

# **Design of Robust Heterogeneous Catalysts for Sustainable Chemistry**

**DISSERTATION**

Zur Erlangung des akademischen Grades eines  
Doktors der Naturwissenschaften (Dr. rer. nat.) im Fach Chemie der  
Fakultät für Biologie, Chemie und Geowissenschaften der Universität  
Bayreuth

vorgelegt von

**M. Phil. Muhammad Zaheer**

geboren in Rawalakot (A.J.K) Pakistan

Bayreuth, 2013

This doctoral thesis was prepared at the Chair of Inorganic Chemistry II, University of Bayreuth from October 2009 to June 2013 under the supervision of Professor Dr. Rhett Kempe.

This is a full reprint of the dissertation submitted to obtain the academic degree of Doctor of Natural Sciences (Dr. rer. nat.) and approved by the Faculty of Biology, Chemistry and Geosciences of the University of Bayreuth.

Dean: Prof. Dr. Rhett Kempe

Thesis submitted: 03-07-2013

Date of defense (disputation): 08-10-2013

Doctoral committee:

1<sup>st</sup> reviewer: Prof. Dr. Rhett Kempe

2<sup>nd</sup> reviewer: Prof. Dr. Jürgen Senker

Chairman: Prof. Dr. Andreas Fery

Prof. Dr. Matthias Breuning

*To Ammi & Abba Ji*

# Abbreviations

---

$\theta$	theta
$\delta$	chemical shift (ppm)
$^{\circ}$	degree
$^{\circ}\text{C}$	degree celsius
$\mu\text{L}$	microliter
$\text{\AA}$	Ångström
cod	cis-1,5-cyclooctadiene
DTA	differential thermal analysis
EDX	energy-dispersive X-ray spectroscopy
equiv.	equivalent
FT-IR	fourier transform infrared spectroscopy
g	gram
GC	gas chromatography
h	hours
K	Kelvin
$\text{m}^2/\text{g}$	square metre per gram
min	minute
mL	milliliter
mmol	millimol
MS	mass spectrometry
NLDFT	nonlocal density functional theory
nm	nanometre
NMR	nuclear magnetic resonance
NPs	nanoparticles
PCS	polycarbosilane
Pd/C	palladium at charcoal
PDCs	polymer derived ceramics
PE	polyethylene
PXRD	powder X-ray diffraction
rpm	revolutions per minute
SiC	silicon carbide
SiCN	silicon carbonitride
TEM	transmission electron microscopy
TGA	thermogravimetric analysis
THF	tetrahydrofuran

# Table of Contents

---

<b>1. Summary / Zusammenfassung.....</b>	<b>1</b>
1.1 Summary.....	1
1.2 Zusammenfassung.....	4
<b>2. Introduction.....</b>	<b>7</b>
<b>3. Overview of Thesis Results .....</b>	<b>13</b>
3.1 Overview and the Interconnection of the Publications.....	13
3.2 Individual Contribution to Joint Publication .....	18
<b>4. The Generation of Palladium Silicide Nanoalloy Particles in a SiCN Matrix and their Catalytic Applications .....</b>	<b>21</b>
4.1 Introduction.....	22
4.2 Experimental .....	23
4.3 Results and Discussion.....	25
4.4 Conclusions.....	34
4.5 References.....	35
<b>5. Polymer Derived Non-oxide Ceramics (PDCs) Modified with Late Transition Metals.....</b>	<b>40</b>
5.1 Introduction.....	40
5.2 General strategies for the synthesis of PDCs.....	41
5.3 Metal modified SiC ceramics.....	42
5.4 Metal modified SiCN ceramics.....	55
5.5 Applications.....	65
5.6 Conclusions and outlook.....	70
5.7 References.....	71
<b>6. Robust Microporous Monoliths with Integrated Catalytically Active Metal Sites Investigated by Hyperpolarized <sup>129</sup>Xe NMR .....</b>	<b>77</b>
6.1 Introduction.....	78
6.2 Experimental .....	80
6.3 Results and discussion .....	84
6.4 Conclusions.....	102
6.5 References.....	104
6.6 Supporting information.....	110
<b>7. Robust Heterogeneous Nickel Catalysts with Tailored Porosity for the Selective Hydrogenolysis of Aryl Ethers .....</b>	<b>116</b>

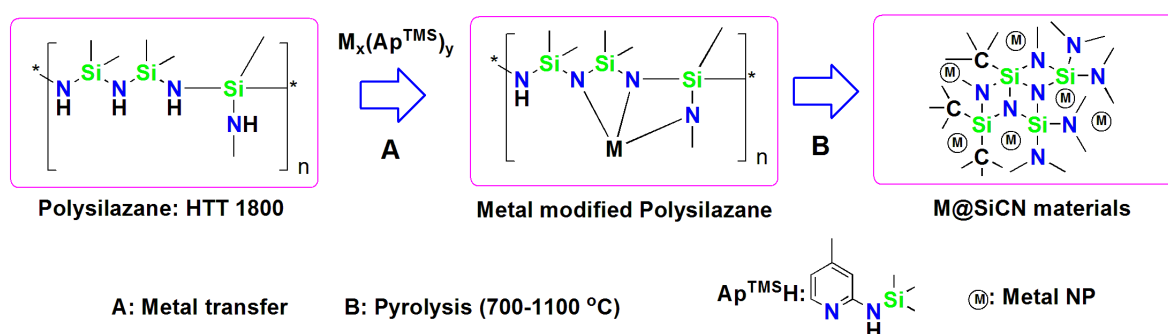
---

7.1 Experimental .....	125
7.2 References .....	126
7.3 Supporting information .....	129
<b>8. Robust Nanoporous Materials with Very Small, Highly Accessible Palladium Nanoparticles .....</b>	<b>137</b>
8.1 References .....	144
8.2 Supporting information .....	148
<b>9. List of Publications.....</b>	<b>151</b>
<b>10. Acknowledgments / Danksagung .....</b>	<b>152</b>
<b>11. Declaration / Erklärung .....</b>	<b>156</b>

# 1. Summary/Zusammenfassung

## 1.1 Summary

Robust heterogeneous catalysts based on polymer derived non-oxide ceramics (SiC/SiCN) with integrated late transition metal (Ni, Pd) nanoparticles (NPs) were designed, characterized and tested for their catalytic potential. For the decoration of SiCN support with metal NPs, a molecular approach was applied which makes the use of amido metal complexes  $[M_x(\text{Ap}^{\text{TMS}})_y]$  (M: Transition metals,  $\text{Ap}^{\text{TMS}}\text{H}$ : 4-Methyl-2-((trimethylsilyl)amino)pyridine) for the chemical modification of the preceramic polymer (commercially known as HTT 1800, Clariant Advanced Materials GmbH, Sulzbach, Germany) by the transfer of metal to its nitrogen functions (scheme 1.1). The modified polymer was transformed to an amorphous SiCN material containing metal NPs by controlled pyrolysis under an inert atmosphere. By following aforementioned approach, Cu@SiCN materials (non-porous) have already been developed in our research group.

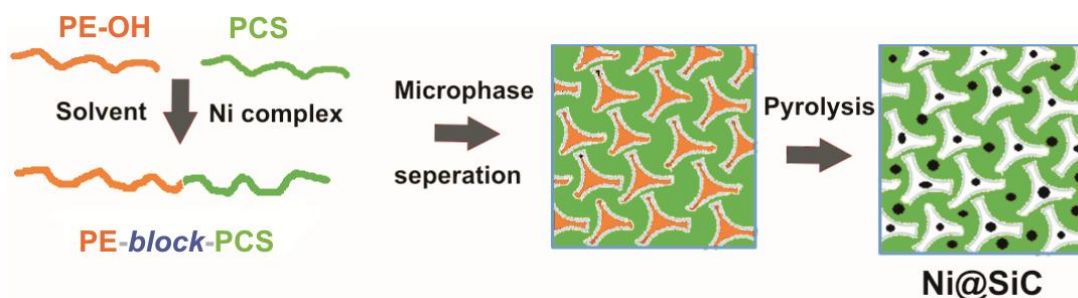


**Scheme 1.1** The synthesis of M@SiCN ceramics.

In present thesis, attempts were made to fabricate porous SiCN/SiC materials with good accessibility of metal (Ni and Pd) NPs. Firstly, the synthesis of palladium containing SiCN materials by the pyrolysis of palladium modified polysilazane was attempted. It was found that during polymer to ceramic transformation, palladium reacts with silicon to form intermetallic palladium silicide ( $\text{Pd}_2\text{Si}$ ) particles. The materials were characterized (TGA, FT-IR, NMR, PXRD and TEM) and applied in catalytic hydrogenation reactions. The activity of the catalysts was found low because of the silicidation of metal and non-porous SiCN support.

The issues of the low porosity of SiCN ceramics and the formation of metal silicides were addressed in the synthesis of Ni@SiCN materials. Controlled pyrolysis of Ni modified polysilazane at 600°C provided microporous Ni@SiCN materials, whereas at 1100°C the formation of nickel silicides in non-porous SiCN matrix was observed. Ni@SiCN materials were characterized by solid state NMR, FT-IR, PXRD, TGA, N<sub>2</sub>-physisorption and TEM. Hyperpolarized <sup>129</sup>Xe NMR was used to study the effect of nickel loading and annealing time on pore structure. The microporous materials showed good thermal stability and activity in selective hydrogenation of aryl acetylenes but as polymer to ceramic conversion was not complete at 600°C, the materials possessed low hydrothermal stability at higher temperatures due to the hydrolysis of Si-N bonds.

In order to replace Si-N bonds with more stable Si-C bonds, a commercial polycarbosilane was used to fabricate SiC materials with integrated Ni NPs by the pyrolysis of nanostructured polycarbosilane-*block*-polyethylene (PCS-*b*-PE) polymer. PCS-*b*-PE was synthesized by the reaction of PCS with PE-OH catalyzed by an amido nickel complex followed by its nanostructuring *via* microphase separation technique. The length of PE block affected the type of pores generated in SiC material and the synthesis of highly porous materials with micro-, meso- and hierarchical porosity was achieved. Ni@SiC materials were characterized by TGA, PXRD, N<sub>2</sub>-physisorption and TEM. Hierarchically porous Ni@SiC selectively cleaves aromatic C-O bond of aryl ethers in water and was found a reusable catalyst.



**Scheme 1.2** Synthesis of Ni@SiC ceramics.

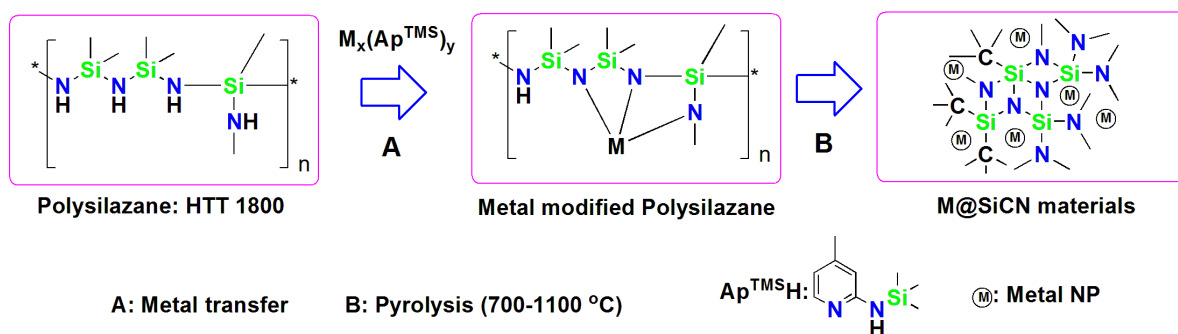
Lastly, controlled pyrolysis of palladium modified polysilazane provided nanoporous SiCN materials with very small and highly accessible Pd NPs. This shows the role of SiCN support whose nitrogen atoms have a stabilizing effect on small metal nanoparticles. Moreover, SiCN support interacts nicely with the NPs leading to the prevention of their leaching. In general, NPs have agglomeration tendencies with

increasing metal loading but in the case of Pd@SiCN, size of metal NPs remained small even with a palladium loading of 14 wt%. Pulse titration with hydrogen showed high accessibility of Pd. Pd@SiCN materials showed better activity than commercial Pd/C catalyst in oxidation of alcohols in the absence of air or oxygen with the evolution of hydrogen.

M@SiCN/SiC materials may find applications in sustainable production of chemicals and fuels from renewable sources, for instance, from lignocellulosic biomass.

## 1.2 Zusammenfassung

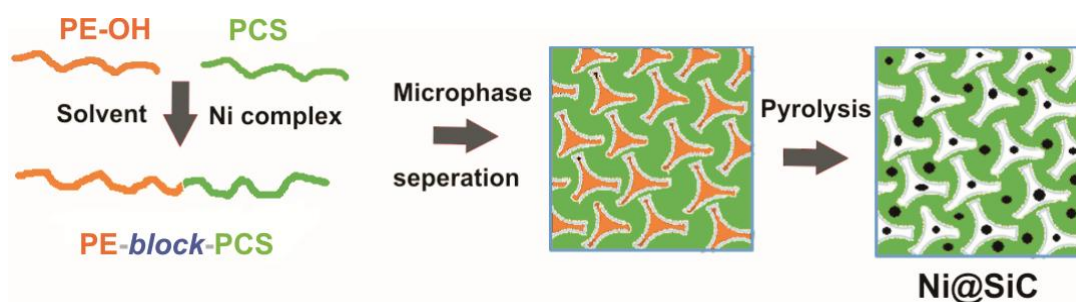
Im Rahmen der Doktorarbeit wurden stabile heterogene Katalysatoren, bestehend aus nicht oxidischen Keramiken (SiC/SiCN) mit integrierten metallischen Nanopartikeln (NP) der Späten Übergangsmetalle (Ni, Pd) entwickelt, charakterisiert und auf ihre katalytischen Eigenschaften untersucht. Das als Ausgangsmaterial verwendete präkeramischen Polymer, kommerziell erhältlich als HTT 1800 (Clariant Advanced Materials GmbH; Sulzbach; Germany), wurde auf molekularem Wege durch Metallübertragung auf die Stickstofffunktionen unter Verwendung von Amidometallkomplexen  $[M_x(\text{Ap}^{\text{TMS}})_y]$  (M: Übergangsmetall,  $\text{Ap}^{\text{TMS}}\text{H}$ : 4-Methyl-2-((trimethylsilyl)amino)pyridinat) (Schema 1.1) modifiziert. Das mit Metall beladene Polymer wurde anschliessend durch kontrollierte Pyrolyse unter Inertgasbedingungen in ein amorphes, metallische NP enthaltendes SiCN Material umgewandelt. Durch diese Vorgehensweise wurden bereits nichtporöse Cu@SiCN Materialien in unserer Forschungsgruppe entwickelt.



**Schema 1.1** Die Synthese von M@SiCN Keramiken.

In der vorliegenden Arbeit wurden Bestrebungen unternommen poröse SiCN/SiC Materialien mit guter Zugänglichkeit zu den Metallischen NP (Ni, Pd) zu generieren. Zunächst wurde die Synthese Palladium enthaltender SiCN Materialien durch Pyrolyse von Palladium modifizierten Polysilazanen untersucht. Dabei wurde beobachtet dass während der Umwandlung des Polymers in die Keramik Palladium mit Silizium unter Bildung intermetallischer Palladiumsilizid-partikel ( $\text{Pd}_2\text{Si}$ ) reagiert. Die Materialien wurden charakterisiert (TGA, FT-IR, NMR, PXRD und TEM) und in Hydrierreaktionen als Katalysator eingesetzt. Die Aktivität des Katalysators blieb aufgrund von Silicidbildung des Metall und unporösen SiCN Träger gering. Die Problematik geringer Porosität der SiCN Keramiken und die Bildung von Metallsiliziden wurde mit der Synthese von Ni@SiCN Materialien studiert. Die

kontrollierte Pyrolyse von Ni modifiziertem Polysilazan lieferte bei 600°C mikroporöse Ni@SiCN Materialien wohingegen bei 1100°C die Bildung von Nickelsiliziden in einer unporösen SiCN Matrix beobachtet wurde. Die Ni@SiCN Materialien wurden mittels Festkörper NMR, FT-IR, PXRD, TGA, N<sub>2</sub>-Physisorption und TEM charakterisiert. Unter Verwendung von hyperpolarisiertem <sup>129</sup>Xe NMR Experimenten wurde der Effekt von Nickelbeladung und Ausglühzeit auf die Porenstruktur untersucht. Die Materialien zeigten gute thermische Stabilität und Aktivität in der selektiven Hydrogenierung von Arylacetylenen. Da aber die Umwandlung von Polymer zu Keramik bei Pyrolysetemperaturen von 600°C noch nicht vollständig ist, besitzen die Materialien aufgrund der Hydrolyse von Si-N Bindungen eine geringe hydrothermale Stabilität bei höheren Temperaturen. Um die Si-N Bindungen durch stabilere Si-C Bindungen zu ersetzen, wurde kommerzielles Polycarbosilan verwendet, um SiC Materialien mit integrierten Ni NP mittels Pyrolyse von nanostrukturiertem Polycarbosilan-*block*-polyethylen (PCS-*b*-PE) Polymer zu erzeugen. PCS-*b*-PE wurde durch eine Amido-Nickel-Komplexbekatalysierte Reaktion von PCS mit PE-OH und anschließender Nanostrukturierung durch Mikrophasenseparationstechnik synthetisiert. Die Länge des PE Blockes beeinflusst den im SiC Material generierten Porentypus. Die Synthese hochporöser Materialien mit Mikro-, Meso- und hierarchischer Porosität wurden erreicht. Ni@SiC Materialien wurden mittels TGA, PXRD, N<sub>2</sub>-Physisorptionsmessungen und TEM charakterisiert. Hierarchisch poröses Ni@SiC spaltet selektiv aromatische C-O Bindungen von Arylethern in Wasser bei guter Wiederverwendbarkeit.



**Schema 1.2** Synthese von Ni@SiC Keramiken.

Zum Schluß lieferte die kontrollierte Pyrolyse von Palladium modifiziertem Polysilazan mikroporöse SiCN Materialien mit sehr kleinen und gut zugänglichen Pd NP. Dies zeigt die Bedeutung des SiCN Trägers, dessen Stickstoffatome einen

stabilisierenden Effekt auf kleine Metall NP haben. Darüber hinaus wechselwirkt der SiCN Träger gut mit den NP und verhindert so deren Herauslösen (Leaching).

Im Allgemeinen besitzen NP die Tendenz mit steigender Metallbeladung zu agglomerieren. Jedoch bleiben Metallischen NP im Falle des Pd@SiCN auch bei 14 wt% stabil. Die Pulstitrations mit Wasserstoff zeigt eine bessere Zugänglichkeit des Palladiums als es für kommerzielle Pd/C Katalysatoren der Fall ist. Pd@SiCN Materialien zeigen ebenso in der Sauerstofffreien Oxidation von Alkoholen zu Aldehyden und Ketonen, unter Bildung von Wasserstoff, eine bessere Aktivität als kommerzielle Pd/C Katalysatoren. M@SiCN/SiC Materialien könnten Anwendung in der nachhaltigen Produktion von Chemikalien und Brennstoffen aus erneuerbaren Quellen, wie beispielsweise lignocellulärer Biomasse finden.

## 2. Introduction

We are living in an oil-based society where most of the fuels and major chemicals are obtained from fossil resources (coal, oil and natural gas). Currently, the building blocks for about 95% of all the carbon-containing chemicals that are required to sustain our everyday lives are derived from crude oil.<sup>[1]</sup> In fact, 70.6% of the crude oil pumped out from earth is used for the production of fuels and 3.4% feeds the chemical industry for the production of chemicals (Fig. 1).<sup>[2]</sup> Interestingly, both fuel market and petrochemicals create revenues that roughly correspond to almost the same amount of money in USA (385 billion US\$).<sup>[2]</sup> Unfortunately, oil reservoirs are depleting tremendously and are currently available to provide fuels and chemicals for a limited period of time.<sup>[3]</sup> Therefore, diminishing fossil resources together with increasing oil prices and emission of green house gases demand alternate renewab-

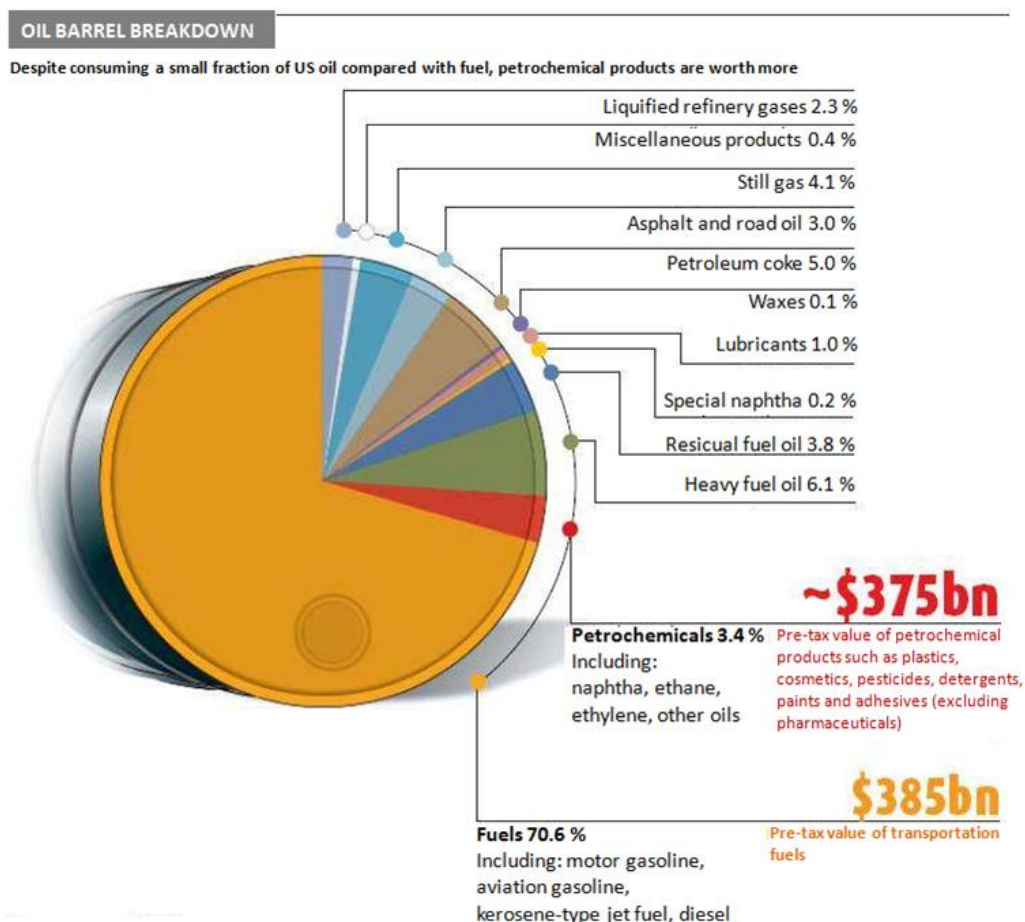


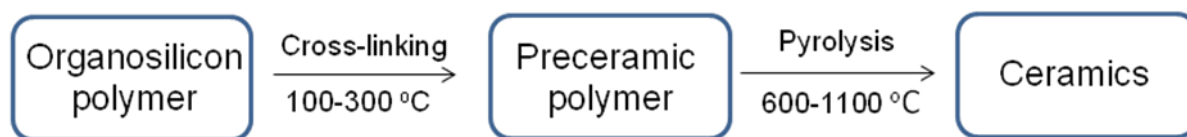
Figure 1. Production of fuels and chemicals from crude oil. Adopted from reference 1.

-le feedstocks for the production of both fuels and chemicals.<sup>[4]</sup> Biomass, in this regard is the only renewable and sustainable source for the production of both fuels and chemicals.<sup>[5]</sup> Whereas there has been a strong focus on the use of biomass for the production of fuels, much less attention has been given to its utilization as a feedstock for organic chemicals.<sup>[6]</sup> Replacement of petroleum-derived chemicals with those from biomass will play a key role in sustaining the growth of the chemical industry.<sup>[7]</sup> The US department of energy, in this regard, has set up a goal that by 2030, 20% of transportation fuel and 25% of chemicals will be produced from biomass.<sup>[8]</sup>

Biomass is a myriad of complex substances that amount to ca.  $170 \times 10^9$  tons per year.<sup>[9]</sup> Lignocellulosic biomass is the most abundant bio-resource available and consists of three major components: Cellulose (40%), hemicelluloses (25%) and lignin (20%).<sup>[10]</sup> Non-edible biomass (lignocelluloses) offers advantages such as their utilization will not compete with the food supply, their lower cost and faster growth as compared to food crops.<sup>[11]</sup>

Catalysts are the philosopher's stones of the chemical industry as most of the industrial processes utilize them. Among others (molecules, enzymes) solid catalysts dominate the chemical industry due to the ease of their separation after the reaction. It is estimated that almost 80-85% of the processes use them<sup>[12]</sup> including the industrial production of fine chemicals.<sup>[13]</sup> Other than biotechnological processes,<sup>[14]</sup> chemical routes in general<sup>[15]</sup> and heterogeneous catalysis in particular find potential use in the efficient utilization of biomass for the production of fuels and chemicals.<sup>[16]</sup> The utilization of biomass as a substituent feedstock for crude oil would be a shift from gaseous phase to liquid phase catalysis demanding additional special features both from the catalyst and the support. As most of the biomass transformations are carried out in aqueous or highly polar solvents, the catalyst needs to be stable against dissolution and leaching in these media under different pH conditions. Tunable porosity is another characteristic required as it would allow the effective transport of substances for effective catalysis.<sup>[17]</sup> Therefore, design of solid catalysts with tunable porosity, high surface area and hydrothermal stability is vital in the efficient utilization of biomass for sustainable chemistry.

Polymer derived ceramics (PDCs) are versatile materials derived from organosilicon



**Scheme 1.** Synthesis of polymer derived ceramics from organosilicon polymers.

polymers (scheme 1) possessing high (hydro)thermal stability and can withstand harsh chemical environment.<sup>[18]</sup> These features make them suitable candidates as support materials for catalytic biomass conversion. Due to the polymer route of synthesis, PDCs offer several advantages over the conventional oxide ceramics synthesized *via* solid state methods. Firstly, they have lower processing temperatures and allow the fine tuning of structure at a molecular level. Secondly, the fabrication of a wide variety of structures like films, fibers, sheets and coatings is facilitated.<sup>[19]</sup> Among other PDCs, SiCN ceramics are interesting in particular because of the presence of nitrogen as a part of three dimensional covalent Si-C-N network. Nitrogen functions, in first place, facilitate the transfer of metal ions from amido metal complexes to silzane polymer. Secondly, they can stabilize small metal nanoparticles (NPs) anchoring them firmly with the support which in turn avoids the metal leaching. The introduction of metal NPs can be achieved by the use of metal (oxide) powders, coordination compounds or employing metal containing polymers. Our group has developed a molecular approach in which amido metal complexes of transition metals are used for the chemical modification of polysilazane which upon its pyrolysis under an inert atmosphere provided M@SiCN materials.<sup>[20]</sup> Although Cu@SiCN catalysts synthesized by this approach, showed appreciable catalytic activity in air oxidation of alkanes, non-porous SiCN support afforded severe mass transport constraints.

The present thesis focuses on the design of robust, porous and recyclable M@SiCN/SiC catalysts for sustainable chemistry applications. Due to broad spectrum of catalytic applications offered by palladium, we decided to extend our approach developed for Cu@SiCN materials to synthesize palladium containing SiCN ceramics. Unfortunately, the activity of the catalysts was low due to the formation of intermetallic Pd<sub>2</sub>Si phase instead of palladium NPs. Moreover the catalysts possessed very low surface area which would have avoided effective mass transport of materials through them. As nickel is an inexpensive metal finding applications in a wide range of catalytic transformations, we tried to fabricate SiCN

supported porous nickel catalysts. It was found that fine tuning of pyrolysis conditions was crucial in addressing the porosity issues as well as in preventing the formation of metal silicides. With slower heating rate (1K/min) and longer dwelling times it was possible to get highly microporous nickel NPs containing SiCN materials. Ni@SiCN materials manifested appreciable thermal stability and good activity in selective hydrogenation of aryl acetylenes. Unfortunately, Si-N bonds of the materials were attacked by water at higher temperatures so it was decided to replace them with more stable Si-C bonds. In order to tune the porosity of materials we made the use of a cheap organic polymer synthesized in our group by the use of molecular catalysts. A commercially available polycarbosilane was reacted with polyethylene having –OH end groups which can react with Si-H group of the pre-ceramic polymer (polycarbosilane) in the presence of an amido nickel complex to provide polycarbosilane-*block*-polyethylene (PCS-*b*-PE) polymer. This block copolymer can be self assembled into ordered structures which upon pyrolysis provided highly porous Ni@SiC materials. The length of organic block greatly affected the type of pores generated within the materials and it was possible to fabricate materials with micro- meso- and hierarchical porosity. Selective hydrogenolysis of lignin model compounds was carried out in water and catalysts were found to be selective and reusable in the cleavage of aromatic C-O bonds.

Last part of the thesis discusses the role of nitrogen functions of SiCN support in the stabilization of very small metal particles. By controlled pyrolysis of polysilazane modified with palladium, nanoporous SiCN materials with very small, highly accessible palladium NPs were achieved. Pd@SiCN materials were found active catalysts in dehydrogenation of alcohols under anaerobic conditions. This reaction is important in the sense that liquid alcohols can be transported easily and stored hydrogen can be regenerated from them by the use of Pd@SiCN catalysts for its use as a clean source of energy. Moreover, the dehydrogenation of alcohols is a key step in sustainable synthesis.<sup>[21]</sup>

## References

- [1] C. H. Christensen, J. Rass-Hansen, C. C. Marsden, E. Taarning, K. Egeblad, *ChemSusChem*. **2008**, *1*, 283-289.

- 
- [2] J. Marshall, *New Sci.* **2007**, *195*, 28-31.
- [3] J. N. Chheda, G. W. Huber, J. A. Dumesic, *Angew. Chem. Int. Ed.* **2007**, *46*, 7164-7183.
- [4] P. L. Dhepe, A. Fukuoka, *ChemSusChem.* **2008**, *1*, 969-975.
- [5] a) D. L. Klass, *Biomass for Renewable Energy, Fuels and Chemicals*, Academic Press, California, **1998**; b) P. Gallezot, *Chem. Soc. Rev.* **2012**, *41*, 1538-1558; c) G. W. Huber, S. Iborra, A. Corma, *Chem. Rev.* **2006**, *106*, 4044-4098; d) B. Kamm, *Angew. Chem. Int. Ed.* **2007**, *46*, 5056-5058.
- [6] J. van Haveren, E. L. Scott, J. Sanders, *Biofuels Bioprod. Bioref.* **2008**, *2*, 41-57.
- [7] D. R. Dodds, R. A. Gross, *Science* **2007**, *318*, 1250-1251.
- [8] US department of energy, Accession No. ADA 436527, **2002**.
- [9] B. Kamm, P. R. Gruber, M. Kamm, *Biorefineries - Industrial Process and Products*, Vol. 1, Wiley-VCH, Weinheim, **2006**, p. 15.
- [10] E. Taarning, C. M. Osmundsen, X. Yang, B. Voss, S. I. Andersen, C. H. Christensen, *Energy Environ. Sci.* **2011**, *4*, 793-804.
- [11] a) J. C. Serrano-Ruiz, R. M. West, J. A. Dumesic, *Annu. Rev. Chem. Biomol. Eng.* **2010**, *1*, 79-100; b) S. P. S. Chundawat, G. T. Beckham, M. E. Himmel, B. E. Dale, *Annu. Rev. Chem. Biomol. Eng.* **2011**, *2*, 121-145.
- [12] G. Ertl, H. Knözinger, F. Schüth, J. Weitkamp, *Handbook of Heterogeneous Catalysis*, Vol. 1, Wiley-VCH, Weinheim, **2008**.
- [13] a) J. H. Clark, D. J. Macquarrie, *Org. Process Res. Dev.* **1997**, *1*, 149-162; b) M. J. Climent, A. Corma, S. Iborra, *Chem. Rev.* **2011**, *111*, 1072-1133.
- [14] H. Danner, R. Braun, *Chem. Soc. Rev.* **1999**, *28*, 395-405.
- [15] A. Corma, S. Iborra, A. Velty, *Chem. Rev.* **2007**, *107*, 2411-2502.

- [16] a) H. Kobayashi, H. Ohta, A. Fukuoka, *Catal. Sci. Technol.* **2012**, 2, 869-883; b) J. Z. Pieter, C. A. Bruijninx, A. L. Jongerius, B. M. Weckhuysen, *Chem. Rev.* **2010**, 110, 3552–3599; c) D. M. Alonso, S. G. Wettstein, J. A. Dumesic, *Chem. Soc. Rev.* **2012**, 41, 8075-8098; d) C. –H. Zhou, X. Xia, C. –X. Lin, D. – S. Tong, J. Beltramini, *Chem. Soc. Rev.* **2011**, 40, 5588-5617.
- [17] R. Rinaldi, F. Schüth, *Energy Environ. Sci.* **2009**, 2, 610-626.
- [18] P. Colombo, R. Riedel, G. D. Soraru, H. –J. Kleebe, *Polymer Derived Ceramics-From Nanostructure to Applications*, DEStech Publications, Inc. Pennsylvania, **2010**.
- [19] P. Colombo, G. Mera, R. Riedel, G. D. Soraru, *J. Am. Ceram. Soc.* **2010**, 93, 1805-1837.
- [20] M. Zaheer, T. Schmalz, G. Motz, R. Kempe, *Chem. Soc. Rev.* **2012**, 41, 5102-5116.
- [21] S. Michlik, R. Kempe, *Nat. Chem.* **2013**, 5, 140-144.

### 3. Overview of Thesis

---

An overview and the interconnection of the publications presented in the thesis (chapters 4-8) are described here.

#### 3.1 Overview and the Interconnection of the Publications

For the development of robust heterogeneous catalysts for the sustainable production of chemicals, polymer derived ceramics (PDCs: SiCN/SiC) were chosen as support materials. Polymer derived non-oxide ceramics modified with late transition metals are reviewed in chapter 5. In addition to the main synthetic strategies for modified SiC and SiCN ceramics, an overview of the morphologies, structures and compositions of both, ceramic materials and metal (nano) particles, is presented. PDCs can broadly be classified into SiC and SiCN ceramics. They are characterized by high thermal stability, oxidation resistance and stability under harsh chemical environment. The chemical modification of organosilicon polymers followed by their pyrolysis can provide metal containing PDCs. For the modification of polymers, either metal (oxide) powders or alternatively coordination complexes can be used, the later being advantageous as they allow the control at a molecular level. Direct pyrolysis of metallopolymers can also provide M@PDCs. The characterization of M@PDCs with various analytical tools is also reviewed. In the applications part, magnetic, biological and catalytic applications of the materials are discussed in depth (Fig. 3.1).

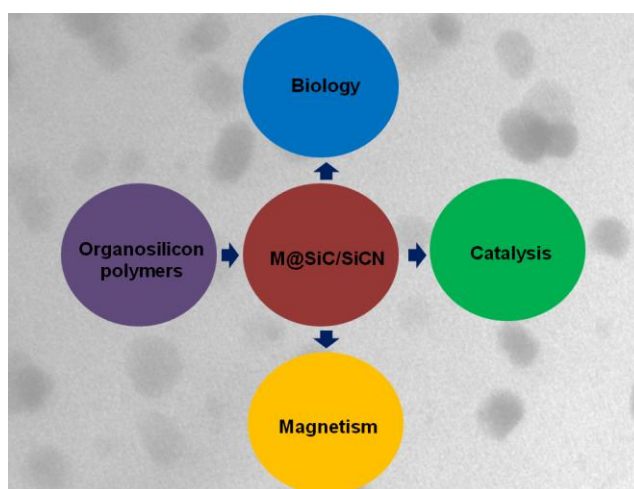


**Figure 3.1** Flow chart of the synthesis and applications of PDCs modified with late transition metals.

For the introduction of active metal particles to SiCN support, a molecular approach utilizing the amido metal complexes was recently developed in our group. During the reaction of metal complex with the polysilazane, metal is transferred to the nitrogen functions of the polymer providing a metallopolymer. The metal modified polymer upon its pyrolysis under an inert atmosphere provides M@SiCN materials. Cu@SiCN catalysts synthesized this way were used in the air oxidation of cycloalkanes. Unfortunately, such catalysts offered low activity because of the non-porous SiCN support and low accessibility of the active metal particles. Aformentioned approach was extended to other metals in order to synthesize M@SiCN composites for various catalytic applications. As palladium offers a wide range of applications in catalytic hydrogenation, oxidation and coupling reactions, an attempt to synthesize Pd@SiCN robust catalysts was made (chapter 4). Amido palladium complex (**2**) not only transferred the metal to N-functions of polysilazane (**1**) but also initiated cross-linking of preceramic polymer by hydrosilylation and dehydrocoupling reactions (Fig. 3.2). After pyrolysis of palladium modified polymer (**3**) the formation of palladium silicide (Pd<sub>2</sub>Si) particles in a SiCN matrix was observed. As the preceramic polymer is rich in silicon (~ 50% Si), palladium reacts with silicon at higher temperature (1100°C) to form palladium silicide. The size of the Pd<sub>2</sub>Si was found dependent on the solvent used in the chemical modification of polysilazane as smaller particles were generated in hexane than those formed with the use of THF. The materials were characterized by NMR (<sup>1</sup>H and <sup>13</sup>C), FT-IR, TGA, PXRD and TEM. Pd<sub>2</sub>Si@SiCN materials were found active, selective and reusable catalysts in the hydrogenation of aryl ketones to alcohols. Conversion increased with increase in temperature keeping constant selectivity to alcoholic product. Overall

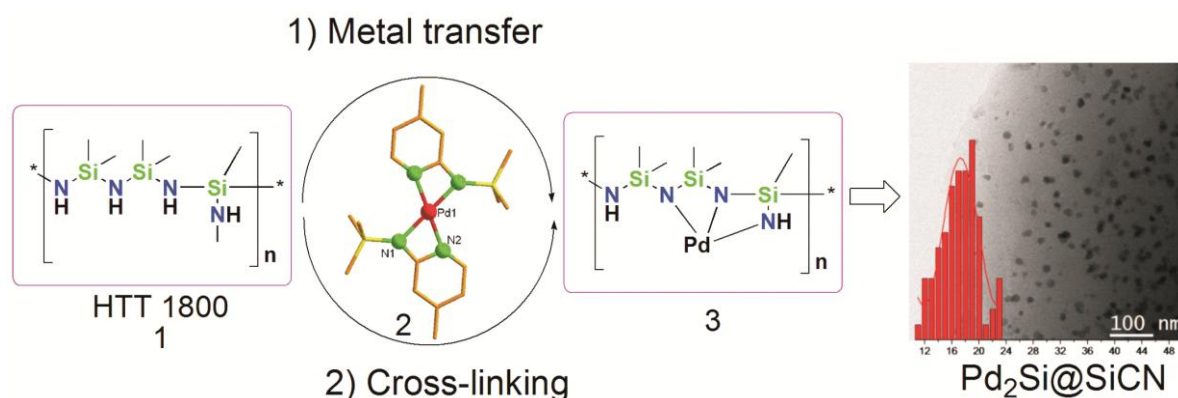


**Figure 3.2** Schematic presentation of the synthesis of Pd<sub>2</sub>Si@SiCN materials.

conversion decreased both with the increase in alkyl chain length and its branching at alpha carbon of the ketone.

As an inexpensive metal widely used for various catalytic transformations, nickel containing SiCN ceramics were planned to be synthesized (chapter 6). The issues of non-porous SiCN support and the formation of metal silicides were addressed in the synthesis of Ni@SiCN materials (Fig. 3.3). The pyrolysis of polysilazane (HTT 1800) at various temperatures (300-1100°C) revealed that the surface area of obtained SiCN materials increased up to 500°C and then decreased to almost zero at 1100°C. This transient porosity arises due to the emission of gases during pyrolysis and is lost above 600°C. Thus, highly microporous Ni@SiCN materials were obtained by the pyrolysis of nickel modified polysilazane (HTT 1800) at 600°C and were characterized by TGA, DTA, FT-IR, PXRD, N<sub>2</sub>-physisorption, TEM and solid state <sup>13</sup>C and <sup>29</sup>Si NMR spectroscopy. Nickel complex not only acted as a metal transfer reagent but also catalyzed the cross-linking of polysilazane *via* hydrosilylation reaction. Moreover, it catalyzed the formation of graphitic carbon within the materials which provided mechanical strength to the materials leading to the retention of porosity at 600°C. Slow heating rates and longer dwelling times were also found useful in this regard. As investigated by <sup>13</sup>C and <sup>29</sup>Si solid state NMR, increase in Ni amount increased the population of SiN<sub>4</sub> sites and the graphitic carbon content within the materials. The surface area, pore size and size of Ni NPs can be tuned. Pyrolysis temperature had tremendous effect on both porosity and nature of particles formed in SiCN matrix. High temperature (1100°C) provided nickel silicide particles in nonporous SiCN matrix. When temperature was decreased to 600°C microporous SiCN materials with integrated Ni NPs were obtained. The materials showed shape

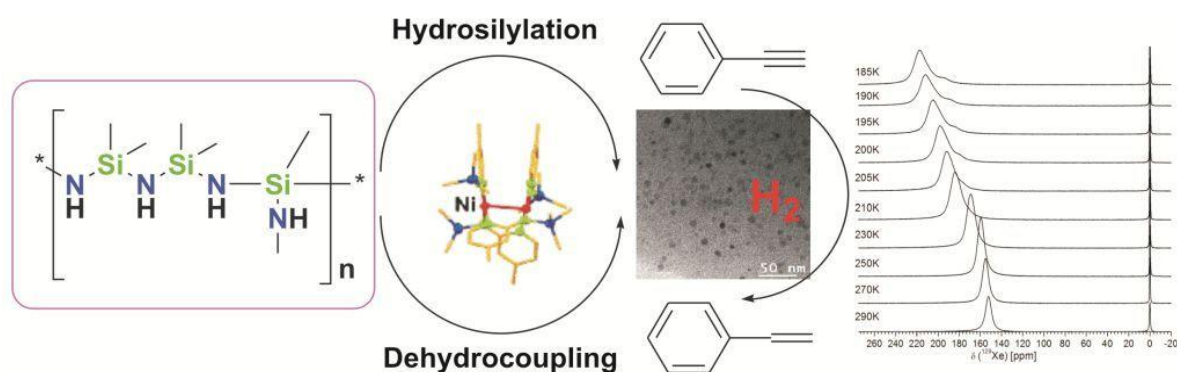


**Figure 3.3.** Pictorial presentation of the synthesis and applications of Ni@SiCN materials.

retention and thermal stability up to 600°C as investigated by TGA studies. Continuous flow hyperpolarized  $^{129}\text{Xe}$  NMR spectroscopy was used to elucidate the effect of nickel loading and annealing time on the pore structure of the materials. The adsorption enthalpy was found independent of the particle size inclusion and particles were located near the external surface and within the internal voids. The composite materials were applied as catalysts in the selective hydrogenation of aryl acetylenes which showed their potential as catalyst or catalyst support materials.

Porosity issues associated with SiCN support as well as the formation of intermetallic phases with noble metals (Ni, Pd, and Pt) were somehow solved by the pyrolysis of chemically modified polysilazane at lower temperatures (600°C). Microporous Ni@SiCN materials in this way showed appreciable thermal stability but as the pyrolysis was carried out at a temperature (600°C), where polymer to ceramic conversion was not complete, the obtained materials suffered the problem of lacking hydrothermal stability. It was found that Si-N bonds are attacked by water leading to their hydrolysis so it was decided to replace them with more stable Si-C bonds. A commercial polycarbosilane (SMP-10) was used in this regard to fabricate SiC materials with integrated Ni NPs. As gaseous emissions at 450-550°C during the pyrolysis of preceramic polymer generates porosity which could be retained in the presence of nickel, addition of a sacrificial carbon source could be beneficial. Without the addition of a sacrificial filler, controlled pyrolysis of Ni modified PCS provided materials with low surface area ( $S_{\text{BET}}$ : 100 m<sup>2</sup>/g) but when a hydroxy-terminated polyethylene (PE) was added, highly microporous Ni@SiC materials ( $S_{\text{BET}}$ : 550 m<sup>2</sup>/g) were obtained. Ni complex catalyzed the dehydrocoupling reaction between Si-H and -OH bonds leading to the formation of a polycarbosilane-*block*-polyethylene (PCS-*b*-PE). Chapter 7 discusses the synthesis of Ni@SiC materials with tunable porosity from the self assembly of (PCS-*b*-PE) polymer (Fig. 3.4). The block copolymer owing to the covalent linkage between the two blocks could be self assembled into ordered microdomains. The organic block was burnt off during pyrolysis under an inert gas providing porous Ni@SiC materials. Slow heating rates and long dwelling times during pyrolysis were found beneficial in terms of structural retention. The length of PE block greatly affected the types of pores generated and the fabrication of Ni@SiC materials with micro-, meso- and hierarchical porosity was achieved. The materials were characterized by PXRD, TGA, N<sub>2</sub>-physisorption and TEM. Ni@SiC materials -

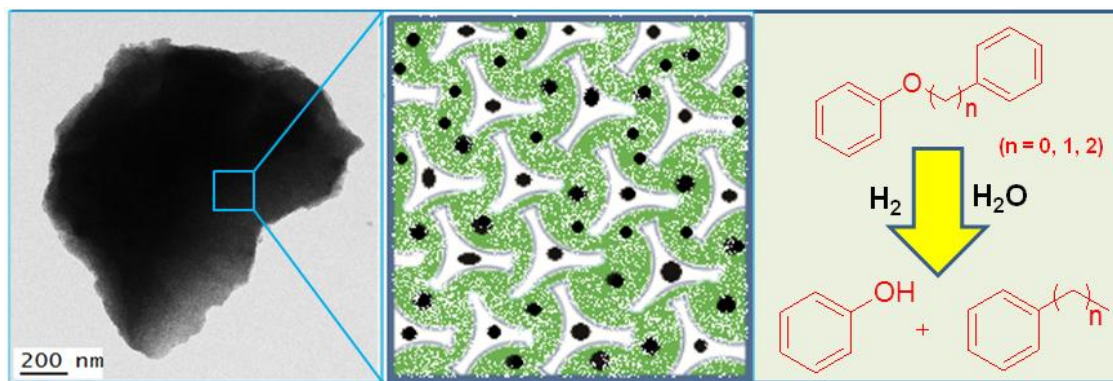


**Figure 3.4** Graphical abstract showing the structure and applications of Ni@SiC materials.

were applied as reusable catalysts for the selective hydrogenolysis of lignin model compounds (aryl ethers). Hierarchical material was found to be the most active as compared to the micro and mesoporous Ni@SiC in the selective cleavage of C-O bond present in aryl ethers.

Inspired by all these investigations in which low temperature pyrolysis ( $\sim 700^\circ\text{C}$ ) and long dwelling times lead to highly porous materials, the reinvestigation of Pd@SiCN was carried out. In a previous attempt to synthesize such materials, the formation of nanoalloy Pd<sub>2</sub>Si particles in a non-porous SiCN matrix was observed. Firstly, Polysilazane (HTT 1800) was chemically modified with an amido palladium complex (Fig. 3.5) and metal got transferred to the nitrogen functions of the polymer. Secondly, controlled pyrolysis of the metallopolymer at  $700^\circ\text{C}$  with slow heating rates and long dwelling times, provided nanoporous Pd@SiCN materials. The loading of metal was varied from 2-14 wt% and materials were characterized by PXRD, N<sub>2</sub>-physisorption and TEM. Pd@SiCN materials contained very small Pd NPs ( $\sim 2.5$  nm) as investigated by TEM. The nitrogen functions of the SiCN network seemed to play a vital role in the stabilization of very small palladium NPs. The preceramic polymer stabilized Pd ions (Pd<sup>+2</sup>), at first place by their coordination to the nitrogen functions of polysilazane. Once reduced to elemental Pd due to the reductive atmosphere during pyrolysis, NPs are capped by N-atoms of the amorphous SiCN network in the second place. In this way, stabilization of very small NPs was achieved which were anchored firmly to the SiCN support and avoided any possible metal leaching. Despite of the agglomeration tendencies of NPs with increasing metal content, the size of NPs remained small even when the metal loading was increased from 2 to 14 wt%. Hydrogen pulse titration was used to determine the metal dispersion. When

fresh Pd@SiCN was heated at 90°C for 24 hours in methanol-water mixture, the metal dispersion increased from 0.25% to 22% which is comparable to the commercial Pd/C catalyst (20%). The activity of the catalysts was expected to be high due to the highly accessible and small Pd NPs. Moreover Pd@SiCN materials possessed porosity and their surface area increased with an increase in metal content. The materials were applied in acceptorless and base free dehydrogenation of alcohols in water. At 90°C, a competitive hydrogenolysis reaction was found along with the dehydrogenation which could be avoided by decreasing the reaction temperature and the amount of water. The activity decreased with an increase in the amount of water used. Both aliphatic and cyclic alcohols were successfully dehydrogenated under mild reaction conditions.

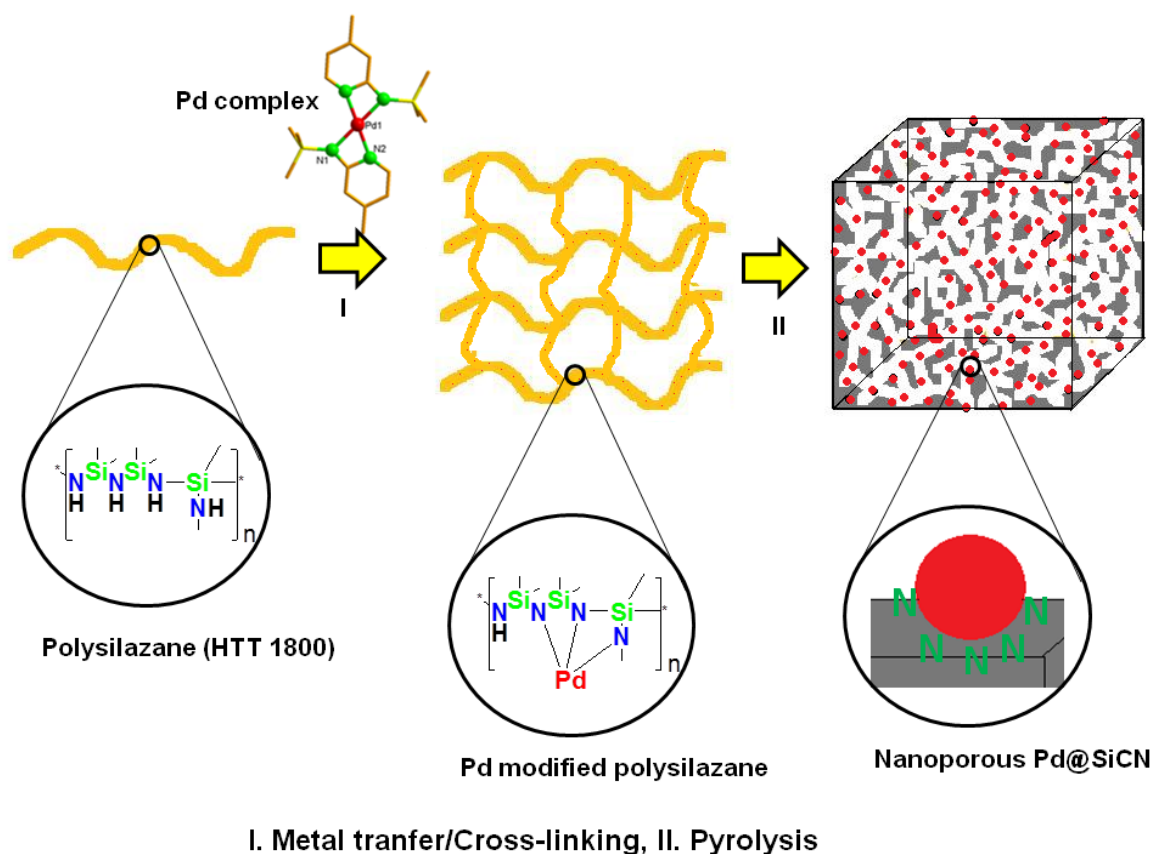


**Figure 3.5** The synthesis of Pd@SiCN and the stabilization of small Pd NPs are shown in the figure.

### 3.2 Individual Contribution to Joint Publication

The results presented in this thesis were gathered with the collaboration of others and are either published, submitted or to be submitted for their publication as

mentioned below. The contribution of co-authors to each publication is acknowledged here. The asterick denotes the corresponding author(s).

### 3.2.1 Chapter 4

This work was published in *J. Mater. Chem.* **2011**, *21*, 18825-18831 with the title '**The Generation of Palladium Silicide Nanoalloy Particles in a SiCN Matrix and Their Catalytic Applications**'

M. Zaheer, G. Motz, R. Kempe\*

I synthesized, characterized and studied the catalytic applications of the materials presented in this work. The paper was written by me while Günter Motz and Rhett Kempe were involved in scientific discussion and in the correction of the manuscript. Rhett Kempe supervised this work also.

### 3.2.2 Chapter 5

This review article was published in *Chem. Soc. Rev.* **2012**, *41*, 5102-5116 with the title '**Polymer Derived Non-oxide Ceramics Modified with Late Transition Metals**'

M. Zaheer, T. Schmalz, G. Motz\*, R. Kempe\*

I wrote the review except the introduction which was written by T. Schmalz. G. Motz and R. Kempe were involved in scientific discussions and manuscript correction.

### 3.2.3 Chapter 6

This work was published in *Chem. Mater.* **2012**, *24*, 3952-3963 with the title '**Robust Microporous Monoliths with Integrated Catalytically Active Metal Sites Investigated by Hyperpolarized  $^{129}\text{Xe}$  NMR**'

M. Zaheer, C. D. Keenan, J. Hermannsdörfer, E. Roessler\*, G. Motz\*, J. Senker\*, R. Kempe\*

I synthesized the materials, did the catalytic experiments and wrote the manuscript. C. D. Keenan performed solid state NMR experiments and wrote the part with  $^{129}\text{Xe}$  NMR. J. Hermannsdörfer took TEM images of the materials. E. Roessler, G. Motz, J. Senker and R. Kempe were involved in scientific discussions and in the correction of the manuscript. The work was planned under the supervision of R. Kempe.

### 3.2.4 Chapter 7

This work was published in *ChemCatChem* with the title '**Robust Heterogeneous Nickel Catalysts with Tailored Porosity for the Selective Hydrogenolysis of Aryl Ethers**'

M. Zaheer, J. Hermannsdörfer, W. P. Kretschmer, G. Motz, R. Kempe\*

The synthesis, characterization and catalytic studies of the materials were performed by me as well as the writing of the manuscript. J. Hermannsdörfer analyzed the materials by TEM while W. P. Kretschmer synthesized the polyethylene. G. Motz and R. Kempe contributed in terms of scientific discussions and correction of the manuscript. The work was supervised by R. Kempe.

### 3.2.5 Chapter 8

This work is to be submitted for publication with the title '**Robust Nanoporous Palladium Catalysts for Oxidant Free Dehydrogenation of Alcohols under Mild Conditions**'

M. Zaheer, G. Motz, R. Kempe\*

The materials were synthesized and characterized by me. I did the catalytic studies with the materials and wrote the manuscript. G. Motz and R. Kempe corrected the manuscript and were involved in scientific discussions. The work was supervised by R. Kempe.

## 4. The Generation of Palladium Silicide Nanoalloy Particles in a SiCN Matrix and Their Catalytic Applications

---

Muhammad Zaheer,<sup>[a]</sup> Günter Motz<sup>[b]\*</sup> and Rhett Kempe<sup>[a]\*</sup>

[a] Inorganic Chemistry II, University of Bayreuth, 95440 Bayreuth, E-mail:

[kempe@uni-bayreuth.de](mailto:kempe@uni-bayreuth.de)

[b] Ceramic Materials Engineering, University of Bayreuth, 95447 Bayreuth, E-mail: [guenter.motz@uni-bayreuth.de](mailto:guenter.motz@uni-bayreuth.de)

**Published in:** *J. Mater. Chem.* **2011**, *21*, 18825-18831.

**Abstract:** The synthesis, characterization and catalytic studies of single phase palladium silicide nanoalloy particles supported by a polymer derived, non-oxide SiCN matrix (Pd<sub>2</sub>Si@SiCN) is reported. Simultaneous chemical modification of a polyorganosilazane as well as its cross-linking was achieved by the use of an aminopyridinato palladium complex at room temperature. Cross-linking takes place with an evolution of hydrogen and increases the ceramic yield by the retention of carbon and nitrogen atoms. Liberation of ligand, as confirmed by <sup>1</sup>H NMR spectroscopy provides an indirect evidence of the transfer of palladium to the nitrogen functions producing metal modified polyorganosilazane whose pyrolysis at 1100°C under nitrogen atmosphere provides Pd<sub>2</sub>Si@SiCN. Powder X-ray diffraction (PXRD) studies confirmed the presence of the hexagonal Pd<sub>2</sub>Si phase in the amorphous SiCN matrix. The size of the particles formed depends upon the nature of the solvent used in cross-linking step. The amount of palladium complex added seems not to affect the size of particles formed but does increase their population density. Pd<sub>2</sub>Si@SiCN catalysts were found active for the hydrogenation of ketones. The selectivity of the reaction towards alcoholic product remains very high. The conversion of the reaction however, decreases both with increase in alkyl chain length as well as its branching at alpha carbon. The recyclable Pd<sub>2</sub>Si@SiCN could be a suitable choice for the catalytic transformations under harsh chemical environment and at higher temperatures.

### 4.1 Introduction

Nanoalloys, owing to their improved structural, electronic and optoelectronic properties as compared to their (metallic) counterparts, find intensive applications in many areas of technological importance.<sup>[1]</sup> For instance, bimetallic alloy nanoparticles have been applied in light emitting diodes (LED)<sup>[2,3]</sup> data storage devices<sup>[4,5]</sup> and thermoelectric devices.<sup>[6]</sup> A salient feature of nanoalloy particles is the superior catalytic performance and their applications, in this regard, range from electrochemical fuel cell reactions,<sup>[7-12]</sup> to various oxidation reactions,<sup>[13-16]</sup> and renewable energy production.<sup>[17,18]</sup>

Polymer derived ceramics (PDC) have been investigated intensively in the past two decades.<sup>[19]</sup> The PDCs based on SiCN ternary system are highly robust materials possessing extraordinary high temperature properties<sup>[20,21]</sup> and oxidation resistance up to 1600°C<sup>[22]</sup> without showing any prominent mechanical creep.<sup>[23]</sup> On the account of their polymer route synthesis, fabrication of fibers,<sup>[24]</sup> films<sup>[25]</sup> and coatings<sup>[26]</sup> is facilitated. Introduction of metal not only improves the electrical<sup>[27]</sup> thermal and magnetic properties<sup>[28]</sup> of these materials but also extends their application profile to catalysis, where such robust systems have successfully been used as catalysts for fuel reforming,<sup>[29]</sup> total oxidation of methane<sup>[30]</sup> and the decomposition of ammonia.<sup>[31]</sup> In addition, metal containing SiCN ceramics have been reported to be selective catalysts in the oxidation of alkanes using air as an oxidant.<sup>[32]</sup> The synthetic strategies for metal containing polymer derived ceramics can broadly be divided into three categories. Firstly, the chemical modification of organosilicon polymers by the use of metal powders<sup>[33]</sup> or by metal oxides;<sup>[34]</sup> secondly, modification at a molecular level by the use of metal complexes<sup>[35,36]</sup> followed by its pyrolysis to obtain metal containing ceramics. The third approach makes the use of metal containing organosilicon polymers<sup>[37-40]</sup> and their subsequent ceramization. We recently reported a molecular approach utilizing aminopyridinato transition metal complexes for the chemical modification of polyorganosilazane<sup>[41,32]</sup> (HTT 1800) whose pyrolysis provided metal particles containing SiCN ceramics. This synthetic protocol is advantageous in the sense that it avoids entry of any foreign element as the aminopyridinato complexes contain the same elements as contained by the polysilazane. Such complexes can be synthesized in good yields and are available for almost all the transition elements.<sup>[42]</sup> Moreover, the dispersion of metal within the

ceramic is assured owing to the covalent linkages of metal with the nitrogen functionalities of the polysilazane. This molecular approach for the synthesis of metal containing SiCN ceramics is (here) extended to the synthesis of so called intermetallic nanoparticles (nanoalloys). The aminopyridinato complex of palladium used here generates palladium silicide nanoparticles by the chemical modification of the polysilazane. Moreover, it cross-links the polymer efficiently at room temperature increasing the ceramic yield by the retention of carbon and nitrogen atoms within the ceramic. Conventional synthesis of palladium silicides involves the annealing of palladium on silicon substrates which, depending upon the stoichiometric ratio and annealing temperature generates different silicide phases (Pd<sub>x</sub>Si<sub>y</sub>).<sup>[43]</sup> Although the growth and structure of palladium silicide has been studied extensively in past, there are only a few reports on the nanosizing of palladium silicides.<sup>[44]</sup> Here we report on the synthesis of palladium silicide nanoparticles and their size control within a SiCN support and their catalytic applications.

## 4.2 Experimental

### 4.2.1 General remarks

All reactions were carried out under dry argon using standard Schlenk and glove box techniques. Solvents were dried and distilled from sodium benzophenone before use. Deuterated solvents obtained from Cambridge Isotope Laboratories were degassed, dried using molecular sieves and distilled prior to use. *n*-butyllithium, 2-amino-4-picoline, chlorotrimethylsilane, acetophenone, 1-phenyl-1-ethanol (ACROS Chemicals), dichloropalladium(II) (Alfa Aesar) and polysilazane (HTT 1800, Clariant, GmbH) were used as received without any further purification.

### 4.2.2 Ligand and complex synthesis

The starting material 4-methyl-2-((trimethylsilyl)amino)pyridine **1**,<sup>[45]</sup> dichloro(1,5-cyclooctadiene)palladium(II)<sup>[46]</sup> and complex **2**<sup>[47]</sup> were synthesized following reported methods (Fig. 1).

### 4.2.3 Cross-linking, metal transfer and pyrolysis

Polysilazane HTT 1800 (3.218 g) was reacted with palladium aminopyridinato complex **2** (Pd/Si 1/20, 1.16 g, 2.49 mmol; Pd/Si 1/40, 0.581 g, 1.25 mmol; Pd/Si 1/60

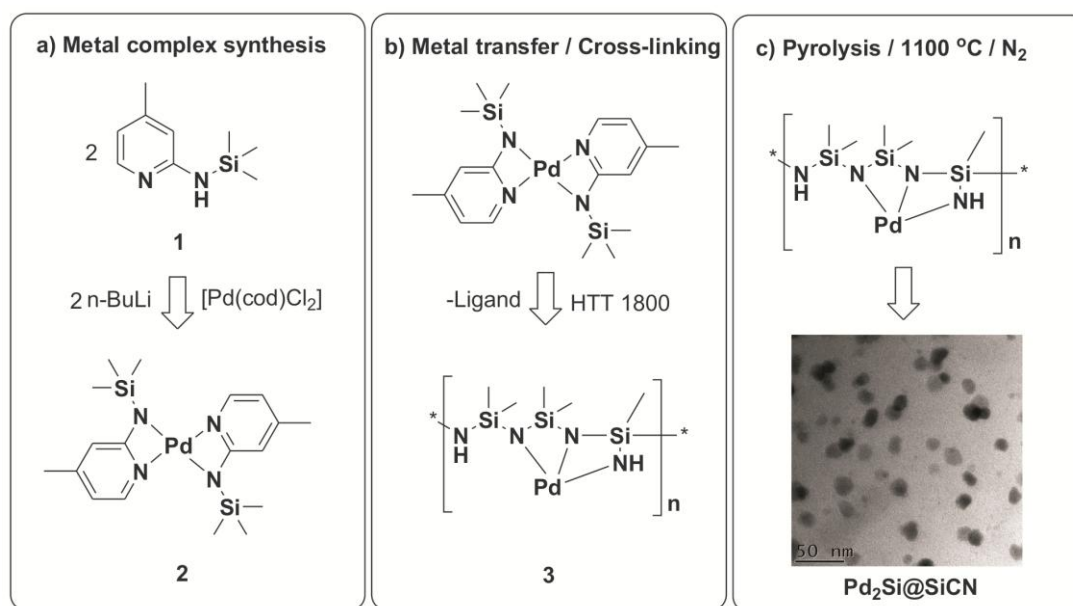


**Figure 1.** Scheme for the synthesis of Pd<sub>2</sub>Si nanoparticles containing SiCN ceramics; a) synthesis of complex **2** from the ligand **1**; b) the polysilazane (HTT 1800) is chemically modified by its reaction with the complex along with the liberation of the ligand; c) metal modified polysilazane **3** produces dipalladium silicide nanoparticles supported SiCN ceramics upon pyrolysis at 1100°C under nitrogen atmosphere. *n*-BuLi: *n*-butyllithium; cod: 1,5-cyclooctadiene; HTT 1800: polyorganosilazane.

0.38 g, 0.83 mmol; Pd/Si 1/80, 0.29 g, 0.62 mmol; Pd/Si 1/100, 0.23 g, 0.5 mmol) in tetrahydrofuran (THF) (5 mL) (Table 1). No cross-linking agent was added as the complex itself acts as a cross-linking agent and changes the orange solution into a black solid. The solvent was evaporated under vacuum and solid obtained was pyrolyzed under nitrogen atmosphere at 1100°C (5 K/min; holding time: 30 min) to get the ceramics.

**Table 1.** Designation of the samples synthesized by using different mounts of palladium complex reacted with HTT 1800, respective palladium to silicon ratio and palladium loading in resulting ceramics.

Sample ID (CL/FC <sup>[a]</sup> )	Pd complex (wt % HTT 1800)	Pd/Si (ratio)	Pd loading <sup>[b]</sup>	
			(calculated)	(actual)
Pd20	36.0	1/20	8.17	6.91
Pd40	18.0	1/40	4.86	3.36
Pd60	12.0	1/60	3.32	2.50
Pd80	9.0	1/80	2.61	1.31
Pd100	7.2	1/100	2.09	0.74
Pd1000	0.2	1/1000	0.22	-

[a] Suffixes CL and FC correspond to the cross-linked and ceramic form respectively. [b] Palladium loading in wt%.

#### 4.2.4 Characterization

Nuclear magnetic resonance (NMR) spectra were recorded using a Varian INNOVA 400 spectrometer. Chemical shifts are reported relative to deuterated solvent. Ceramization was carried out under nitrogen in a high temperature furnace (Nabertherm LH 60/14, Nabertherm, Germany). Gas chromatography (GC) analyses were performed using an Agilent 6890N gas chromatograph equipped with a flame ionization detector (FID) and an Agilent 19091 J-413 FS capillary column using dodecane as internal standard. All X-ray powder diffractograms were recorded by using a STOE STADI-P-diffractometer (CuK<sub>α</sub> radiation, 1.54178 Å) in  $\theta$ -2 $\theta$  -geometry and with a position sensitive detector. Transmission electron microscopy (TEM) was carried out by using a Varian LEO 9220 (200 kV) instrument. The sample was suspended in chloroform and sonicated for 5 min. Subsequently a drop of the suspended sample was placed on a grid (Plano S 166–3) and allowed to dry.

Elemental analysis was performed by standard protocols employing digestion in HNO<sub>3</sub>/HCl/H<sub>2</sub>O<sub>2</sub> and inductively coupled plasma optical emission spectrometry (ICP-OES) using a Varian, Vista-Pro radial. FT-IR-measurements were performed using a Perkin–Elmer FTIR-Spectrum 100 over a range of 4000 to 450 cm<sup>-1</sup>.

#### 4.2.5 Catalytic studies

1 mmol of ketone in toluene (0.4 mL) was taken in a glass tube along with a magnetic bar and 60 mg of milled ceramics (particle size: <100 μm) was added. This tube was placed in a Parr autoclave under a hydrogen pressure of 40 bar. The reactor was heated to the respective temperature within 20 min and stirring (400 rpm) was continued at this temperature for 24 hours. Afterwards, reaction mixture was diluted with THF and dodecane as internal standard was added. The conversion and selectivity were determined by GC.

### 4.3 Results and discussion

#### 4.3.1 Synthesis (palladium complex, metal modified polysilazane and ceramics)

Fig. 1a shows the schematic presentation of the synthesis of the palladium complex (a), chemical modification of Si-H and vinyl-silicon groups containing HTT 1800 (b) and the generation of dipalladium silicide nanoparticles supported by SiCN ceramics

(c). Polysilazane HTT 1800 was reacted with different amounts of palladium complex **2** (Table 1) to get the metal modified and cross-linked thermosets **3** whose pyrolysis at 1100°C provided Pd<sub>2</sub>Si@SiCN.

Complex **2** was reacted with polysilazane HTT 1800 in THF (5 mL). Upon mixing of the complex with polysilazane, an exothermic reaction takes place with effervescence and solution gradually changes its color until it completely converts into a black solid. The shape of the solid can be controlled by the amount of solvent added. With a relatively small amount of solvent more volume expansion and foaming were observed which could be avoided by the addition of more solvent. GC analysis of the gaseous products of the cross-linking reaction shows predominance of hydrogen.

The Seyferth group had reported on the dehydrocoupling between Si-H bonds by the reaction of Ru<sub>3</sub>(CO)<sub>12</sub> with alkylsilyl hydrides.<sup>[48]</sup> On the basis of hydrogen evolved during cross-linking we assume the same kind of dehydrocoupling between Si-H functions (besides cross-linking *via* hydrosilylation and vinyl polymerization).<sup>[49]</sup> FT-IR studies of the reaction of HTT 1800 with the palladium complex (Fig. 3) show the decrease in the intensities of the vibrations characteristic of vinylic (2998-3084 cm<sup>-1</sup>), Si-H (2150 cm<sup>-1</sup>) and N-H (3300-3500 cm<sup>-1</sup>) bonds. This supports the hydrosilylation and dehydrocoupling cross-linking mechanisms to be operative and the formation of palladium amides. Improved yields of the ceramics also support the dehydrocoupling mechanism as it will result in the retention of carbon and nitrogen atoms within the ceramics. The use of free radical initiators for the initiation of cross-linking could be avoided by the use of the palladium aminopyridinato complex.

Kinetic studies of metal transfer reaction (cross-linking) were performed using <sup>1</sup>H NMR. HTT 1800 was reacted with complex **2** in deuterated benzene (C<sub>6</sub>D<sub>6</sub>) and spectra were recorded after every 2 min (Fig. 2a). The characteristic signals of the complex gradually decrease in intensities until they are totally absent after 20 minutes of reaction time. At this time, the spectrum of the reaction mixture shows only the characteristic resonance signals of the ligand (Fig. 2a and b). Moreover resonance of the -NH- function, originally absent in the spectrum of the complex again appears at 3.89 ppm confirming the evolution of free protonated ligand in the reaction mixture. This liberation of ligand provides an indirect evidence of the transfer of palladium to the nitrogen functions of polysilazane most probably due to the availability of more coordination sites in the polymer. Based upon aforementioned

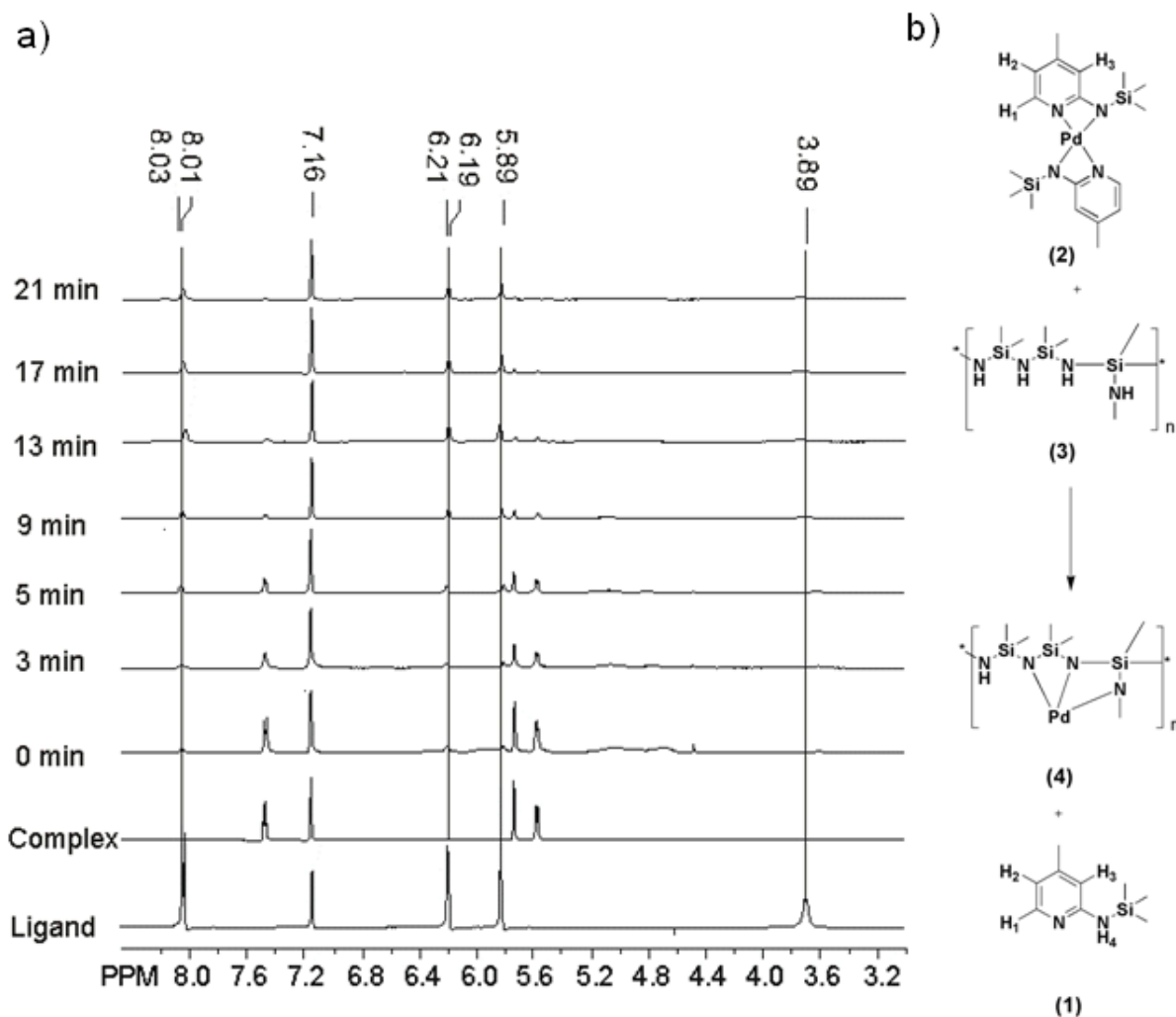


**Figure 2.** a) <sup>1</sup>H NMR spectra of the reaction mixture (HTT 1800 and complex **2** in benzene) at different time intervals; b) schematic representation of metal transfer reaction which produces metal modified polysilazane (**4**) by the reaction of palladium aminopyridinato complex **2** with HTT 1800 **3**. The palladium is transferred to the nitrogen functions of the polymer with the liberation of protonated ligand **1**.

observations, it may be concluded that the palladium complex chemically modifies the polysilazane by coordination of palladium to its nitrogen atoms. The solvent free, metal modified and cross-linked polysilazane was then shifted to a furnace for pyrolysis.

#### 4.3.2 Pyrolysis and ceramization

The metal modified cross-linked polymers were heated under nitrogen atmosphere in a furnace with a heating rate of 5 K/min upto 1100°C to get an amorphous metal containing SiCN ceramics.

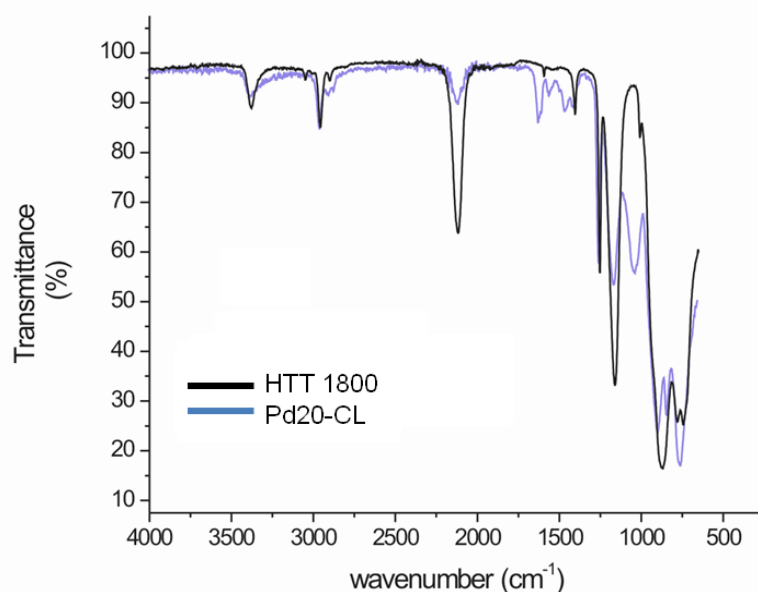


**Figure 3.** FT-IR spectrum of HTT 1800 before and after the addition of complex. The decrease in the intensities of Si-H and CH<sub>2</sub>=CH- vibrational was observed upon the addition of the palladium complex.

### 4.3.3 Characterization of Pd<sub>2</sub>Si@SiCN

#### 4.3.3.1 Thermogravimetric analysis (TGA)

TGA analysis of the cross-linked precursors was carried out with a heating rate of 5 K / min upto 1100°C under nitrogen atmosphere (Fig. 4). Major mass loss (21-26%) occurs between 100-730°C and may be attributed to the loss of gases (methane, ammonia and hydrogen).<sup>[50]</sup> Above 730°C, the observed mass loss was only 1.2-1.5 % giving ceramic yields of 78% (Pd100-FC, curve b) and 73% (Pd20-FC, curve a). Theoretically speaking, a total yield of 65% was expected in the case of Pd20-FC assuming the total loss of ligand and complete retention of palladium during ceramization. An increase in yield by 8% suggests that ligand is not totally lost during ceramization and contributes towards ceramic yield. This may be attributed to the retention of silicon and palladium atoms contained by the ligand during pyrolysis. Moreover, the evolution of hydrogen during cross-linking reaction suppresses the emission of methane and ammonia (at 300-500°C) gases resulting in the retention of carbon and nitrogen atoms. The loss of oligomers in the temperature regime of 100-300°C is avoided owing to the efficient cross-linking of polysilazane by the palladium complex. It is evident from TGA data (Fig. 4) that as expected, ceramic yield decreases with the increase in the amount of the complex.

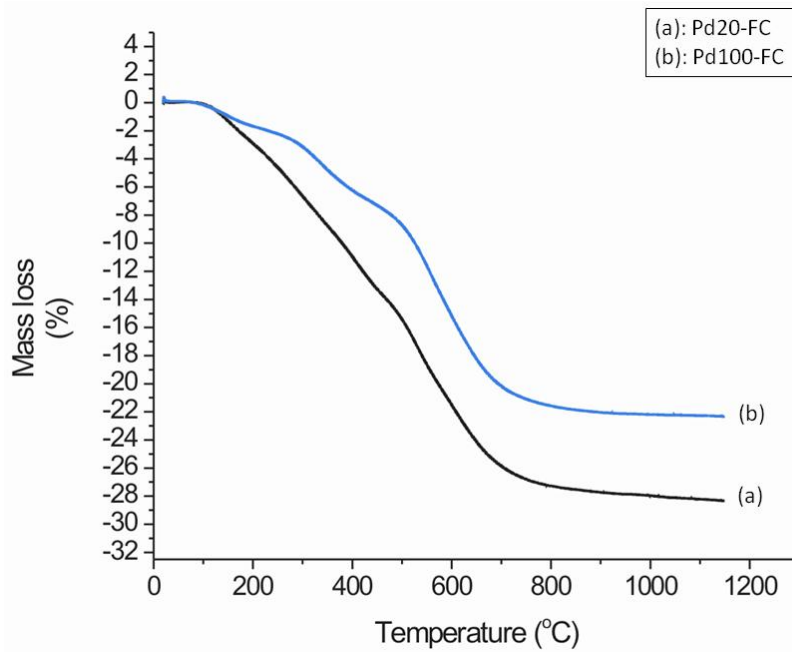


**Figure 4.** TGA analysis of Pd20-FC (8 wt% Pd) in comparison with Pd100-FC (2 wt% Pd); major mass loss occurs between 100-730°C giving ceramic yields of 78% for Pd100-FC (b) and 73% for Pd20-FC (a).

#### 4.3.3.2 Powder X-ray diffraction (Powder XRD)

Powder XRD of palladium containing SiCN ceramics was carried out to confirm the amorphous nature of the matrix as well as the presence of the metallic phase. The reflection pattern of cubic phase of palladium was totally absent in the diffractograms and reflections characteristic of hexagonal phase of Pd<sub>2</sub>Si were observed. Powder XRD data of dipalladium silicide (Pd<sub>2</sub>Si) were assimilated from the single crystal XRD data<sup>[51]</sup> and were used as reference for the interpretation of Powder XRD results (Fig. 5). The peaks at 2θ value of 38.1°, 41.4°, 42.4°, 48.5° in Pd20-FC (8 wt% Pd) can be assigned to the reflections of (201), (210), (300) and (110) planes of hexagonal Pd<sub>2</sub>Si. With the decrease in the amount of metal within the support, only the most intense peaks at 38.1°, 41.4° and 42.4° can be seen in the diffractograms of all the Pd<sub>2</sub>Si@SiCN composites synthesized. Reflection patterns corresponding to other silicide phases (PdSi and Pd<sub>3</sub>Si), as evident from the phase diagram of Pd-Si system,<sup>[52]</sup> are not found in powder XRD. Reflections at 20.8°, 26.8° and 36.5° may be assigned to quartz. The formation of quartz may arise because of the exposure of thermosets to air during their transfer to furnace for pyrolysis. Palladium rich β-Pd<sub>2</sub>Si is stable in the temperature regime of 1090-1404°C above which it melts congruently and below 1090°C, it transforms to its silicon rich polymorph (α-Pd<sub>2</sub>Si). The formation

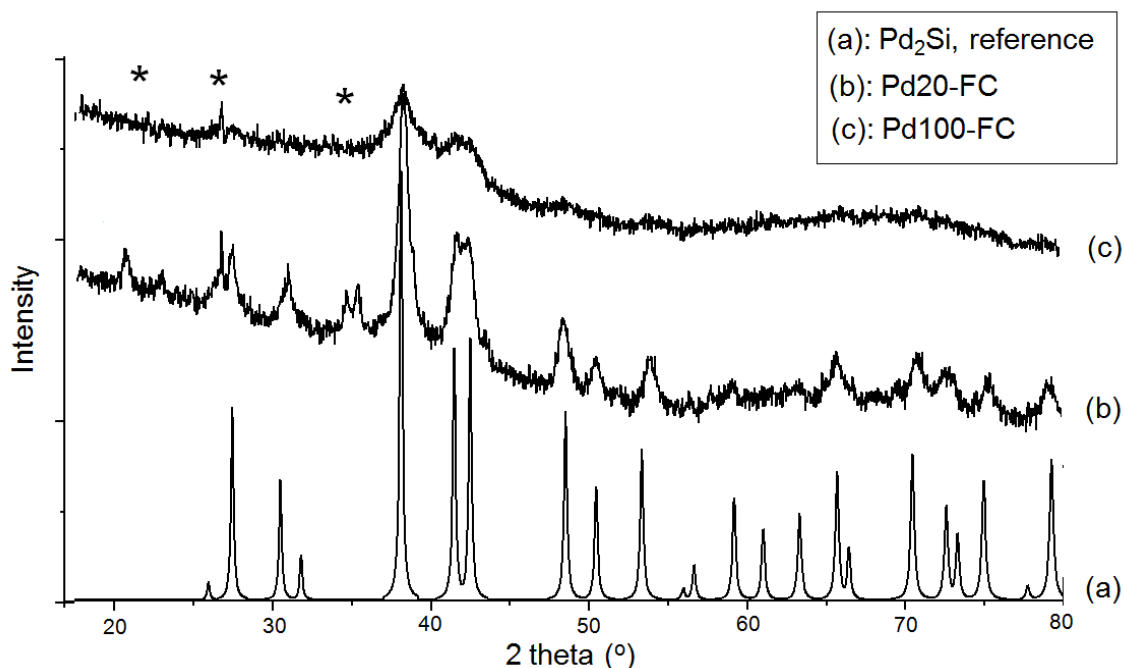


**Figure 5.** PXRD of ceramics (pyrolyzed at 1100°C under nitrogen atmosphere) in comparison with the assimilated PXRD pattern of hexagonal Pd<sub>2</sub>Si, the most intense peaks at 38.1°, 41.4° and 42.4° correspond to (201), (210) and (300) planes. \* Reflections at 20.8°, 26.8° and 36.5° may be assigned to quartz.

of hexagonal Pd<sub>2</sub>Si phase could be the result of the interaction of amorphous SiCN with palladium at pyrolysis temperature of 1100°C. In our previous report,<sup>[32]</sup> formation of metallic phase instead of metal silicide phases was confirmed by powder XRD and solid state copper NMR studies. In fact, formation of copper silicide requires much higher amount of loaded copper (>80 wt%) within the system<sup>[53]</sup> which is very unlikely at a maximal copper loading of 13.7% in Cu@SiCN system.<sup>[32]</sup>

#### 4.3.3.3 TEM Investigations

TEM micrographs of the samples provide further insight to the microstructure of the supported palladium silicide nanoparticles (Fig. 6 and 7). The size of the particles generated on the ceramic support depends on the cross-linking step. The two samples pyrolyzed under same conditions but using different solvents (in cross-linking step) generate particles with different sizes. On the other hand, samples with different loadings of palladium but cross-linked under identical conditions give the same size of the nanoparticles (Fig. 6b and d). Thus, size can be controlled in terms of the nature of the solvent used for the mixing the of palladium complex with polysilazane. Since the palladium complex is highly soluble in THF, only a small

amount of the solvent (5 mL) was enough for its complete dissolution. A much faster exothermic reaction takes place upon the addition of palladium complex solution to the polymer resulting in an immediate cross-linking along with the chemical modification of polysilazane. The metal modified polymer upon its pyrolysis generates palladium silicide particles with an average size of 18 nm (Fig. 6d) with a uniform distribution over the surface (Fig. 6c). In the case where hexane was used as solvent, palladium complex requires relatively large amount of solvent (15 mL as compared to 5 mL of THF in the first approach) for its dissolution. The nanoalloy particles generated in this case are 5-6 nm in size (Fig. 7c) and are homogeneously distributed over the support with the population density comparable to those synthesized using THF as solvent (Fig. 7a-d). When the amount of THF was incre-

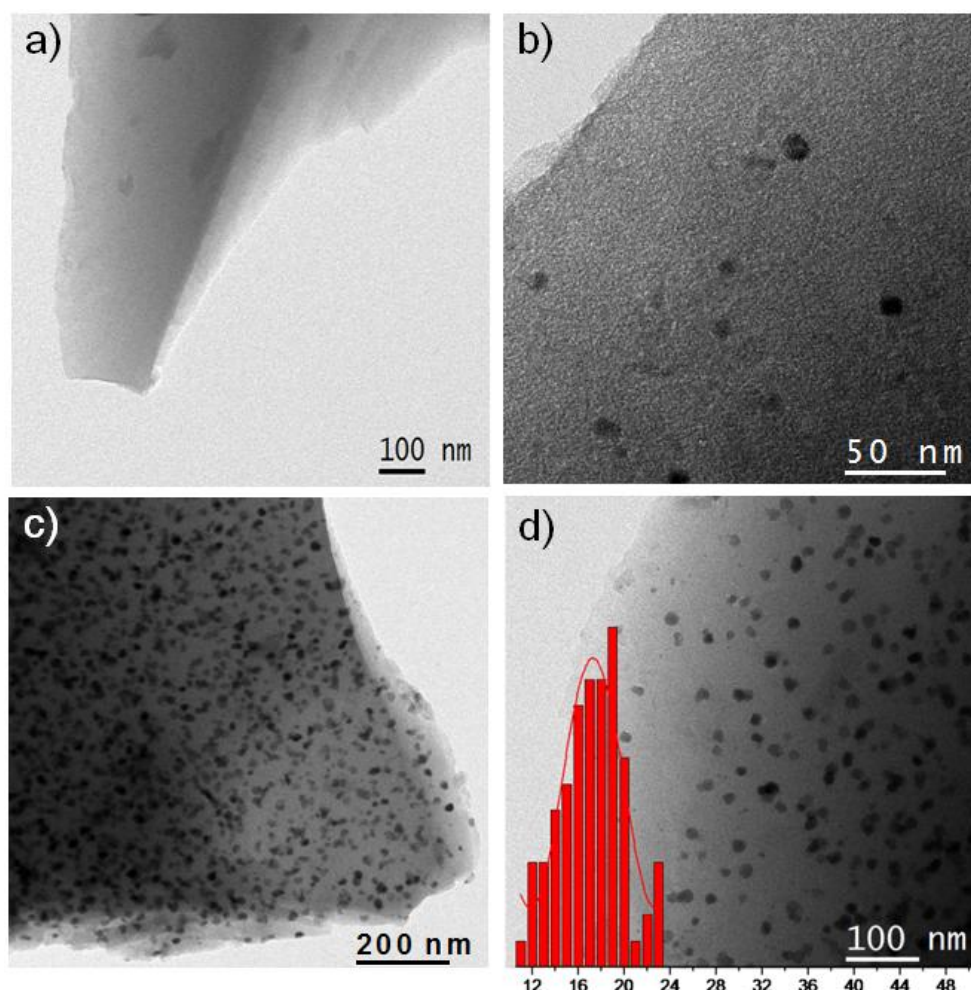


**Figure 6.** TEM micrographs of ceramic materials. a) SiCN ceramic without palladium loading does not show any particles on the surface; b) lower loading of palladium (0.2 wt%, Pd1000-FC) decreases the density of particles on the surface keeping their size in the same regime; c) Pd<sub>2</sub>Si particles uniformly distributed over the surface of Pd<sub>20</sub>-FC (8 wt% Pd); d) dipalladium silicide nanoparticles on the surface of Pd<sub>20</sub>-FC with particles size distribution.

-ased to 15 mL, the cross-linking took place with a much slower rate but the particles generated were within the same size regime (~18 nm). Thus it is the nature of the solvent and not the extent of dilution which controls the size of the particles formed. It is evident from the Fig. 6a that without the addition of palladium complex to The population density of the particles formed depends upon the amount of metal complex reacted with the polymer (Fig. 6b) keeping their size the same (16-18 nm).

#### 4.3.4 Catalytic studies

In the case of palladium based nanoalloys, both unsupported<sup>[54]</sup> and supported Pd-Ga<sup>[55,56]</sup> have recently been reported as efficient selective catalysts for semihydrogenation of alkynes. The alloys of palladium with silicon are worthment-

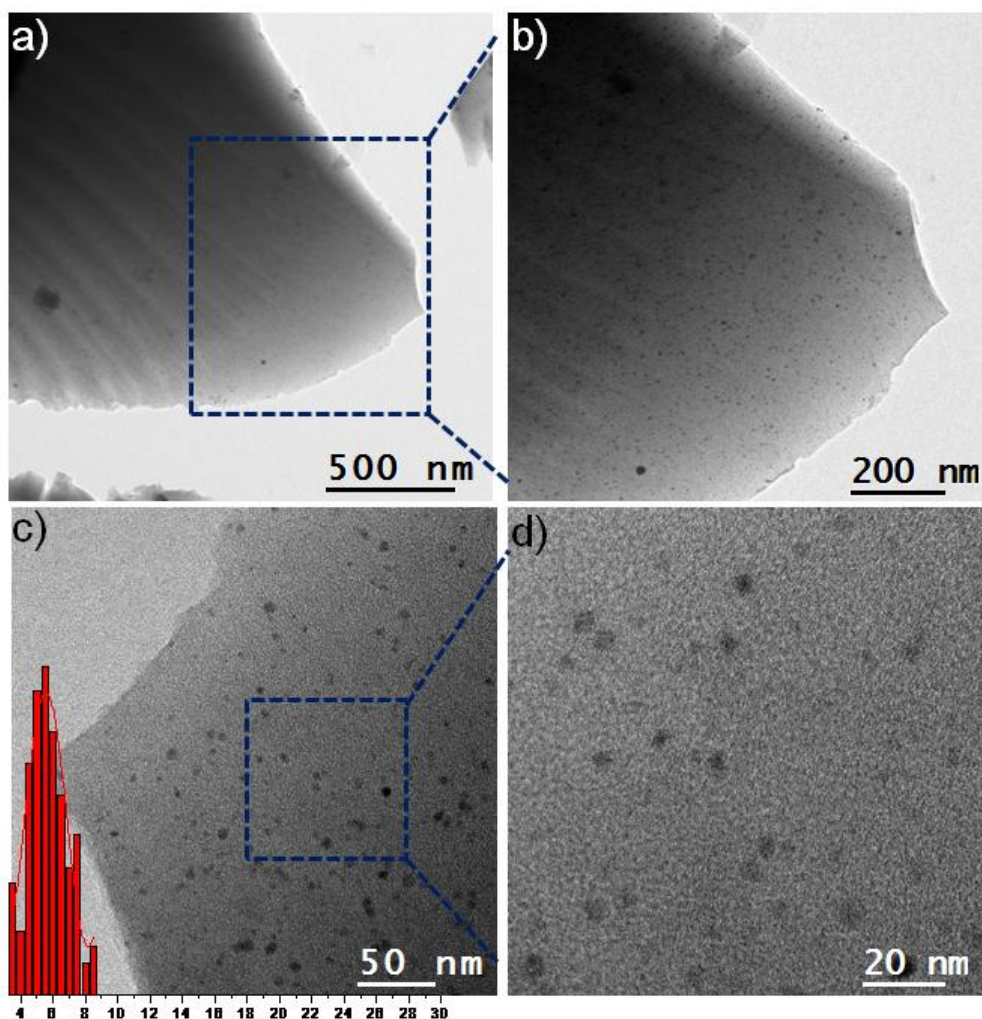


**Figure 7.** a-d) TEM micrographs of Pd<sub>20</sub>-FC synthesized in hexane (15 mL); a uniform distribution of palladium silicide particles over the ceramic has been shown at different magnification in figures (a) and (b) while figure (c) shows palladium silicide particles (~4-6 nm) with size distribution.

-tioning here in this regard as these materials show excellent catalytic activities for many reactions of industrial importance.<sup>[57-59]</sup> According to Bartok and coworkers<sup>[60]</sup> semihydrogenation of alkynes over Pd-Si alloy provides better selectivity in comparison to the Pd-Ge and pure palladium catalysts. Baiker *et al.* found high conversion and selectivity for Pd<sub>81</sub>Si<sub>19</sub> alloy in semihydrogenation of propargylic alcohol and phenylacetylene in supercritical carbon dioxide.<sup>[61,62]</sup> Palladium silicide phases generated as a result of metal support interactions in Pd/SiO<sub>2</sub> system have been reported to be selective catalysts in semihydrogenation of phenylacetylene to styrene<sup>[63]</sup> and for neopentane isomerization.<sup>[64-66]</sup> The group of Massardier reported on the catalytic activity of palladium silicides containing Pd/SiC catalysts for methane total oxidation.<sup>[67]</sup> A promising feature of palladium silicides is their chemical and electrochemical stability<sup>[68]</sup> which makes them ideal candidates as anode materials for fuel cells applications.<sup>[69,70]</sup>

#### 4.3.4.1 Catalytic hydrogenation of ketones

Catalytic hydrogenation of aromatic ketones to various products (Fig. 8a) was investigated using Pd<sub>2</sub>Si@SiCN catalyst system. All the catalysts with a palladium loading ranging from 2-8 wt% (Pd100-FC to Pd20-FC) show selective hydrogenation of ketones to alcoholic products. Pd20-FC (8 wt% Pd) shows higher performance (Fig. 8b) than other ceramics (Pd40-FC, Pd60-FC, Pd80-FC and Pd100-FC) and was selected for further studies. The conversion increases both with the increase in catalyst amount and temperature (Fig. 8c) but selectivity remains the same. Alkyl phenyl ketones with alkyl length ranging from 1-7 carbon atoms (acetophenone to heptanophenone) and those having branching at alpha carbon (2-methyl-1-propiophenone and 2,2-dimethyl-1-propiophenone) were applied in the investigations. Catalytic studies were performed both at 85 and 50°C under 40 bar hydrogen pressure for 24 hours. It was found that at 85°C both the conversion and the selectivity to alcohol were above 95%. At 50°C, however, the conversion decreases both with the increase in alkyl chain length and its branching at alpha carbon. The selectivity again remains above 99% to alcoholic product (Table 2). The catalyst does not show any deactivation after a reaction time of 75 hours. Recycling of the catalyst was studied at 50% conversion by adjusting the amount of catalyst added. After 24 hours, the reaction was stopped and catalyst was separated by cent-

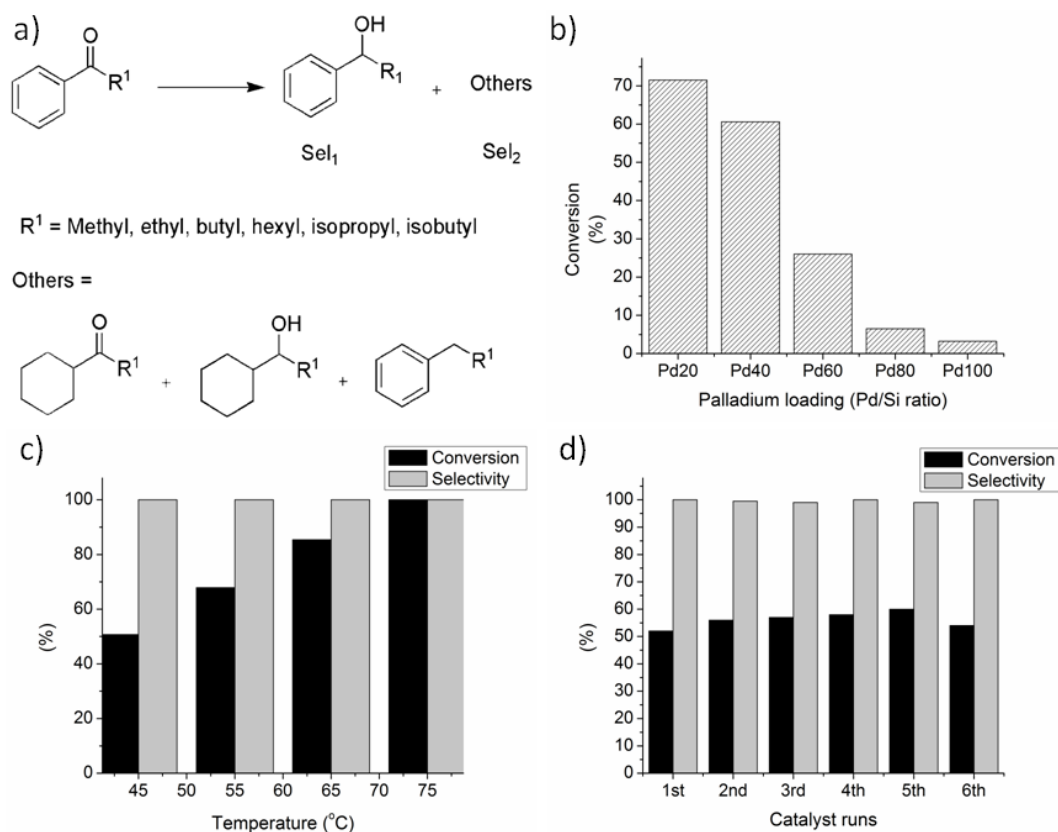


**Figure 8.** a) Schematic representation of catalytic hydrogenation of ketones to different products; b) hydrogenation of acetophenone (2 mmol) with 60 mg of catalyst at 75°C under 20 bar hydrogen for 24 hours. The conversion decreases with decrease in the amount of palladium contained by the ceramics; c) Hydrogenation of acetophenone (2 mmol) using Pd20-FC (120 mg) under 20 bar hydrogen pressure for 24 hours. The conversion increases with temperature keeping the selectivity constant; d) hydrogenation of acetophenone (2 mmol) with the catalyst Pd20-FC (60 mg) under 20 bar hydrogen pressure for 24 h. The figure shows reusability of the catalyst up to six catalyst runs.

-rifugation and dried under vacuum at 120°C for 6 hours. A slight increase in conversion was observed after first run and no loss of activity was observed over six consecutive catalyst runs (Fig. 8d).

#### 4.4 Conclusions

Pd<sub>2</sub>Si nanoparticles supported by a polymer derived SiCN matrix have been synthesized following a molecular approach making the use of an aminopyridinato palladium complex. The complex cross-links the polysilazane *via* hydrogen evolution increasing the ceramic yield. Moreover it chemically modifies the precursor by the transfer of palladium to its amido nitrogen atoms. The metal modified polymer, upon its pyrolysis at 1100°C provides dipalladium silicide nanoparticles. The size of the

**Table 2.** Hydrogenation of the ketones using the catalyst Pd20-FC (8 wt% Pd) at 85 and 50°C; 1 mmol of substrate, 0.4 mL toluene and 60 mg of the catalyst were used under 40 bar hydrogen pressure.

Substrate	85°C		50°C	
	Conversion <sup>[a]</sup>	Sel <sub>1</sub> /Sel <sub>2</sub> <sup>[b]</sup>	Conversion	Sel <sub>1</sub> /Sel <sub>2</sub>
Acetophenone	100	99/1	46	99/1
Propiophenone	100	99/1	48	99/1
Valerophenone	100	99/1	42	99/1
Heptanophenone	98	99/1	33	99/1
2-Methyl-1-propiofenone	100	99/1	11	99/1
2,2-Dimethyl-1-propiofenone	93	99/1	4	99/1

[a] Conversion in mol% units. [b] Sel<sub>1</sub> and Sel<sub>2</sub> denote selectivity to alcoholic and other products respectively.

particles formed depends upon the solvent used and is independent of the amount of loaded metal. Higher metal loading, results in a higher density of particles. Catalysts show selective formation of alcohols from the hydrogenation of ketones. Overall conversion of the reaction increases with catalyst amount and temperature keeping the selectivity constant. A decrease in activity was observed with an increase in alkyl chain length and branching at alpha carbon of the ketone.

### Acknowledgements

The authors are grateful to Justus Hermannsdörfer for TEM analysis, Kathrin Inzenhofer for TGA studies and Dr. Wolfgang Milius for powder XRD measurements. Financial support from Deutsche Forschungsgemeinschaft (DFG, SPP 1181) is gratefully acknowledged. M. Zaheer is thankful to Higher Education Commission of Pakistan (HEC) and Deutscher Akademischer Austausch Dienst (DAAD) for the fellowship.

### 4.5 References

- [1] R. Ferrando, J. Jellinek, R. L. Johnston, *Chem. Rev.* **2008**, *108*, 845-910.
- [2] Q. J. Sun, Y. A. Wang, L. S. Li, D. Wang, T. Zhu, J. Xu, C. Yang, Y. Li, *Nat. Photon.* **2007**, *1*, 717-722.

- [3] S. Coe, W. -K. Woo, M. Bawendi, V. Bulovic, *Nature* **2002**, *420*, 800-803.
- [4] M. Wuttig, N. Yamada, *Nat. Mater.* **2007**, *6*, 824-832.
- [5] D. Alloyeau, C. Ricolleau, C. Mottet, T. Oikawa, C. Langlois, Y. L. Bouar, N. Braidy, A. Loiseau, *Nat. Mater.* **2009**, *8*, 940-946.
- [6] T. C. Harman, P. J. Taylor, M. P. Walsh, B. E. LaForge, *Science* **2002**, *297*, 2229-2232.
- [7] B. Lim, M. Jiang, P. H. C. Camargo, E. C. Cho, J. Tao, X. Lu, Y. Zhu, Y. Xia, *Science* **2009**, *324*, 1302-1305.
- [8] A. Kowal, M. Li, M. Shao, K. Sasaki, M. B. Vulkmirovik, J. Zhang, N. S. Marinkovic, P. Liu, A. I. Frenkel, R. R. Adzic, *Nat. Mater.* **2009**, *8*, 325-330.
- [9] V. R. Stamenkovic, B. S. Mun, M. Arenz, K. J. J. Mayrhofer, C. A. Lucas, G. Wang, P. N. Ross, N. M. Markovic, *Nat. Mater.* **2007**, *6*, 241-247.
- [10] F. Maroun, F. Ozanam, O. M. Magnussen, R. J. Behm, *Science* **2001**, *293*, 1811-1814.
- [11] J. Greeley, I. E. L. Stephens, A. S. Bondarenko, T. P. Johansson, H. A. Hansen, T. F. Jaramillo, J. Rossmeisl, I. Chorkendorff, J. K. Nørskov, *Nat. Chem.* **2009**, *1*, 552-556.
- [12] X. Ji, K. T. Lee, R. Holden, L. Zhang, J. Zhang, G. A. Botton, M. Couillard, L. F. Nazar, *Nat. Chem.* **2010**, *2*, 286-293.
- [13] L. Kesavan, R. Tiruvalam, M. H. Ab Rahim, M. I. bin Saiman, D. I. Enache, R. L. Jenkins, N. Dimitratos, J. A. Lopez-Sanchez, S. H. Taylor, D. W. Knight, C. J. Kiely, G. J. Hutchings, *Science* **2011**, *331*, 195-199.
- [14] D. I. Enache, J. K. Edwards, P. Landon, B. S. -Espriu, A. F. Carley, A. A. Herzing, M. Watanabe, C. J. Kiely, D. W. Knight, G. J. Hutchings, *Science* **2006**, *311*, 362-365.
- [15] S. Alayoglu, A. U. Nielkar, M. Mavrikakis, B. Eichhorn, *Nat. Mater.* **2008**, *7*, 333-338.
- [16] M. Schrunner, S. Proch, Y. Mei, R. Kempe, N. Miyajima, M. Ballauff, *Adv. Mater.* **2008**, *20*, 1928-1933.
- [17] F. Besenbacher, I. Chorkendorff, B. S. Clausen, B. Hammer, A. M. Molenbroek, J. K. Nørskov, I. Stensgaard, *Science* **1998**, *279*, 1913-1915.
- [18] G. W. Huber, J. W. Shabaker, J. A. Dumesic, *Science*, **2003**, *300*, 2075-2077.

- [19] P. Colombo, R. Riedel, G. D. Soraru, H. -J. Kleebe in *Polymer Derived Ceramics: From Nanostructure to Applications*, DEstech Publications, Inc. Pennsylvania, USA, **2010**.
- [20] H.-J. Kleebe, H. Störmer, S. Trassl, G. Ziegler, *Appl. Organomet. Chem.* **2001**, *15*, 858-866.
- [21] R. Riedel, H.-J. Kleebe, H. Schönfelder, F. Aldinger, *Nature* **1995**, *374*, 526-528.
- [22] W. Weibelzahl, G. Motz, D. Suttor, G. Ziegler, *Key Eng. Mat.* **1999**, *161-163*, 111-114.
- [23] G. Thurn, J. Canel, J. Bill, F. Aldinger, *J. Eur. Ceram. Soc.* **1999**, *19*, 2317-2323.
- [24] G. Motz, *Adv. Sci. Technol.* **2006**, *50*, 24-30.
- [25] A. Izumi, K. Oda, *Thin Solid Films* **2006**, *501*, 195-197.
- [26] H. Hoche, D. Allebrandt, R. Riedel, C. Fasel, *Plasma Processes Polym.* **2009**, *6*, S649-S654.
- [27] H.-Y. Ryu, R. Raj, *J. Am. Ceram. Soc.* **2007**, *90*, 295-297.
- [28] S. I. Andronenko, A. Leo, I. Stiharu, S. K. Misra, *Appl. Magn. Reson.* **2010**, *39*, 347-356.
- [29] I. K. Sung, Christian, M. Mitchell, D. Kim, P. Kenis, *Adv. Funct. Mater.* **2005**, *15*, 1336-1342.
- [30] M. Kamperman, A. Burns, R. Weissgraeber, N. V. Vegten, S. C. Warren, S. M. Gruner, A. Baiker, U. Wiesner, *Nano Lett.* **2009**, *9*, 2756-2762.
- [31] Christian, M. Mitchell, D. -P. Kim, P. J. A. Kennsi, *J. Catal.* **2006**, *241*, 235-242.
- [32] G. Glatz, T. Schmalz, T. Kraus, F. Haarmann, G. Motz, R. Kempe, *Chem. Eur. J.* **2010**, *16*, 4231-4238.
- [33] X. Yan, X. Cheng, C. Li, R. Hauser, R. Riedel, *Material Sci. Forum* **2007**, *546-549*, 2269-2272.
- [34] A. Saha, S. R. Shah, R. Raj, *J. Mater. Sci.* **2003**, *18*, 2549-2551.
- [35] R. Hauser, A. Francis, R. Theismann, R. Riedel, *J. Mater. Sci.* **2008**, *43*, 2042-2049.
- [36] D. Seyferth, H. Lang, C. A. Sobon, J. Borm, H. J. Tracy, N. Bryson, *J. Inorg. Organomet. Polym.* **1992**, *2*, 59-77.

- [37] M. J. MacLachlan, M. Ginzburg, N. Coombs, T. W. Coyle, N. P. Raju, J. E. Greedan, G. A. Ozin, I. Manners, *Science* **2000**, *287*, 1460-1463.
- [38] M. Ginzburg, M. J. MacLachlan, S. M. Yang, N. Coombs, T. W. Coyle, N. P. Raju, J. E. Greedan, R. H. Herber, G. A. Ozin, I. Manners, *J. Am. Chem. Soc.* **2002**, *124*, 2625-2639.
- [39] B. -Z. Tang, R. Peterson, D. A. Foucher, A. Lough, N. Coombs, R. Sodhi, I. Manners, *J. Chem. Soc. Chem. Commun.* **1993**, 523-525.
- [40] R. Peterson, D. A. Foucher, B. Tang, A. Lough, N. P. Raju, J. E. Greedan, I. Manners, *Chem. Mater.* **1995**, *7*, 2045-2053.
- [41] T. Schmalz, T. Kraus, M. Guenther, C. Liebscher, U. Glatzel, R. Kempe, G. Motz, *Carbon* **2011**, *49*, 3065-3072.
- [42] a) R. Kempe, *Eur. J. Inorg. Chem.* **2003**, 791-803; b) G. Glatz, S. Demeshko, G. Motz, R. Kempe, *Eur. J. Inorg. Chem.* **2009**, 1385-1392; c) S. Deeken, G. Motz, R. Kempe, *Z. Anorg. Allg. Chem.* **2007**, *633*, 320-325; d) A. Spannenberg, A. Tillack, P. Arndt, R. Kirmse, R. Kempe, *Polyhedron* **1998**, *17*, 845-850; e) S. Deeken, S. Proch, E. Casini, H. F. Braun, C. Mechtler, C. Marschner, G. Motz, R. Kempe, *Inorg. Chem.* **2006**, *45*, 1871-1879; f) G. Glatz, G. Motz, R. Kempe, *Z. Anorg. Allg. Chem.* **2008**, *634*, 2897-2902.
- [43] H. Okamoto, *J. Phase Equilib. Diff.* **2007**, *28*, 231-232.
- [44] R. K. Joshi, M. Yoshimura, K. Tanaka, K. Ueda, A. Kumar, N. Ramgir, *J. Phys. Chem. C*, **2008**, *112*, 13901-13904.
- [45] R. Kempe, P. Arndt, *Inorg. Chem.* **1996**, *35*, 2644-2649.
- [46] J. Wiedermann, K. Mereiter, K. Kirchner, *J. Mol. Catal. A. Chem.* **2006**, *257*, 67-72.
- [47] A. Spannenberg, P. Arndt, R. Kempe, *Angew. Chem. Int. Ed.* **1998**, *37*, 832-835.
- [48] D. Seyferth, H. Lang, C. A. Sobon, J. Borm, H. J. Tracy, N. Bryson, *J. Inorg. Organomet. Polym.* **1992**, *2*, 59-77.
- [49] N. S. Choong Kwet Yive, R. J. P. Corriu, D. Leclercq, P. H. Mutin, A. Vioux, *Chem. Mater.* **1992**, *4*, 141-146.
- [50] A. Francis, E. Ionescu, C. Fasel, R. Riedel, *Inorg. Chem.* **2009**, *48*, 10078-10083.
- [51] A. Nylund, *Acta Chem. Scan.* **1966**, *20*, 2381-2386.

- [52] C. Boxi, T. B. Massalski, *J. Phase Equil.* **1991**, *12*, 349-356.
- [53] R. W. Olensinski, G. J. Abbaschian, *Bull. Alloy Phase Diagrams*, **1986**, *7*, 170-178.
- [54] M. Armbrüster, G. Wowsnick, M. Friedrich, M. Heggen, R. C. –Gil, *J. Am. Chem. Soc.* **2011**, *133*, 9112-9118.
- [55] A. Ota, M. Arbrüster, M. Behrens, D. Rosenthal, M. Friedrich, I. Kasatkin, F. Girgsdies, W. Zhang, R. Wagner, R. Schlögl, *J. Phys. Chem. C.* **2011**, *115*, 1368-1374.
- [56] L. Shao, W. Zhang, M. Armbrüster, D. Teschner, F. Girgsdies, B. Zhang, O. Timpe, M. Friedrich, R. Schlögl, D. S. Su, *Angew. Chem. Int. Ed.* **2011**, *50*, 1-6.
- [57] A. N. Correia, L. H. Mascaro, S. A. S. Machado, L. A. Avaca, *J. Braz. Chem. Soc.* **1999**, *10*, 478-482.
- [58] A. Molnar, G. V. Smith, M. Bartok, *Adv. Catal.* **1989**, *36*, 329-383.
- [59] H. Walter, G. Roewer, K. Bohmhammel, *J. Chem. Soc. Faraday Trans.* **1996**, *92*, 4605-4608.
- [60] A. Molnar, G. V. Smith, M. Bartok, *J. Catal.* **1986**, *101*, 67-72.
- [61] R. Tschan, R. Wandler, M. S. Schneider, M. Burganer, M. M. Schubert, A. Baiker, *Appl. Catal. A-Gen.* **2002**, *223*, 173-185.
- [62] R. Tschan, R. Wandeler, M. S. Schneider, M. M. Schubert, A. Baiker, *J. Catal.* **2001**, *204*, 219-229.
- [63] J. Panpranot, K. Phandinthong, T. Sirikajorn, M. Arai, P. Prasertthdam, *J. Mol. Catal. A. Chem.* **2007**, *261*, 29-35.
- [64] W. Juszczyk, Z. Karpinski, D. Lomot, J. Pielaszek, , *J. Catal.* **2003**, *220*, 299-308.
- [65] W. Juszczyk, Z. Z. Karpinski, J. Pielaszek, J. W. Sobczak, *New J. Chem.* **1993**, *17*, 573-576.
- [66] W. Juszczyk, Z. Karpinski, *J. Catal.* **1989**, *117*, 519-532.
- [67] Ch. Methivier, B. Beguin, M. Brun, J. Massardier, J. C. Bertolini, *J. Catal.* **1998**, *173*, 374-382.
- [68] A. K. Vijh, G. Belanger, *J. Mater. Sci. Lett.* **1995**, *14*, 982-984.
- [69] A. K. Vijh, G. Belanger, R. Jacques, *J. Mater. Sci. Lett.* **1993**, *12*, 113-115.
- [70] N. V. Vlasenko, N. I. Ilchenko, *React. Kinet. Catal. Lett.* **1988**, *36*, 189-193.

## 5. Polymer Derived Non-Oxide Ceramics Modified With Late Transition Metals

---

Muhammad Zaheer,<sup>[a]</sup> Thomas Schmaltz,<sup>[b]</sup> Guenter Motz<sup>[b]\*</sup> and Rhett Kempe<sup>[a]\*</sup>

[a] Inorganic Chemistry II, University of Bayreuth, 95440 Bayreuth, E-mail: [kempe@uni-bayreuth.de](mailto:kempe@uni-bayreuth.de) [b] Ceramic Materials Engineering, University of Bayreuth, 95447 Bayreuth, E-mail: [guenter.motz@uni-bayreuth.de](mailto:guenter.motz@uni-bayreuth.de)

**Published in:** *Chem. Soc. Rev.* **2012**, *41*, 5102-5116.

**Abstract:** This tutorial review highlights the methods for the preparation of metal modified polymer derived ceramics (PDCs) and concentrates on the rare non-oxide systems enhanced with late transition metals. In addition to the main synthetic strategies for modified SiC and SiCN ceramics, an overview of the morphologies, structures and compositions of both, ceramic materials and metal (nano) particles, is presented. Potential magnetic and catalytic applications have been discussed for the so manufactured metal containing non-oxide ceramics.

### 5.1 Introduction

In contrast to the classical manufacturing of ceramic powders at high temperatures the processing of polymer derived ceramics (PDCs) is a relatively young technology and offers a number of advantages over the conventional way.

By using different educts and different types of reactions the chemical and physical properties of the preceramic polymers (precursors) such as elemental composition, solubility, fusibility and viscosity are adjustable. On the one hand special functional groups enable a further modification of the polymer to produce completely new ceramic materials with high purity and homogenous distribution of the elements. On the other hand they provide for a 3-dimensional cross-linking to an unmeltable polymer (green body), which is the precondition for ceramization. The transformation

of the thermoset to the ceramic materials already occurs at relatively low temperatures (<1000°C). Due to the different properties of the preceramic polymers and of the resulting ceramics, various applications as e.g. ceramic fibres, porous ceramics, polymeric and ceramic coatings and as ceramic matrices are established. Due to these applications in combination with the versatile shaping methods precursors such as polysiloxanes, polysilazanes, polycarbosilazanes, polyborosilazanes and polysilylcarbodiimides are becoming more and more important. Recently published review articles and books summarize the interdisciplinary research devoted to PDCs and guide towards earlier summaries and pioneering work in the field.<sup>[1-5]</sup> PDCs, like other technical ceramics, can broadly be categorized into two classes: those having an oxygen moiety (oxide ceramics) and the ones without any oxygen (non-oxide ceramics). The characteristic features of the non-oxide systems include their resistance to crystallisation and the high thermal and chemical stabilities. Wide ranging applications are observed for these materials including high performance coatings, sensors, nanocomposites and fibres. The potential of these and further applications, for instance, in energy technologies and catalysis can be extended by the incorporation of metallic or intermetallic nanoparticles or phases. Late transition metals form metallic particles or phases during pyrolysis due to the reductive conditions in combination with their noble character, and they are highly relevant for catalytic applications. In a more general sense, two of the oldest and very different classes of materials, ceramics and metals, are combined and structured on a nano-scale. In this review we describe and summarize the initial attempts made to synthesis late transition metal modified polymer derived non-oxide ceramics and the applications of these materials.

## **5.2 General strategies for the synthesis of metal modified PDCs**

Synthesis of late transition metal enhanced polymer derived non-oxide ceramics can broadly be divided into three categories:

- (i) blending of the precursor with metal or metal oxide powders,
- (ii) synthesis from metallopolymers, and
- (iii) the chemical modification of precursor polymers using coordination compounds.

In the first approach, preformed metal (or metal oxide) particles are simply blended with the preceramic polymers followed by cross-linking and pyrolysis. This method is

limited with the particle sizes of the used metal (oxide) powders. In the second and third approach the desired nanoparticles are built-up, most likely *via* the formation of clusters, starting from the atomic scale. So well defined metallopolymers, in which the metal atoms are already bonded to the monomer units before polymerisation, can be formed in the first place. The modified polymers are then pyrolyzed to obtain the metal containing ceramic. Finally, in the third approach, coordination compounds (also called (metal) complexes) react with the polymeric preceramic precursors. A metal transfer from the complex to the polymer chain can occur, giving rise to metal modified precursors, which are cross-linked and pyrolyzed, yielding the metal enhanced PDCs. Each of these approaches will be discussed in detail for two classes of polymer derived non-oxide ceramics: SiC and SiCN. This review also concentrates on the modification using late transition metals, including the elements from groups 8–11 (especially Fe, Co, Ni, Pd, Pt, Cu, Ag and Au).

### 5.3 Metal modified SiC ceramics (M@SiC)

#### 5.3.1 Modification by metal (oxide) powders

In 1976, Yajima *et al.*<sup>[6]</sup> reported the synthesis of polycarbosilane (PCS) followed by its mixing with Fe–Cr alloy powder containing 13 wt% Cr in the ratio of 1 : 9. After air drying the mixture was hot pressed and heated with a rate of 5 K min<sup>-1</sup> up to 1100°C and kept for 1/2 hour. This resulted in the formation of spherical or ellipsoidal particles of Cr<sub>7</sub>C<sub>3</sub> and CrSi<sub>2</sub>. The material was resistant to oxidation and showed hardly any increase in weight after heating at 1000°C for 50 hours under air.

More recently, poly[(silylene)diacetylenes] were modified by dispersing metal oxides (Co<sub>3</sub>O<sub>4</sub>, NiO, PdO, PtO<sub>2</sub>).<sup>[7]</sup> Subsequent pyrolysis of the dispersions above 1400°C under argon afforded metal silicides (CoSi, Ni<sub>2</sub>Si, Pd<sub>3</sub>Si/Pd<sub>4</sub>Si, Pt<sub>3</sub>Si/Pt<sub>5</sub>Si) and graphitic carbon as detected by powder XRD. The metal silicides were formed through the reaction of SiC with the metal particles with the release of graphitic carbon. The formation of metal silicides (in the case of Ni) from the pyrolysis of mixture of metal powder and polysilane under argon atmosphere was also reported by Seyferth *et al.*<sup>[8]</sup>

### 5.3.2 Metal modified SiC ceramics from metallopolymers

#### 5.3.2.1 Iron containing precursors

Ferrocene based metallopolymers were investigated intensively as precursors for ceramic materials by Whittell and Manners.<sup>[9]</sup> In 1993 this group reported<sup>[10]</sup> the formation of magnetic ceramics from the pyrolysis of poly(ferrocenylsilanes) (PFSs) (Fig. 1, 1 and 2) at 500°C under nitrogen atmosphere. High molecular weight PFSs were prepared by the ring-opening polymerization of [1]sila-ferrocenophane precursors.

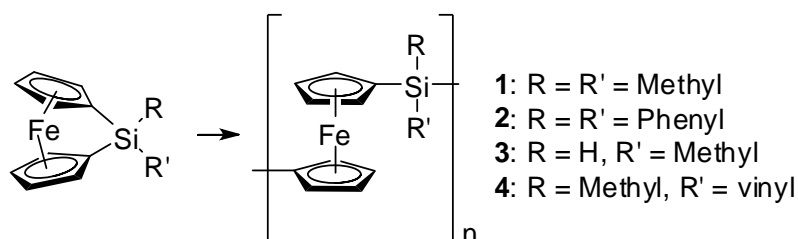


**Figure 1.** Synthesis of Poly(ferrocenylsilanes) *via* ring-opening polymerization.

The ceramic yields were rather low (35–40%) for **1** and **2**. Ceramics were attracted by bar magnets and powder XRD confirmed their amorphous nature. EDX analysis indicated the presence of iron, silicon and carbon together with trace amounts of oxygen. Poly(ferrosinylsilanes) with Si–H- and vinyl-functions (**3** and **4** in Fig. 1) provided the highest yields (60–65%) at 600°C under nitrogen.<sup>[11]</sup> Pyrolysis of a 1:1 blend of the polymers **3** and **4** afforded the ceramic in 62% yield at 600°C and the highest ceramic yield at 1000°C (56%) owing to the efficient cross-linking of the polymer *via* hydrosilylation. Analysis of the ceramics with SEM and EDX indicated that these materials were iron/silicon carbides. The ceramic formed at 600°C was found to be amorphous, whereas the corresponding one formed at 1000°C contained  $\alpha$ -Fe crystallites (by powder XRD). The formation of polymer **1** (Fig.1) followed by subsequent pyrolysis inside the channels of mesoporous silica produced magnetic ceramic composites.<sup>[12]</sup> Data collected from powder XRD, solid-state NMR, DSC, TEM and EDX provided support to the claim that the products of both, polymerization and pyrolysis reactions, remained predominantly inside the channels of the host material. The presence of  $\alpha$ -Fe nanoparticles with a size of 20 Å was confirmed by

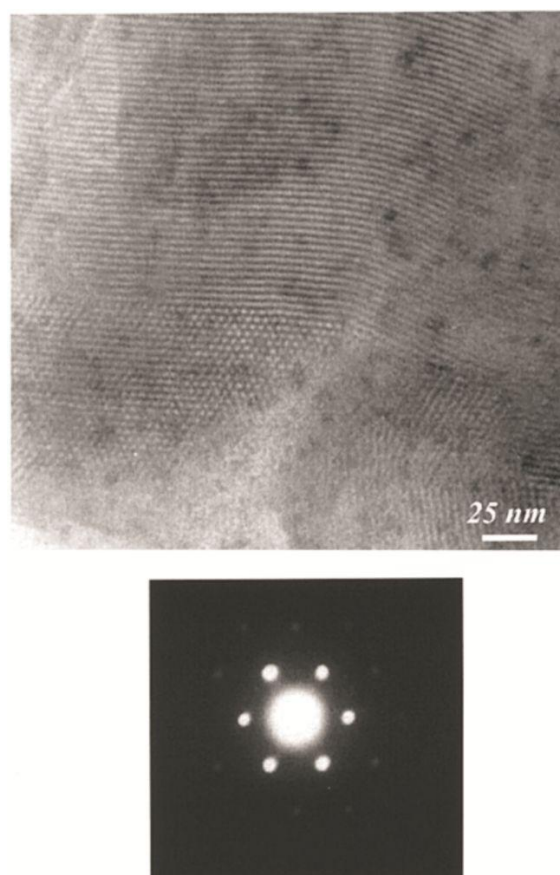


**Figure 2.** TEM micrograph of ceramic-MCM-41 composite (top) with electron diffraction pattern (bottom) showing the hexagonal order in the ceramics. (Reproduced from ref. 13 after permission. Copyright 2000 American Chemical Society).

powder XRD studies. The product obtained from the pyrolysis of polymer **1** in the channels of MCM-41 contained much smaller sized iron than those observed in the pyrolysis of bulk polymer **1**.<sup>[13]</sup> (Fig. 2) The ceramic yield is an important consideration while choosing a suitable ceramic precursor because this ultimately determines the utility, bulk properties and shape retention in the resulting ceramic. Cross-linking the preceramic polymer is a prevalent method for increasing the ceramic yield because it reduces the amount of volatile products.

In 2000, the Manners group<sup>[14]</sup> was successful in the synthesis of magnetic ceramics with high yields from highly cross-linked spirocyclic[1]silaferrocenophane (**B** in Fig. 3). Under nitrogen atmosphere ceramic yield was above 90% resulting in ceramic containing iron nanoclusters together with SiC and Si<sub>3</sub>N<sub>4</sub> as verified by powder XRD and TEM studies. With the increase in pyrolysis temperature, an increase in the size of the iron particles was confirmed (**D** and **E** in Fig. 3). In a full account, details of the pyrolysis (under nitrogen) of a well characterized cross-linked poly(ferrocenylsilane)

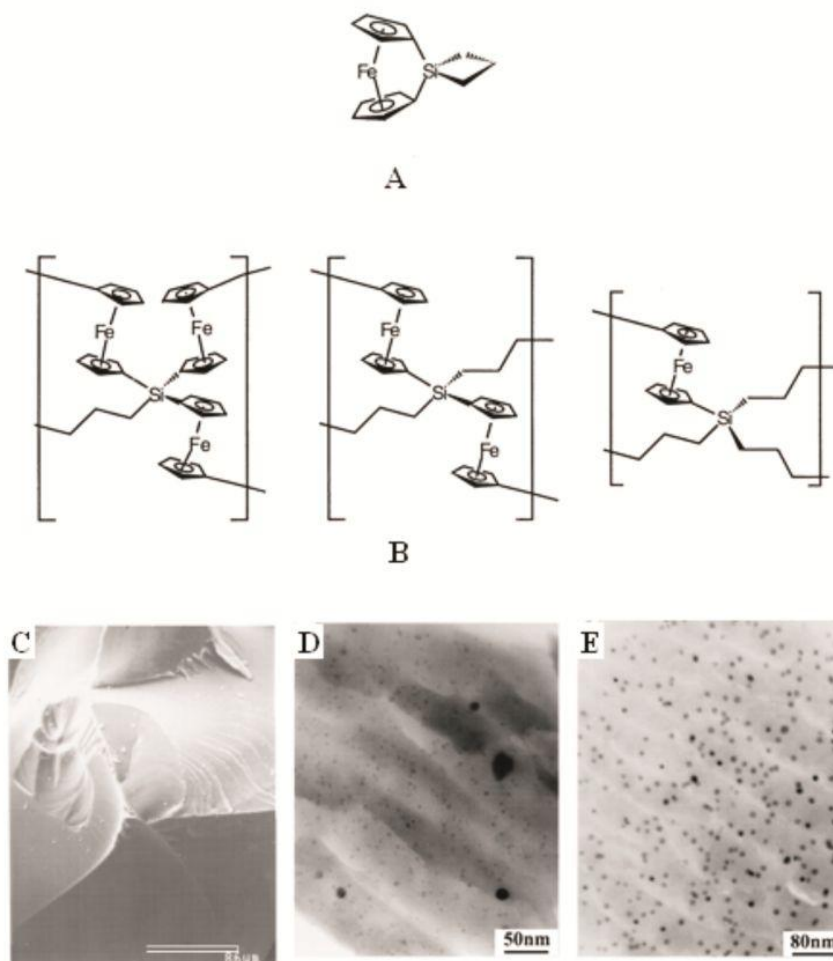


**Figure 3.** Spirocyclic [1]silaferrocenophane (**A**), its polymerization product (**B**). SEM (**C**) and TEM micrographs of bulk ceramic obtained by the pyrolysis of **B** at 600°C (**D**) and 550°C (**E**). (reproduced from ref. 14 after permission. Copyright 2000 Science, AAAS).

network derived from the polymerization of  $\text{fcSi}(\text{CH}_2)_3$  (see Fig. 3) were disclosed.<sup>[15]</sup> Variation of both, pyrolysis temperature and holding time, permitted control over the nucleation and growth of the  $\alpha$ -Fe particles, which ranged in size from around 15 to 700 Å. Also the crystallization of the surrounding matrix could be influenced by these parameters (Fig. 4).

The ceramics contained smaller  $\alpha$ -Fe particles when prepared at temperatures lower than 900°C and displayed superparamagnetic behavior, whereas the materials prepared at 1000°C contained larger particles and were ferromagnetic. In addition, the composition of the ceramic was altered by changing the pyrolysis atmosphere to argon, which yielded ceramics that contain  $\text{Fe}_3\text{Si}_5$ .

Pyrolysis of hyperbranched poly[1,1-ferrocenylene(methyl)-silyne] provided magnetic ceramics.<sup>[16]</sup> Sintering at high temperatures (1000–1200°C) under nitrogen and argon

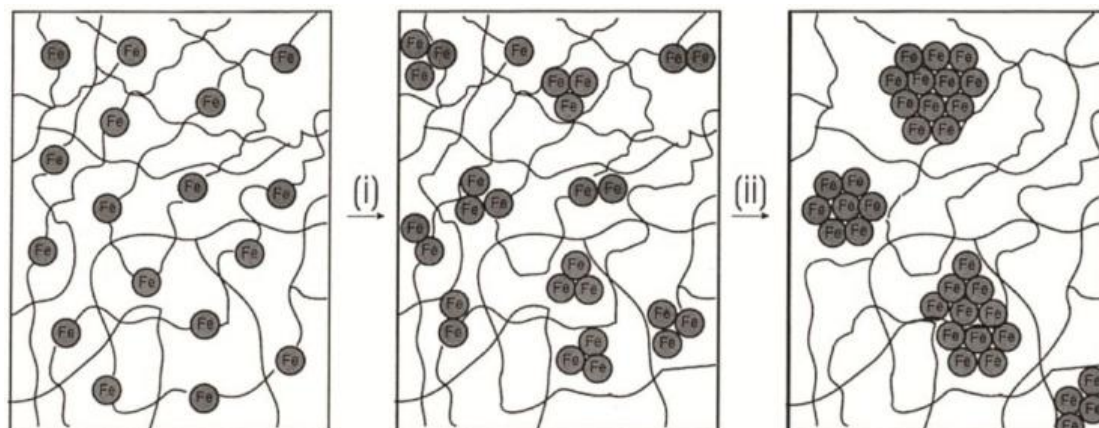


**Figure 4.** Graphical representation of a nucleation and growth model that illustrates the genesis of the magnetic ceramic from (i) iron atom release from polymer (see Fig. 3A) followed by (ii) nucleation and growth of iron nanoparticles. (reprinted after permission from ref. 15. Copyright 2009 American Chemical Society).

generated ceramics in 48–62% yields. Hyperbranched polymers were found superior, in terms of the ceramic yield, to the linear ones as ceramic precursors. The ceramics were electrically conductive and possessed a porous architecture constructed of interconnected nanoclusters. The iron content was estimated by EDX to be 36–43%, much higher than that (11%) of the ceramic prepared from the linear precursor. The nanocrystals in the ceramics were mainly  $\alpha$ - $\text{Fe}_2\text{O}_3$  and  $\text{Fe}_3\text{Si}$ . Using porous anodic alumina rods as hard template, magnetic ceramic nanorods were synthesized by the polymerization of silaferrocenophanes within the pores. The pyrolysis of the composite at  $900^\circ\text{C}$  under nitrogen followed by the chemical etching (with 1% NaOH) provided iron oxide ( $\text{Fe}_2\text{O}_3$ ) containing magnetic ceramic nanorods (NRs).<sup>[17]</sup> Highly ordered magnetic ceramic NR arrays were synthesized similarly from poly(ferrocenylsilane) by nanoimprint lithography with anodic aluminium oxide templates.<sup>[18]</sup> The key to the method was the controlled infiltration of the precursor in the nanochannels. The resulting ceramic nanorods could precisely replicate the size and shape of their PFS precursor nanorods in the template (Fig. 5).

Inverted opal structures were synthesized using a template consisting of a 3-dimensional arrangement of silica spheres. The ferrocenyl monomers were infiltrated into the void spaces within the silica sphere template. The polymerization at  $250^\circ\text{C}$  under nitrogen provided polymer silica composites which were etched with aqueous hydrogen fluoride (HF) solution and pyrolyzed ( $600$  and  $900^\circ\text{C}$  for 6 hours) under nitrogen. Ceramic yield was found to be in the range of 70–85% and  $\text{Fe}_2\text{O}_3$  nanoparticles were uniformly distributed over the composite.<sup>[19]</sup> Iron containing

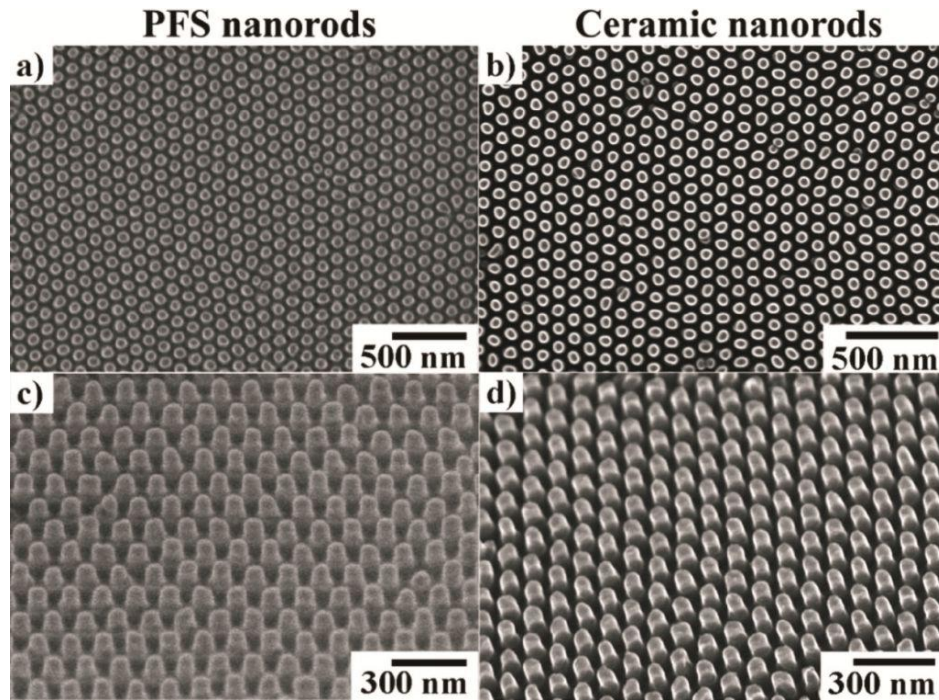


**Figure 5.** Large area highly ordered arrays of PFS NRs and their consequent ceramic NRs prepared by pyrolysis at 700°C for 5 h: (a, b) SEM top view- and (c, d) angle view-micrographs. (Modified and reproduced from ref. 18 after permission, copyright 2009 American Chemical Society).

SiC(O) magnetoceramics were recently synthesized using iron nitrate and a polycarbosilane.<sup>[20]</sup> The Fe@PCS precursors were pyrolyzed at 600–1200°C to produce magnetoceramics. The powder XRD and TEM analysis showed that the ceramics contained Fe<sub>3</sub>Si nanoparticles, which were dispersed in a amorphous SiC(O) matrix. Moreover, the crystallization of β-SiC was observed at 1200°C. Very recently, thermolysis of poly(ferrocenylsilane) at 1000°C or poly[[(dimethylsilyl)-ferrocenyl]diacetylene] at 850°C was reported.<sup>[21]</sup> The formation of ferromagnetic Fe<sub>3</sub>Si nanoparticles, well distributed in a SiC/C matrix, was observed. The average size of the formed nanoparticles, their size distribution and their agglomeration behavior depend strongly on the choice of polymer and the thermolysis conditions.

### 5.3.2.2 Fe@SiC ceramics from nanostructured block copolymers.

Block copolymers can be self-assembled into a variety of nanoscale morphologies as a result of immiscibility between the constituent blocks. If the structuring of the system can be maintained during pyrolysis nanostructured ceramic materials are possible. The block copolymer **BC1** (Fig. 6) forms stable cylindrical micelles in *n*-hexane.<sup>[21]</sup> These well-characterized micelles can be used to form oriented nanoscopic ceramic lines by hydrogen plasma treatment.<sup>[23]</sup> Shell cross-linking of the

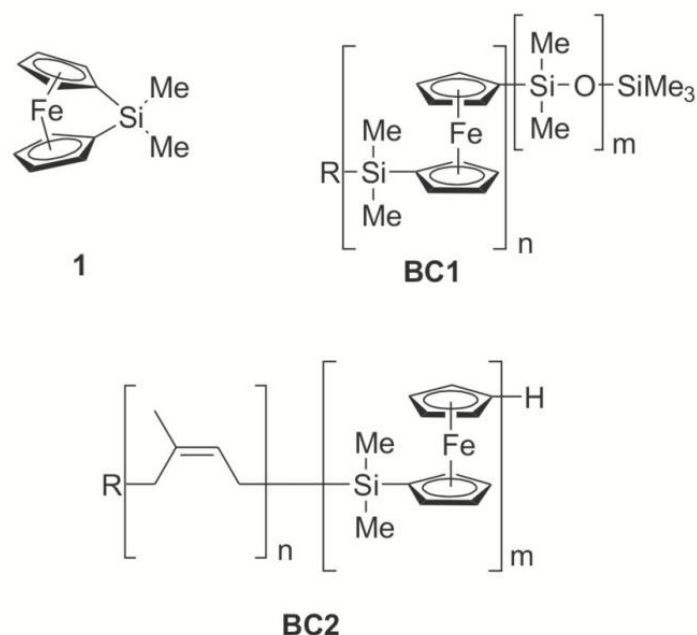


**Figure 6.** Structural formulas of [1]silaferrocenophane (**1**) and block copolymers synthesized from it, poly(ferrocenyldimethylsilane-*b*-dimethylsiloxane, **BC2**) and poly(isoprene-*b*-ferrocenyl-dimethylsilane, **BC3**). (R = alkyl).

cylindrical micelles was achieved for **BC2** (Fig. 6) by Pt-catalyzed hydrosilylation. The presence of a cross-linked corona was found to permit the pyrolysis-induced formation of cylindrical ceramic replicas with shape retention up to 600°C.<sup>[24]</sup> Furthermore, these micelles were deposited on a Si substrate from solution and upon etching continuous ceramic nanolines with lengths of micrometre and widths of as small as 8 nm were created. The presence of iron was confirmed by X-ray photoelectron spectroscopy (XPS).<sup>[25]</sup> The pyrolysis of cylinder-forming samples of the diblock copolymer PS-*b*-PFEMS in bulk and in thin films produced semi-ordered arrays of C/SiC ceramics containing Fe nanoparticles (Fig. 7). The pyrolysis of thin films stabilized by cross-linking the PS domains with UV light demonstrated high areal yields, improved shape retention, and the presence of cylinder-centered magnetic nanoparticles.<sup>[26]</sup>

Pt(0)-catalyzed ring-opening precipitation copolymerization of fcSiMe<sub>2</sub> (see **1** in Fig. 6) and fcSi(CH<sub>2</sub>)<sub>3</sub> (see Fig. 3A) was used to prepare polymer microspheres under mild conditions. Their pyrolysis led to spherical magnetic ceramic replicas (Fig. 8).<sup>[27]</sup> Thin films of PS-*b*-PFS were synthesized by spin coating on a silicon wafer and were subjected to UV radiation to cross-link the PS matrix. Subsequent pyrolysis (600°C, 2 hours) resulted in the formation of ceramic nanodots on the surface of the silicon wafer with a repeating space of 40 nm. The XPS studies revealed the presence of

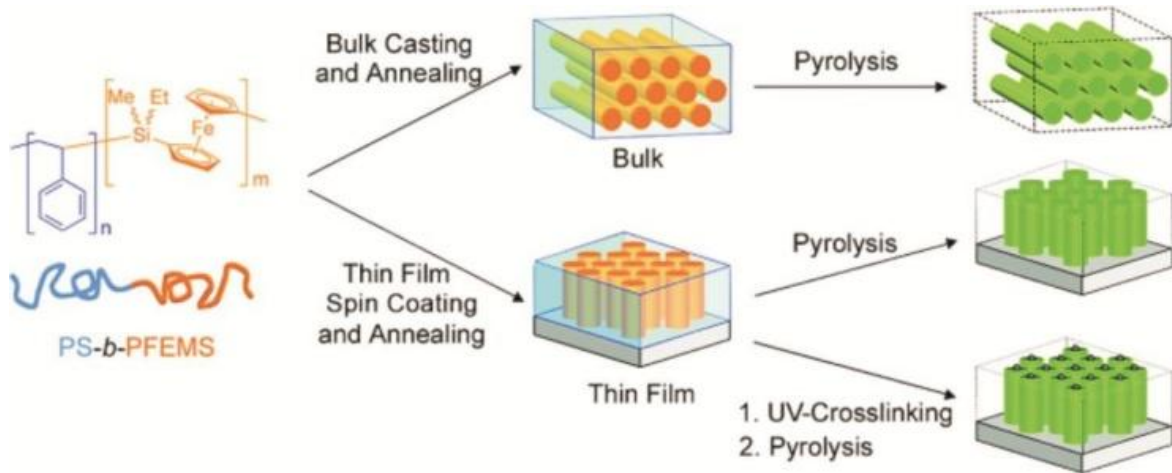


**Figure 7.** Generation of ceramic materials from the pyrolysis of bulk samples (top) and thin films (bottom) of polystyrene-*block*-poly(ferrocenylethylmethylsilane) (PS-*b*-PFEMS). (Reprinted from ref. 26 after permission, copyright 2008 American Chemical Society).

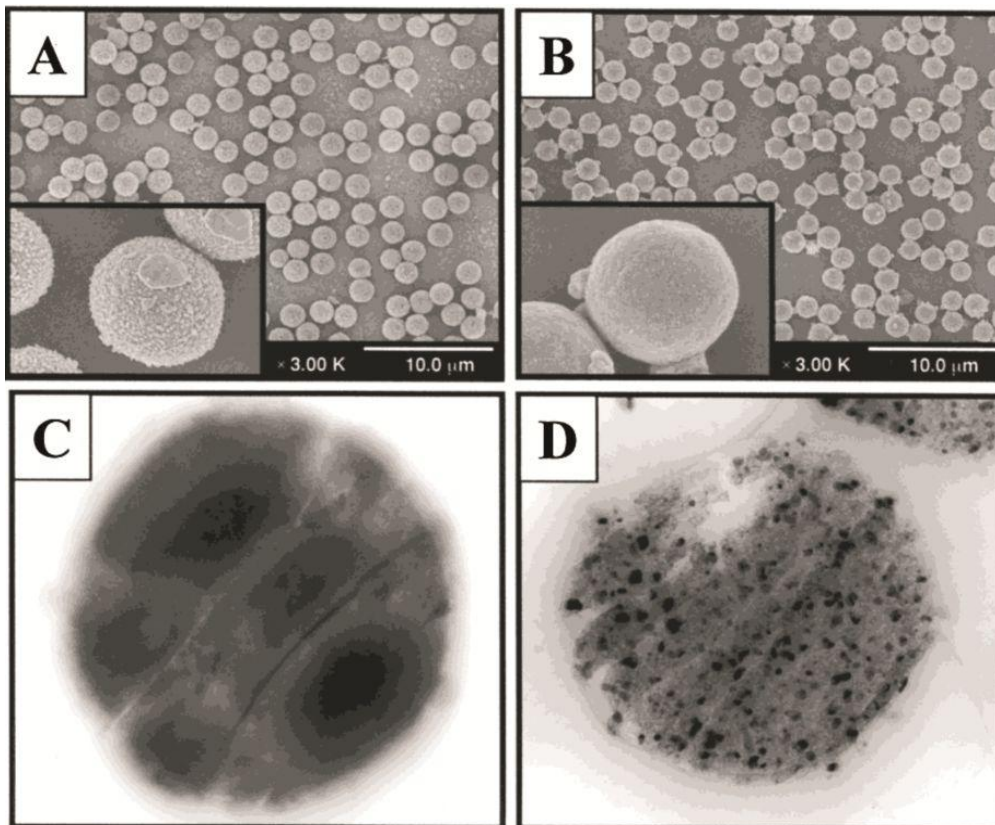


**Figure 8.** SEM and thin-section TEM micrographs of ceramic particles obtained from pyrolysis of organometallic microspheres under a nitrogen atmosphere for (A, C) 2 h at 600°C and (B, D) 2 h at 900°C. (Reprinted after permission from ref. 27, copyright 2002 American Chemical Society).

$\text{Fe}_2\text{O}_3$  and  $\text{Fe}_3\text{O}_4$  species. The cylindrical morphology of the block copolymer is lost upon pyrolysis which may be attributed to the lack of the cross-linking of PFS block. The inefficient cross-linking leads to the loss of volatile products during the pyrolysis

which in turn destroys the structure. The low yield of the ceramics (30%) also supports the inefficient cross-linking.<sup>[28]</sup>

### 5.3.2.3 Bimetallic systems (FeM@SiC ceramics)

Sila[1]ferrocenophanes having acetylenic substituents were polymerized and reacted with  $\text{Co}_2(\text{CO})_8$  to get a bimetallic polymer (polymer **2** in Fig. 9).

In a typical reaction 75–100% acetylenic moieties are substituted with cobalt carbonyl. The bimetallic polymer is stable in air and moisture.<sup>[29]</sup> The ceramic yield was 72% and 59% at 600 and 900°C, respectively. The black ceramic obtained was attracted by a bar magnet. Powder XRD confirmed the amorphous SiC/C and TEM

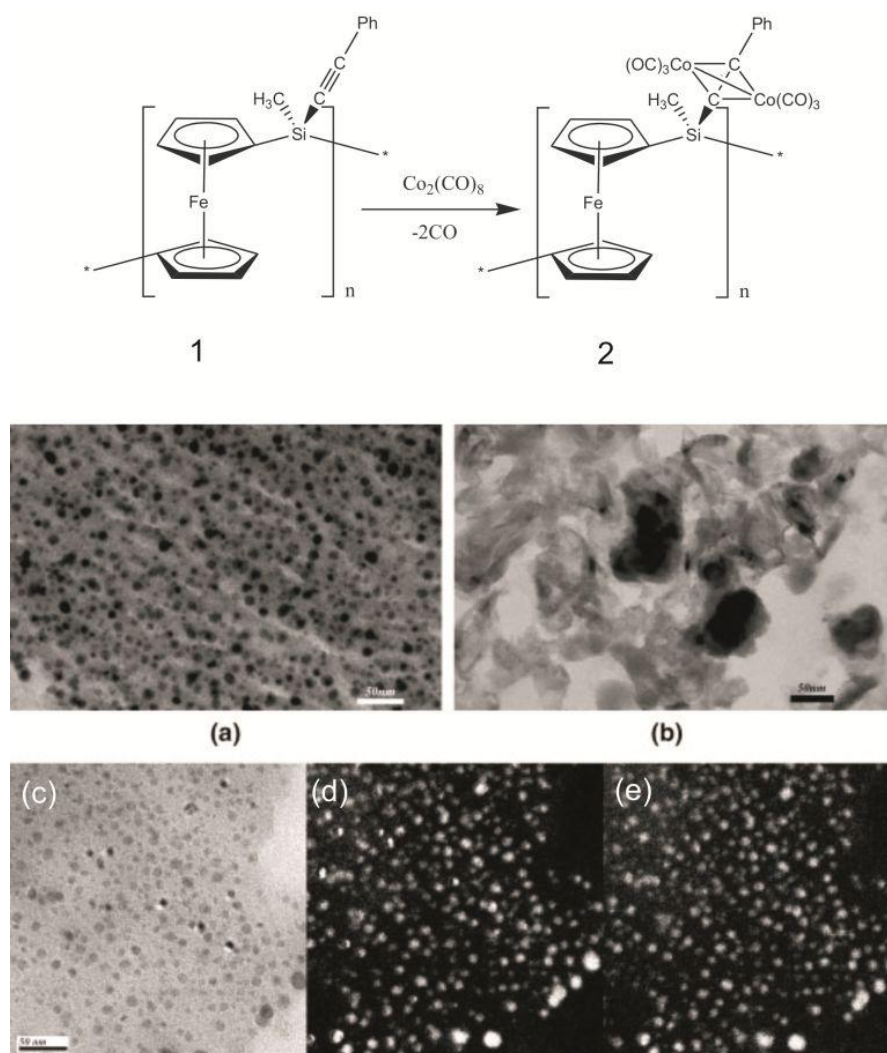


**Figure 9.** Synthesis of cobalt modified poly(ferrocenylsilane) (**2**) from acetylene substituted poly(ferrocenylsilane) (**1**). TEM images of cross sections of ceramics pyrolyzed at (a) 600°C and (b) at 900°C. TEM micrographs of ceramic cross section (c) with the corresponding EDS maps for (d) iron and (e) cobalt. (Reprinted after permission from ref. 29, copyright 2003 Wiley-VCH Verlage GmbH & Co).

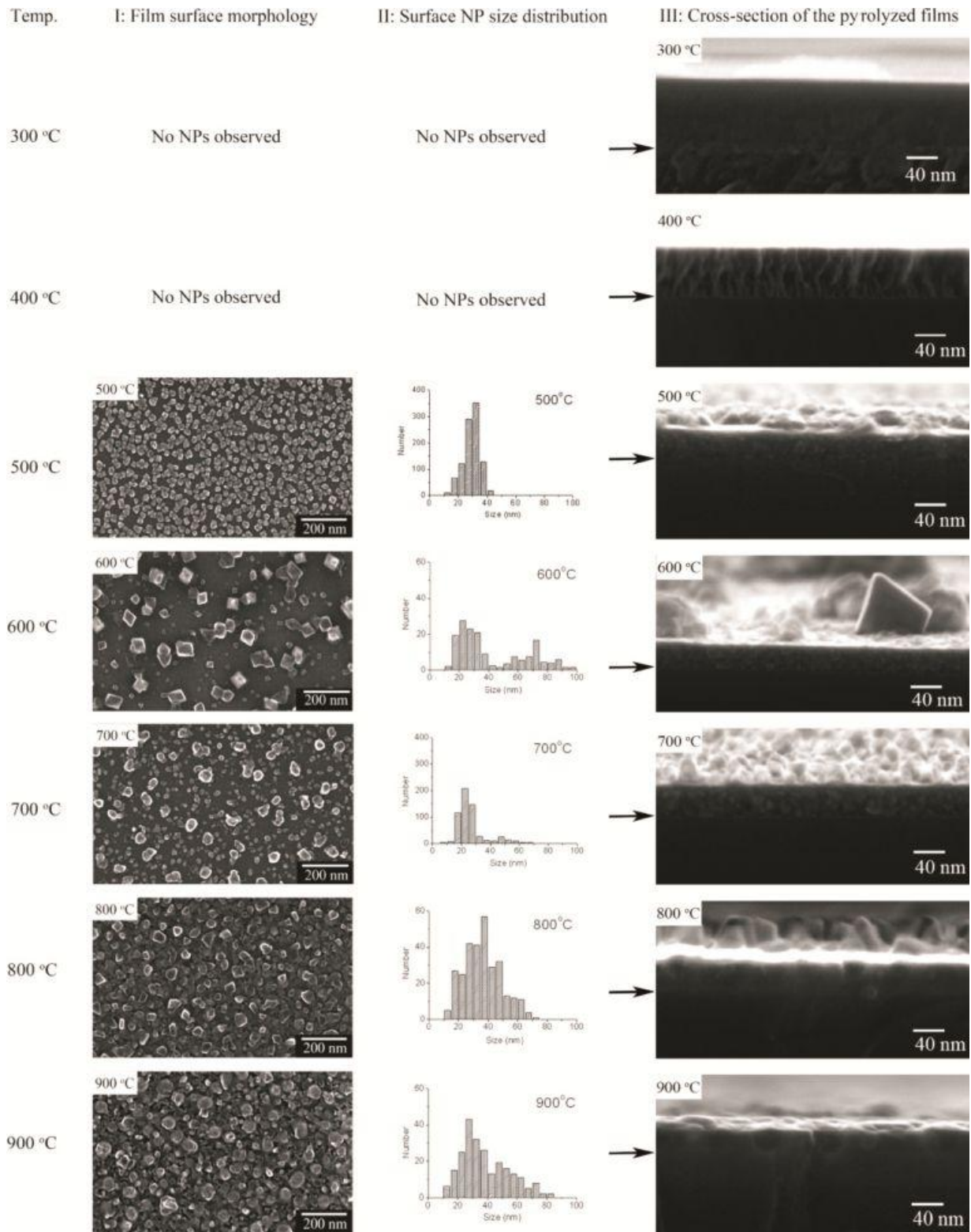


**Figure 10.** Vertical view SEM micrographs (series I), surface particle size distributions (series II), and cross-sectional SEM micrographs (series III) for Co@PFS thin films pyrolyzed at 300, 400, 500, 600, 700, 800 and 900 °C. The original film thickness before pyrolysis was about 200 nm. The arrows in series III indicate the interface of the Si substrate and the pyrolyzed film. (Reprinted after permission from ref. 33, copyright 2006 American Chemical Society).

with EDX shows the presence of Fe and Co within the same nanoparticle ((d) and (e) in Fig. 9).

A similar approach was used to synthesize ordered 2D arrays of ferromagnetic Fe/Co alloy nanoparticle rings with diameters of 2–12  $\mu\text{m}$ .<sup>[30]</sup> The highly metallized poly(ferrocenylsilane) precursors were structured *via* template directed self-assembly followed by plasma etching and pyrolysis. Furthermore, thin films (Fig. 10) were made of Co@PFS whose pyrolysis afforded patterned ferromagnetic ceramics with excellent shape retention.<sup>[31–33]</sup>

Solution processing is a facile method to generate magnetic thin films. Poly(ferrocenylethylmethylsilane) (PFEMS, Fig. 11A) was doped with Pd using two methods: sublimation of  $[\text{Pd}(\text{acac})_2]$  (acac = acetylacetonate) to form Pd NPs in the polymer films and direct mixing of  $[\text{Pd}(\text{acac})_2]$  with the polymer precursor prior to film deposition. Pyrolysis of the precursors yielded ferromagnetic ceramics (Fig. 11B–D). The effect of the pyrolysis temperature and atmosphere on magnetic properties, chemical composition and crystalline structure of the ceramics was explored. For the ceramics derived from pyrolysis (1000°C, under argon) of Pd@PFEMS, the formation of Fe/Pd alloys was observed. All the samples show characteristic reflection patterns of  $\text{Fe}_3\text{O}_4$  and  $\text{Fe}_2\text{O}_3$  suggesting an incorporation of oxygen during their handling and storage.<sup>[34]</sup>

### 5.3.2.4 Other M@SiC ceramics

Ferrocene is a very stable and easy to modify organometallic molecule, and thus ideal to incorporate into metallopolymers. Unfortunately, this chemistry is restricted to iron, but for other late transition metals strategies to incorporate these elements into non-oxide ceramics have to be developed. Following the aforementioned protocol, synthesis and pyrolysis of a series of nickel containing polycarbosilanes (Ni@PCS, Fig. 12) was described.<sup>[35]</sup>

Pyrolysis of the Ni@PCSs yielded ceramics with embedded Ni or Ni silicide nanoparticles. By adjusting the pyrolysis temperature, it was possible to control the formation of either nickel (400 and 600°C) or nickel silicide ( $\text{Ni}_3\text{Si}$  and  $\text{Ni}_{31}\text{Si}_{12}$ ) nanoparticles (900°C) (see TEM micrographs in Fig. 12). The substituent group (phenyl or *t*-butyl), the clusterization percentage and the pyrolysis time, all influenced the yield and the properties of ceramic materials.

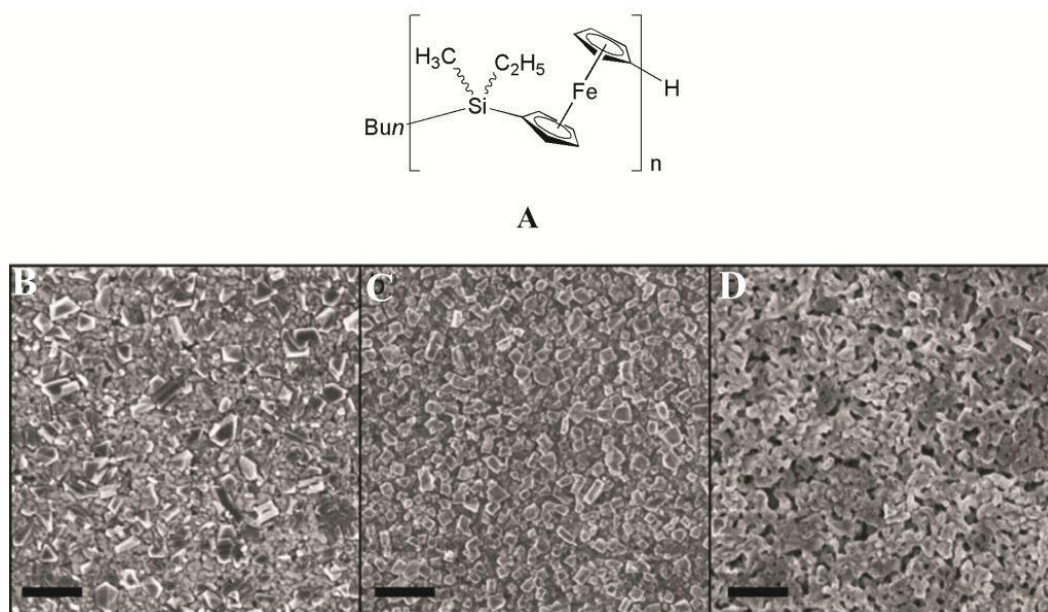


**Figure 11.** Structural formula of poly(ferrcenyethylmethylsilane) (PFEMS, A) with SEM micrographs of the ceramics obtained from the pyrolysis of PFEMS (B), PFEMS containing Pd nanoparticles (C) and PFEMS containing Pd(acac)<sub>2</sub> pyrolyzed under argon stream at 1000°C (D). (Scale bar: 1 μm). (Reprinted after permission from ref. 34, copyright 2011 American Institute of Physics).

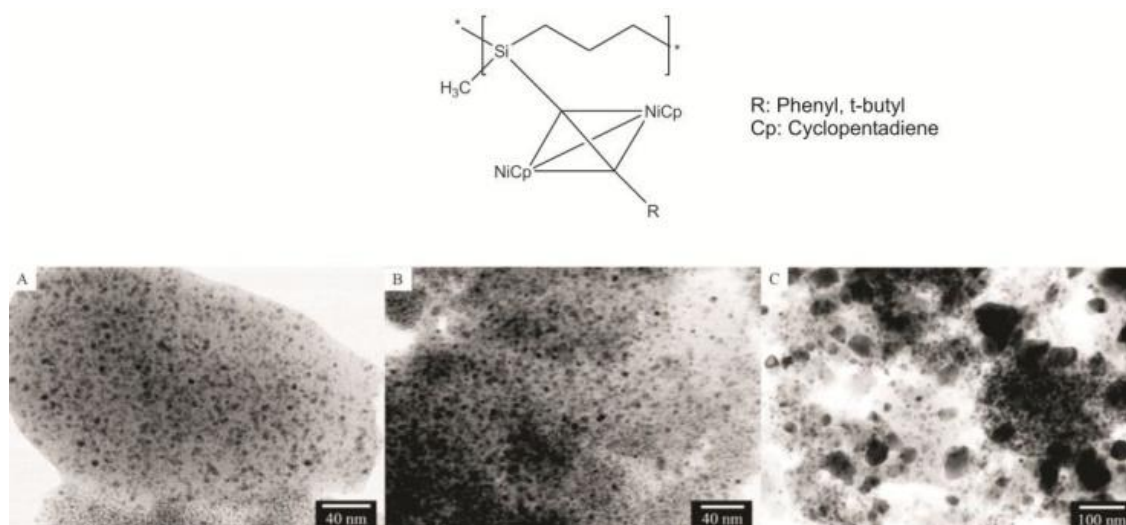


**Figure 12.** Structural formula of nickel containing poly(ferrocenylsilane) (Ni@PFS) along with the TEM images of pyrolyzed ceramics at (A) 400, (B) 600, and (C) 900°C for 1 h. (Reproduced after permission from ref. 35, copyright 2007 American Chemical Society).

The pyrolysis of poly[[(diorganosilylene)diacetylene]dicobalt-hexacarbonyls] (Fig. 13) at 1350°C gave Co<sub>2</sub>Si and graphite-like carbon. Evolution of part of the carbon monoxide in the early stage of the pyrolysis (100°C) showed that the cross-linking of diacetylene units was induced by reactive cobalt species. Furthermore, at higher temperatures (200–500°C), cobalt clusters catalyze the formation of the ceramic.

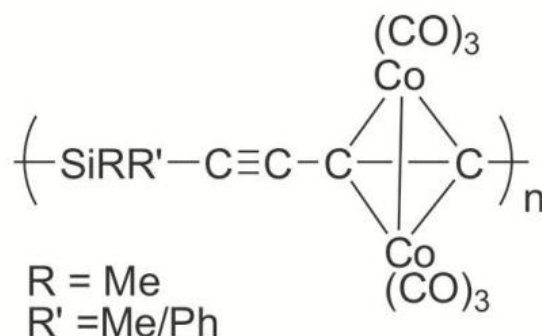


**Figure 13.** Structural formula of poly[[(diorganosilylene)diacetylene]-dicobalthexacarbonyls].

$\text{Co}_2\text{Si}$  was shown to result from the reaction of SiC with Co above  $1000^\circ\text{C}$ , both formed during the pyrolysis process. Finally, at  $1100^\circ\text{C}$ , a carboreduction reaction led to the elimination of the oxygen incorporated in the carbon matrix during the cross-linking process.<sup>[36]</sup> Furthermore, porous  $\text{CeO}_2/\text{Pt}$ -polycarbosilane composites, using an aqueous hexachloroplatinic acid as a hydrosilylation catalyst causing cross-linking of allyl groups in the liquid PCS, were reported.<sup>[37]</sup> The cross-linked polymers showed high specific surface areas and well dispersed ceria nanoparticles in the matrix. Pyrolysis at  $1200\text{--}1500^\circ\text{C}$  and post-oxidative treatment at various temperatures produce porous ceramic structures with surface areas up to  $423 \text{ m}^2 \text{ g}^{-1}$ . X-Ray diffraction investigations showed that the crystallinity of the SiC matrix could be controlled by the pyrolysis temperature.

### 5.3.3 Modification by coordination compounds

First investigations on reactions between precursor polymers and coordination compounds were reported by Seyferth and coworkers.<sup>[38]</sup> The presence of Si–H- and Si–Si-functions in Nicalon polycarbosilane (PCS) provided an opportunity to add polynuclear transition metal carbonyls ( $\text{Ru}_3(\text{CO})_{12}$ ,  $\text{Fe}_3(\text{CO})_{12}$ ,  $\text{Os}_3(\text{CO})_{12}$ ,  $\text{Rh}_6(\text{CO})_{16}$ ,  $\text{Co}_4(\text{CO})_{12}$ ,  $\text{Co}_2(\text{CO})_8$ ) to the polymer backbone.<sup>[39]</sup> Their addition resulted in the desired cross-linking of the polycarbosilane and provided an increased ceramic yield. For instance, the addition of 2 wt% of  $\text{Ru}_3(\text{CO})_{12}$  to PCS provided a ceramic yield of 76% at  $1000^\circ\text{C}$  under argon atmosphere. The chemical composition of the pyrolysis product at  $1500^\circ\text{C}$  was found to be 88.8% SiC and 11.1% C. However no details about the fate and behavior of the metals inside the resulting ceramics were reported. The pyrolysis of an iron containing polycarbosilane (1300C/Ar) was used to synth-

-esize magnetic SiC nanowires.<sup>[40]</sup> Therefore poly(dimethylsilane) was simply mixed with  $[\text{Fe}(\text{acac})_3]$  (acac = acetylacetonate). The powder XRD spectrum of the material showed the presence of typical diffraction lines of a  $\beta$ -SiC crystal along with diffraction lines related to  $\text{Fe}_5\text{Si}_3$ ,  $\text{Fe}_3\text{Si}$  and FeC. Similarly, the formation of silicon carbide (SiC) fibers using an iron containing polycarbosilane was reported.<sup>[41]</sup> Iron pentacarbonyl  $[\text{Fe}(\text{CO})_5]$  was first reacted with PCS. Nanosized  $\alpha$ -Fe domains rather uniformly distributed were found inside the ceramic fibres. The formation of  $\text{Si}_3\text{N}_4$  and SiC nanowires using an iron ( $\text{FeCl}_2$ )<sup>[42]</sup> or a cobalt compound ( $\text{CoCl}_2$ )<sup>[43]</sup> and poly(methyl-phenylsilsesquioxane) was described. Powder XRD analysis of the iron samples pyrolyzed at  $1250^\circ\text{C}$  under nitrogen flow showed the crystallization of  $\beta$ -SiC,  $\alpha$ - $\text{Si}_3\text{N}_4$ ,  $\text{Fe}_3\text{Si}$  and  $\text{Si}_2\text{ON}_2$ . Moreover at  $1350^\circ\text{C}$ , the formation of single crystalline  $\text{Si}_3\text{N}_4$  nanowires took place. In the case when samples were pyrolyzed at  $1400^\circ\text{C}$  under argon atmosphere, SiC nanowires with spherical tips (iron silicide) were generated as confirmed by HR-TEM coupled EELS and EDX measurements. Powder XRD studies showed the presence of  $\beta$ -SiC,  $\text{Fe}_3\text{Si}$  and amorphous carbon as major phases present in the samples pyrolyzed at  $1250$ – $1300^\circ\text{C}$  under argon atmosphere. Authors obtained the similar results using  $\text{CoCl}_2$  assisted pyrolysis of the precursor. The resulting ceramics containing nanowires showed a specific surface area up to  $110 \text{ m}^2 \text{ g}^{-1}$ .

#### 5.4. Metal modified SiCN ceramics (M@SiCN)

##### 5.4.1 Modification by metal (oxide) powders

One of the first examples on the modification of PSZs with metal (oxide) powders for the synthesis of metal containing SiCN ceramics was reported in 2003.<sup>[44]</sup> The composites were synthesized by the mixing of  $\text{Fe}_3\text{O}_4$  powder with a liquid PSZ, followed by pyrolysis at different temperatures. Investigations of the products by powder XRD revealed that above  $600^\circ\text{C}$  only the diffraction peaks for  $\text{Fe}_3\text{O}_4$  could be found. At  $700^\circ\text{C}$ ,  $\text{Fe}_3\text{O}_4$  begins to reduce to  $\alpha$ -Fe, accompanied by the formation of iron-silicate. This reaction is complete at  $1000^\circ\text{C}$ . At temperatures above  $1100^\circ\text{C}$ ,  $\alpha$ -Fe begins to convert to FeN.

In 2007, the synthesis of metal enhanced SiCN ceramics by the mixing of metal powders with a commercial PSZ (Ceraset®, Kion Inc., USA) was reported.<sup>[45,46]</sup> The

PSZ was first thermally cross-linked by heating up to 280°C under an argon atmosphere followed by milling. The green body powders were mixed with metal powders (Fe, Co and Ni), homogenized with milling, warm pressed and pyrolyzed at 1000°C under an argon atmosphere. Phase evolution of the ceramics was carried out by powder XRD. Whereas Ni and Fe form silicides, cobalt exists solely in the metallic phase. The same strategy was applied to mixed metal systems. In these cases, formation of ternary metal silicides was observed.

The formation of nickel silicides was also observed by others.<sup>[47]</sup> Nickel powder was mixed with PSZ (Ceraset®) to obtain 10 vol% metal fractions in the resulting metal–ceramic composite. This composite slurry was cross-linked, warm pressed in a graphite die and pyrolyzed at 1000°C under nitrogen atmosphere, followed by heat treatment at 1200°C for 1 and 10 hours. The powder XRD data from the composite annealed for 1h at 1200°C in argon showed the formation of crystalline Ni<sub>2</sub>Si and also the presence of metallic Ni. As the annealing time is increased, the peaks corresponding to Ni<sub>2</sub>Si increased in strength while the Ni peaks subsided. After annealing for 10h, a new phase, corresponding to Si<sub>3</sub>N<sub>4</sub>, was found. Similar observations were made in the SiCN ceramics synthesized by the mixing of Fe and Co with PSZ (Ceraset®).<sup>[48]</sup> The formation of Fe<sub>3</sub>Si and Co<sub>2</sub>Si was confirmed by quantitative powder XRD analysis. In a different publication the same authors investigated the crystallization behavior of iron containing SiCN ceramics at temperatures well above 1000°C.<sup>[49]</sup> The synthesis of a Fe<sub>3</sub>Si/SiCN composite was accomplished *via* pyrolysis at 1100°C in an argon stream. At 1300°C, the crystalline phases Fe<sub>3</sub>Si, Fe<sub>5</sub>Si<sub>3</sub>, and SiC were observed. The crystallization of SiC was assumed to occur from the liquid Fe/Si/C alloy being formed during the molten state of silicides at 1300°C.

The group of Kroke<sup>[50]</sup> used a different approach and synthesized silver nanoparticles containing SiCN ceramics by the mixing of 3 wt% as-synthesized Ag nanoparticles with Ceraset® followed by pyrolysis under flowing nitrogen and/or ammonia. Bulk samples as well as coatings were investigated. Powder X-ray diffraction (XRD), transmission electron microscopy (TEM), thermal analysis (TGA, DTA), absorption spectroscopy (UV-vis) and infrared (IR) spectroscopy were used to characterize the products. At temperatures in the range of 800–1000°C silver particles with an average size of 5-7 nm was observed.

#### 5.4.2 Metal modified SiCN ceramics from metallopolymers

Like in the case of PCSs, again iron containing polymers were the first successful attempts in this field. So poly(ferrocenylsilazanes) with linear or linear–cyclic structure were synthesised *via* hydrosilylation, a reaction during which no by-product is formed.<sup>[51]</sup> The ceramic yields of these metallopolymers were estimated by thermogravimetric analysis (TGA) and bulk pyrolysis, and were found to depend on the molecular structures. Compared with that of their linear counterparts the ceramic yields of linear–cyclic polymers were much higher.

The preparation of iron-containing PSZs by mixing of  $\text{Fe}[\text{N}(\text{SiMe}_2\text{Vi})_2]_3$  ( $\text{Vi} = -\text{CH}=\text{CH}_2$ ) and a vinyl group containing PSZ afforded magnetic ceramics after cross-linking at  $350^\circ\text{C}$  (no peroxide addition) and pyrolysis in  $\text{N}_2$ .<sup>[52]</sup> (Fig. 14) The ceramics produced were investigated by X-ray diffraction, transmission electron microscope and vibrating sample magnetometer at room temperature. It was indicated that  $\alpha\text{-Fe}$  is the only magnetic crystalline iron phase embedded in the amorphous SiCN matrix from 500 to  $900^\circ\text{C}$ . Iron particle size increases with an increase in the pyrolysis temperature (Fig. 14).

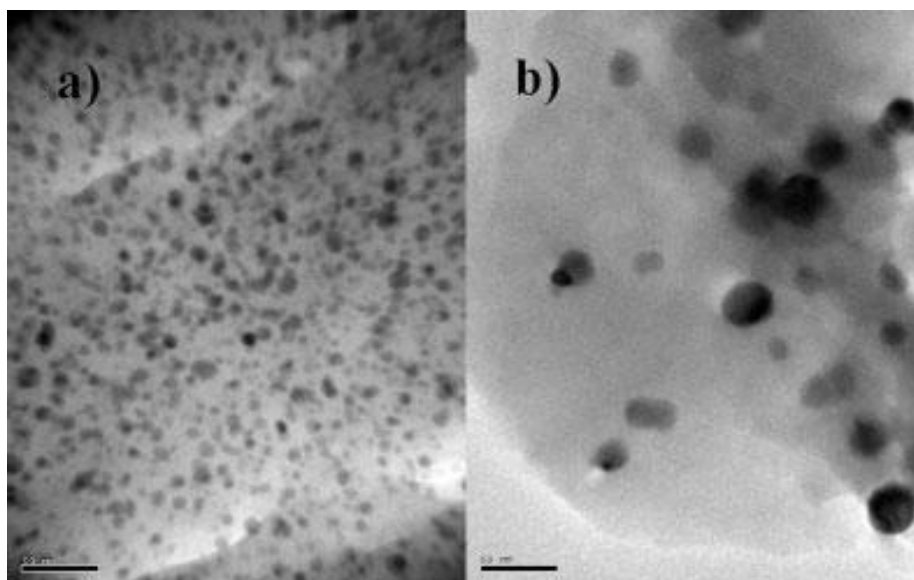


**Figure 14.** TEM micrographs of the samples prepared at (a)  $500^\circ\text{C}$  and (b)  $900^\circ\text{C}$ . (Scale bar: 50 nm). (Reproduced after permission from ref. 52, copyright 2007 Wiley Periodicals, Inc.).

The synthesis of silazane and silazane–iron polymers was also performed in an improved configuration of plasma assisted chemical vapor deposition coupled with

chemical transport reaction.<sup>[53]</sup> The resulted (nano-structured) polymers were then pyrolyzed at 1200°C under nitrogen atmosphere. Evidence for the presence of Fe<sub>3</sub>C and Si<sub>3</sub>N<sub>4</sub> in the pyrolysis products of the iron containing polymer is presented. Hexamethyldisilazane and ferrocene/ hexamethyldisilazane were used as molecular precursors, respectively.<sup>[54,55]</sup>

### 5.4.3 Modification by coordination compounds

Among the many polysilazanes (PSZs) available, especially those containing vinyl- and Si–H functionalities are widely used for the fabrication of SiCN ceramics since they show a very good cross-linking behavior resulting in good ceramic yields. Additionally, the availability of reactive N–H-, vinyl- and Si–H-functionalities in these precursors allows the incorporation of metal atoms into the polymer chains. So covalent bonds between the metal ions and the polysilazanes can be established by their reaction with coordination compounds. During this metal transfer the ligand of the coordination compound is released and after cross-linking may become a part of the preceramic polymer. Polymer–metal binding is essential in the regard that it avoids the loss of metal *via* sublimation during pyrolysis. This molecular approach is advantageous, owing to the dispersion of the metal at an atomic level, the broad applicability (coordination compounds of many metals can be used) and the use of rather inexpensive (commercially available) polymer precursors.

A metal containing SiCN ceramic was synthesized by reacting lithiated polysilazanes with FeCl<sub>3</sub> followed by pyrolysis under argon, nitrogen and ammonia.<sup>[56]</sup> Ceramic yields were found to be higher than in the case of the unmodified silazanes. Powder XRD of the ceramics pyrolyzed under argon and nitrogen showed crystalline Fe while those heated under ammonia showed Fe<sub>4</sub>N, Fe<sub>3</sub>N and Fe. One drawback of this approach is the difficulty of removing unreacted FeCl<sub>3</sub> and formed LiCl completely because of their poor solubility in organic solvents. Also along the investigation of PSZ cross-linking reactions induced by iron chloride addition,<sup>[57]</sup> some Fe@SiCN ceramics were detected. The cross-linked solids were pyrolyzed at 500–1000°C under nitrogen atmosphere after curing at 130°C for 24 hours. A ceramic yield of 80% at 800°C was observed. Powder XRD measurements at 500°C showed the presence of crystalline iron along with the NH<sub>4</sub>Cl and Fe<sub>3</sub>C while at 1000°C the crystallization of Si<sub>3</sub>N<sub>4</sub> and Fe<sub>3</sub>Si was observed. The crystallization of Si<sub>3</sub>N<sub>4</sub> at a

temperature of about 900°C is quite unusual. Electron paramagnetic resonance (EPR) and ferromagnetic resonance (FMR) studies of SiCN ceramics doped with iron revealed a variety of iron species.<sup>[58]</sup> Different oxygen containing iron complexes were dissolved in a liquid PSZ followed by cross-linking at 160°C (DCP addition) and pyrolysis in the temperature range of 600–1600°C for these studies. After pyrolysis between 950–1150°C, nanocrystalline particles in the ferromagnetic state and Fe ions incorporated into the free-carbon in the superparamagnetic state were found. Powder XRD studies of the samples show the crystallization of Si<sub>3</sub>N<sub>4</sub> above 130°C while at 1100°C the existence of Fe<sub>5</sub>Si<sub>3</sub> and graphitic carbon was confirmed. In this approach the use of metal carbonyls can be advantageous in the sense that they can initiate hydrosilylation and dehydro-coupling reactions (even at room temperature as shown in the case of [Co<sub>2</sub>(CO)<sub>8</sub>]) leading to the simultaneous cross-linking and metal modification of the polymer.<sup>[48]</sup> The formation of intermetallic compounds Fe<sub>3</sub>Si and Co<sub>2</sub>Si was confirmed by XRD and TEM studies using Fe and Co carbonyls. The chemical modification of HTT1800 by the use of a Ni(II) complex resulted in the formation of nanoporous silicon oxycarbo-nitride ceramics modified by Ni nanoparticles.<sup>[59]</sup> The as-obtained Ni modified PSZ precursors were thermolyzed at 700°C and transformed into ceramic nanocomposites, manifesting a nanoporous structure, revealing a BET surface area of 215 m<sup>2</sup> g<sup>-1</sup>. Recently, a molecular approach<sup>[60]</sup> for the modification of the PSZ HTT1800 making the use of minopyridinato metal complexes<sup>[61,62]</sup> was developed (Fig. 15).

Amido complexes can be synthesized in good yields on a large scale and are soluble in common organic solvents, so a good polymer/coordination compound mixing is possible. Moreover, they contain the same elements as contained by the precursor polymer, thus avoiding the entry of any alien element into the ceramic composites. The amido ligand contributes towards ceramic yield by providing Si, C and N atoms to the ceramic. Furthermore, nearly all transition metals are addressable.<sup>[63]</sup> On the account of the availability of more coordination sites within the PSZ backbone and the intrinsic reactivity of the complex, the metal transfer (here copper) from the complex to the polymer takes place. As a result of this transfer, the liberation of a protonated ligand was observed. The <sup>1</sup>H and <sup>13</sup>C NMR studies of the reaction between the copper aminopyridinato complex (see Fig. 15 for its structure) and the used PSZ showed the liberation of protonated ligand Ap<sup>TMS</sup>H providing indirect

evidence of the transfer of the metal to the nitrogen functions of the polymer (Fig. 16). The copper transfer was additionally supported by a model reaction, the reaction of  $[\text{Cu}_2(\text{Ap}^{\text{TMS}})_2]$  with an excess of  $\text{HN}(\text{SiMe}_3)_2$  (Me = methyl) simulating the polymer backbone. In this reaction the formation of a tetrameric Cu silylamide was observed. A metal modified polymer was cross-linked using DCP and pyrolyzed at  $1000^\circ\text{C}$  to form copper containing SiCN ( $\text{Cu@SiCN}$ ). The copper cations bound to the polymer backbone are reduced to a copper metal during the pyrolysis step as observed by solid-state  $^{65}\text{Cu}$  NMR spectroscopy, SEM micrographs and energy dispersive spectroscopy (EDS). Furthermore, powder diffraction experiments verified the presence of crystalline copper.

The loading of copper could be varied over a large range up to a Si to Cu ratio of 5. The size of the Cu particles found in  $\text{Cu@SiCN}$  increases with a higher loading of copper complex (Fig. 17). Owing to the availability of aminopyridinato complexes, the aforementioned bottom-up approach should be extendable to other (nearly all) transition metals. Interestingly, a very different behavior was found for palladium aminopyridinates (in comparison to copper) which generate intermetallic nanoparticles. Simultaneous chemical modification of the polyorganosilazane HTT-1800 as well as its cross-linking was achieved by the use of an aminopyridinato palladium complex at room temperature.<sup>[64]</sup> Cross-linking takes place with an evolution of hydrogen supporting a dehydrocoupling mechanism in parallel to hydrosilylation, which increases the ceramic yield by the retention of carbon and nitrogen atoms (which otherwise are lost in the form of  $\text{CH}_4$  and  $\text{NH}_3$ ). The ceramic yield was found to be even higher than in the case of the pure PSZ, cross-linked by the addition of free radical initiators like DCP. Liberation of the ligand, as confirmed again by  $^1\text{H}$  NMR spectroscopy, provides indirect evidence of the transfer of palladium to the nitrogen functions producing palladium modified PSZ. Pyrolysis at  $1100^\circ\text{C}$  under nitrogen atmosphere provides  $\text{Pd}_2\text{Si@SiCN}$ . Powder X-ray diffraction studies confirmed the presence of the hexagonal  $\text{Pd}_2\text{Si}$  phase in the amorphous SiCN matrix. The size of the particles formed depends upon the nature of the solvent Used in the cross-linking step. The amount of the palladium complex added seems not to affect the size of particles formed but does increase their population density (Fig. 18). For the catalytic applications of  $\text{Pd}_2\text{Si@SiCN}$  see chapter 5.2.

The Wiesner group<sup>[65]</sup> developed a highly innovative bottom-up approach to fabricate

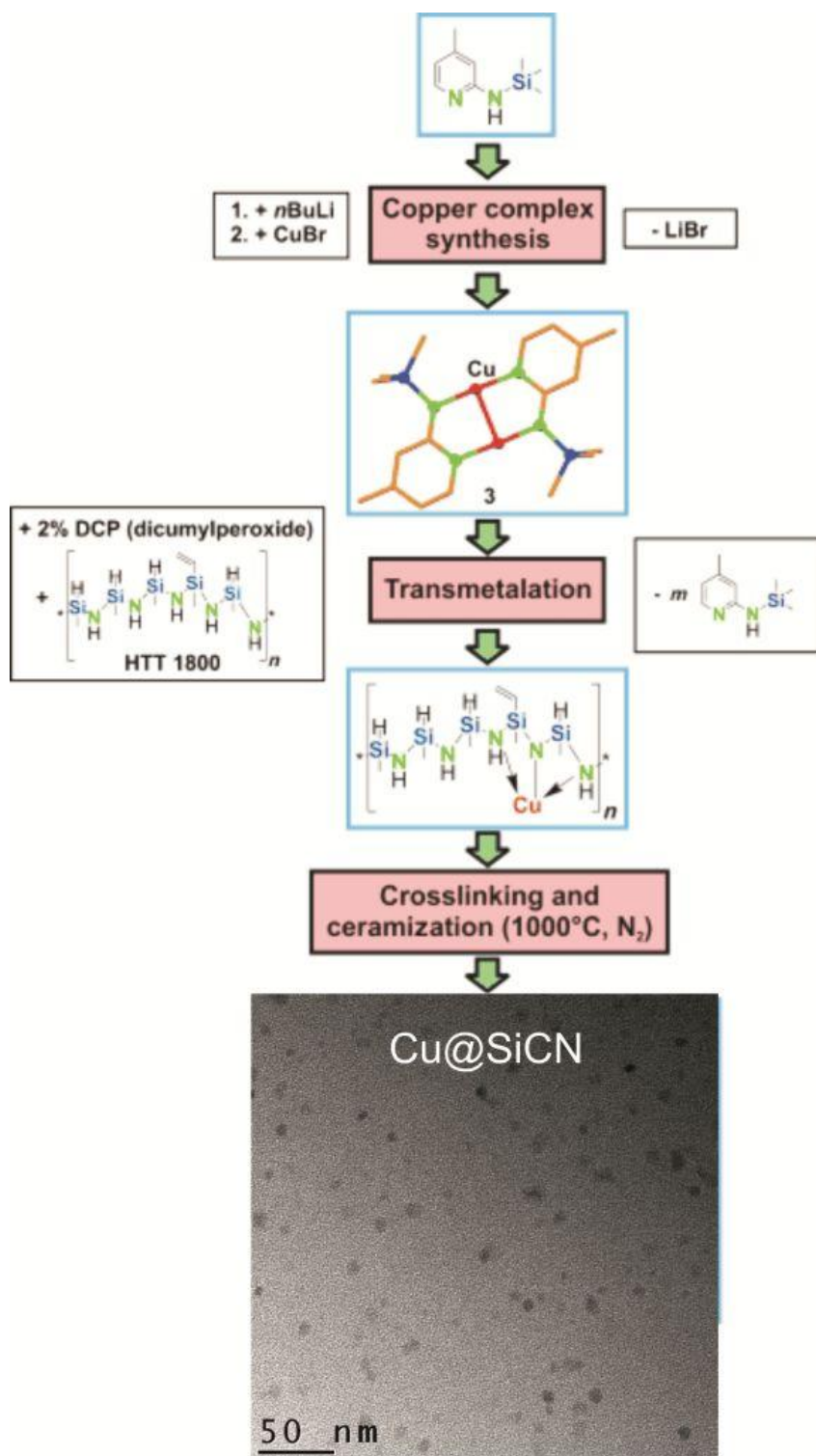


**Figure 15.** The approach to Cu@SiCN precursor ceramics *via* modification by coordination compounds: 4-methyl-N-(trimethylsilyl)pyridin-2-amine ( $\text{Ap}^{\text{TMS}}\text{H}$ ) is deprotonated with butyl lithium ( $n\text{-BuLi}$ ) and subsequently reacted with  $\text{CuBr}$  to yield the copper aminopyridinato complex  $[\text{Cu}_2(\text{Ap}^{\text{TMS}})_2]$ . This coordination compound undergoes a metal transfer reaction with the PSZ, here HTT1800, with the release of  $\text{Ap}^{\text{TMS}}\text{H}$ . After cross-linking with dicumylperoxide (DCP) at  $120^\circ\text{C}$  the preceramic green body is formed. Pyrolysis affords an amorphous SiCN ceramic enhanced by Cu nanoparticles (Cu@SiCN). For the catalytic applications of Cu@SiCN in alkane oxidation reactions using air as an oxidant please see chapter 5 b). (Reproduced after permission from ref.60, copyright 2010 Wiley-VCH Verlag GmbH & Co. KGaA, Weinheim).

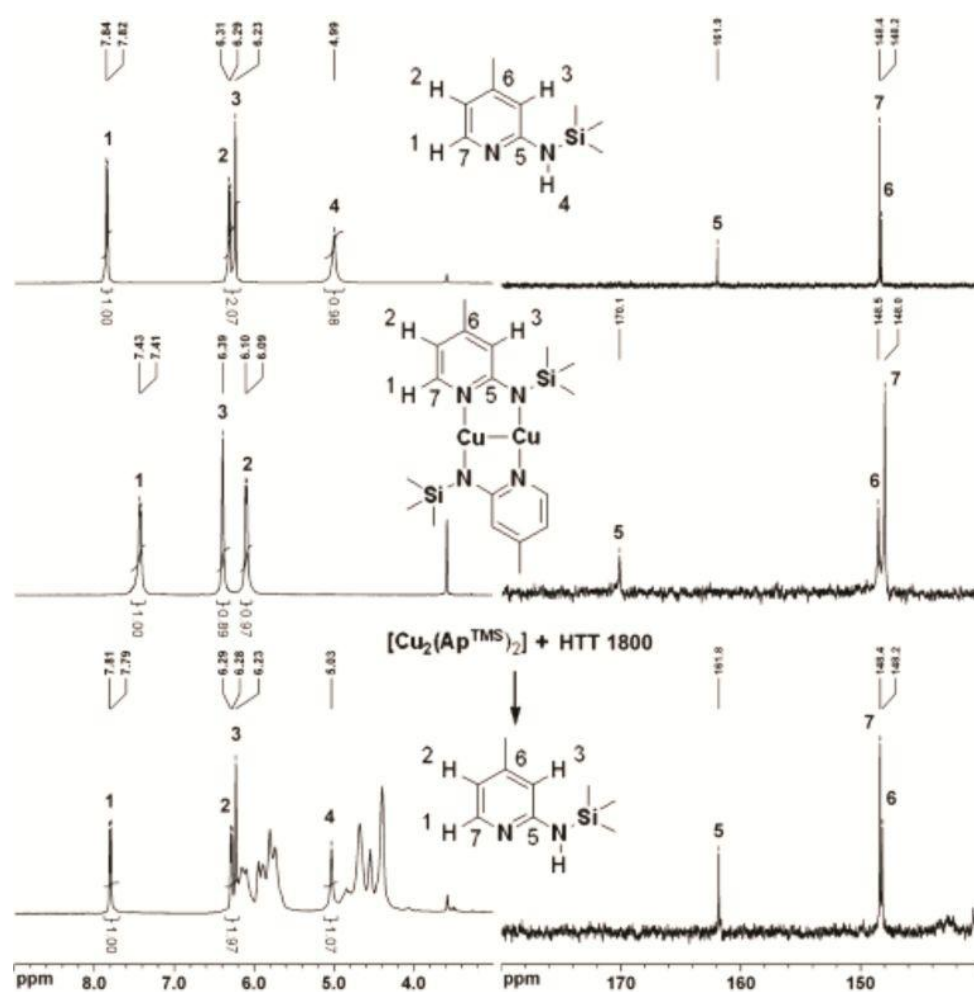


**Figure 16.**  $^1\text{H}$  (left) and  $^{13}\text{C}$  NMR spectra (right) of  $\text{Ap}^{\text{TMS}}\text{H}$  (top),  $[\text{Cu}_2\text{Ap}^{\text{TMS}}_2]$  (middle), and after its reaction with HTT1800 (bottom). (Reproduced with permission from ref. 60. Copyright 2010 Wiley-VCH Verlag GmbH & Co. KGaA, Weinheim).

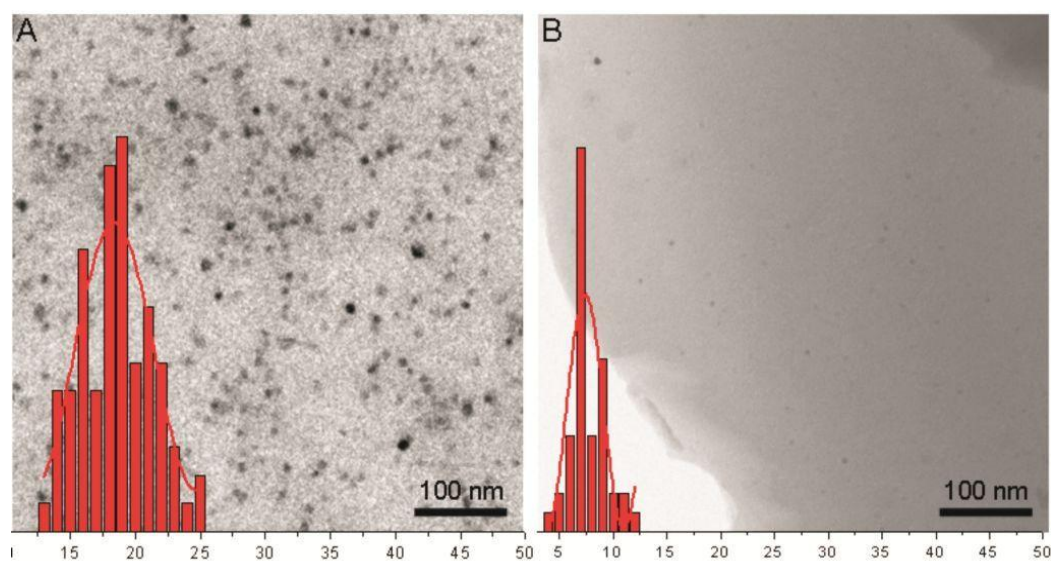


**Figure 17.** TEM micrographs of Cu@SiCN (a) Si/Cu =10 (b) Si/Cu =100 including particle size distribution statistics.

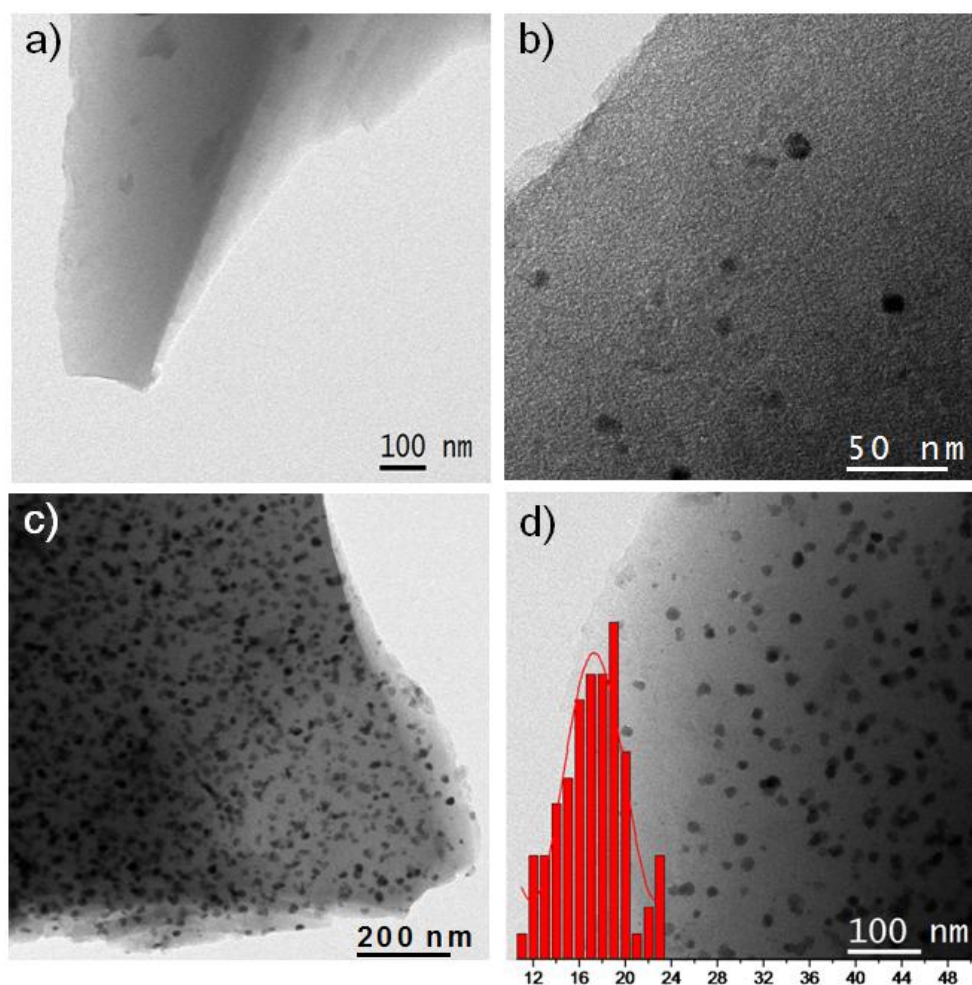


**Figure 18.** TEM micrographs of ceramic materials. a) SiCN ceramic without palladium loading does not show any particles; b) lower loading of palladium (0.2 wt%, Si/Pd ratio 1000) decreases the density of particles keeping their size in the same regime; c) Pd<sub>2</sub>Si particles uniformly distributed over the ceramic support Si/Pd = 20 (8 wt% Pd); d) particles size distribution for the sample shown in (c). (Reproduced after permission from ref. 64, copyright 2011 Royal Society of Chemistry).

porous SiCN ceramics with integrated platinum nanoparticles. Structuring of the material was achieved through a combination of micromolding and multicomponent colloidal self-assembly. The coordination compound [(cod)PtMe<sub>2</sub>] (COD = 1,5-cyclooctadiene) was used as platinum precursor. Heat treatment (1000°C under inert atmosphere) resulted in hierarchically structured porous ceramic material functionalized with Pt nanoparticles (Fig. 19).

In an attempt to couple the generation of metal nanoparticles and porosity within SiCN ceramics the chemical modification of HTT1800 with aminopyridinato complexes along with the addition of the sacrificial filler (polyethylene) was investigated.<sup>[66]</sup> In a simultaneous process, both porosity (Fig. 20) and carbon nanotubes (CNTs) (Fig. 20c, Fig. 21) were generated. The thermal decomposition of

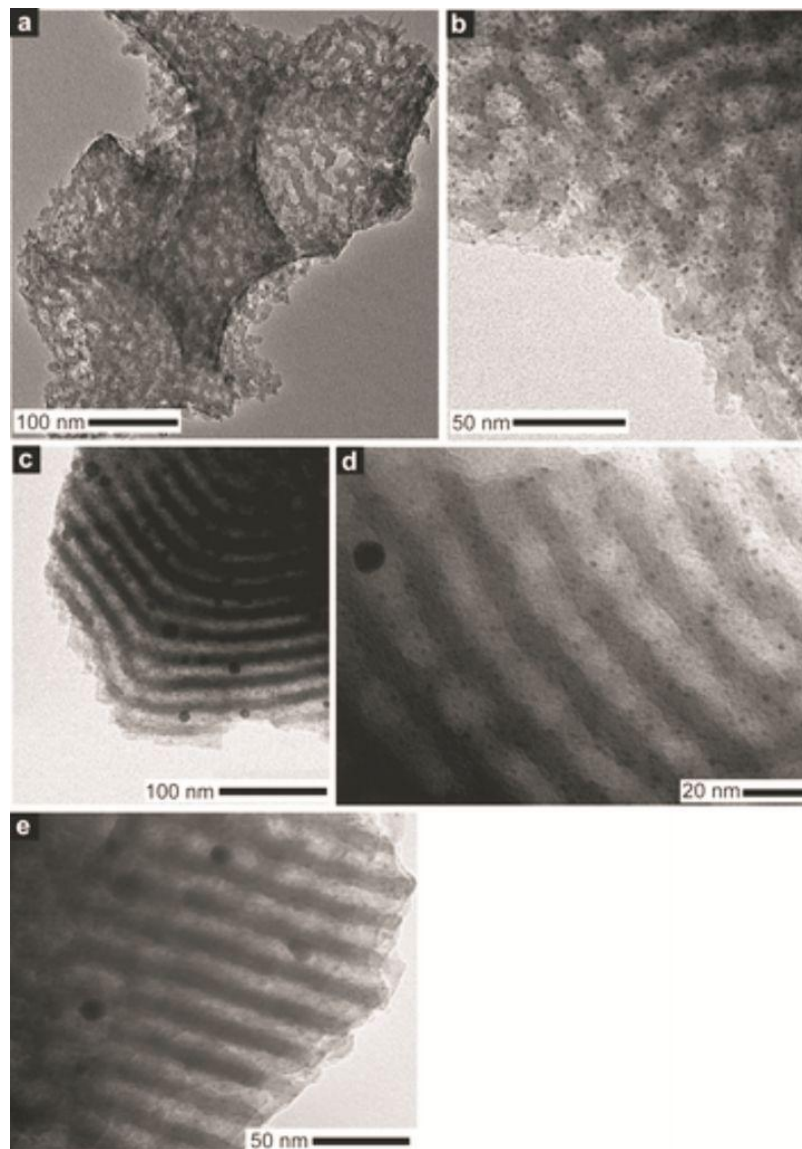


**Figure 19.** (a,b) TEM micrographs showing the Pt nanoparticles homogeneously distributed throughout the material. (c,d) TEM micrographs of material post heat treated to 600°C in air for 1 min and (e) for an additional 10h. (Reproduced after permission from ref. 65, copyright 2009 American Chemical Society).

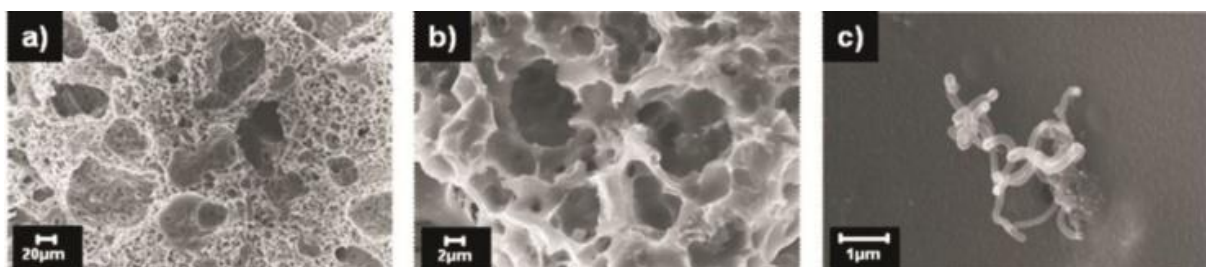


**Figure 20.** (a-c) SEM micrographs of a Au@SiCN ceramic (1000°C/N<sub>2</sub>; Au:Si = 1:50). (Reproduced after permission from ref. 66, copyright 2011 Elsevier Ltd).

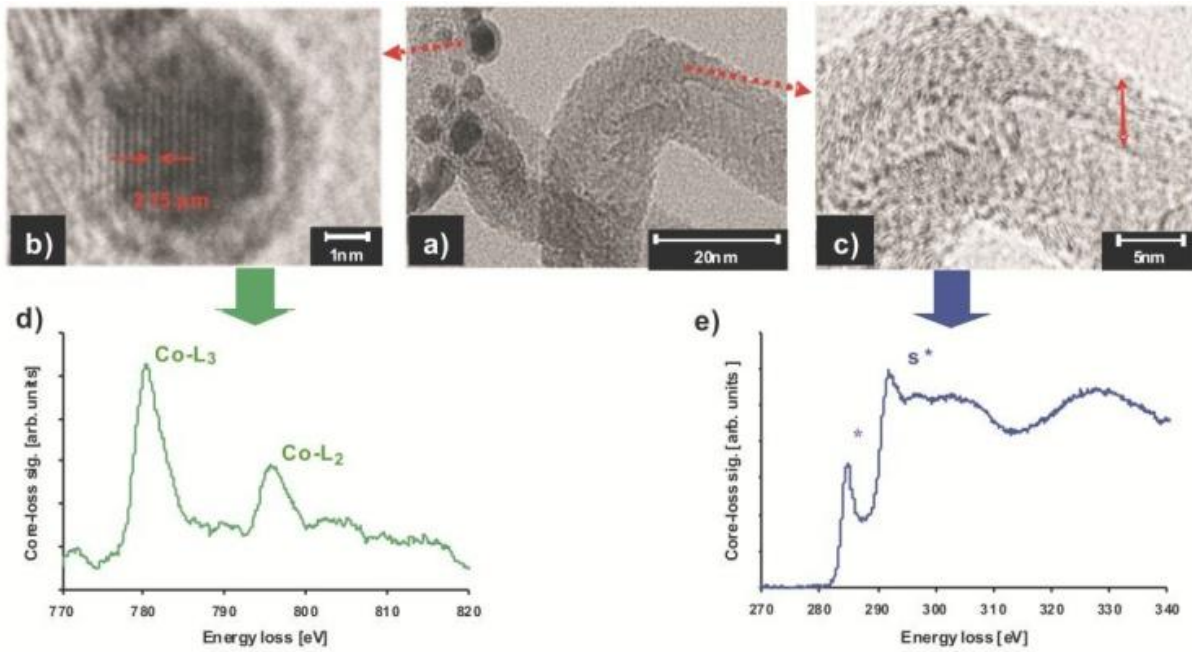


**Figure 21.** TEM micrographs of a Co@SiCN ceramic (Co:Si ratio = 1:50) (d) core-loss EELS of the metal particle (e) coreloss EELS of the carbon nanotube. (Reproduced after permission from ref. 66, copyright 2011 Elsevier Ltd).

the polyethylene leads not only to the formation of an open porosity, but also to an *in situ* reaction of its pyrolysis products with the metal nanoparticles to form the CNTs in the pores. Depending on the metal, carbon nanotubes as well as turbostratic carbon were formed in different amounts. During pyrolysis, gaseous hydrocarbons are formed whose decomposition results in the generation of CNTs *via* a chemical vapor deposition (CVD) process. Cobalt and iron were found to be more effective in the generation of nanotubes than the other metals employed.

## 5.5. Applications

### 5.5.1 Magnetic applications

Incorporating metals into non-oxide, polymer derived ceramics gives interesting magnetic properties to the ceramics depending upon the nature and size of nanosized species generated into the resulting ceramics. The crystallization of transition metals, metal oxides, carbides, nitrides and silicides leads to the magnetic properties of such composite materials. Ferromagnetism is the most commonly observed type of magnetism in these materials. Ferromagnetic materials are attracted by the applied

magnetic field owing to the presence of unpaired electrons which align parallel to each other even after the applied field is completely removed. A ferromagnetic material can further be transformed into 'superpara-magnetic material' which occurs when ferromagnetic crystallites are rather small (1–10 nm). In sufficiently small sized nanoparticles, magnetization can randomly flip direction under the influence of temperature. Thus the materials behave like a paramagnetic material but the magnetic moment of the crystallites aligns with the external magnetic field. Above a specific temperature (Curie temperature  $T_c$ ) the parallel alignment of magnetic spins is completely disordered and the material becomes paramagnetic.

SiCN ceramics synthesized by the mixing of  $\text{Fe}_3\text{O}_4$  powder with the polysilazane precursor<sup>[44]</sup> showed lower saturation magnetization ( $M_s$ : increase in the strength of the external magnetic field cannot increase the magnetization of the material further. A characteristic of the ferromagnetic materials) when pyrolyzed at 600°C than the one pyrolyzed at 1000°C. This difference in magnetization can be explained by the lower magnetization of  $\text{Fe}_3\text{O}_4$  species present at 600°C than that of  $\alpha\text{-Fe}$  particles present at 1000°C. The mixing and ball milling of Fe powder with Ceraset® resulted in the crystallization of  $\text{Fe}_3\text{Si}$  and the material showed a high saturation magnetization ( $M_s$ ) of 57 emu  $\text{g}^{-1}$ . The formation of ferromagnetic phase was attributed to the formation of  $\text{Fe}_3\text{Si}$ .<sup>[48]</sup>

The formation of metal silicides in SiCN ceramics synthesized by the mixing of metal powders with Ceraset® affects the magnetic properties which were studied at both -196°C and room temperature. The ceramics containing iron silicide ( $\text{Fe}_3\text{Si}$ ) particles show soft magnetism at both temperatures and can be easily saturated with the magnetization vector. The composites filled with Co powder show better magnetic properties than those containing Mn or Ni powder. This could be attributed to the formation of Mn and Ni silicides by the metal–matrix interactions which are absent in the case of Co.<sup>[45,46]</sup>

The Fe@SiCN ceramic synthesized by the pyrolysis of iron containing polysilazane at 500–900°C under nitrogen stream resulted in the formation of iron nanoparticles and an increase in  $M_s$  was observed with an increase of the pyrolysis temperature. When pyrolyzed under ammonia, saturation magnetization of the materials increases up to 700°C and then decreases. This behavior may be explained by the change of major magnetic crystallites present at different pyrolysis temperatures ( $\text{Fe}_3\text{N}$  at 500

and 600°C; Fe<sub>4</sub>N and Fe at 700°C; Fe at 800°C).<sup>[56]</sup>

Ceramics synthesized by the pyrolysis of ferrocene based organosilicon polymers show superparamagnetism or ferro-magnetism depending upon the pyrolysis temperature which in turn decides the size of iron nanoparticles formed.<sup>[14,52]</sup> At lower temperatures smaller size particles are formed which give superparamagnetic materials.<sup>[13,28]</sup> At higher temperatures iron clusters become larger in size giving ferromagnetic properties to the material.<sup>[15,27]</sup> A similar behavior was observed in the ceramics containing alloy particles (Co/Fe),<sup>[30,33]</sup> metal silicide particles<sup>[16,21,35]</sup> and ceramic nanowires<sup>[40]</sup> or thin films containing iron.<sup>[34]</sup> The superparamagnetic and ferromagnetic properties of the materials can also be tuned in terms of the composition of metallopolymer precursor which in turn controls the nature of crystallites formed within the ceramics.<sup>[54]</sup>

### 5.5.2 Heterogeneous catalysis

The robust nature of a ceramic makes it an ideal candidate for a catalytic support. The thermal robustness might be suitable for high temperature application like dry reforming, the conversion of methane and CO<sub>2</sub> to 'syn-gas' (CO and H<sub>2</sub>). It is also of advantage if the catalysis itself is done at lower temperature, but the catalyst reactivation, like removal of coke and other impurities, may involve high temperature steps. Secondly, a support like non-oxide SiC and SiCN ceramics differs from an oxide support in terms of polarity and acidic properties. Thirdly, non-oxide ceramics are comparatively inert and can be applied for solution phase catalysis under chemically harsh conditions, like high pH values for instance, under which oxide supports may simply dissolve. The shortage of petroleum and the resulting price increase of this fossil carbon source as well as environmental concerns require more use of alternative, preferentially, renewable resources. The different catalytic chemistry related to this change may require solution phase catalysts, which are chemically rather inert. The use of non-oxide ceramics as catalytic support materials is quite rare and only a few reports could be found in the literature. Cu@SiCN was studied in the catalytic oxidation of alkanes (cyclooctane) using air as an oxidant.<sup>[60]</sup> Oxidation of non-activated alkanes is very challenging especially if the cheap oxidant air is used. Alkanes are rather inert and thermodynamically preferred total oxidation is highly competitive. The selective formation of cyclooctanone

(monoxygenated product) was observed, which increase with a higher copper content of the used ceramics (see Fig. 22). The catalysts did not show any loss of activity up to four consequent catalytic runs. Copper is also regarded as a catalytically interesting metal due to its low price.

Furthermore, the oxidation of methane by  $O_2$  was investigated using platinum nanoparticles supported by a hierarchically structured porous SiCN ceramic.<sup>[65]</sup> Thermogravimetric analysis (TGA) did not show any substantial change in the weight of pyrolyzed structure under oxygen atmosphere at 600°C. Moreover, postpyrolysis order retention as verified by small angle X-ray scattering (SAXS) confirmed the stability of the catalyst in an oxidizing environment. The size of the particles, however, increased from 1–2 nm to 10 nm after heat treatment at 600°C. The carbon dioxide was the only product detected suggesting the total oxidation of methane under experimental conditions.

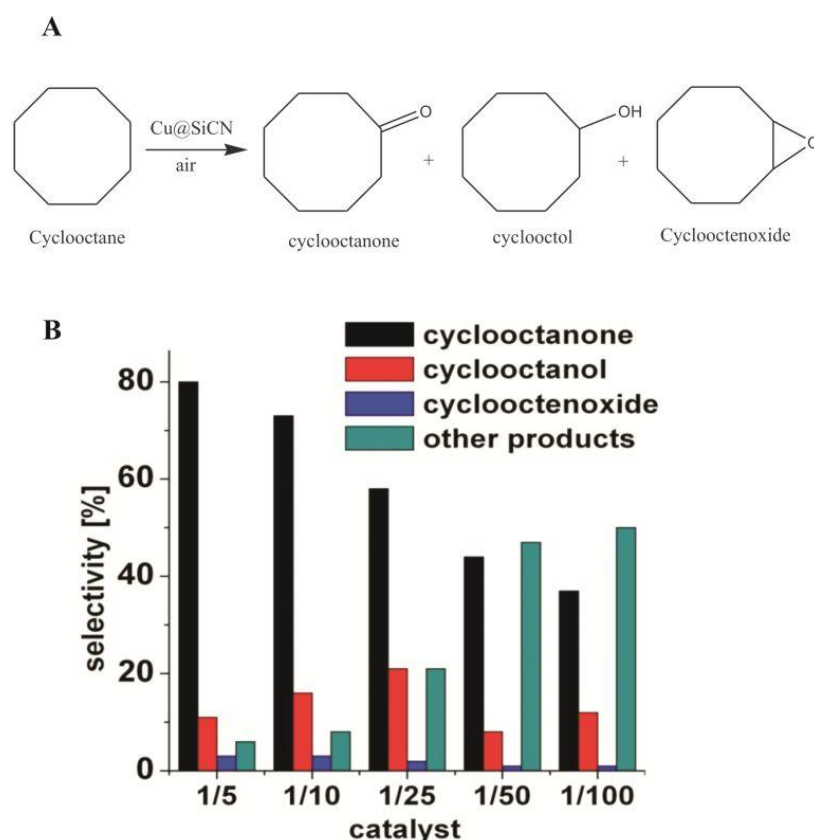


**Figure 22.** Scheme showing the formation of different products obtained by the oxidation of cyclooctane using Cu@SiCN as catalyst (A). Selectivities [%] of different catalysts (B). The copper to silicon ratios vary from 1:5 to 1:100. (Reproduced from ref. 60 after permission, copyright 2010 Wiley-VCH Verlag GmbH & Co. KGaA, Weinheim).

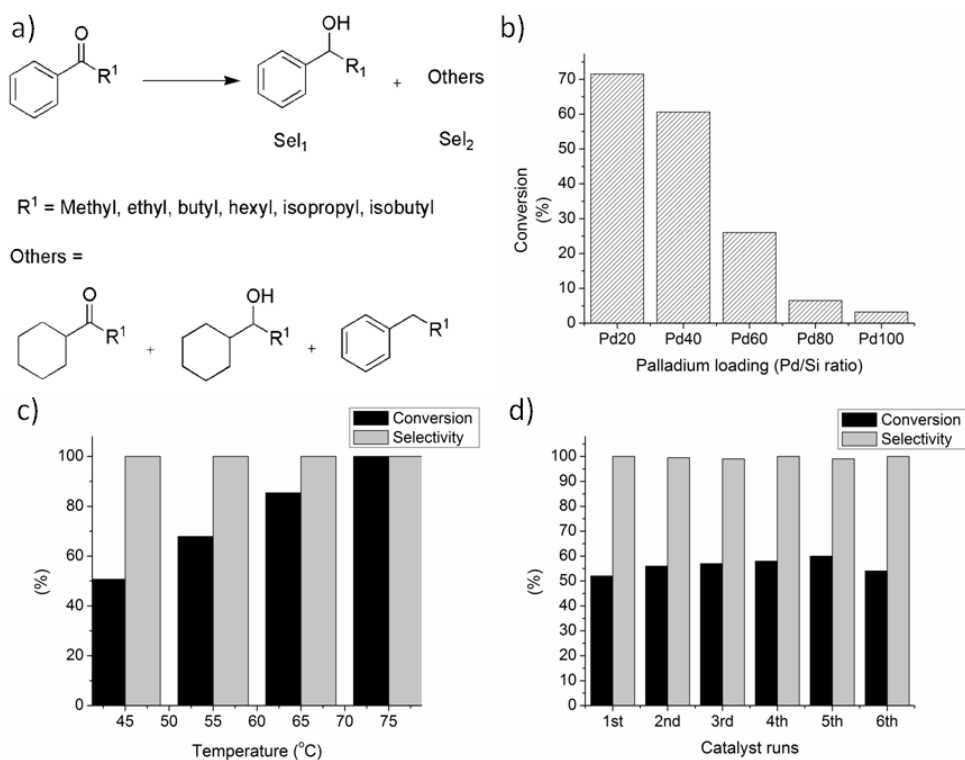


**Figure 23.** (a) Schematic representation of catalytic hydrogenation of ketones to different products; (b) hydrogenation of acetophenone (2 mmol) with 60 mg of catalyst at 75°C under 20 bar hydrogen for 24 hours. The conversion decreases with decrease in the amount of palladium contained by the ceramics; (c) hydrogenation of acetophenone (2 mmol) using Pd20 (120 mg) under 20 bar hydrogen pressure for 24 hours. The conversion increases with temperature keeping the selectivity constant; (d) hydrogenation of acetophenone (2 mmol) with the catalyst Pd20 (60 mg) under 20 bar hydrogen pressure at 75°C for 24 hours. The figure shows reusability of the catalyst up to six catalyst runs. (Reproduced with permission from ref. 64, copyright 2011 The Royal Society of Chemistry).

The catalytic total oxidation of methane was also investigated using Pt/CeO<sub>2</sub>/SiC composites.<sup>[37]</sup> The catalysts showed good catalytic activity and stability towards methane oxidation which was attributed to the presence of nanosized platinum and ceria species. The catalytic activity decreased both with the decrease in specific surface area and the amount of ceria contained by the catalysts. Palladium silicide containing SiCN catalysts (Pd<sub>2</sub>Si@SiCN) were used for the selective hydrogenation of aromatic ketones.<sup>[64]</sup> The selectivity of the reaction towards alcoholic products remained very high and did not change with the amount of palladium or with the amount of catalysts added. The conversion increased both with the increase in the reaction temperature and the amount of catalyst used, while it decreased with the increase in alkyl chain length and its branching at  $\alpha$ -carbon. The catalysts manifested appreciable reusability and no loss in the activity of the catalysts was observed up to six consecutive catalyst runs (Fig. 23).

### 5.5.3 Other applications

Some M@SiCN ceramics, containing copper or silver nanoparticles, could be used in medical applications, as they can act as fungicides (Cu) or bactericides (Ag). So, for example, some silver modified PDCs have been tested in detail for their antibacterial potentials and show strong activities against some of the bacterial species (*Escherichia coli* and *Staphylococcus aureus*).<sup>[50]</sup>

### 5.6. Conclusions and outlook

The relatively young materials based on polymer derived ceramics should be a promising technology for different challenging applications in the future. This article gives an overview of the rather rare examples of non-oxide PDCs modified by late transition metals. The different possible synthesis strategies for the desired metal modification of SiC and SiCN ceramics are the simple addition of metal (oxide) powders to the precursors (i), the development of well defined metallopolymers (ii), and the rather new way of using metal coordination compounds for the metal transfer reactions (iii).

The first mentioned way is limited by the size of the used metal (oxide) powders, while in the case of (ii) and (iii) a bottom-up approach, coming from the atomic scale, is realized. This offers, at least theoretically, the possibility to tune the size of the formed metal nanoparticles inside the derived PDCs.

In content with metallopolymers a lot of work dealing with ferrocene containing systems was published, while in the case of the modification by coordination compounds, the use of amino-pyridinato complexes is very actual. Up to now it was possible to synthesize and characterize several chemically modified precursors using a series of specially developed, partially new aminopyridinato complexes, which act as metal transfer reagents towards the N-functionalities of polysilazanes. One important point along this way, was getting analytical evidence exactly for these metal–nitrogen bonds, which we were able to receive from NMR spectroscopy, at least in parts. This new technique for highly disperse loading of active particles onto ceramic structures by a direct chemical bond between the metal and precursor has been successfully demonstrated and the considerable advantages gained over other, conventional processes, could be verified. As these coordination compounds are

available for nearly all transition elements, the corresponding modifications should be possible.

For all the manufactured metal containing non-oxide ceramics numerous analytical techniques were used to get evidence for the present morphologies, structures and compositions of both ceramic materials and metal (nano) particles.

Some examples of potential applications of the iron modified polymer derived ceramics, especially in the use of their magnetic properties, are given. The use of M@SiC/SiCN systems for different catalytic transformations is described.

As ceramics will have increasing applications as membranes, filter materials or catalysts in future, also the materials based on precursor derived ceramics should be further developed in these fields. The metal modified polymer systems, which can be thermally converted into the ceramic materials, are promising candidates therefore. In future, new combinations of metal/precursor should be tested to enable the development of “tailored” precursor ceramics for more and other applications in catalysis, filter technique or also for example the fields of energy conservation (e.g. hydrogen storage), environmental protection or fuel cells. Clearly, therefore much additional development work is necessary.

### **Acknowledgements**

Financial support from the Deutsche Forschungsgemeinschaft (DFG) in context of the SPP 1181: ‘Nanoscaled Inorganic Materials by Molecular Design: New Materials for Advanced Technologies’ is gratefully acknowledged.

### **5.7 References**

- [1] *Polymer derived Ceramics—From Nano-Structure to Applications*, ed. P. Colombo, R. Riedel, G. D. Soraru and H.-J. Kleebe, DEStech Publications, Pennsylvania, **2010**.
- [2] R. Riedel, G. Mera, R. Hauser and A. Klönczyski, *J. Ceram. Soc. Jpn.* **2006**, *114*, 425–444.
- [3] P. Miele, S. Bernard, C. Cornu and B. Toury, *Recent developments in polymer-derived ceramic fibers (PDCFs): preparation, properties and*

- applications—A review*, *Soft Mater.* Vol. 4, Taylor & Francis, Inc. **2007**, vol. 4, p. 249–286.
- [4] P. Miele and S. Bernard, *Boron- and nitrogen-containing polymers for advanced materials*, *Macromolecules Containing Metal and Metal-Like Elements*, 8 (boron-containing polymers), John Wiley & Sons, Inc. **2007**, p. 103–120.
- [5] H. Schmidt, *Si-(B-)C-N ceramics derived from preceramic polymers: stability and nano-composite formation*. *Soft Mater.* Vol. 4, Taylor & Francis, Inc. **2007**, p. 143–164.
- [6] S. Yajima, T. Shishido and H. Kayano, *Nature* **1976**, 264, 237–238.
- [7] R. J. P. Corriu, P. Gerbier, C. Guerin and B. Henner, *J. Mater. Chem.* **2000**, 10, 2173–2182.
- [8] D. Seyferth, H. Lang, C. A. Sobon, J. Borm, H. J. Tracy and N. Bryson, *J. Inorg. Organomet. Polym. Mater.* **1992**, 2, 59–77.
- [9] G. R. Whittell and I. Manners, *Adv. Mater.* **2007**, 19, 3439–3468.
- [10] B.-Z. Tang, R. Petersen, D. A. Foucher, A. Lough, N. Coombs, R. Sodhib and I. Manners, *J. Chem. Soc., Chem. Commun.* **1993**, 523–525.
- [11] R. Petersen, D. A. Foucher, B.-Z. Tang, A. Laugh, N. P. Raju, J. E. Greedan and I. Manners, *Chem. Mater.* **1995**, 7, 2045–2053.
- [12] M. J. MacLachlan, P. Aroca, N. Coombs, I. Manners and G. A. Ozin, *Adv. Mater.* **1998**, 10, 144–149.
- [13] M. J. MacLachlan, M. Ginzburg, N. Coombs, N. P. Raju, J. E. Greedan, G. A. Ozin and I. Manners, *J. Am. Chem. Soc.* **2000**, 122, 3878–3891.
- [14] M. J. MacLachlan, M. Ginzburg, N. Coombs, T. W. Coyle, N. P. Raju, J. E. Greeden, G. A. Ozin and I. Manners, *Science* **2000**, 287, 1460–1463.

- [15] M. Ginzburg, M. J. MacLachlan, S. M. Yang, N. Coombs, T. W. Coyle, N. P. Raju, J. E. Greedan, R. H. Herber, G. A. Ozin and I. Manners, *J. Am. Chem. Soc.* **2002**, *124*, 2625–2639.
- [16] Q. Sun, J. W. Y. Lam, K. Xu, H. Xu, J. A. K. Cha, P. C. L. Wong, G. Wen, X. Zhang, X. Jing, F. Wang and B. Z. Tang, *Chem. Mater.* **2000**, *12*, 2617–2624.
- [17] M. G. Margau, S. F. Bidoz, N. Coombs, G. A. Ozin and I. Manners, *Chem. Commun.* **2002**, 3022–3023.
- [18] K. Liu, S. F. Bidoz, G. A. Ozin and I. Manners, *Chem. Mater.* **2009**, *21*, 1781–1783.
- [19] J. Galloro, M. Ginzburg, H. Miguez, S. M. Yang, N. Coombs, A. S. Stéfati, J. E. Greedan, I. Manners and G. A. Ozin, *Adv. Funct. Mater.* **2002**, *12*, 382–388.
- [20] Y. Yu, L. An, Y. Chen and D. Yang, *J. Am. Ceram. Soc.* **2010**, *93*, 3324–3329.
- [21] V. A. Du, A. Sidorenko, O. Bethge, S. Paschan, E. Bertagnolli and U. Schubert, *J. Mater. Chem.* **2011**, *21*, 12232–12238.
- [22] J. Massey, K. N. Power, I. Manners and M. A. Winnik, *J. Am. Chem. Soc.* **1998**, *120*, 9533–9540.
- [23] J. A. Massey, M. A. Winnik and I. Manners, *J. Am. Chem. Soc.* **2001**, *123*, 3147–3148.
- [24] X.-S. Wang, A. Arsenault, G. A. Ozin, M. A. Winnik and I. Manners, *J. Am. Chem. Soc.* **2003**, *125*, 12686–12687.
- [25] L. Cao, J. A. Massey, M. A. Winnik, I. Manners, S. Riethmüller, F. Banhart, J. P. Spatz and M. Möller, *Adv. Funct. Mater.* **2003**, *13*, 271–276.
- [26] D. A. Rider, K. Liu, J.-C. Eloi, L. Vanderark, L. Yang, J.-Y. Wang, D. Grozea, Z.-H. Lu, T. P. Russell and I. Manners, *ACS Nano* **2008**, *2*, 263–270.

- [27] K. Kulbaba, A. Cheng, A. Bartole, S. Greenberg, R. Resendes, N. Coombs, A. S. Sefat, J. E. Greedan, H. D. A. Stöver, G. A. Ozin and I. Manners, *J. Am. Chem. Soc.* **2002**, *124*, 12522–12534.
- [28] K. Temple, K. Kulbaba, K. N. P. Billard, I. Manners, K. A. Leach, T. Xu, T. P. Russell and C. J. Hawker, *Adv. Mater.* **2003**, *15*, 297–300.
- [29] A. Berenbaum, M. G. Margau, N. Coombs, A. J. Lough, A. S. Sefat, J. E. Greedan, G. A. Ozin and I. Manners, *Adv. Mater.* **2003**, *15*, 51–55.
- [30] S. B. Clendenning, S. F. Bidoz, A. Pietrangelo, G. Yang, S. Han, P. M. Brodersen, C. M. Yip, Z.-H. Lu, G. A. Ozin and I. Manners, *J. Mater. Chem.* **2004**, *14*, 1686–1690.
- [31] A. Y. Cheng, S. B. Clendenning, G. Yang, Z.-H. Lu, C. M. Yip and I. Manners, *Chem. Commun.* **2004**, 780–781.
- [32] S. B. Clendenning, S. Han, N. Coombs, C. Paquet, M. S. Rayat, D. Grozea, P. M. Brodersen, R. N. S. Sodhi, C. M. Yip, Z.-H. Lu and I. Manners, *Adv. Mater.* **2004**, *16*, 291–296.
- [33] K. Liu, S. B. Clendenning, L. Friebe, W. Y. Chan, X. Zhu, M. R. Freeman, G. C. Yang, C. M. Yip, D. Grozea, Z.-H. Lu and I. Manners, *Chem. Mater.* **2006**, *18*, 2591–2601.
- [34] K. R. Thomas, A. Ionescu, J. Gwyther, I. Manners, C. H. W. Barnes, U. Steiner and E. Sivaniah, *J. Appl. Phys.* **2011**, *109*, 073904.
- [35] L. Friebe, K. Liu, B. Obermeier, S. Petrov, P. Dube and I. Manners, *Chem. Mater.* **2007**, *19*, 2630–2640.
- [36] R. J. P. Corriu, N. Devylder, C. Guerin, B. Henner and A. Jean, *J. Organomet. Chem.* **1996**, *509*, 249–257.
- [37] E. Kockrick, R. Frind, M. Rose, U. Petasch, W. Boehlmann, D. Gieger, M. Herrmann and S. Kaskel, *J. Mater. Chem.* **2009**, *19*, 1543–1553.
- [38] D. Seyferth, H. Lang, C. A. Sobon, J. Borm, H. J. Tracy and N. Bryson, *J. Inorg. Organomet. Polym.* **1992**, *2*, 59–77.

- [39] D. Seyferth, C. A. Sobon and J. Borm, *New J. Chem.* **1990**, *14*, 545–547.
- [40] R. Mishra, R. K. Tiwari and A. K. Saxena, *J. Inorg. Organomet. Polym. Mater.* **2009**, *19*, 223–227.
- [41] X. Chen, Z. Su, L. Zhang, M. Tang, Y. Yu, L. Zhang and L. Chen, *J. Am. Ceram. Soc.* **2010**, *93*, 89–95.
- [42] C. Vakifahmetoglu, E. Pippel, J. Woltersdorf and P. Colombo, *J. Am. Ceram. Soc.* **2010**, *93*, 959–968.
- [43] C. Vakifahmetoglu, P. Colombo, S. M. Carturan, E. Pippel and J. Woltersdorf, *J. Am. Ceram. Soc.* **2010**, *93*, 3709–3719.
- [44] A. Saha, S. R. Shah and R. Raj, *J. Mater. Res.* **2003**, *18*, 2549–2551.
- [45] X. Yan, X. Cheng, G. Han, R. Hauser and R. Riedel, *Key Eng. Mater.* **2007**, *353–358*, 1485–1488.
- [46] X. Yan, X. Cheng, C. Li, R. Hauser and R. Riedel, *Mater. Sci. Forum* **2007**, *546–549*, 2269–2272.
- [47] H.-Y. Ryu and R. Raj, *J. Am. Ceram. Soc.* **2007**, *90*, 295–297.
- [48] R. Hauser, A. Francis, R. Theismann and R. Riedel, *J. Mater. Sci.* **2008**, *43*, 2042–2049.
- [49] A. Francis, E. Ionescu, C. Fasel and R. Riedel, *Inorg. Chem.* **2009**, *48*, 10078–10083.
- [50] V. Bakumov, K. Gueinzius, C. Hermann, M. Schwarz and E. Kroke, *J. Eur. Ceram. Soc.* **2007**, *27*, 3287–3292.
- [51] X. Hu, Y. Li and C. Xu, *J. Appl. Polym. Sci.* **2010**, *118*, 3384–3390.
- [52] J. Li, Z. Zhang, Z. Zheng, L. Guo, G. Xu and Z. Xie, *J. Appl. Polym. Sci.* **2007**, *105*, 1786–1792.
- [53] A. Dumitru, I. Stamatina, A. Moroza, C. Mirea and V. Ciupina, *Mater. Sci. Eng. C*, **2007**, *27*, 1331–1337.

- [54] A. Dumitru, A. Morozan, C. Mirea, D. Mihaiescu, C. Panaiotu, V. Ciupina and I. Stamatina, *Combust. Sci. Technol.* **2005**, *65*, 713–717.
- [55] A. Dumitru, V. Ciupina, I. Stamatina, G. Prodan, A. Morozan and C. Mirea, *J. Optoelectron. Adv. Mater.* **2006**, *8*, 50–54.
- [56] Y. Li, Z. Zheng, C. Reng, Z. Zhang, W. Gao, S. Yang and Z. Xie, *Appl. Organomet. Chem.* **2003**, *17*, 120–126.
- [57] J. H. Park, K. H. Park and D. P. Kim, *J. Ind. Eng. Chem.* **2007**, *13*, 27–32.
- [58] S. I. Andronenko, I. Stiharu, D. Menard, C. Lacroix and S. K. Misra, *Appl. Magn. Reson.* **2010**, *38*, 385–402.
- [59] M. S. Bazarjani, H.-J. Kleebe, M. M. Müller, C. Fasel, M. B. Yazdi, A. Gurlo and R. Riedel, *Chem. Mater.* **2011**, *23*, 4112–4123.
- [60] G. Glatz, T. Schmalz, T. Kraus, F. Haarmann, G. Motz and R. Kempe, *Chem. Eur. J.* **2010**, *16*, 4231–4238.
- [61] For a review article on aminopyridinato ligands see: R. Kempe, *Eur. J. Inorg. Chem.* **2003**, 791–803.
- [62] For discussion of the binding modes see: S. Deeken, G. Motz and R. Kempe, *Z. Anorg. Allg. Chem.* **2007**, *633*, 320–325.
- [63] For the general applicability of these ligands please see: G. Glatz, G. Motz and R. Kempe, *Z. Anorg. Allg. Chem.* **2008**, *634*, 2897–2902.
- [64] M. Zaheer, G. Motz and R. Kempe, *J. Mater. Chem.* **2011**, *21*, 18825–18831.
- [65] M. Kamperman, A. Burns, R. Weissgraeber, N. V. Vegten, S. C. Warren, S. M. Gruner, A. Baiker and U. Wiesner, *Nano Lett.* **2009**, *9*, 2756–2762.
- [66] T. Schmalz, T. Kraus, M. Guenther, C. Liebscher, U. Glatzel, R. Kempe and G. Motz, *Carbon* **2011**, *49*, 3065–3072.

## 6. Robust Microporous Monoliths with Integrated Catalytically Active Metal Sites Investigated by Hyperpolarized $^{129}\text{Xe}$ NMR

---

Muhammad Zaheer,<sup>[a]</sup> Caroline D. Keenan,<sup>[b]</sup> Justus, Hermannsdörfer,<sup>[a]</sup> Ernest Roessler,<sup>[c]</sup> Guenter Motz,<sup>[d]</sup> Jürgen Senker,<sup>[b]</sup> Rhett Kempe<sup>[a]\*</sup>

[a] Inorganic Chemistry II, University of Bayreuth, 95440 Bayreuth, E-mail: [kempe@uni-bayreuth.de](mailto:kempe@uni-bayreuth.de) [b] Inorganic Chemistry III, University of Bayreuth, 95440 Bayreuth, E-mail: [juegen.senker@uni-bayreuth.de](mailto:juegen.senker@uni-bayreuth.de) [c] Experimental Physics II, University of Bayreuth, 95440 Bayreuth, E-mail: [ernest.roessler@uni-bayreuth.de](mailto:ernest.roessler@uni-bayreuth.de) [d] Ceramic Materials Engineering, University of Bayreuth, 95447 Bayreuth, E-mail: [guenter.motz@uni-bayreuth.de](mailto:guenter.motz@uni-bayreuth.de)

**Published in:** *Chem. Mater.* **2012**, *24*, 3952-3963.

**Abstract:** Robust microporous nanocomposites (specific surface area  $\approx 400 \text{ m}^2/\text{g}$ ) containing nickel nanoparticles have been synthesized and characterized by thermogravimetric analysis (TGA), differential thermal analysis (DTA), Fourier transform infrared (FT-IR) spectroscopy, nitrogen physisorption, powder X-ray diffraction (XRD), transmission electron microscopy (TEM), and  $^{13}\text{C}$  and  $^{29}\text{Si}$  solid-state nuclear magnetic resonance (NMR) spectroscopy. The commercially available polysilazane (HTT-1800) is chemically modified using an N-ligand-stabilized nickel complex that catalyzes the cross-linking of the polymer *via* hydrosilylation at room temperature. Upon pyrolysis at  $600^\circ\text{C}$  under an inert atmosphere, nickel nanoparticles and micropores are generated in a concerted process. The specific surface area, pore volume, and size of the nickel particles can be tuned. The materials show excellent shape retention upon pyrolysis providing the possibility to fabricate monoliths. The composites are stable in the presence of moisture and are

both thermally and solvothermally robust, as indicated by the nitrogen adsorption, FT-IR, and TGA measurements. Continuous-flow, hyperpolarized  $^{129}\text{Xe}$  NMR methods were used in tandem to evaluate the effects of the nickel content and annealing time on the pore structure of the microporous nanocomposite. The adsorption enthalpy is rather independent of nickel particle inclusion. The interior adsorption sites are lined with methyl groups and the nickel particles seem to be located near the external surface of the composites and within the internal voids. The nickel nanoparticles were used to catalyze selective hydrogenation reactions indicating applications of the nanocomposites as catalyst itself or as catalyst support.

## 6.1 Introduction

The design of microporous materials (MPMs) is of high scientific and technological interest, because of the wide range of applications offered by these materials in sorption, separation, and catalysis.<sup>[1-6]</sup> The distribution of the size, shape, and volume of the pores decides the ability of solids to perform a specific function in a particular application.<sup>[7]</sup> Highly crystalline zeolites are perhaps the most widely used MPMs. They possess pores with molecular dimensions that allow the selective movement of molecules through them.<sup>[8]</sup> Together with the presence of acidic sites and narrow pore size distribution, zeolites have been used as acid- and shape-selective catalysts<sup>[9]</sup> in petrochemical industries<sup>[10]</sup> and, more recently, biomass conversion.<sup>[11-12]</sup>

Although zeolites offer higher thermal and hydrothermal stabilities,<sup>[13]</sup> compared to the carbon and other silica-based porous materials,<sup>[7]</sup> they do not facilitate the fabrication of monoliths, which afford lower pressure drops at a given geometric surface area.<sup>[14]</sup> Moreover, the characteristic small pores, typically in the 0.3–0.7 nm range, impose severe mass transport constraints.<sup>[15]</sup> This limitation led to the development of other zeotypes (metallophosphates, and related materials<sup>[16]</sup>) and metal-organic frameworks (MOFs).<sup>[17]</sup> These microporous materials possess larger pores, compared to zeolites, but are usually less stable.<sup>[7]</sup>

MOFs have been intensively used as heterogeneous catalysts<sup>[18]</sup> but are limited only to low-temperature catalytic transformations, because of the poor thermal and hydrothermal stability offered by them.<sup>[7]</sup> In the past decade, amorphous microporous materials such as polymers of intrinsic porosity (PIMs),<sup>[19]</sup> porous aromatic

frameworks (PAFs),<sup>[20]</sup> covalent organic frameworks (COFs),<sup>[21]</sup> porous polymer networks (PPNs),<sup>[22]</sup> and sol-gel-derived materials<sup>[23,24]</sup> have been synthesized and investigated for their potential applications. These materials show very high surface areas and high uptake of gases (hydrogen, carbon dioxide) but afford less thermal and hydrothermal stability, compared to the conventional microporous solids, which limits their potential use as catalyst support materials.

We have recently studied the formation of metal nanoparticles in SiCN nanocomposites, as well as catalytic applications of these hybrid materials.<sup>[25-28]</sup> Unfortunately, most of the generated metal nanoparticles are not accessible for catalysis, since they are deeply embedded in the ceramic support material. On the other hand, we developed M@MOF catalysts, metal nanoparticles stabilized in highly porous MOFs that suffer from low thermal stability of the porous host or catalyst support.<sup>[29-32]</sup> Here, we report on the synthesis and characterization of a new type of microporous nanocomposites with catalytically active nickel nanoparticles. In addition to standard characterization methods,  $^{13}\text{C}$  and  $^{29}\text{Si}$  solid-state nuclear magnetic resonance (NMR) spectroscopic techniques are used to elucidate the effect of the size and amount of nickel on the chemical structure of the nanocomposite with increasing nickel content and metal particulate size. The materials manifest good thermal stabilities and fine-tuning of surface area and the size of metal particles are possible. The selective catalytic hydrogenation demonstrates the catalytic potential of these materials. Furthermore, applications as robust catalyst supports can be expected. The presence of nitrogen sites may also provide basic properties to the composites extending their application to base catalysis.<sup>[33]</sup>

Continuous-flow hyperpolarized (CF-HP)  $^{129}\text{Xe}$  NMR was employed as a noninvasive probe of the pore architecture and Xe adsorption capacities within the microporous SiCN nanocomposite materials. The observed  $^{129}\text{Xe}$  chemical shift ( $\bar{\delta}_{\text{obs}}$ ) reflects even small changes in the local environment of Xe, indicating modifications in porosity, enthalpies of adsorption, as well as pore connectivity and accessibility.<sup>[34-39]</sup> As such, it is an invaluable tool to detect subtle changes in physical and chemical environments within porous materials, because of the high polarizability of its electron cloud. The significant increase in the signal-to-noise ratio afforded by hyperpolarization methods reduce the experiment time from hours to seconds.<sup>[39-42]</sup> The resulting spectral enhancement is unique in that it has the capability to allow

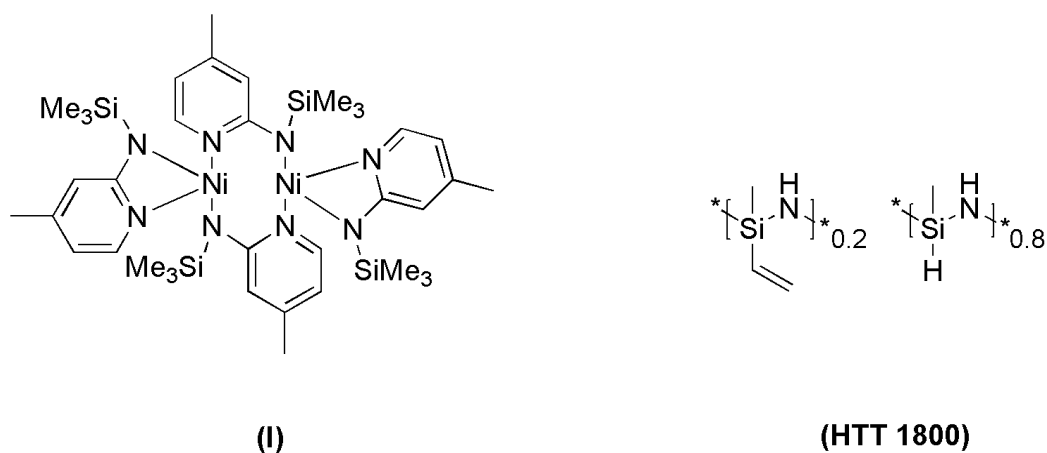
one to probe specific Xe surface interactions, which can yield information about micropore size<sup>[43]</sup> and degree of surface heterogeneity.<sup>[44]</sup> It has not only been proven sensitive to the changes in amorphous polymer structure with cross-linking,<sup>[45]</sup> but also has been shown to be useful in the characterization of paramagnetic metal particles confined within zeolites with varying cluster size.<sup>[46, 47]</sup> Here, we use  $^{129}\text{Xe}$  NMR as a tool to monitor the subsequent effects of Ni-particle inclusion on the internal surfaces of the hybrid nanocomposite material.

## 6.2 Experimental

### 6.2.1 General Remarks

All reactions were carried out under dry argon using standard Schlenk and glovebox techniques. Solvents were dried and distilled from sodium benzophenone before use. Deuterated solvents obtained from Cambridge Isotope Laboratories were degassed, dried using molecular sieves, and distilled prior to use. 2-Amino-4-picoline, chlorotrimethylsilane, phenylacetylene (Sigma–Aldrich), *n*-butyl lithium, dodecane (ACROS Chemicals), *p*-tolylacetylene, *m*-tolylacetylene, 4-*tert*-butylphenylacetylene, 4-fluorophenylacetylene, 4-methoxyphenylacetylene (Alfa-Aesar), and polyorganosilazane (HTT-1800, Clariant GmbH, Sulzbach, Germany) were used as-received without any further purification.

The starting materials 4-methyl-2-((trimethylsilyl)amino)pyridine ( $\text{Ap}^{\text{TMSH}}$ ), and complex I (see Scheme 1) were synthesized following reported methods.<sup>[48, 49]</sup>



**Scheme 1.** The molecular structure of polysilazane (HTT-1800) and the amido nickel complex (I).

### 6.2.2 Cross-Linking, Metal Transfer, and Pyrolysis

Polyorganosilazane HTT-1800 (3.218 g) was reacted with  $[\text{Ni}(\text{Ap}^{\text{TMS}})_2]_2$  (Ni-10: Si/Ni 10/1, 2.08 g, 2.49 mmol; Ni-20: Si/Ni 20/1, 1.04 g, 1.25 mmol; Ni-100: Si/Ni 100/1, 0.20 g, 0.25 mmol; Ni-133: Si/Ni 133/1, 0.15 g, 0.18 mmol) in 5 mL Tetrahydrofuran (THF). The solvent was evaporated under vacuum and obtained gels were pyrolyzed in a furnace (Nabertherm LH 60/14, Nabertherm, Germany) under nitrogen stream (from room temperature to 300°C (holding for 2 h) in 5 h, heating from 300°C to 600°C (holding for 2 h) in 5 h and finally cooling back to room temperature.

### 6.2.3 Solid-State NMR

All data were acquired at room temperature and externally referenced to TMS using adamantane and tris(trimethylsilyl)amine for  $^{13}\text{C}$  and  $^{29}\text{Si}$  nuclei, respectively. A broad band  $^1\text{H}$  decoupling with a SPINAL-64 sequence ( $\nu_{\text{nut}} = 70$  kHz) was used for all measurements.

Solid-state  $^{29}\text{Si}$  and  $^{13}\text{C}$  NMR spectra of the cross-linked HTT-1800 were carried out on a DSX 400 Bruker Avance NMR spectrometer using a Hahn-echo pulse sequence under magic-angle spinning (MAS). The rotational frequency was set to 12.5 kHz. The spectra were recorded with a recycle delay of 600 and 60 s for the  $^{29}\text{Si}$  and  $^{13}\text{C}$  MAS NMR, respectively. A  $\pi/2$  pulse length of  $\sim 3.3$   $\mu\text{s}$  was used for both.

Pyrolyzed samples were characterized by ramped  $^{29}\text{Si}\{^1\text{H}\}$  and  $^{13}\text{C}\{^1\text{H}\}$  cross-polarization (CP) MAS and single-pulse excitation (HPDEC)  $^{29}\text{Si}$  MAS NMR techniques, recorded on a commercial Avance II 300 Bruker spectrometer equipped with a standard triple resonance 7-mm MAS probe.<sup>[50]</sup> Typical recycle delays were 3.0 and 60 s, respectively. Spectra were accumulated at a rotation frequency of 4.0 kHz. The average  $^1\text{H}$  field strength was set to 60 kHz. The X channel nutation frequency was adjusted to 56 kHz to match the Hartmann–Hahn condition. The contact time ( $T_{\text{CP}}$ ) was set between 2 ms and 5 ms, depending on the sample.

The  $^{29}\text{Si}$  MAS spectra from both the CP and HPDEC experiments were deconvoluted using a scripted MATLAB protocol, fitting Lorentz–Gaussian peaks with upper and lower bounds for spectral linewidth, chemical shift, and amplitude. Comparison of the two experiments showed little difference in relative peak amplitudes, although the two peaks furthest upfield exhibit a weaker  $^1\text{H}$  dipolar interaction, which is expected.

Quantification of  $^{29}\text{Si}$  silicate populations from HPDEC and Hahn-Echo  $^{29}\text{Si}$  MAS NMR measurements were performed on both the cross-linked HTT-1800 and pyrolyzed samples. Overlapping resonances within  $^{13}\text{C}$  CP/MAS spectra were also deconvoluted in order to help differentiate between  $-\text{CH}_3$  and aliphatic carbon units.

#### 6.2.4 Hyperpolarized $^{129}\text{Xe}$ NMR

$^{129}\text{Xe}$  NMR experiments were performed on a home-built hyperpolarization (HP) generator located at the University of Bayreuth. Specific details concerning the design principles and performance quality are to be published in a subsequent article. Variable-temperature  $^{129}\text{Xe}$  NMR spectra were obtained on an Avance II 300 Bruker spectrometer with a static probe head, modified to incorporate continuous flow (CF) of HP  $^{129}\text{Xe}$  through a 3.0-mm inner diameter PEEK sample holder. Variable-temperature spectra were acquired using a single-pulse excitation with a  $\pi/2$  pulse length of 2.6  $\mu\text{s}$ , 2 to 16 transients, and a 10 s recycle delay. Unlike conventional  $^{129}\text{Xe}$  NMR methods, here, the recycle delay is limited by the flow rate instead of the relaxation time.<sup>[51]</sup> Applying a hard  $90^\circ$  pulse essentially destroys all nuclear polarization; the signal is then only observable if the unpolarized Xe atoms are replaced by fresh HP gas. Our gas mixture was comprised of 1:1:98, Xe:N<sub>2</sub>:He (by vol%) and was polarized using 15 W of diode laser power (Coherent, Inc.) tuned to the Rb D<sub>1</sub> line ( $\lambda \cong 794$  nm). The Xe partial pressure was maintained at 0.06 bar and the flow rate was held relatively constant during the experiment time (~100 sccm). All spectra were referenced to the gas-phase spectral frequency obtained in a nickel-free environment.

#### 6.2.5 Sorption Analysis

The specific surface area measurements were carried out on a Quantachrome (NOVA 2000 e-Series) surface area and pore size analyzer. The pore width and average pore volume was calculated using quenched solid density functional theory (QSDFT, adsorption branch) and a carbon kernel (cylindrical/slit/spherical pore geometry) was applied.

### 6.2.6 Powder X-ray Diffraction (PXRD)

All powder X-ray diffractograms were recorded by using a STOE STADI-P-diffractometer (Cu K $\alpha$  radiation,  $\lambda = 1.54178 \text{ \AA}$ ) in  $\theta$ – $2\theta$  geometry and with a position-sensitive detector. All powder samples were introduced into glass capillaries (diameter of 0.7 mm, Mark-tubes Hilgenberg, No. 10) in a glovebox and sealed prior to the measurements.

### 6.2.7 Fourier Transform Infrared (FT-IR) Spectroscopy and Thermal analysis (DTA/TGA)

Measurements were performed at a Perkin–Elmer FTIR-Spectrum 100 over a range from  $4400 \text{ cm}^{-1}$  to  $650 \text{ cm}^{-1}$ . Thermal analysis (TGA/DTA) was performed over Thermowaage L81 (Linseis, Germany).

### 6.2.8 Transmission Electron Microscopy (TEM)

Transmission electron microscopy (TEM) was performed using a Varian LEO 9220 (200 kV) instrument. The sample was suspended in chloroform and sonicated for 5 min. Subsequently, a drop of the suspended sample was placed on a grid (Plano S 166-3) and allowed to dry.

### 6.2.9 Gas Chromatography (GC)

Gas chromatography (GC) analyses were performed using an Agilent 6890N gas chromatograph equipped with flame ionization detection (FID) device and an Agilent 19091 J-413 FS capillary column, using dodecane as an internal standard.

### 6.2.10 Catalysis

The catalytic-selective hydrogenation of alkynes was done in a Parr autoclave under hydrogen pressure (20 bar). The catalyst was activated by heating at  $100^\circ\text{C}$  for 24 h under a hydrogen pressure of 20 bar. A glass tube was charged with a magnetic bar and milled catalyst (particle size of  $<100 \mu\text{m}$ ) and placed in the reactor, which was then filled with hydrogen at room temperature. The reactor was heated to respective

temperature within 20 min and stirring was continued at this temperature for 24 h. Afterward, the reaction mixture was diluted with THF and dodecane was added as an internal standard. The conversion and selectivity were determined by GC.

### 6.3 Results and Discussion

The preceramic polymer HTT-1800 was reacted with nickel complex (see Table 1). Upon the addition of polymer to a solution of nickel complex in THF, an exothermic reaction took place with an immediate solidification and darkening of polysilazane.

**Table 1.** The identification of experimental parameters for specific nanocomposite materials.

Sample ID	Ni-complex loading (wt%)	Si/Ni (ratio)	Ni-loading <sup>[a]</sup> (wt%)
Ni-10	64.8	10	8.1
Ni-20	32.4	20	4.3
Ni-100	6.4	100	1.0
Ni-133	2.0	133	0.3

[a] Theoretical loading of nickel in materials pyrolyzed at 600°C under nitrogen.

The gelation time was dependent on the amount of the complex added and ranged from 2 min (Ni-10, Ni-20) to 2 h (Ni-131). After the removal of solvent, the gels were pyrolyzed in a furnace under an atmosphere of nitrogen and were found to retain their shape after the pyrolysis at 600°C (see Figure 1). Abbreviations identifying the specific loading of nickel complex, with respect to HTT-1800, the silicon-to-nickel

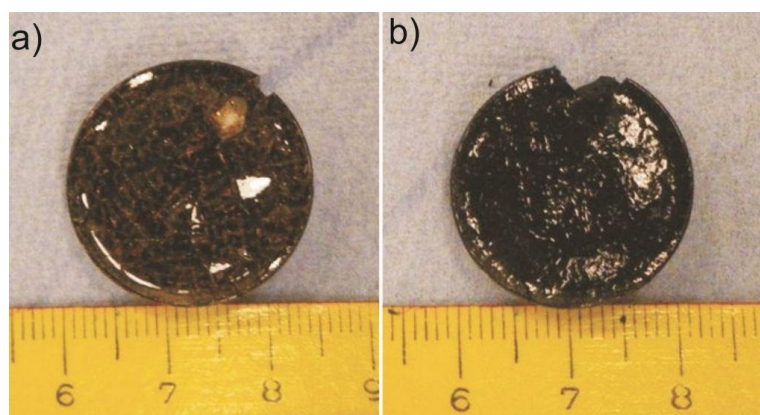


**Figure 1.** Pictorial presentation of Ni-131 (2 wt% nickel complex) before (a) and after pyrolysis at 600 °C for 2 hours (b).

(Si/Ni) ratio, and the loading of nickel in the resulting materials pyrolyzed at 600°C ( $\text{N}_2$ ) are found in Table 1. The Si/Ni ratio, which increases with decreasing the amount of added nickel complex, was used to adjust the amount of nickel in the final materials.

### 6.3.1 Characterization

#### 6.3.1.1 Solid-State Magic Angle Spinning–Nuclear Magnetic Resonance Spectroscopy (MAS NMR)

The Hahn-Echo  $^{13}\text{C}$  and  $^{29}\text{Si}$  MAS NMR measurements of the gels obtained at room temperature by the reaction of nickel complex with HTT-1800 provide an explanation about the solidification of the polysilazane. As shown in Figure 2a, the Hahn-Echo  $^{13}\text{C}$  MAS NMR spectrum of the Ni-100-RT gel shows characteristic resonance peaks for both  $\text{Si}-\underline{\text{C}}\text{H}_3$  (2.97 ppm)<sup>[52, 53]</sup> and  $\text{Si}-\underline{\text{C}}\text{H}_2\text{-Si}$  (9.36 ppm).<sup>[54]</sup> The latter linkages arise as a result of addition of  $\text{Si}-\text{H}$  to the  $\text{CH}_2=\text{CH}-$  bond. The absence of any peak at 132 ppm ( $\text{sp}^2$  carbon of vinyl) confirms the operative cross-linking *via* hydrosilylation.

After pyrolysis, the signals assigned to methyl or methylene carbon atoms become broader (Figure 2). The additional resonance at 24 ppm is assigned to the  $\text{Si}_4\underline{\text{C}}$  environment (feature S2 in the Supporting Information). The presence of peaks at 132 and 141 ppm in the materials obtained from polysilazane show the existence of a vinylic group, which becomes totally consumed in the case of samples with nickel. The nickel-containing hybrid materials also show the presence of graphitic carbon, as confirmed by the peak at 135 ppm. The most intense signal in the Hahn-Echo  $^{29}\text{Si}$  NMR spectrum Ni-100-RT (see Figure 2b) at -22.6 ppm is assigned to  $\underline{\text{Si}}\text{H}(\text{Csp}^3)\text{N}_2$  environment<sup>[55]</sup> originally present in the polymer (HTT-1800 in Scheme 1), while the additional resonance at -31.0 ppm is attributed to  $\text{SiHC}(\text{sp}^2)\text{N}_2$ .<sup>[56,57]</sup> After hydrosilylation,  $\underline{\text{Si}}\text{H}(\text{Csp}^3)\text{N}_2$  changes into  $\text{C}(\text{sp}^3)_2\underline{\text{Si}}\text{N}_2$  (see feature S1 in the Supporting Information), which appears in the spectrum at a chemical shift of -8.7 ppm.<sup>[58]</sup> The utilization of this function was also confirmed by FT-IR studies of the gels (Figure 3a). After pyrolysis at 600°C for 2 h, the same sample (Ni-100-2h) shows an intense peak at -24.0 ppm in its  $^{29}\text{Si}$  CP/MAS spectrum, corresponding to  $\text{C}\underline{\text{Si}}\text{N}_3$ , formed as a result of a dehydrocoupling reaction between  $\text{Si}-\text{H}$  and  $\text{N}-\text{H}$  functions.<sup>[58]</sup> The additional peaks observed at -8.5 ppm and

-43.6 ppm are assigned to  $\text{C}_2\text{SiN}_2$  and  $\text{SiN}_4$  environments, respectively. The former peak can be attributed to the hydrosilylation reaction while the latter appears at the expense of  $\text{C}_2\text{SiN}_2$  and  $\text{CSiN}_3$  (breaking of Si-C bonds and the emission of methane) (see feature S1 in the Supporting Information). This is confirmed by (i) the decrease in the  $\text{C}_2\text{SiN}_2$  and  $\text{CSiN}_3$  intensities and annealing time, as shown by the integrated HPDEC  $^{29}\text{Si}$  MAS NMR (summarized in Table 2) and (ii) the decrease within the FT-IR spectral intensity at  $1255\text{ cm}^{-1}$  with the increasing nickel content (see Figure 3b). The  $\text{C}_2\text{SiN}_2$  also forms  $\text{CSiN}_3$  by the expulsion of methane (feature S1 in the Supporting Information). This explains why the abundance of the latter environment shows negligible change with increasing nickel content (samples pyrolyzed for 2 h; see Table 2).

Quantitative analysis of the relative signal intensities within the acquired  $^{29}\text{Si}$  HPDEC MAS spectra yields additional insight into compositional changes between the various nanocomposite materials. The results of which are summarized in Table 2.

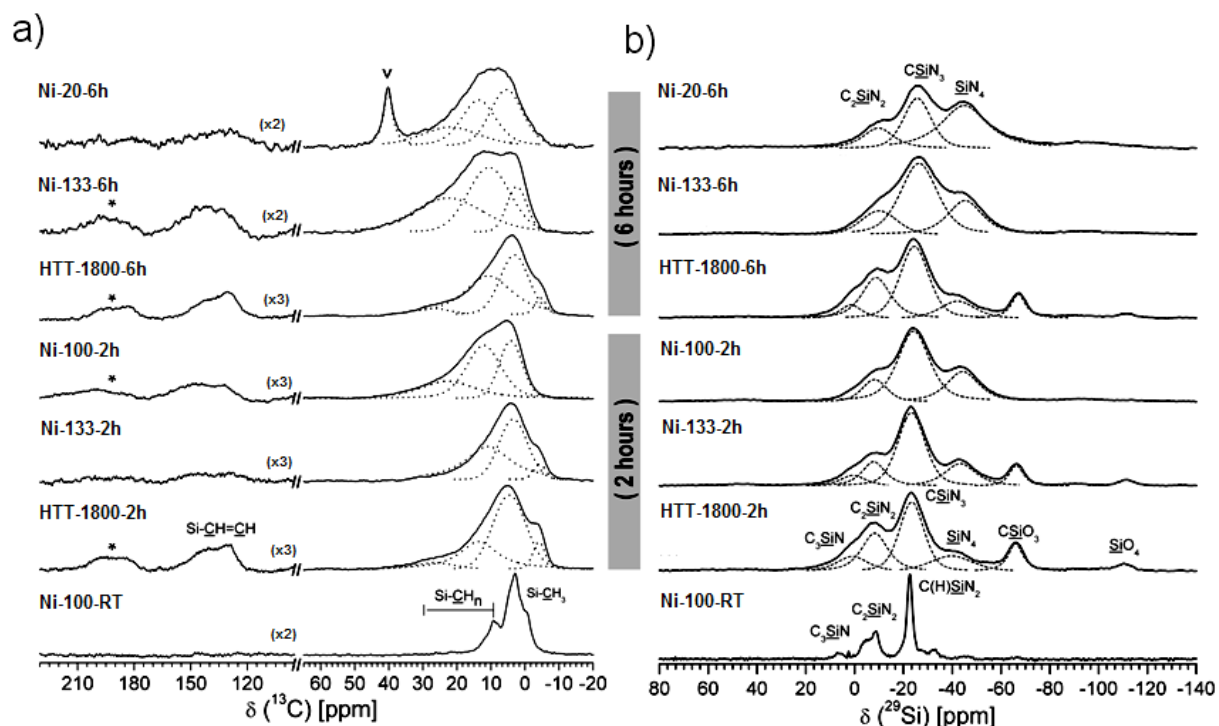


**Figure 2.** The quantitative  $^{13}\text{C}$  (a) and  $^{29}\text{Si}$  (b) Hahn-echo MAS NMR spectra of cross-linked HTT-1800 (Ni-100-RT) is compared to CP/MAS NMR spectra of pyrolyzed materials with varying Ni content and annealing times. Asterisks denote spinning side bands while the dashed lines are the deconvolution. The annealing time is specified by the addition of -2h (2 hours) or -6h (6 hours) to the sample name. The intensity of the Si-CH=CH environment (95-230 ppm) is enlarged by  $n$  times ( $nx$ ). The index ( $\nu$ ) indicates erroneous solvent (dimethylsulfoxide) peak introduced after pyrolysis.

**Table 2.** Percent contribution of different silicon environments extracted from deconvoluted single-pulse (HPDEC) <sup>29</sup>Si MAS NMR spectra.

Pyrolysis conditions	Sample	(Csp <sup>3</sup> )Si(H)N <sub>2</sub>	(Csp <sup>3</sup> ) <sub>2</sub> SiN <sub>2</sub>	C(sp <sup>2</sup> )Si(H)N <sub>2</sub>	C <sub>3</sub> SiN	Si-Si	Si(H)N <sub>2</sub>		
25 °C	Ni-100-RT	51.6	32.6	6.7	5.1	1.9	1.2		
		(Csp <sup>3</sup> )SiN <sub>3</sub>	SiN <sub>4</sub>	(Csp <sup>3</sup> ) <sub>2</sub> SiN <sub>2</sub>	(Csp <sup>3</sup> )SiO <sub>3</sub>	C <sub>3</sub> SiN	SiO <sub>4</sub>	Composition <sup>[a]</sup>	
600 °C	HTT-1800	43.6	7.57	30.5	7.8	4.8	5.8	SiC <sub>0.32</sub> N <sub>0.91</sub>	
(2 hours)	Ni-133	42.8	21.7	14.9	9.2	9.0	4.8	SiC <sub>0.29</sub> N <sub>1.23</sub>	
	Ni-100	51.9	29.5	11.7	< 1	< 1	1.8	SiC <sub>0.38</sub> N <sub>1.31</sub>	
600 °C	HTT-1800	31.7	20.0	22.7	6.9	10.1	8.4	SiC <sub>0.26</sub> N <sub>1.17</sub>	
(6 hours)	Ni-133	35.1	28.6	32.9	< 1	< 1	3.3	SiC <sub>0.26</sub> N <sub>1.09</sub>	
	Ni-20	19.9	56.1	14.2	< 1	< 1	9.7	SiC <sub>0.25</sub> N <sub>1.38</sub>	

[a] Calculated from percentage intensities of C<sub>2</sub>SiN<sub>2</sub>, CSiN<sub>3</sub>, SiN<sub>4</sub> (the major Si environments) following the method discussed in ref. 54. The contribution of oxygenated Si environments (CSiO<sub>3</sub>, SiO<sub>4</sub>) and Ni is not shown.

The most notable trend is the growth in the SiN<sub>4</sub> peak intensity with increasing nickel content and annealing time, from 7.5% in the pure polysilazane (HTT-1800–2h) to 56.0% in the case of Ni-20–6h. The corresponding C<sub>2</sub>SiN<sub>2</sub> and CSiN<sub>3</sub> intensities decrease from 30.5% to 14.2% and 43.6% to 19.9%, respectively (see Table 2). The materials obtained from pure polysilazane and Ni-133–2h (low nickel content) showed incorporation of oxygen when stored under air most probably by the hydrolysis of Si-NH bonds by moisture, as indicated by the appearance of signals at -67.0 ppm (CSiO<sub>3</sub>) and -110.0 ppm (SiO<sub>4</sub>). The small amount of oxygen might have come by the exposure of the samples to the air during their transportation to the furnace, as seen in the case of Ni-20.

The percent composition of each material, summarized in Table 2, is based on the relative intensities extracted from integrals of their individual HPDEC <sup>29</sup>Si MAS NMR spectra, using quantitative methods. The composition of hybrid materials obtained at 600°C was then calculated assuming the C<sub>2</sub>SiN<sub>2</sub>, CSiN<sub>3</sub>, and SiN<sub>4</sub> as the major silicon environments, following the procedure as discussed elsewhere.<sup>[54]</sup> Whereas the N/Si ratio in the materials obtained from pure polysilazane is almost equal to unity (same as in the polymer), the materials with nickel contain more nitrogen (SiC<sub>0.2</sub>N<sub>1.2</sub>, in the case of Ni-133) and it increases with the increase in the amount of nickel (SiC<sub>0.3</sub>N<sub>1.3</sub> in the case of Ni-100-RT) as well as the holding time at 600°C

( $\text{SiC}_{0.25}\text{N}_{1.38}$  in the case of Ni-20). The increased nitrogen content suggests that transamination reactions<sup>[59]</sup> during pyrolysis are not favored and the loss of nitrogen in the form of ammonia is avoided. On the other hand, the C/Si ratio decreases from 1.4 in the polymer to 0.2–0.3 in the pyrolyzed materials. This trend might be attributed to the loss of methane from the polymeric network during pyrolysis, which reduces the carbon content of the Si–C–N network but increases the amount of free carbon (graphitic carbon) in the materials.

### 6.3.1.2 Fourier Transform Infrared Spectroscopy (FT-IR)

Ni-100-RT sample pyrolyzed at different temperatures under a nitrogen atmosphere was analyzed *via* FT-IR (Figure 3a). At room temperature, the characteristic stretching vibrations assigned to Si–H functions ( $2117\text{ cm}^{-1}$ ) decrease in intensity, which is indicative of the hydrosilylation reaction. Moreover, the stretching frequency

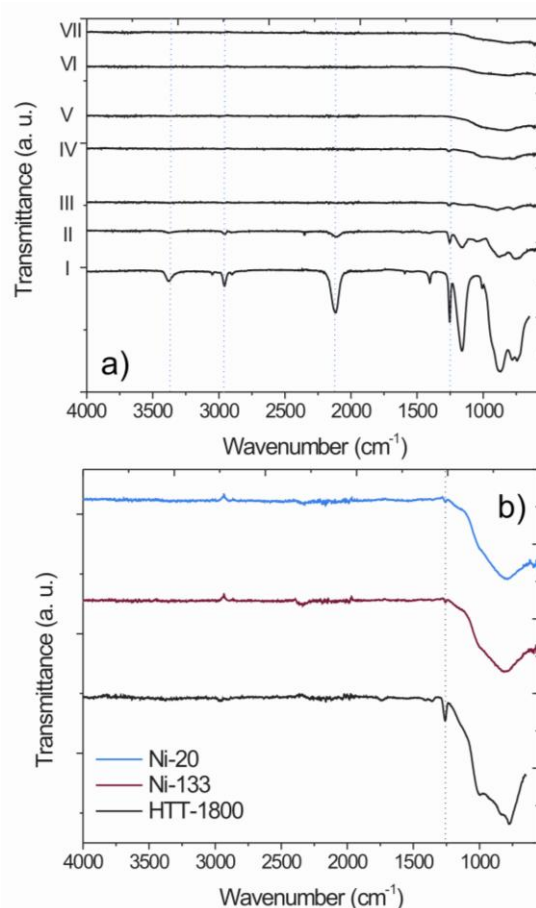


**Figure 3.** a) FT-IR spectra of Ni-100-RT at room temperature (II), 300 (III), 500 (IV), 700 (V) 900 (VI) and  $1100^{\circ}\text{C}$  (VII) in comparison to the spectrum of HTT-1800 (I). b) FT-IR spectra of materials pyrolyzed at  $600^{\circ}\text{C}$  under nitrogen for 6 hours.

for the N–H bond ( $3382\text{ cm}^{-1}$ ) shifts slightly toward higher wavenumbers. The amido-metal bond is formed as a result of the transfer of the metal from aminopyridinato complexes to the nitrogen functions of the polysilazane, producing a metal-modified polymer.<sup>[25]</sup> The stretching vibration for vinylic linkage ( $3049, 1404\text{ cm}^{-1}$ ) became totally absent at  $300^\circ\text{C}$ , confirming the completion of cross-linking reactions. In particular, almost complete utilization of Si–H ( $2117\text{ cm}^{-1}$ ) and N–H ( $3382, 1158\text{ cm}^{-1}$ ) functions at a pyrolyzing temperature of  $300\text{--}600^\circ\text{C}$  is contradictory to the results of Trassl et al., who observed the existence of N–H bonds at  $800^\circ\text{C}$  in the same type of polymer having much fewer N–H bonds, compared to HTT-1800.<sup>[57]</sup> The utilization of these functions provides a clear indication of dehydrocoupling reactions between Si–H and N–H functions,<sup>[60]</sup> along with the operative hydrosilylation. At  $500\text{--}600^\circ\text{C}$ , the materials show a small peak at  $1255\text{ cm}^{-1}$  (Si–CH<sub>3</sub>) and a broad band at  $1200\text{--}600\text{ cm}^{-1}$  due to the stretching of Si–C and Si–N bonds. When samples were held at this temperature for 6 h, the peak at  $1255\text{ cm}^{-1}$  almost vanished which is in accordance to <sup>13</sup>C MAS NMR, where the intensity of Si–CH<sub>3</sub> decreased with increase in amount of nickel and holding time (see Figure 2a and feature S2 in the Supporting Information). In the case of sample without nickel (HTT-1800), the same peak was quite prominent. This suggests the formation of more ceramic like materials (SiCN ceramics) at as low temperature as  $600^\circ\text{C}$ , because of the presence of nickel. At and above  $700^\circ\text{C}$ , the infrared (IR) spectra show only broad bands characteristic of Si–C–N ceramics.

#### 6.3.1.3 Thermogravimetric Analysis (TGA) and Differential Thermal Analysis (DTA)

Thermogravimetric analysis (TGA) of the sample (Figure 4) with a lower loading of nickel complex (Ni-100) shows a mass loss of 16% from  $25^\circ\text{C}$  to  $600^\circ\text{C}$  and an additional 6% loss between  $600^\circ\text{C}$  and  $1100^\circ\text{C}$ , providing materials in a good yield (86% and 80% at  $600^\circ\text{C}$  and  $1100^\circ\text{C}$ , respectively). The mass loss between  $25^\circ\text{C}$  and  $450^\circ\text{C}$  was related to the loss of hydrogen and oligomeric silazane fragments, while that above  $530^\circ\text{C}$  is due to the loss of methane. The ceramic yield of Ni-100 (80%) at  $1100^\circ\text{C}$  was found to be higher than the ceramics obtained from pure HTT-1800 (78%) cross-linked with the addition of dicumylperoxide (DCP). Increasing the amount of loaded nickel complex decreases the yield of the materials obtained at different temperatures. For instance, Ni-10 (64.8 wt% nickel complex) shows a mass loss of 29% and 4% in the temperature ranges of  $25\text{--}600^\circ\text{C}$  and  $600\text{--}1100^\circ\text{C}$ , resp-

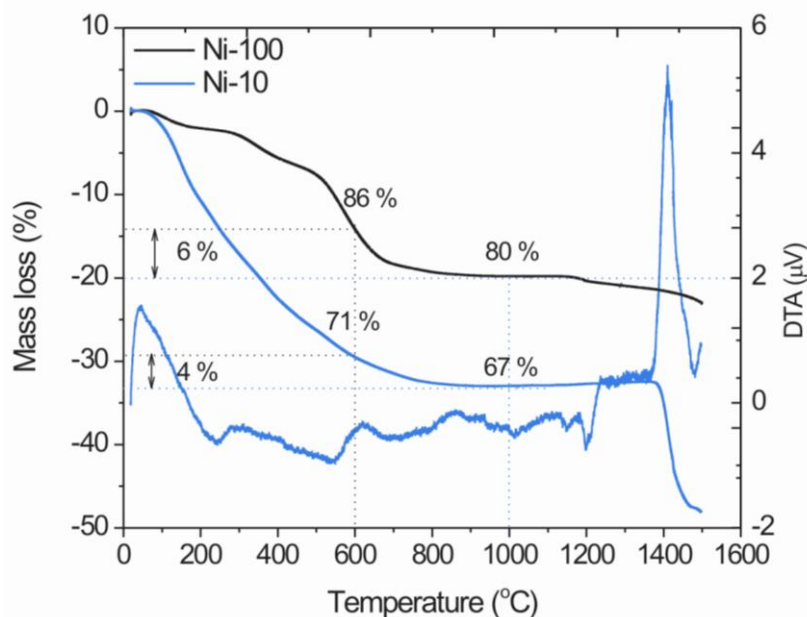


**Figure 4.** TGA (5 K/ min,  $\text{N}_2$ ) of Ni-100 (black line) and Ni-10 (blue line). Percentages are expressed as relative yield within set temperature ranges described within the text. DTA of Ni-10 is characterized by a sharp endothermic at  $1406^\circ\text{C}$  (melting point of silicon, bottom blue line).

actively (see Figure 4). DTA of the gel (Ni-10) showed broad endothermic peaks at  $25\text{--}600^\circ\text{C}$  and were attributed to the loss of oligomeric silazane species ( $25\text{--}200^\circ\text{C}$ ) and methane ( $600^\circ\text{C}$ ) from the polymer. Powder XRD analysis of the Ni-10 pyrolyzed at  $1100^\circ\text{C}$  showed the crystallization of silicon nitride (see Figure 5). A sharp and intense endothermic peak above  $1400^\circ\text{C}$  was assigned to the melting of silicon. A weight loss of 13% (TGA) is associated with this peak.<sup>[61]</sup> Powder XRD analysis of the materials analysis of the materials (initially pyrolyzed at  $1100^\circ\text{C}$  under nitrogen) post-heated to  $1500^\circ\text{C}$  (argon) indicates crystallization of silicon carbide (see feature S3 in the Supporting Information).

#### 6.3.1.4 Powder X-ray Diffraction (PXRD)

The evolution of phases in Ni-10 at different pyrolyzing temperatures was investigated by powder XRD studies. The sample remains X-ray amorphous up to  $500^\circ\text{C}$ , above which the graphitic carbon arises at a  $2\theta$  value of  $26.4^\circ$  (see Figure 5). At  $1100^\circ\text{C}$ , the characteristic reflection pattern of  $\beta\text{-Si}_3\text{N}_4$  appears in the diffractogram, in accordance to the HPDEC MAS NMR studies, which show an increase in the  $\text{SiN}_4$  sites with nickel content (see Table 2) and DTA studies (Figure 4). The samples pyrolyzed at  $600^\circ\text{C}$  (under nitrogen) show a broad peak at  $\sim 26^\circ$  ( $2\theta$ ), which was assigned to the amorphous carbon and is in accordance with

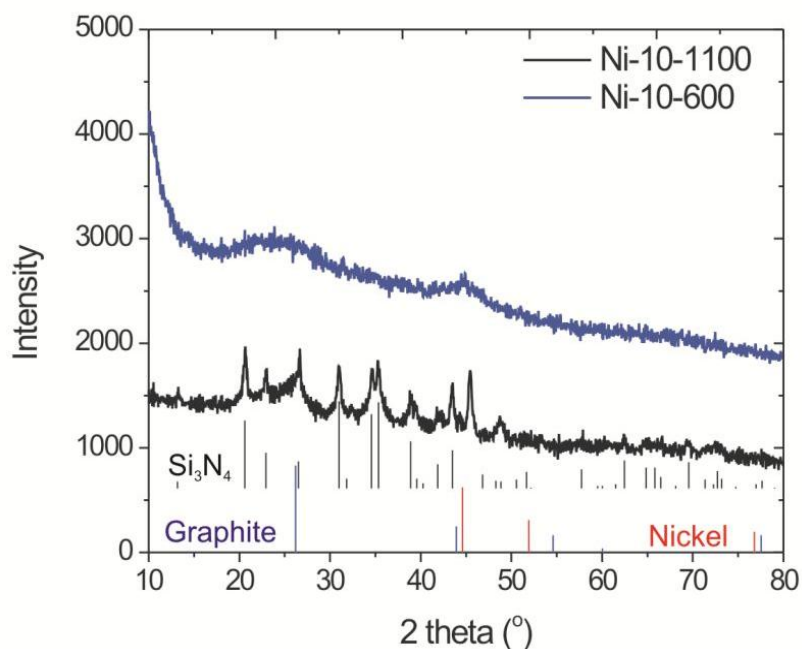


**Figure 5.** Powder XRD of Ni-10 pyrolyzed at 600°C (N<sub>2</sub> / 2 hours) shows characteristic reflection pattern of cubic phase of nickel (PDF: 00-001-1260) and graphite (PDF: 00-003-0401), as indicated by red and grey vertical bars, respectively. Crystallization of hexagonal phase (black vertical bars) of silicon nitride (PDF: 00-041-0360) takes place at 1100°C (N<sub>2</sub>)°C.

the <sup>13</sup>C MAS NMR studies. A broad reflection peak at 44.6° corresponds to the (111) plane of cubic nickel and the broadening is due to the small size of the particles, as seen in TEM images (see Figures 6d and 6f). The size of the nickel nanoparticles decreases with decreasing nickel content and in the case of samples with lower loadings (Ni-20 and Ni-100-RT), the particles are too small to be detected *via* powder XRD.

#### 6.3.1.5 Nickel Particle Size Distribution

The microstructure of the nanocomposites was analyzed by transmission electron microscopy (TEM). The materials obtained at 600°C show homogeneous distribution of nickel particles whose size increased as the nickel content increased (see Figure 6). The hybrid materials with lower loading of nickel (Ni-100) show a narrow distribution of particle size (2–3 nm), which somehow broadened with increasing nickel content (6–9 nm in the case of Ni-10). In order to have an idea about the formation and growth of nickel particles with temperature, Ni-100 was pyrolyzed at different temperatures, followed by the analysis of the products with TEM. The formation of the metal nanoparticles seems to start above 300°C, because they were not observed in the samples pyrolyzed below this temperature. The nickel complex decomposes in the temperature range of 200–300°C and results in the generation of

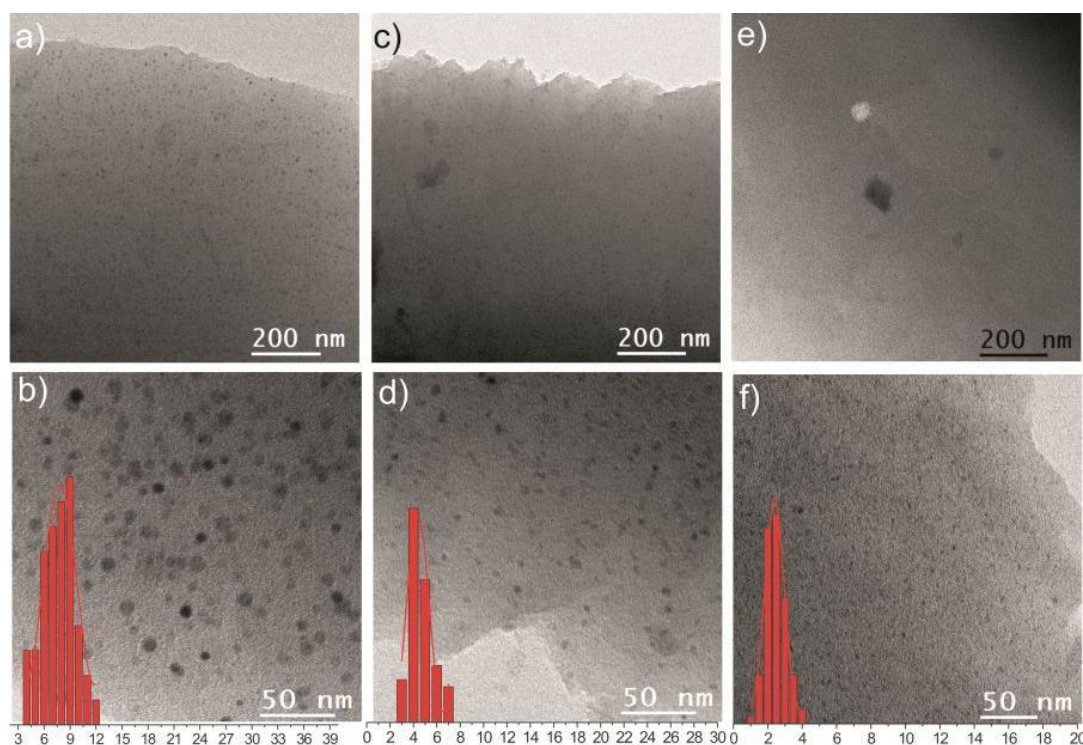


**Figure 6.** TEM micrographs of Ni-10 (a and b), Ni-20 (c and d) and Ni-100 (e and f) pyrolyzed at 600 °C (2 hours) along with the particle size count (red bars). The size of the particles increased with an increase in the amount of nickel complex contained by the materials.

Ni ions, which are then reduced in the reductive pyrolysis atmosphere, because of the emission of hydrogen and methane.<sup>[25]</sup> At 500°C, small nickel nanoparticles were seen which seem to be loosely bonded to the surface as they moved to the copper grid used for TEM analysis (see feature S4 in the Supporting Information). The size of the particles increased as the pyrolyzing temperature increased.

#### 6.3.1.6 Stability Studies

The porous hybrid materials are stable up to 600°C, with regard to mass loss under an inert atmosphere, as depicted by the TGA analysis (Figure S5 in the Supporting Information). The composites (Ni-133 and Ni-10, 600°C/6 h) were heated up to 600°C in air and exhibit surface area retention up to 500°C. Increasing the nickel content in the materials seemed to enhance the stability as the Ni-10 showed only a small change in surface area when heated to 600°C. FT-IR spectra of the composites at 500–600°C show the appearance of Si–O and Si–O–Si bonds in the range of 1000–800  $\text{cm}^{-1}$ , which is due to the incorporation of a sufficient amount of oxygen. Ni-133 was stirred in water and THF at room temperature for 24 h, followed by nitrogen adsorption studies, which show only a small decrease in surface area,

indicating the stability of materials in water and organic solvents (see feature S6 in the Supporting Information). The remarkable resistivity in an oxidative environment and thermal stability of our nickel-containing hybrid material might be attributed to the richness in SiN<sub>4</sub> sites, which provides robustness (ceramic property) to the material.

### 6.3.1.7 Porosity and Surface Studies

There are few reports about the synthesis of nanoporous metal-free materials from oligo or polysilazanes,<sup>[62-65]</sup> but the resulting silicon imidontride structures are highly reactive and prone to hydrolysis, due to the presence of Si–NH functions.<sup>[49]</sup> The hybrid materials reported here offer better stability (hydro (solvo)thermal), compared to the aforementioned materials, because of the restructuring catalyzed by nickel nanoparticles (NPs). Recently, the synthesis of nanoporous SiOCN ceramics from the pyrolysis of a polysilazane modified with a nickel aminoethanol complex was reported.<sup>[66]</sup> Although the generation of metal nanoparticles and the porosity was achieved in a single step, a higher amount of oxygen (~30%) coming from the complex could not be avoided.

The nanocomposites were subjected to N<sub>2</sub>-physisorption studies in order to evaluate

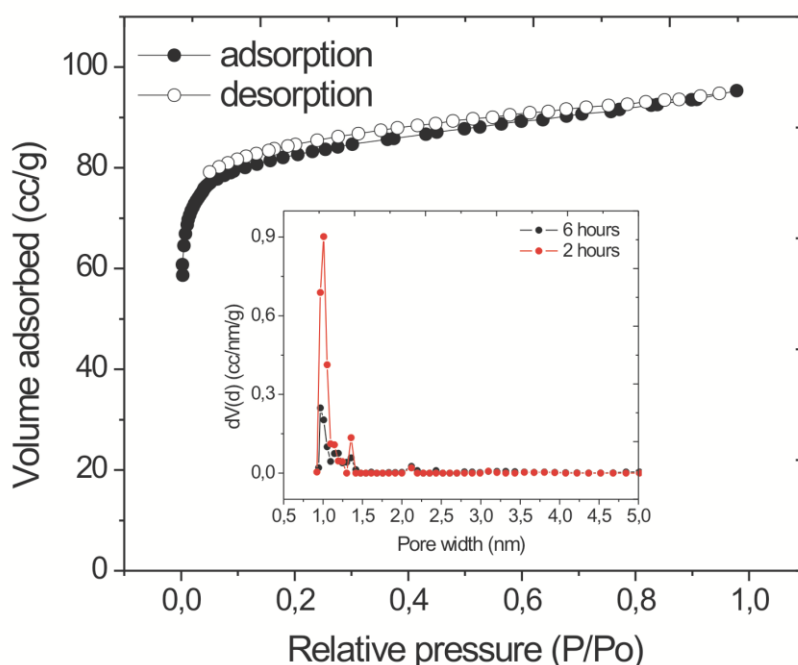


**Figure 7.** Nitrogen adsorption-desorption isotherm of Ni-100-RT pyrolyzed at 600°C for 2 hours. The inset shows the pore size distribution calculated by QS-DFT model for the same sample held at 600°C for 2 and 6 hours.

**Table 3.** Specific surface area, average pore width and pore volume of hybrid material pyrolyzed at 600°C ( $\text{N}_2$ / 2 hours or 6 hours).

Sample		SSA <sup>[a]</sup> ( $\text{m}^2/\text{g}$ )	Pore width <sup>[b]</sup> (nm)	Pore volume ( $\text{cc}/\text{g}$ )
HTT-1800	2 hrs	294	1.0	0.119
	6 hrs	382	0.9	0.168
Ni-10	2 hrs	83	1.1	0.046
	6 hrs	160	1.0	0.085
Ni-20	2 hrs	232	1.1	0.101
	6 hrs	330	0.9	0.139
Ni-100	2 hrs	323	1.0	0.126
	6 hrs	217	0.9	0.104
Ni-133	2 hrs	374	0.9	0.159
	6 hrs	200	1.1	0.095

[a] Specific surface area measured by Brunauer-Emmett-Teller method, [b] pore size distribution calculated by Quenched Solid Density Functional Theory (QS-DFT) method.

the generation of porosity under pyrolyzing conditions. It was found that the apparent surface area increased with the pyrolyzing temperature up to 500°C (400  $\text{m}^2/\text{g}$ ) and then decreased to 18  $\text{m}^2/\text{g}$  at 1100°C. The generation of porosity at 500–600°C may be related to the loss of methane from the three-dimensional (3D) network of cross-linked polymer. The hybrid materials obtained at 600°C show typical type-I adsorption isotherms (Figure 7) and both surface area and the average pore volume of the materials increase as the amount of nickel complex decreases (see Figure 7 and Table 3). The dwelling time at 600°C seems to affect the pore volume as well as the surface area, both of which increased with an increase in holding time, in the case of the materials with high nickel content (Ni-10, Ni-20). However, the pore widths slightly decreased when the dwelling time was increased from 2 h to 6 h. It is worth mentioning here that the carbon kernel used for the calculation of pore widths would be less polar than SiCN, thus a slight underestimation of the pore widths is expected.

### 6.3.1.8 <sup>129</sup>Xe NMR Studies

The static CF-HP <sup>129</sup>Xe NMR spectra for selected nanocomposite materials at 298 K are displayed in Figure 8. Xe adsorbed on the Ni-free polymer, pyrolyzed at 600°C for 6 h (HTT-1800–6h) shows a narrow gas resonance centered at 0 ppm and a broader, yet symmetric resonance at 150.3 ppm, demonstrating the accessibility of the pore volume to Xe. As a general rule, the larger the observed shift ( $\bar{\delta}_{\text{obs}}$ ), the smaller the pore size.<sup>[42, 67]</sup> Briefly,  $\bar{\delta}_{\text{obs}}$  represents a sum of potential interactions:<sup>[68, 69]</sup>  $\bar{\delta}_{\text{obs}} = \bar{\delta}_{\text{ref}} + \bar{\delta}_{\text{S}} + \bar{\delta}_{\text{Xe-Xe}} + \bar{\delta}_{\text{SAS}} + \bar{\delta}_{\text{E,M}}$ , where  $\bar{\delta}_{\text{ref}}$  is the gas-phase Xe shift extrapolated to zero pressure (0 ppm) and  $\bar{\delta}_{\text{S}}$  is the component arising from Xe surface interactions;  $\bar{\delta}_{\text{Xe-Xe}}$  refers to contributions from Xe–Xe collisions,  $\bar{\delta}_{\text{SAS}}$  arises from its interaction with strong adsorption sites (SAS), and  $\bar{\delta}_{\text{E,M}}$  manifests from electric and/or magnetic fields induced by the presence of metal particles acting as SAS. HP methods typically employ dilute Xe densities which effectively limits the Xe–Xe contribution to the  $\bar{\delta}_{\text{obs}}$  at ambient temperature (298 K). It should be noted that reducing the sample temperature leads to an increase in either  $\bar{\delta}_{\text{Xe-Xe}}$  or  $\bar{\delta}_{\text{S}}$ , depending on whether micropores or mesopores are present.<sup>[38, 70]</sup>

Because the HTT-1800–6 h sample does not contain any nickel, the observed <sup>129</sup>Xe chemical shift is attributed to Xe confined within internal voids. However, this shift is too large to reflect Xe occupying the pore diameters indicated by N<sub>2</sub>-adsorption measurements. As such, we suggest that this shift arises from Xe interacting with organic moieties<sup>[71]</sup> (e.g., –CH<sub>3</sub> groups) lining the pore surface, which solid-state <sup>13</sup>C and FTIR measurements show are in abundance. Preferred adsorption within organic macrocycles has been shown to exhibit similar effects.<sup>[72, 73]</sup>

The addition of 2 wt% nickel complex (Ni-133–2h) has a negligible effect on the  $\bar{\delta}_{\text{obs}}$  value. The observed decrease in the  $\bar{\delta}_{\text{obs}}$  line width from 701 Hz to 530 Hz may indicate a more homogeneous structure of internal voids, compared to the pyrolyzed HTT-1800–6h (see Figure 8). A subsequent increase in the nickel content (Ni-100–2h) induces noticeable broadening in both the adsorbed and gas-phase resonances, indicating a strong influence due to the inclusion of Ni particles. The signal for the adsorbed Xe remains rather symmetric, while the resonance centered near 0 ppm starts to exhibit some asymmetry and a new resonance near 14.6 ppm, indicating the presence of larger void space. These features become more pronounced with longer

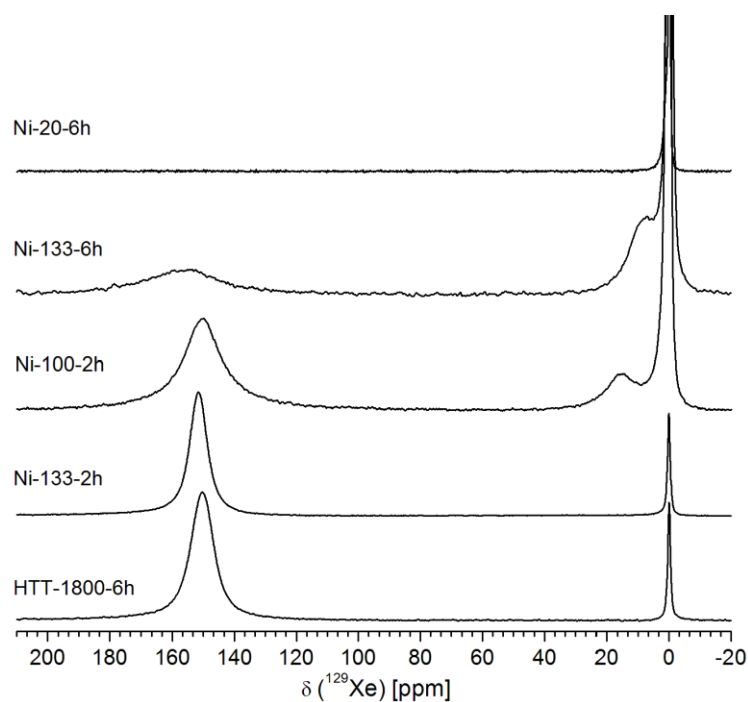


**Figure 8.** CF-HP  $^{129}\text{Xe}$  NMR spectra obtained at room temperature for nanocomposite materials having different Ni-loading and holding times. The addition of either '-2h' or '-6h' indicates 2 hour or 6 hour pyrolysis.

annealing times. The resonance attributed to the adsorbed Xe in Ni-133-6h is further broadened to 13 kHz and shifted downfield to 157 ppm (Figure 8). The downfield shift may be due to the increase in  $\text{SiN}_4$  units (compared to both Ni-133-2h and Ni-100-2h matrices); the removal of larger amorphous voids may promote the formation of more ordered phases with condensed void space. As shown previously by TEM images, longer annealing times lead to larger Ni-particle aggregates (Figure 6). More agglomeration of the nickel particles within the nanocomposite support material would likely increase the probability of surface roughness, which have been shown to promote the formation of Xe clusters.<sup>[74,75]</sup> The strong local dipole fields induced by the superparamagnetic nature of the nickel particles may be responsible for the severe broadening of the resonances due to the shortening of the  $^{129}\text{Xe}$  spin-lattice relaxation. The paramagnetic nature of the nickel particles near the external surface would have an additional depolarizing effect on the HP  $^{129}\text{Xe}$ . The higher metallic character of the particles will eventually limit the detectable amount of Xe sampling the internal voids, because of an increase in the depolarization potential and broadening. This justifies our observations on the Ni-20 sample, which contains the highest nickel content and largest nickel particle size (among the measured

materials) where only a multicomponent asymmetric line broadening around the gas phase is observed. A more-detailed discussion is given in the Supporting Information. Recent work by Clewett et al.<sup>[76]</sup> on the surface properties of carbon nanotubes laced with paramagnetic particles attributes the complex structure around the gas-phase resonance to the presence of additional adsorption sites that are not detectable, because of strong paramagnetic relaxation effects. This would effectively reduce the polarization of Xe adsorbed on the nickel particles and average the remaining polarization with that of the gaseous Xe (within the fast exchange regime). The weighting factor of Xe adsorbed into these paramagnetic voids is likely to be small due to a very short time  $T_1$  (on the order of a few nanoseconds),<sup>[77]</sup> resulting in an averaged frequency closer to 0 ppm. As such, we believe that the higher nickel content creates additional domains that manifest as asymmetric line broadening and additional peaks observed near the gas phase.

The temperature dependence of the CF-HP  $^{129}\text{Xe}$  NMR spectra (Figure 9) was investigated for many samples, with the purpose of extracting more-specific information on physical parameters typically hidden within possible exchange processes.

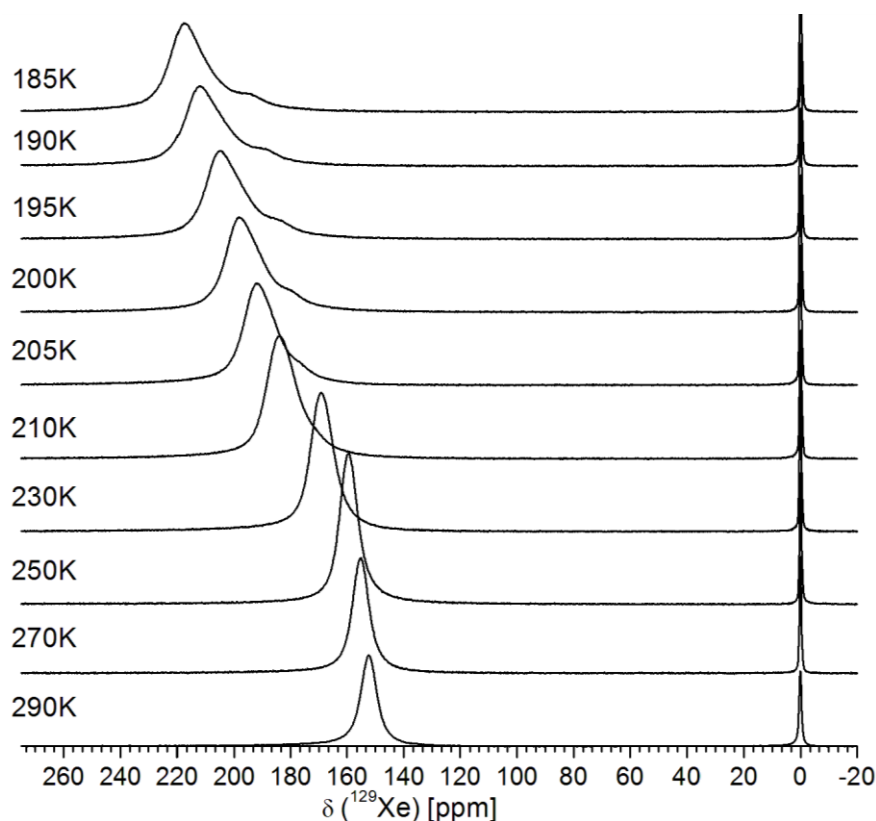


**Figure 9.** Variable temperature CF-HP  $^{129}\text{Xe}$  NMR spectra data of Ni-133-2h.

Reducing the sample temperature not only increases the Xe density within the pore space, but it also slows the diffusion processes and increases residence times within the microporous materials. This makes the identification of additional cavities much more likely. Samples Ni-133–2h and Ni-100–2h were chosen for variable-temperature (VT) analysis, because of their similar temperature treatment (2 h annealing time) and comparable surface-to-volume ratios. Monitoring the changes due to the inclusion of larger nickel particles is of particular interest as Ni-100–2h possesses almost three times more nickel, compared to Ni-133–2h (see Table 1). VT CF-HP  $^{129}\text{Xe}$  spectra for Xe adsorbed within Ni-133–2h are shown in Figure 9. The broad, symmetric line shape of the adsorbed Xe shifts and broadens significantly with cooling. Only a moderate shift of the signal is detected between 290 and 240 K. Below which, a stronger shift and a multimodal line occurs. Spectral deconvolution of the adsorbed  $^{129}\text{Xe}$  resonance suggests the presence of three distinct adsorption sites at 185 K.

The amount of Xe within the gas and pore environments are directly proportional to their relative integrated spectral intensities, assuming a sufficiently long recycle delay and negligible depolarization effects. The extraction of quantitative thermodynamic parameters under low loading conditions (high temperatures) can be obtained by plotting the adsorbed-to-gas phase ratio ( $I_{\text{ads}}/I_{\text{g}}$ ) as a function of temperature.<sup>[70]</sup> The integrated signal intensities extracted from Ni-133–2h and Ni-100–2h are shown in Figure 10. The equilibrium constant describes the activities of the total amount of adsorbed Xe with respect to the gas phase and can be used to relate  $I_{\text{ads}}/I_{\text{g}}$  to the standard Gibbs free energy of the adsorption process. Results are evaluated according to

$$\ln (I_{\text{ads}}/I_{\text{g}}) = \Delta S^{\circ}/R - \Delta H_{\text{ads}}/RT$$

where  $\Delta H_{\text{ads}}$  is the differential enthalpy of adsorption,  $R$  the universal gas constant, and  $\Delta S^{\circ}$  the temperature-independent standard entropy change.

The validity of this model to evaluate the thermodynamics of Xe adsorption is limited to fast diffusion conditions and often manifests as a positive, linear slope in the logarithmic plot. As such, only the linear segment located within the high-temperature region is used to extract pertinent thermodynamic parameters. The initial slope observed in the Ni-100–2 h sample yields a  $\Delta H_{\text{ads}}$  value of  $-10.0$  kJ/mol Xe, and a standard entropy change ( $\Delta S^{\circ}$ ) of  $-41.8$  J/(mol K), which is characteristic of phy-

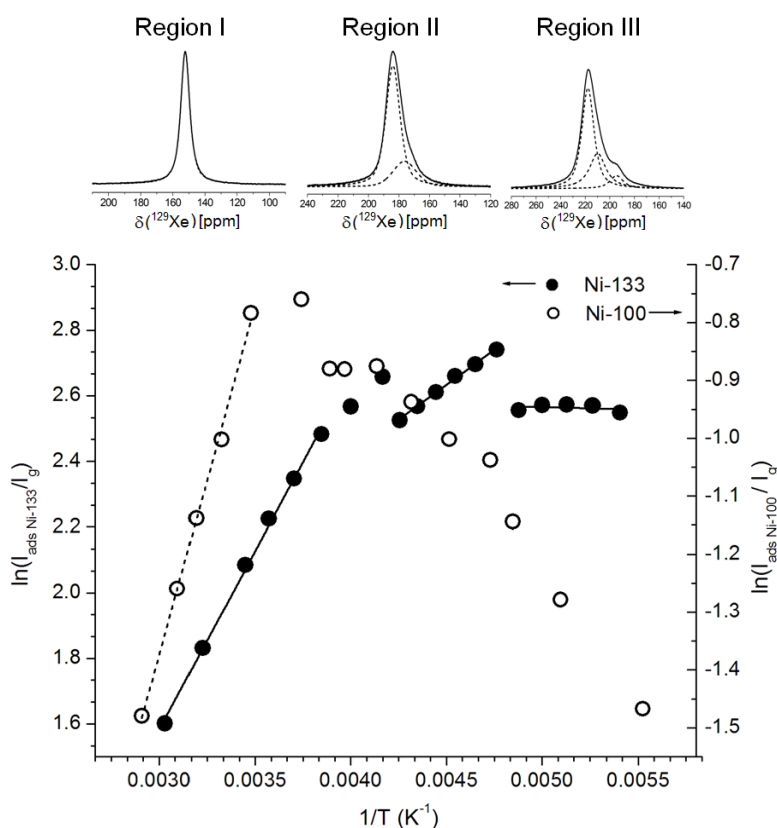


**Figure 10.** Integrated intensity ratios extracted from variable temperature CF-HP  $^{129}\text{Xe}$  NMR spectra data of Ni-100-2h (open symbol) and Ni-133-2h (closed symbol). Inset: spectra on the upper portion of the summary plot refer to the first (Region I), second (Region II) and third (Region III) linear segments within Ni-133-2h, as described in the text.

-isorption (Figure 10). The turning point at 255 K reflects a diffusion limiting process wherein longer residence times limit the replacement of adsorbed gas with freshly HP Xe.<sup>[78]</sup> The fast depolarization observed in Ni-100–2 h is likely due to the elevated nickel content, while the substantial broadening of the resonance from 1 kHz at room temperature, to 2.6 kHz at 185 K is attributed to paramagnetic relaxation effects that are due to increased interactions between Xe and nickel particles with cooling.

Different behavior is observed for Ni-133–2 h, where multiple linear segments are shown to span over several temperature intervals. Similar to Ni-100–2 h, the first segment reflects Henry's law-type behavior (Figure 10, Region I), yielding adsorption enthalpy and entropy of  $-9.0$  kJ/mol Xe and  $-13.9$  J/(mol K), respectively. Here, the higher  $\Delta S^\circ$  value ( $-13.9$  J/(mol K) versus  $-41.8$  J/(mol K)) reflects the larger number of open end groups (like  $-\text{CH}_3$ ), which enhances the flexibility of Ni-133–2 h, compared to Ni-100–2 h. The sudden decrease in the  $I_{\text{ads}}/I_{\text{g}}$  ratio at 240 K with cooling (Figure 10, Region II) suggests a possible change within the internal structural arrangement. An additional, larger reduction in the integrated signal

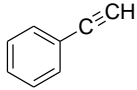
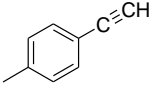
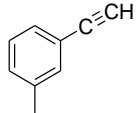
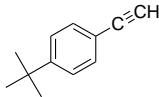
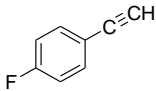
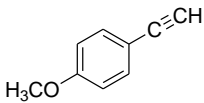
intensities is detected at 210 K (Figure 10, Region III). Interestingly, previously discussed asymmetric contributions to the adsorbed  $^{129}\text{Xe}$  line shape correspond to each of these two observed transitions. As shown in the three deconvoluted  $^{129}\text{Xe}$  spectra shown in Figure 10 (Regions, I, II, and III), each depression and subsequent buildup within  $I_{\text{ads}}/I_{\text{g}}$  is associated with the emergence of an additional resonance, suggesting some change within Xe exchange processes. The  $I_{\text{ads}}/I_{\text{g}}$  ratios measured near these two observed transitions were found to be both reversible and reproducible. These trends are likely more reflective of the relative lifetime of adsorbed HP Xe within these domains, rather than its actual distribution. The temperature dependence of the adsorption behavior was also analyzed using chemical shift analysis (see feature S7 in the Supporting Information). The adsorption enthalpies were found to be comparable to those obtained above.

### 6.3.2 Catalytic Studies

Selective hydrogenation of phenylacetylene to styrene is a reaction of great industrial importance as the small amount of it present in styrene feed can deactivate the polymerization catalysts.<sup>[79]</sup> Among the other supported noble-metal catalysts,<sup>[80-82]</sup> those based on palladium<sup>[83-87]</sup> are the most active and selective and are used industrially for the removal of phenylacetylene from styrene feed.<sup>[88]</sup> Although other catalysts containing inexpensive metals have also been tried, they suffer the problem of being less active and specific,<sup>[89]</sup> and attempts have been made to increase their selectivity by alloying them with silicon.<sup>[90-91]</sup> Nickel nanoparticles supported by porous hybrid materials reported here were found to be highly selective in the hydrogenation of phenylacetylene to styrene. The hydrogenation of phenylacetylene in different organic solvents was studied at 25°C under a hydrogen pressure of 5 bar. Whereas the tetrahydrofuran (THF) and dichloromethane (DCM) afforded better selectivity to styrene, hexane and toluene provided better conversions.

By the adjustment of catalyst amount, hydrogen pressure, volume of toluene, and stirring speed, it was possible to get almost 100% conversion of alkynes with high selectivity (89–99%) to the alkenes (see Table 4). No catalytic activity was detected by applying a SiCN material without nickel. The effect of various substituents on the phenyl ring of phenylacetylene was also studied (see Figure 11a). Whereas an elect-

**Table 4.** Hydrogenation of alkynes at 25 °C using Ni-10 catalyst <sup>[a]</sup>.

Substrate	Conversion (mol%)	Selectivity [b] (mol%)
	99	97
	99*	97
	99	98
	99	94
	99	89
	99	99

[a] Alkyne (0.5 mmol), catalyst (50 mg), Toluene (0.2 mL), hydrogen pressure (20 bar), stirring velocity (1250 rpm). [b] Selectivity in mol% to olefin product. Reaction time (24 hours, \* 32 hours).

-ron donating group (such as methyl) at the para position decreased the activity, the electron-withdrawing groups (fluoro and methoxy) and the bulky (tertiary butyl) group at the same position were found to increase the activity by many folds. An electron-releasing methyl group at the meta position was found to increase the conversion. All of the aforementioned substrates were hydrogenated to olefins with high selectivity (89–99%). The catalyst was consecutively used up to five runs and did not show any prominent change in the conversion and selectivity (see Figure 11b). After every catalytic run, the catalyst was removed and the filtrate was checked for its catalytic activity under the same experimental conditions with the addition of fresh substrate. No activity was observed, which suggests either no or very low leaching of nickel.

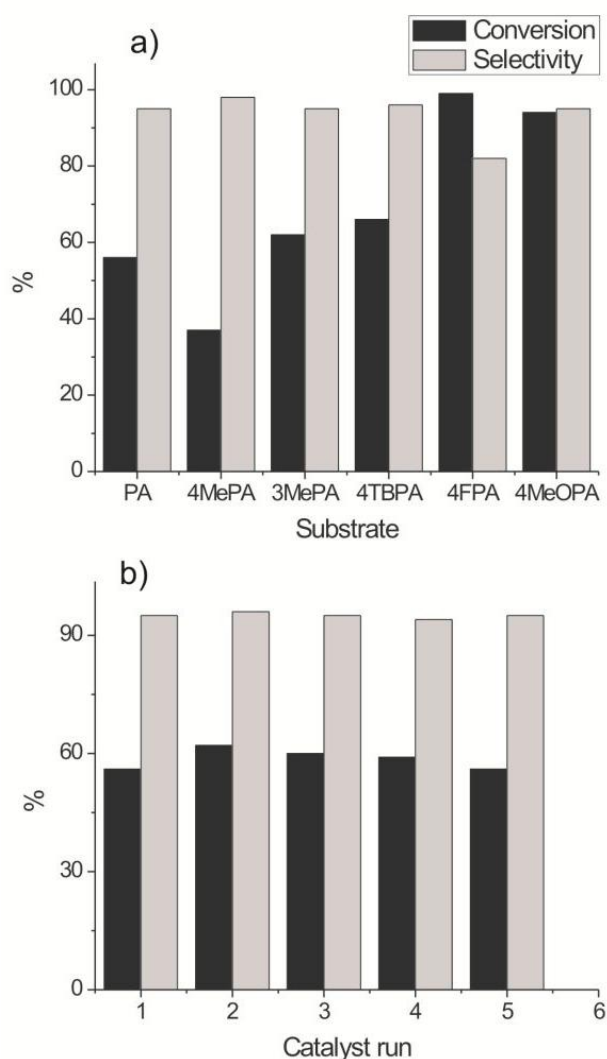


**Figure 11.** a) Hydrogenation of alkynes (0.5 mmol), catalyst (20 mg), Toluene (0.2 mL), hydrogen pressure (20 bar), stirring velocity (750 rpm). Conversion and selectivity (olefin) are given in mol% units. (PA) Phenylacetylene, Me (methyl), TB (tertiarybutyl), F (fluoro), MeO (methoxy). b) Recycling of the catalyst (Ni-10, 20 mg) for five consecutive runs (0.5 mmol of phenylacetylene in toluene (0.2 mL) at 25°C for 24 hours under 5 bar hydrogen).

## 6.4 Conclusions

Simultaneous generation of the porosity and nickel nanoparticles were achieved by the pyrolysis (600°C/N<sub>2</sub>) of a chemically modified commercial polysilazane. An amido nickel complex catalyzes the hydrosilylation reaction, leading to the cross-linking of polysilazane at room temperature, which in turn, affords better yields. Dehydrocoupling reactions lead to the complete utilization of N–H bonds and an enhanced stability of the composites. Increasing the nickel content together with the holding time at 600°C increases the population of SiN<sub>4</sub> sites at the expense of

$\text{C}_2\text{SiN}_2$  and  $\text{CSiN}_3$  sites. In other words, much of the methyl and methylene groups bonded to silicon ( $\text{C}_2\text{SiN}_2$  and  $\text{CSiN}_3$  environments) are lost as methane, producing a  $\text{SiN}_4$  network that renders higher thermal stability to the materials. The surface area and the size of the metal particles can be altered by adjusting the amount of added nickel complex. Moreover, the presence of nickel lowers the crystallization of silicon nitride (at  $1100^\circ\text{C}/\text{N}_2$ ). The fabrication of monolithic microporous materials is possible, which are thermally robust until  $500^\circ\text{C}$  in an oxidative environment and are selective hydrogenation catalysts.

CF-HP  $^{129}\text{Xe}$  NMR methods were used to probe the influence of specific thermal and Ni-complex treatments on the formation of microporous nanocomposites with catalytically active nickel particles. Stronger Xe-nickel interactions are verified by the limited detection of adsorbed Xe and appearance of additional peaks near the gas phase with increasing metal particle size and concentration. Substantial broadening of both adsorbed and gaseous Xe resonances with higher nickel content indicate that nickel particles are not only embedded within the SiCN porous network, but located near the external surface as well. The negligible change in the adsorption enthalpy of Xe with the nickel particle inclusion suggests minimal catalyst support effects. As such, the catalytic activity would be dominated by the nickel particles.

### Supporting Information

Schematic presentation of various silicon environments, a tabular presentation of  $^{13}\text{C}$  chemical shift values, powder XRD of the materials treated at  $1500^\circ\text{C}$ , TEM micrographs of the materials at various pyrolyzing temperatures, and a brief text discussion about the variation of Xe chemical shift with temperature, along with figures. This material is available free of charge *via* the Internet at <http://pubs.acs.org>.

The authors declare no competing financial interest.

### Acknowledgments

The authors thank the Deutsche Forschungsgemeinschaft (DFG) and Sonderforschungsbereich (SFB) 840 Bayreuth for financial support, and they gratefully acknowledge Dr. Wolfgang Milius and Kathrin Inzenhofer for PXRD and

TGA/DTA measurements. M.Z. acknowledges the Higher Education Commission of Pakistan (HEC) and Deutscher Akademischer Austausch Dienst (DAAD) for the fellowship.

## 6.5 References

- [1] G. Ferey, *Chem. Mater.* **2001**, *13*, 3084-3098.
- [2] F. -S. Xiao, S. Qiu, W. Pang, R. Xu, *Adv. Mater.* **1999**, *11*, 1091-1099.
- [3] P. A. Wright, *Microporous Framework Solids*. The Royal Society of Chemistry, Cambridge, England. **2008**.
- [4] V. Valtchev, S. Mintova, M. Tsapatsis, *Ordered Porous Solids: Recent Advances and Prospects* (Ed.) Elsevier, Amsterdam, **2009**.
- [5] G. J. A. A. Soler-Illia, C. Sanchez, B. Lebeau, J. Patarin, *Chem. Rev.* **2002**, *102*, 4013-4138.
- [6] A. Stein, *Adv. Mater.* **2003**, *15*, 763-775.
- [7] M. E. Davis, *Nature* **2002**, *417*, 813-821.
- [8] C. S. Cundy, P. A. Cox, *Chem. Rev.* **2003**, *103*, 663-701.
- [9] A. Corma, *J. Catal.* **2003**, *216*, 298-312.
- [10] A. Corma, *Chem. Rev.* **1997**, *97*, 2373-2419.
- [11] E. Taarning, C. M. Osmundsen, X. Yang, B. Voss, S. I. Andersen, C. H. Christensen, *Energy Environ. Sci.* **2011**, *4*, 793-804.
- [12] T. P. Vispute, H. Zhang, A. Sanna, R. Xiao, G. W. Huber, *Science* **2010**, *330*, 1222-1227.
- [13] R. M. Ravenelle, F. Schuessler, A. D'Amico, N. Danilina, J. A. van Bokhoven, J. A. Lercher, C. W. Jones, C. Sievers, *J. Phys. Chem. C* **2010**, *114*, 19582-19595.

- [14] T. Boger, A. K. Heibel, C. M. Sorensen, *Ind. Eng. Chem. Res.* **2004**, *43*, 4602-4611.
- [15] T. Boger, A. K. Heibel, C. M. Sorensen, *Ind. Eng. Chem. Res.* **2004**, *43*, 4602-4611.
- [16] J. Perez-Ramirez, C. H. Christensen, K. Egeblad, C. H. Christensen, J. C. Groen, *Chem. Soc. Rev.* **2008**, *37*, 2530-2542.
- [17] K. Cheetham, G. Ferey, T. Loiseau, *Angew. Chem. Int. Ed.* **1999**, *38*, 3268-3292.
- [18] S. L. James, *Chem. Soc. Rev.* **2003**, *32*, 276-288.
- [19] A. Corma, H. Garcia, F. X. Liabres i Xamena, *Chem. Rev.* **2010**, *110*, 4606-4655.
- [20] N. B. McKeown, P. M. Budd, *Chem. Soc. Rev.* **2006**, *35*, 675-683.
- [21] T. Ben, H. Ren, S. Ma, D. Cao, J. Lan, X. Jing, W. Wang, J. Xu, F. Deng, J. M. Simmons, S. Qiu, G. Zhu, *Angew. Chem. Int. Ed.* **2009**, *48*, 9457-9460.
- [22] M. Mastalerz, *Angew. Chem. Int. Ed.* **2008**, *47*, 445-447.
- [23] W. Lu, D. Yuan, D. Zhao, C. I. Schilling, O. Plietzsch, T. Muller, S. Bräse, J. Guenther, J. Blümel, R. Krishna, Z. Li, H. -C. Zhou, *Chem. Mater.* **2010**, *22*, 5964-5972.
- [24] M. -J. Munoz-Aguado, M. Gregorkiewitz, *J. Colloid Interface Sci.* **1997**, *185*, 459-465.
- [25] S. -Y. Moon, J. -S. Bae, E. Jeon, J. -W. Park, *Angew. Chem. Int. Ed.* **2010**, *49*, 9504-9508.
- [26] G. Glatz, T. Schmalz, T. Kraus, F. Haarmann, G. Motz, R. Kempe, *Chem. Eur. J.* **2010**, *16*, 4231-4238.
- [27] M. Zaheer, G. Motz, R. Kempe, *J. Mater. Chem.* **2011**, *21*, 18825-18831.

- [28] T. Schmalz, T. Kraus, M. Guenthner, C. Liebscher, U. Glatzel, R. Kempe, G. Motz, *Carbon* **2011**, *49*, 3065-3072.
- [29] M. Zaheer, G. Motz, R. Kempe, *Chem. Soc. Rev.* **2012**, *41*, 5102-5116.
- [30] S. Proch, J. Herrmannsdörfer, R. Kempe, C. Kern, A. Jess, L. Seyferth, J. Senker, *Chem. Eur. J.* **2008**, *14*, 8204-8212.
- [31] J. Herrmannsdörfer, R. Kempe, *Chem. Eur. J.* **2011**, *17*, 8071-8077.
- [32] T. Ahnfeldt, N. Guillou, D. Gunzelmann, I. Margiolaki, T. Loiseau, G. Ferey, J. Senker, N. Stock, *Angew. Chem. Int. Ed.* **2009**, *48*, 5163-5166.
- [33] T. Ahnfeldt, D. Gunzelmann, T. Loiseau, D. Hirsemann, J. Senker, G. Ferey, N. Stock, *Inorg. Chem.* **2009**, *48*, 3057-3067.
- [34] J. Weitkamp, M. Hunger, U. Ryma, *Micro. Meso. Mater.* **2001**, *48*, 255-270.
- [35] T. Ito, J. Fraissard, *J. Chem. Phys.* **1982**, *36*, 124-129.
- [36] M. A. Springuel-Huet, J. L. Bonardet, A. Gédéon, J. Fraissard, *Magn. Reson. Chem.* **1999**, *37*, S1-S13.
- [37] L. -Q. Wang, D. Wang, J. Liu, G. J. Exarhos, S. Pawsey, I. Moudrakovski, *J. Phys. Chem. C* **2009**, *113*, 6577-6583.
- [38] S. Pawsey, K. K. Kalebaila, I. Moudrakovski, J. A. Ripmeester, S. L. Brock, *J. Phys. Chem. C.* **2010** *114*, 13187-13195.
- [39] V. V. Terskikh, I. L. Mudrakovskii, V. M. Mastikhin, *J. Chem. Soc. Faraday Trans.* **1993**, *89*, 4239-4243.
- [40] C. -Y. Cheng, T. C. Stamatatos, G. Christou, C. R. Bowers, *J. Am. Chem. Soc.* **2010**, *132*, 5387-5393.
- [41] D. Raftery, H. Long, T. Meersmann, P. J. Grandinetti, L. Reven, A. Pines, *Phys. Rev. Lett.* **1991**, *66*, 584-587.
- [42] T. G. Walker, W. Happer, *Rev. Mod. Phys.* **1997**, *69*, 629-642.

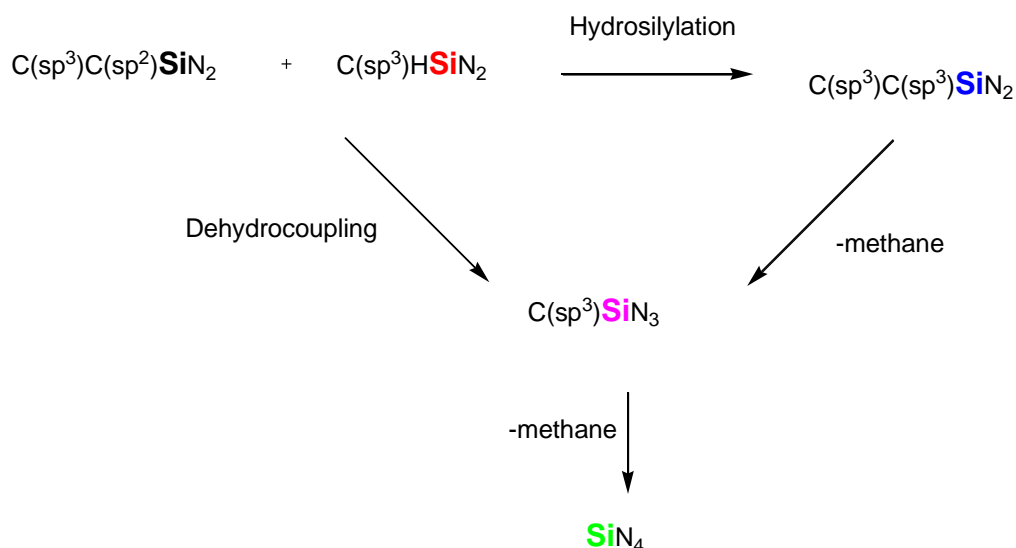
- [43] B. Driehuys, G. D. Gates, E. Miron, K. Sauer, D. K. Walter, W. Happer, *Appl. Phys. Lett.* **1996**, *69*, 1668-1670.
- [44] J. Demarquay, J. Fraissard, *Chem. Phys. Lett.* **1987**, *136*, 314-318.
- [45] M. A. Springuel-Huet, J. L. Bonardet, A. Gedeon, J. Fraissard, *Langmuir* **1997**, *13*, 1229-1236.
- [46] G. J. Kennedy, *Polym. Bull.* **1990**, *23*, 605-608.
- [47] B. Labouriau, G. Panjabi, B. Enderle, T. Pietrass, B. C. Gates, W. L. Earl, K. C. Ott, *J. Am. Chem. Soc.* **1999**, *121*, 7674-7681.
- [48] J. Enderle, A. Labouriau, K. C. Ott, B. C. Gates, *Nano Lett.* **2002**, *2*, 1269-1271.
- [49] R. Kempe, P. Arndt, *Inorg. Chem.* **1996**, *35*, 2644-2649.
- [50] S. Deeken, S. Proch, E. Casini, H. F. Braun, C. Mechtler, C. Marschner, G. Motz, R. Kempe, *Inorg. Chem.* **2006**, *45*, 1871-1879.
- [51] G. Metz G. X. L. Wu, S. O. Smith, *J. Magn. Reson.* **1994**, *110*, 219-227
- [52] B. M. Goodson, *J. Magn. Reson.* **2002**, *155*, 157-216
- [53] N. Brodie, J. –P. Majoral, J. –P. Disson, *Inorg. Chem.* **1993**, *32*, 4646-4649.
- [54] R. J. P. Corriu, D. Leclercq, P. H. Mutin, J. –M. Planeix, A. Vioux, *Organometallics* **1993**, *12*, 454-462.
- [55] C. Gerardin, F. Taulelle, D. Bahloul, *J. Mater. Chem.* **1997**, *7*, 117-126.
- [56] Y. –Li. Li, E. Kroke, R. Riedel, C. Fasel, C. Gervais, F. Babonneau, *Appl. Organomet. Chem.* **2001**, *15*, 820-832.
- [57] M. Weinmann, T. W. Kamphowe, J. Schuhmacher, K. Mueller, F. Aldinger, *Chem. Mater.* **2000**, *12*, 2112-2122.
- [58] S. Trassl, D. Suttor, G. Motz, E. Rössler, G. Ziegler, *J. Eur. Ceram. Soc.* **2000**, *20*, 215-225.

- [59] J. Seitz, J. Bill, N. Egger, F. Aldinger, *J. Eur. Ceram. Soc.* **1996**, *16*, 885-889.
- [60] E. Kroke, Y. -L. Li, C. Konetschny, E. Lecomte, C. Fasel, R. Riedel, *Mater. Sci. Eng.* **2000**, *26*, 97-199.
- [61] W. -D. Wang, R. Eisenberg, *Organometallics* **1991**, *10*, 2222-2227.
- [62] R. M. Prasad, G. Mera, K. Morita, M. Müller, H. -J. Kleebe, A. Gurlo, C. Fasel, R. Riedel, *J. Eur. Ceram. Soc.* **2012**, *32*, 477-484.
- [63] J. P. Dismukes, J. W. Johnson, J. S. Bradley, J. M. Millar, *Chem. Mater.* **1997**, *9*, 699-706.
- [64] J. S. Bradley, O. Vollmer, R. Rovai, U. Specht, F. Lefebvre, *Adv. Mater.* **1998**, *10*, 938-942.
- [65] O. Vollmer, F. Lefebvre, J. S. Bradley, *J. Mol. Catal. A: Chem.* **1999**, *146*, 87-96.
- [66] D. Farruseng, K. Schlichte, B. Spliethoff, A. Wingen, S. Kaskel, J. S. Bradley, F. Schueth, *Angew. Chem. Int. Ed.* **2001**, *40*, 4204-4207.
- [67] M. S. Bazarjani, H.-J. Kleebe, M. M. Müller, C. Fasel, M. B. Yazdi, A. Gurlo, R. Riedel, *Chem. Mater.* **2011**, *23*, 4112-4123.
- [68] F. Chen, C. -L. Chen, S. Ding, Y. Yue, C. Ye, F. Feng, *Chem. Phys. Lett.*, **2004**, *383*, 309-313.
- [69] M. A. Springuel-Huet, J. Demarquay, T. Ito, J. Fraissard, *Stud. Surf. Sci. Catal.* **1988**, *37*, 183.
- [70] M. A. Springuel-Huet, M. A. Bonardet, J. L. Fraissard, *J. Appl. Magn. Reson.* **1995**, *8*, 427-456.
- [71] R. Anedda, D. V. Soldatov, I. L. Moudrakovski, M. Casu, J. A. Ripmeester, *Chem. Mater.* **2008**, *20*, 2908-2920.
- [72] S. -J. Huang, S. Huh, P. -S. Lo, S. -H. Liu, V. S.-Y. Lin, S. -B. Liu, *Phys. Chem. Chem. Phys.* **2005**, *7*, 3080-3087.

- [73] K. J. Ooms, K. Campbell, R. R. Tykwinski, R. E. Wasylshen, R. R. Tykwinski, *J. Mater. Chem.* **2005**, *15*, 4318-4327.
- [74] K. Campbell, K. J. Ooms, M. J. Ferguson, P. J. Stang, R. E. Wasylshen, R. R. Tykwinski, *Can. J. Chem.* **2011**, *89*, 1264-1276.
- [75] A. Jablonski, K. Wandelt, *Surf. Sci.* **1991**, *251–252*, 650-655.
- [76] A. Kuznetsova, J. T. Yates, V. V. Simonyan, J. K. Johnson, C. B. Huffman, R. E.J. Smalley, *Chem. Phys.* **2001**, *115*, 6691-6698.
- [77] F. M. Clewett, S. W. Morgan, B. Saam, T. Pietrass, *Phys. Rev. B.* **2008**, *78*, 235402.
- [78] B. Driehuys, G. D. Cates, W. Happer, *Phys. Rev. Lett.* **1995**, *74*, 4943-4946.
- [79] T. Meersman, J. W. Logan, R. Simonutti, S. Caldarelli, A. Comotti, P. Sozzani, L. G. Kaiser, A. Pines, *J. Phys. Chem. A* **2000**, *104*, 11665-11670.
- [80] T. Vergunst, F. Kapteijn, J.A. Moulijn, *Ind. Eng. Chem. Res.* **2001**, *40*, 2801–2809.
- [81] S. Domínguez-Domínguez, A. Berenguer-Murcia, D. Cazorla-Amorós, A. Linares-Solano, *J. Catal.* **2006**, *243*, 74-81.
- [82] C. Li, Z. Shao, M. Pang, C. T. Williams, C. Liang, *Catal. Today* **2011**, *186*, 69-75.
- [83] B. A. Wilhite, M. J. McCready, A. Varma, *Ind. Eng. Chem. Res.* **2002**, *41*, 3345-3350.
- [84] S. Domínguez-Domínguez, A. Berenguer-Murcia, A. Linares-Solano, D. Cazorla-Amorós, *J. Catal.* **2008**, *257*, 87-95.
- [85] S. Mandal, D. Roy, R. V. chaudhary, M. Sastry, *Chem. Mater.* **2004**, *16*, 3714-3724.
- [86] W. Liu, C. O. Arean, S. Bordiga, E. Groppo, A. Zecchina, *ChemCatChem*, **2011**, *3*, 222-226.

- [87] A. Mastalir, Z. Kiraly, *J. Catal.* **2003**, *220*, 372-381.
- [88] P. Weerachawanasak, O. Mekasuwandumrong, M. Arai, S. –I. Fujita, P. Praserthdam, J. Panpranot, *J. Catal.* **2009**, *262*, 199-205.
- [89] S. Domínguez-Domínguez, A. Berenguer-Murcia, B. K. Pardhan, A. Linares-Solano, D. Cazorla-Amorós, *J. Phys. Chem. C.* **2008**, *112*, 3827-3834.
- [90] M. Bautista, J. M. Campelo, A. Garcia, D. Luna, J. M. Marinas, R. A. Quiros, A. A. Romero, *Catal. Lett.* **1998**, *52*, 205-213.
- [91] X. Chen, A. Zhao, Z. Shao, C. Li, C. T. Williams, C. Liang, *J. Phys. Chem. C.* **2010**, *114*, 16525-16533.
- [92] X. Chen, M. Li, J. Guan, X. Wang, C. T. Williams, C. Liang, *Ind. Eng. Chem. Res.* **2012**, *51*, 3604-3611.

## 6.6 Supporting information

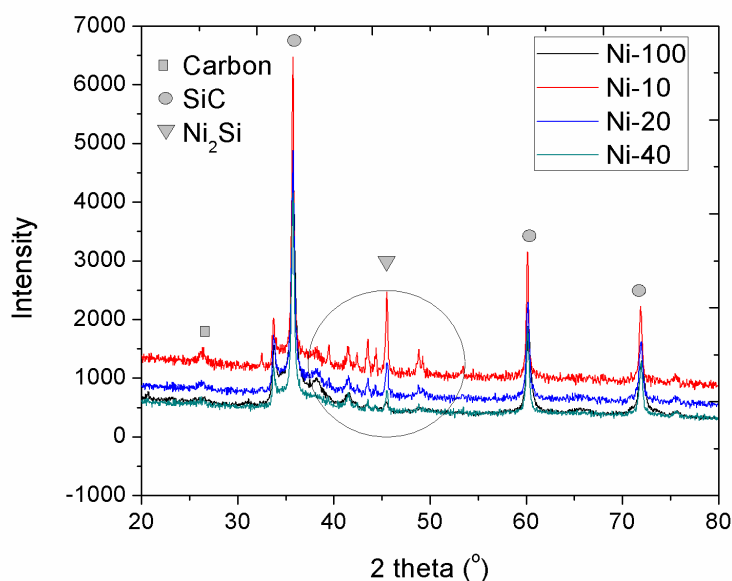


**S1.** Schematic presentation of various silicon environments generated by the catalytic effect of Ni complex and pyrolysis. The hydrosilylation reaction mainly takes place at room temperature while the dehydrocoupling and loss of methane takes place majorly during pyrolysis.

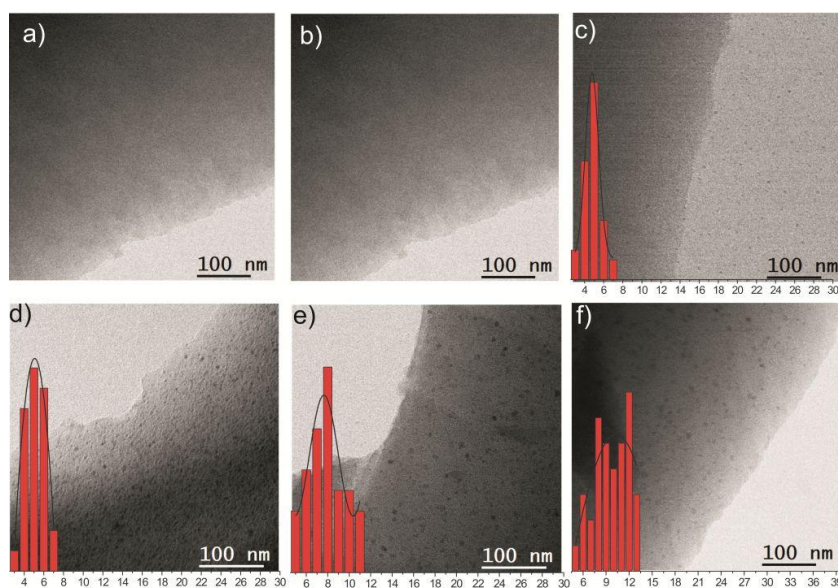
**S2.**  $^{13}\text{C}$  MAS NMR chemical shifts assigned to various carbon environments.

Carbon Function	Si- $\underline{\text{C}}\text{H}_3$	Si-( $\underline{\text{C}}\text{H}_2$ ) $_n$ -Si	Si $\underline{\text{C}}_4$	$\underline{\text{C}}\text{H}_2=\underline{\text{C}}\text{H}-$	graphite
Chemical Shift (ppm) [a]	-4 to 5	12 (n = 1 or 2)	24	132,141	135

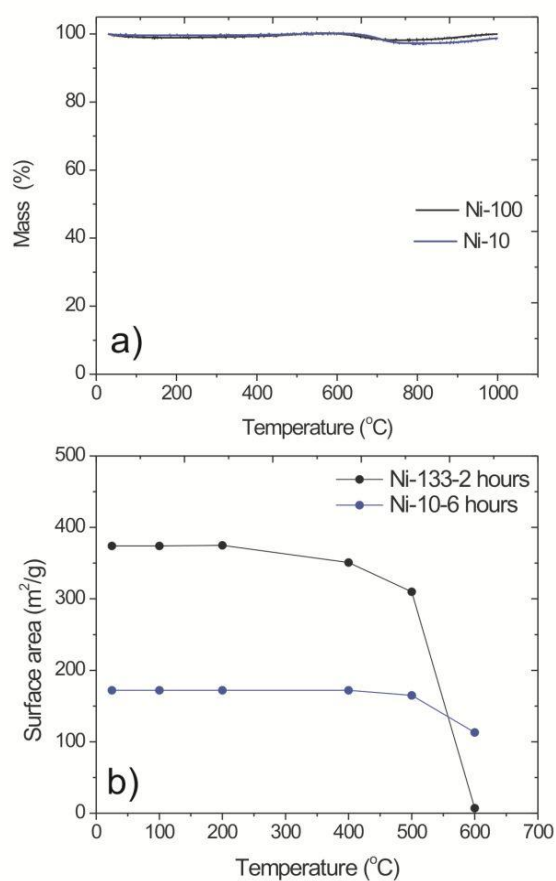
[a] chemical shift values taken from references 32-38.



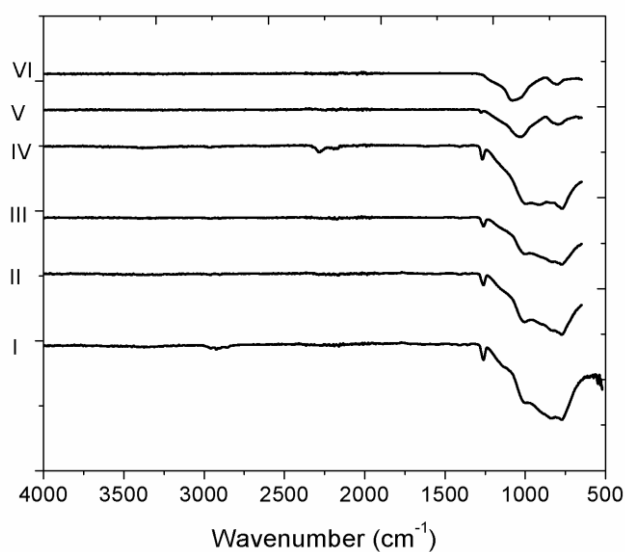
**S3.** Powder XRD pattern of materials pyrolyzed at 1100°C (nitrogen) and post heated to 1500°C (argon).



**S4.** TEM micrographs along with the particle size count of Ni-100 (600°C/ 2 hours) at room temperature (a), 300 (b), 500 (c), 700 (d), 900 (e) and 1100°C (f). The nanoparticles grow in size with an increase in annealing temperature.



**S5.** TGA (5 K/min, Ar) of Ni-10 and Ni-100 (a) along with the change in the surface area with temperature in an oxidative environment (b).



**S6.** FT-IR spectra of Ni-133 (II) after stirring in THF at room temperature (under air) for 24 hours (I) and heating in air at 200 (III), 400 (IV), 500 (V) and 600 °C (VI).

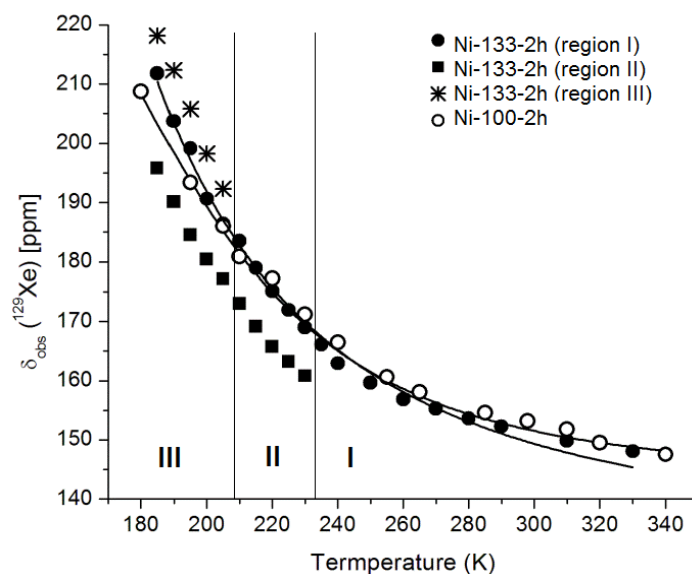
### 6.6.1 <sup>129</sup>Xe Chemical Shift Analysis

Evaluation of the thermodynamic properties within the low temperature regime can provide alternate information as  $\delta_{\text{Xe-Xe}}$ ,  $\delta_{\text{SAS}}$ , and  $\delta_{\text{E,M}}$  contributions become more significant. Slower diffusion rates and higher coverage result in stronger Xe-surface interactions. Previous analysis of the ratio of signal intensities examines the *total* Xe uptake with respect to the gas phase. Here we can further elucidate Xe adsorption parameters as additional amorphous voids become discernible within emerging chemical shifts at higher loadings. The temperature dependencies of the  $\delta_{\text{obs}}$  in both Ni-133-2h and Ni-100-2h are shown in S7. Resonances extracted from deconvoluted CF-HP <sup>129</sup>Xe spectra (Ni-133) are specified by region (I, II or III), the boundaries of which are consistent with previously described phenomena in the high temperature limit. Under fast exchange conditions, the temperature and pressure dependence of the observed chemical shift can be expressed as (Anedda *et al.*):

$$\delta_{\text{obs}} = \delta_{\text{S}} + \Delta\delta \left[ \frac{pk' \exp(-\Delta H_{\text{ads}}/RT)}{T^{0.5} + pk' \exp(-\Delta H_{\text{ads}}/RT)} \right] \quad (1)$$

Terms:  $\Delta\delta$ ,  $p$  and  $k'$  refer to the total variation in the chemical shift, the relative pressure, and extracted pre-exponential factor which is relatable to the standard entropy change. The other terms are the same as described previously within the main text.

Thermodynamic parameters extracted from experimental results are tabulated in S8, where the  $\delta_{\text{S}}$  was obtained directly from the fit and  $\Delta S^{\circ}$  determined from the extracted  $k'$  value. The similar adsorption enthalpies found for Xe in both Ni-133-2h and Ni-100-2h are found in the high temperature regime (low loading). The specific values are provided with the main text. The slight decrease in the  $\Delta H_{\text{ads}}$  value with increased nickel-content and SiN<sub>4</sub> networking suggests further penetration into internal voids. The molecular restriction resulting from sampling more ordered amorphous domains can explain the noticeable loss in mobility (negative  $\Delta S^{\circ}$  value). We tentatively assign the asymmetric downfield resonance off the main adsorption peak to Xe in more confined pore spaces (region III). Despite the loss in resolution due to higher Ni-particle inclusion, a closer examination of the Xe lineshape of Xe adsorbed within Ni-100-RT shows downfield asymmetric broadening off the main resonance at reduced temperatures, similar to that in Ni-133-2h. The difference in  $\Delta S^{\circ}$  between these resonances likely reflects the probing of CSiN<sub>3</sub> and SiN<sub>4</sub> rich

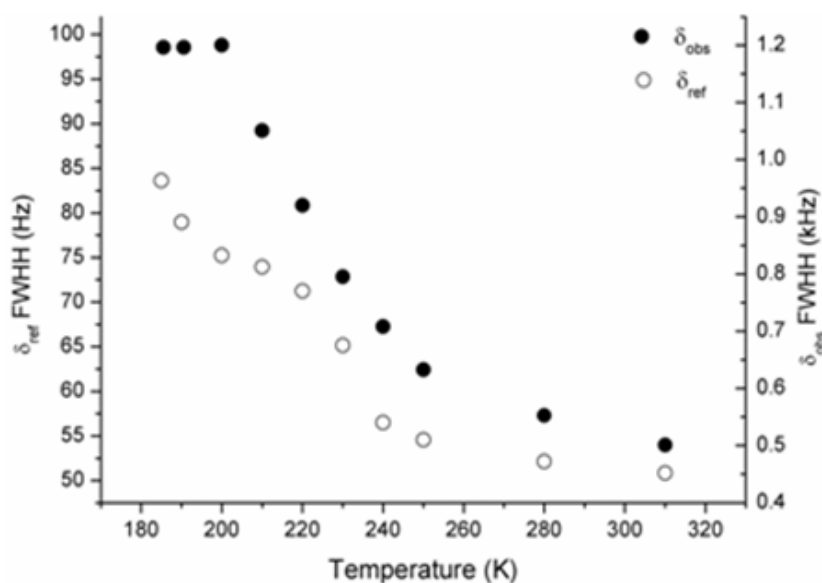


**S7.** Variation in the observed CF-HP  $^{129}\text{Xe}$  chemical shift for Ni-133-2h and Ni-100-2h samples with temperature. Open symbols correspond to Ni-100-2h while and symbols to Ni-133-2h. Regions I, II, and III refer to the previously discussed linear segments shown in Fig. 10 (VT behavior of Ni-133-2h, Fig. 10).

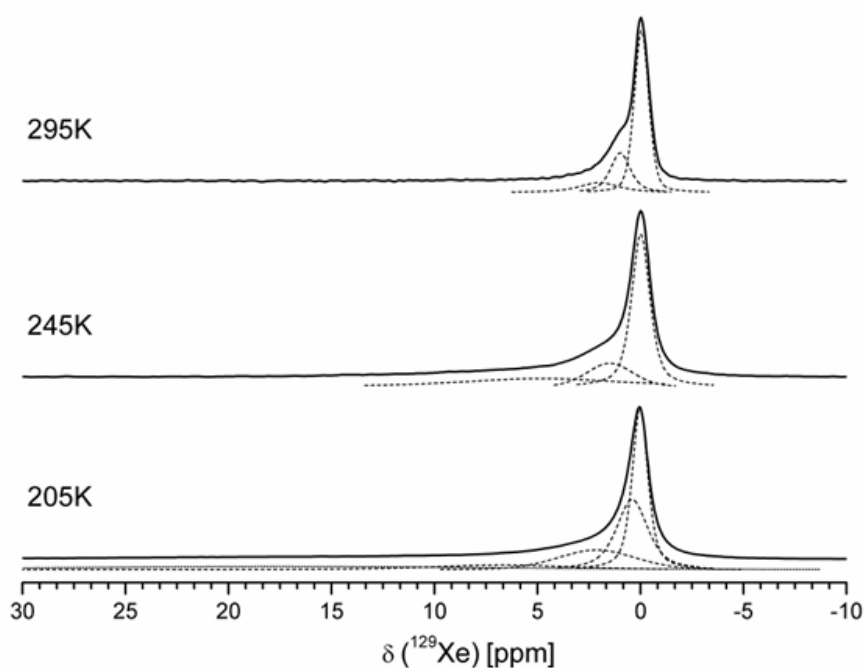
**S8.** Experimentally determined thermodynamic parameters obtained from the evaluation of chemical shift data (S6). Ni-13-2h and Ni-100-2h.

Low Temperature Regime				
(high Xe loading)				
Sample	$\Delta H'_{\text{ads}}$ (kJ/mol Xe)	$\Delta S^\circ$ (J/Kmol Xe)	$\delta_s$ (ppm)	$\Delta\delta$ (ppm)
Ni-133				
-region I	-9.6	-7.5	133.1	161.9
-region II	-14.4	-29.2	146.5	80.5
-region III	-14.5	-29.8	147.1	118.2
Ni-100-RT	-10.3	-7.2	143.2	96.2

environments. The upfield resonance (region II-  $\square$  symbol in S7), may be attributed to structural distortions which trap adsorbed Xe within differing amorphous voids.



**S9.** The substantial broadening of the  $^{129}\text{Xe}$  resonances are observed with cooling.  $\delta_{\text{ref}}$  (%) refers to the peak attributed to the gaseous Xe, and  $\delta_{\text{obs}}$  (●) to Xe adsorbed within the porous environment. Their corresponding y-axis' are placed on the left and right side of the graph, respectively. The linewidths were obtained assuming two-site exchange between a single adsorption site and the gaseous Xe.



**S10.** Variation in the observed CF-HP  $^{129}\text{Xe}$  chemical shift for Ni-20-6h with temperature. Ni-20-6h possesses the highest nickel content and largest nickel particle size. Only a multi-component asymmetric line broadening around the gas phase is observed—cooling significantly enhances these features.

## 7. Robust Heterogeneous Nickel Catalysts with Tailored Porosity for the Selective Hydrogenolysis of Aryl Ethers

---

Muhammad Zaheer,<sup>[a]</sup> Justus Hermannsdörfer,<sup>[a]</sup> Winfried P. Kretschmer,<sup>[a]</sup> Günter Motz<sup>[b]</sup> and Rhett Kempe<sup>[a]\*</sup>

[a] Inorganic Chemistry II, University of Bayreuth, 95440 Bayreuth, Germany, E-mail: [kempe@uni-bayreuth.de](mailto:kempe@uni-bayreuth.de) [b] Ceramic Materials Engineering, University of Bayreuth, 95447 Bayreuth.

**Published in:** *ChemCatChem* **2013**, DOI: 10.1002/cctc.201300763.

The sustainable production of fine chemicals and fuels, from renewable resources is a burgeoning and challenging research area.<sup>[1]</sup> Lignocellulose biomass (cellulose, hemicellulose, lignin), is a key resource whose availability is plentiful and its utilization will allay the fears regarding competition with food supplies.<sup>[2]</sup> Whereas, cellulose can be depolymerized in many ways,<sup>[3]</sup> selective cleavage of aryl ether (C<sub>Ar</sub>-O) and especially diaryl ether substructure of lignin is challenging.<sup>[4]</sup> In spite of the fact that lignin constitutes almost 15-30% of the woody biomass<sup>[5]</sup> with an energy content up to 40%<sup>[6]</sup> its depolymerization *via* hydrogenolysis is crucial for the generation of fuel and chemicals. Selective cleavage of the C<sub>Ar</sub>-O bond of lignin model compounds has been reported by the use of both molecular catalysts (V,<sup>[7]</sup> Ru<sup>[8]</sup> and Ni<sup>[9]</sup> complexes) or applying heterogeneous catalysts (Ni<sup>[10]</sup> Zn/Pd<sup>[11]</sup>). The molecular catalysts offer better chemoselectivity in the selective cleavage of C<sub>Ar</sub>-O bonds and are operative under mild conditions (80-135°C) but are sensitive to large concentration of water whose removal from the crude biomass is challenging and uneconomic. The heterogeneous catalysts, on the other hand, require either higher reaction temperatures (~250°C) or hydrogen pressure (>30 bar)<sup>[9]</sup> which leads to substantial reduction of arenes (and subsequent hydrogen loss). Interestingly, the Lercher group has reported on the use of solid catalysts for the cleavage of ether bonds in water.<sup>[12-14]</sup> The substantial reduction of arenes was also observed. Reports

on the reusability of hitherto applied catalysts are rare. Thus, there is a need for a reusable robust heterogeneous catalyst offering hydrothermal stability for the selective cleave of C<sub>Ar</sub>-O bonds.

In past few years, we and others have developed late transition metals containing polymer derived SiCN materials (M@SiCN) as robust heterogeneous catalysts.<sup>[15]</sup> The Wiesner group fabricated Pt@SiCN materials which, despite of the structural control over multiple length scales, showed very low surface area.<sup>[16]</sup> By the controlled pyrolysis of Ni modified polysilazane, we managed to get high surface area microporous materials which were found selective catalysts in the hydrogenation of phenylacetylene.<sup>[17]</sup> Unfortunately, the Si-N bonds of the materials pyrolyzed at 600°C were sensitive to hydrolysis under harsh conditions. SiC materials do not contain such bonds and, in consequence, should offer additional hydrothermal stability. Commercially available silicon carbide possesses low surface area, which limits the effective transport of substances through it for efficient catalysis.<sup>[18]</sup> Self assembly of block copolymers<sup>[19]</sup> has been applied by Kim and co-workers for the fabrication of mesoporous SiC materials and allows fine tuning of pore morphology.<sup>[20]</sup> Porous iron containing SiC materials have been fabricated by Manners group *via* self assembly of metal containing block copolymers.<sup>[21]</sup>

Here we report on the synthesis of polymer derived porous SiC composites with integrated nickel nanoparticles (Ni NPs) by the self assembly of organic-inorganic block copolymers (BCPs). The synthesis, cross-linking and microphase separation of BCPs is achieved in a concerted process<sup>[22]</sup> followed by controlled pyrolysis which leads to porous Ni@SiC composite materials. The porosity of the materials can be tailored from micro- to meso scale including hierarchical (micro-meso) structures by changing the molecular weight of the organic block. In particular synthesis of mesoporous Ni@SiC materials with an average pore diameter (2-8 nm) was achieved which is challenging due to high Laplace pressure leading to the pore collapse.<sup>[22]</sup> Phenethoxybenzene (PEB) and diphenylether (DPE) mimicking the most frequent  $\beta$ -O-4 (45-62%) and 4-O-5 (4-9%) linkages of lignin (see Fig. 1), are used as model compounds for the chemoselective cleavage of C<sub>Ar</sub>-O bond. Ni@SiC catalysts are active under mild reaction conditions (90-120°C, 6 bar hydrogen) in water providing high selectivity for hydrogenolysis of C<sub>Ar</sub>-O bond and reusability.

The synthesis of Ni@SiC materials is summarized in Scheme 1. An organic-inorganic

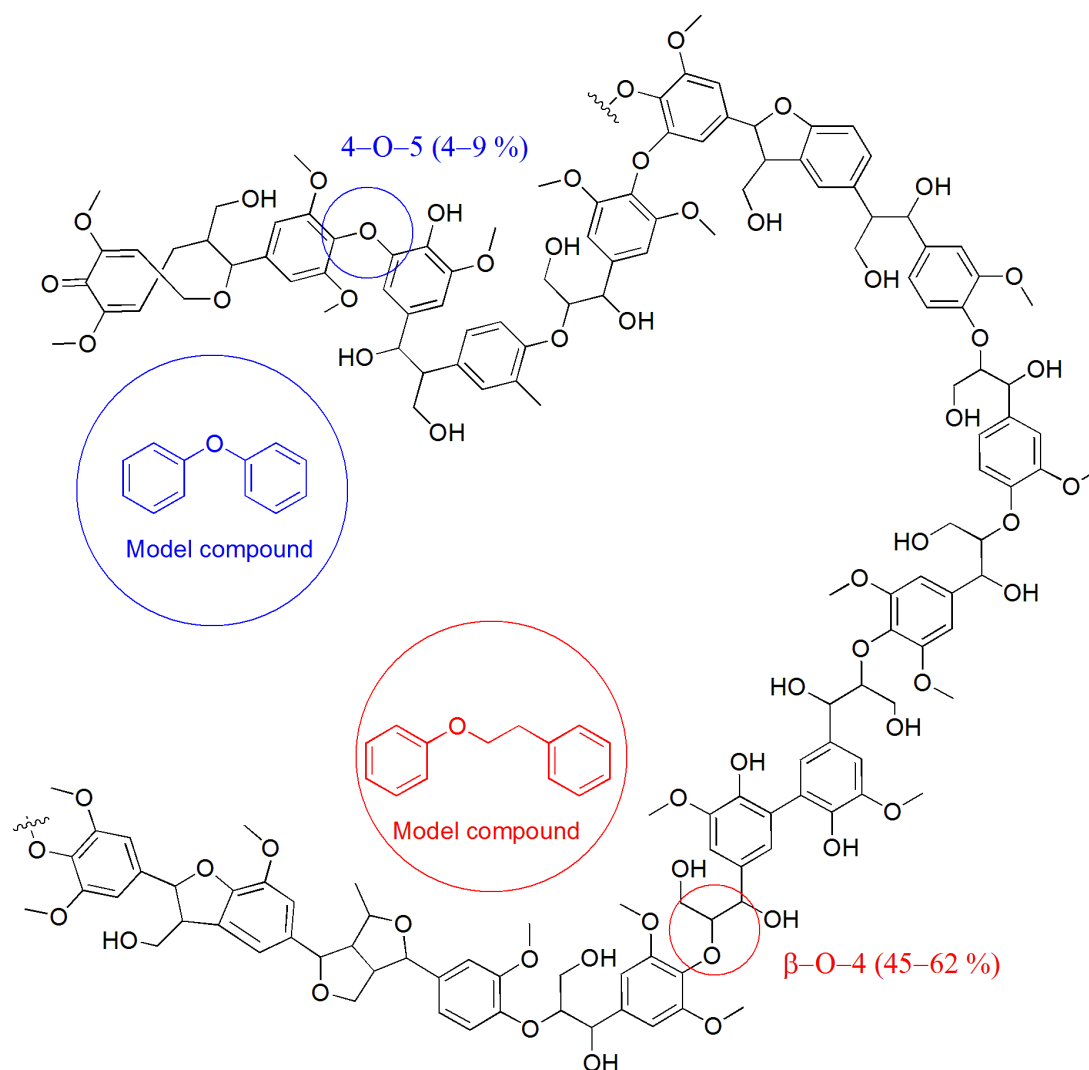
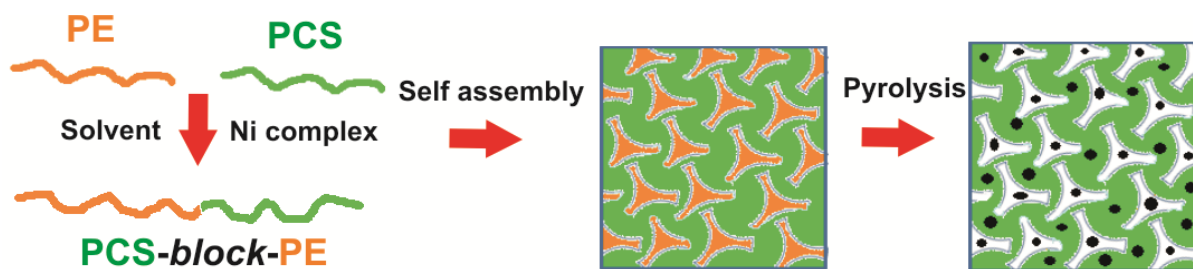


**Figure 1.** A fragment of hard wood lignin.

block copolymer is formed by the reaction (1:1 wt ratio) of polycarbosilane (PCS) with hydroxy-terminated polyethylene (PE) *via* nickel catalyzed dehydrocoupling of Si-H and O-H functions.<sup>[23]</sup> The added nickel complex (see Fig. S1 supporting information (SI) for structure) also catalyzes the cross-linking of polycarbosilane block *via* homocoupling of Si-H bonds. As both blocks are immiscible and covalently linked, the microphases separate in the presence of a solvent into microdomains providing a nanostructured material. The PE block used is inexpensive and can be produced efficiently using molecular catalysts.<sup>[24]</sup> The crystallization behavior of strictly linear PE allows good morphology control even in combination with rather ill-defined inorganic blocks.<sup>[25]</sup> The organic block is burnt out during pyrolysis (700°C/ Ar) whereas Ni (II) species are reduced to elemental nickel. Thus, porous SiC materials



**Scheme 1.** The synthesis of porous Ni@SiC materials *via* the self assembly of polycarbosilane-*block*-polyethylene (PCS-*b*-PE). The BCP is synthesized *via* Ni complex catalyzed dehydrocoupling of polycarbosilane (PCS) with polyethylene (PE).

with integrated Ni NPs are generated. The loading of nickel complex was adjusted so that the final materials after pyrolysis contain 4.3 wt% of nickel with a Si/Ni ratio of 20/1 (Table S2, SI). The molecular weight of the organic block (PE) affects the type of porosity generated in the Ni@SiC catalyst. As the high density PE can be produced inexpensively using efficient molecular catalysts, we decided to use it for the fabrication of SiC materials.<sup>[27]</sup> The use of a PE (1739 g/mole) after self assembly and pyrolysis provided Ni@SiC materials. The structure of the materials was investigated by TEM which indicates that Ni NPs with an average size of 3 nm (Fig. 2c) decorated the porous SiC matrix (Fig. 2). The material is mainly mesoporous as shown by N<sub>2</sub>-adsorption studies. Fig. 2d shows nitrogen adsorption-desorption isotherm with type-IV hysteresis indicative of a mesoporous material. Another evidence of the existence of mesopores comes from the closure of desorption branch at P/P<sub>0</sub> ~0.4, which is due to capillary condensation, a process typically known for mesoporous materials. To a BET surface area ( $S_{\text{BET}}$ ) of 450 m<sup>2</sup>/g, only 38 m<sup>2</sup>/g is contributed by micropores as calculated by t-plot method (see entry 1, Table S3, supporting information). The size of the pores was calculated by NLDFT (adsorption branch) and is in 2 to 8 nm size range which is in close agreement with TEM images. The presence of Ni NPs was confirmed by PXRD analysis of the materials (see Fig. 2d) which shows a broad reflection at 44.6° corresponding to 111 plane of cubic nickel (ICDD PDF number: 00-001- 1260). A broad reflection at 26.5° corresponds to the amorphous graphitic carbon. When molecular weight of the organic block (PE) was decreased to 326 g/mole) microporous materials ( $S_{\text{BET}} = 552 \text{ m}^2/\text{g}$ ) were obtained. The material shows typical type-I adsorption isotherm (see Fig. 3c) with an average pore width of 1.3 nm (Fig. S6, SI). The external surface area (69 m<sup>2</sup>/g) shows a little contribution from mesopores as well (entry 2, Table S3, SI). Ni NPs are

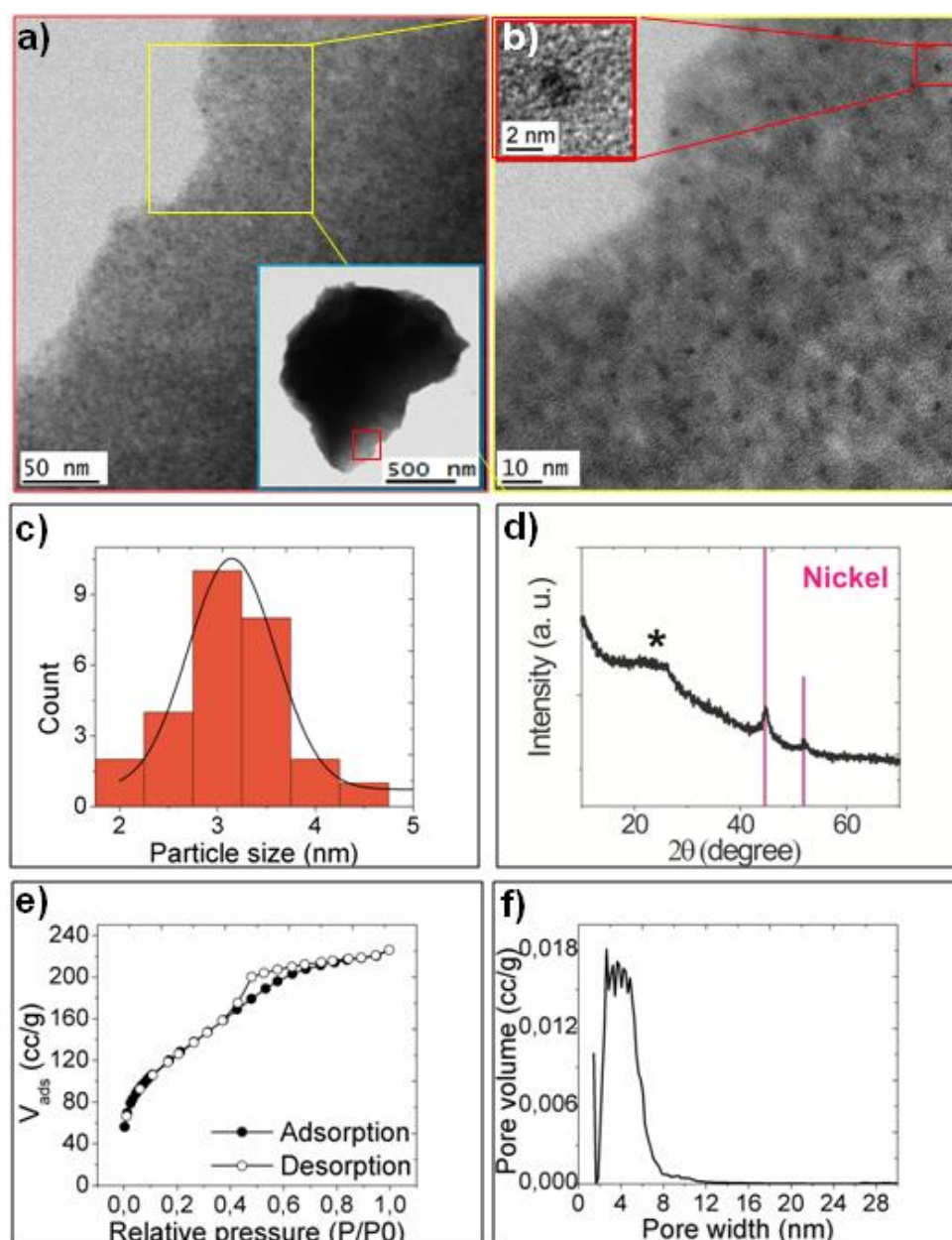


**Figure 2.** a-b) TEM micrographs of mesoporous Ni@SiC (SiC-meso) with Ni NPs and c) corresponding size distribution. d) PXRD pattern with nickel reflexes and asterisk denoting graphitic phases. e)  $N_2$ -adsorption-desorption isotherm and f) corresponding pore size distribution calculated by NL-DFT model using silica kernel with cylindrical pore geometry.

of smaller size (2.3 nm, Fig. 3b) as compared to the mesoporous materials and are uniformly distributed over the material as shown in TEM images (Fig. 3a). PXRD analysis of the material (Fig. S7a) confirms the presence of Ni NP. At this stage, it seems that porosity of the Ni@SiC materials can be tailored by varying the molecular weight of PE used. Whereas, lower molecular weight PE (326 g/mole) provides microporous materials, mesoporous materials can be obtained by higher molecular weight PE (1739 g/mole). We expected to get a hierarchical (micro-meso) material by

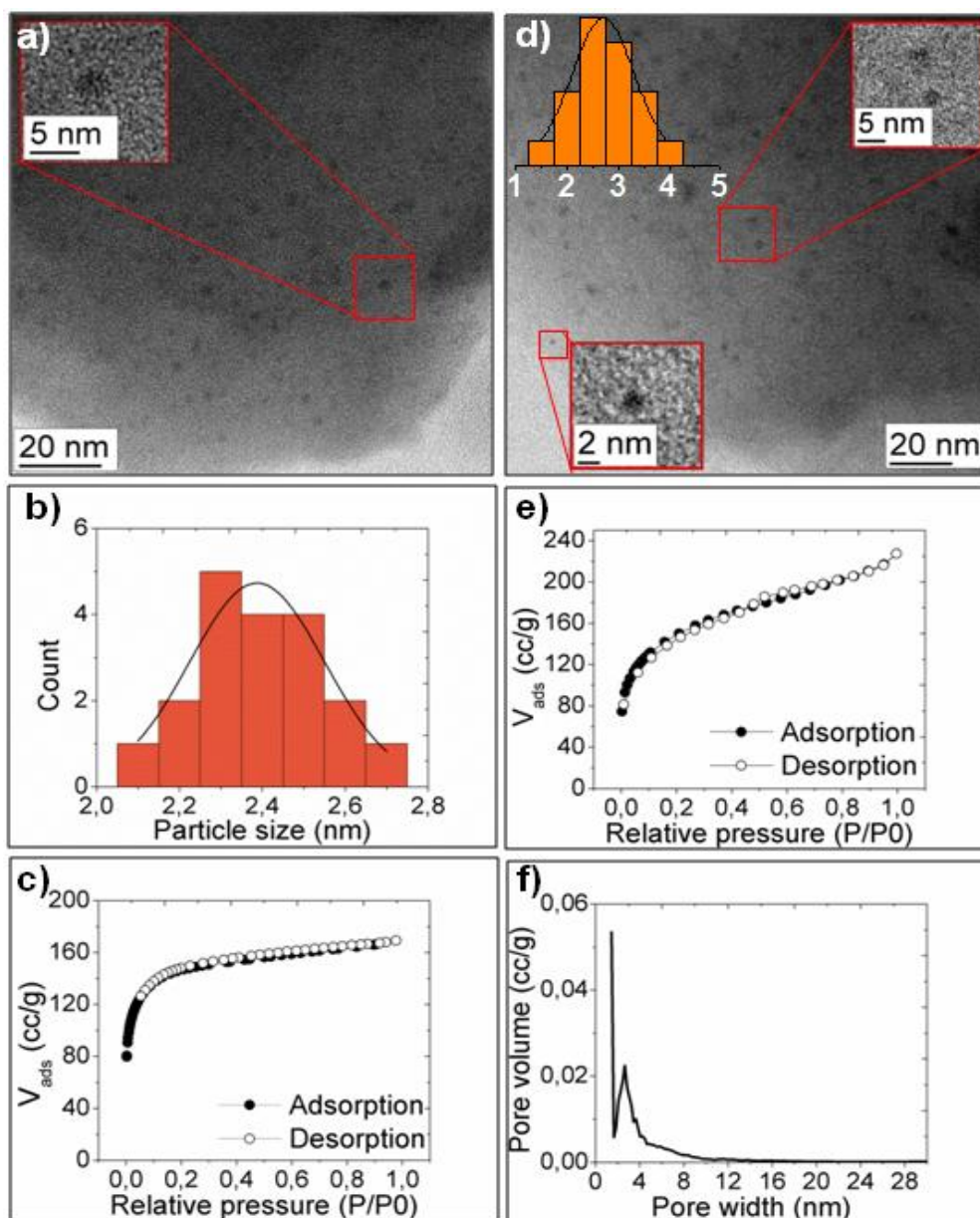


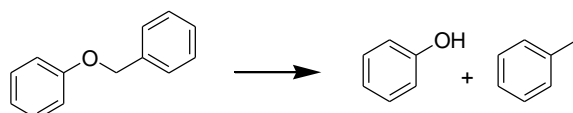
**Figure 3.** a) TEM micrograph with inset HR-TEM, b) particle size distribution and c) N<sub>2</sub>-adsorption isotherm for SiC-micro material. d) TEM micrograph with particle size count and HR-TEM insets, e) N<sub>2</sub>-adsorption isotherm and f) pore size distribution calculated by NLDFT method for SiC-hier material.

the use of a PE with intermediate chain length. When PE with a molecular weight of 550 g/mole was used, materials with hierarchical porosity (SiC-hier) were obtained. The formation of amorphous SiC was confirmed by FT-IR and solid state <sup>29</sup>Si NMR analysis of the materials (Figure S8, SI). The later shows broad peaks at -16 and -65 ppm assigned to SiC<sub>4</sub> and CSiO<sub>3</sub> environments respectively.<sup>[26]</sup> A slight amount of oxygen in the materials comes from the hydroxy-terminated PE. As shown in Fig. 3, materials containing nickel particles with an average size of 2.5 nm were obtained. High uptake of nitrogen both at lower and higher relative pressure values (Fig. 3e) is

indicative of the existence of both micro and meso pores. The NLDFT model applied to the  $N_2$ -adsorption isotherm (Fig. 3f) suggests the presence of micro and mesopores. Contributions to the total surface area of SiC-hier ( $552 \text{ m}^2/\text{g}$ ) came partly from the micropores ( $326 \text{ m}^2/\text{g}$ ) and partly from mesopores ( $202 \text{ m}^2/\text{g}$ ) as tabulated in Table S3 (entry 3, SI). The pores are produced by the gaseous emission (mostly hydrocarbons) from the burning of the organic block (see Fig. S9 for TGA of all the materials).

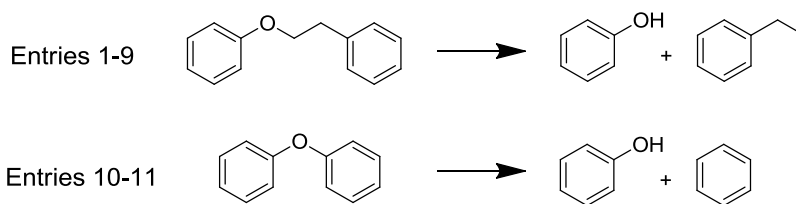
The selective hydrogenolysis of lignin model compounds mimicking the most abundant  $\beta$ -O-4 (phenethoxybenzene) and 4-O-5 (diphenylether) linkages was studied in water under 6 bar hydrogen pressure. The activity comparison of all the three type of Ni@SiC materials was tested in hydrogenolysis of benzylphenylether at  $110^\circ\text{C}$  for 20 hours. SiC-hier with hierarchical porosity was found to be the most active catalyst providing 99% conversion (Entry 2, Table 1) while in the case of microporous SiC-micro, the conversion of substrate ether was 75% (Entry 1). Mesoporous Ni@SiC (SiC-meso) showed only 26% conversion (Entry 3). The selectivity towards aromatic products (phenol and toluene) was high in all the three catalysts tested. As the aryl ethers are insoluble in water, the addition of a phase

**Table 1.** Hydrogenolysis of benzylphenylether (BPE) with Ni@SiC catalysts in water for 20 hours<sup>[a]</sup>.



Entry	catalyst	T ( $^\circ\text{C}$ )	Base (equi)	TBAB (equi)	Conv (%)	Sel <sup>[b]</sup> (%)
1	SiC-micro*	110	-	-	75	94
2	SiC-hier*	110	-	-	99	81
3	SiC-meso*	110	-	-	26	98
4	SiC-micro	90	1	0.3	90	99
5	SiC-hier	90	1	0.3	99	99
6	SiC-meso	90	1	0.3	64	99

[a] Conditions: 0.5 mmol of ether was mixed with either 15 mg of catalyst ( $1.17 \times 10^{-5}$  mole Ni) or \*40 mg catalyst ( $3.13 \times 10^{-5}$  mole Ni) in 2 mL water at a hydrogen pressure of 6 bar (\*10 bar) and stirred (1000 rpm) at a specified temperature for 20 hours. [b] Selectivity to phenol in mol%.

**Table 2.** Hydrogenolysis of phenethoxybenzene (entries 1-9) and diphenylether (entries 10-11) with Ni@SiC catalysts in water for 20 hours<sup>[a]</sup>.

Entry	catalyst	Base (equi)	TBAB (equi)	Conv (%)	Sel <sup>[b]</sup> (%)
1	SiC-hier	-	-	0	0
2	SiC-hier	-	0.3	0	0
3	SiC-hier	NaOH (1)	-	27	99
4	SiC-hier	NaOH (1)	0.3	93	92
5	SiC-hier	K <sub>2</sub> CO <sub>3</sub> (1)	0.3	71	84
6	SiC-hier	NaOtBu(1)	0.3	89	94
7	SiC-hier	KOtBu (1)	0.3	99	96
8	SiC-micro	NaOH (1)	0.3	78	95
9	SiC-meso	NaOH (1)	0.3	25	99
<b>10</b>	<b>SiC-hier</b>	<b>KOtBu (1)</b>	<b>0.3</b>	<b>50</b>	<b>98</b>
<b>11</b>	<b>SiC-hier*</b>	<b>KOtBu(2.5)</b>	<b>1.0</b>	<b>96</b>	<b>97</b>

[a] Conditions: 0.5 mmol of ether was mixed with either 15 mg of catalyst ( $1.17 \times 10^{-5}$  mole Ni) or \*30 mg ( $3.42 \times 10^{-5}$  mole Ni) in 2 mL water at a hydrogen pressure of 6 bar and then stirred (1000 rpm) at a specified temperature for 20 hours. [b] Selectivity to phenol (ethylbenzene/benzene selectivity > 99% in all cases)

transfer catalyst could be advantageous. With the addition of 0.3 equivalents of tetrabutylammoniumbromide (TBAB), hydrogenolysis of benzylphenyl ether was achieved even at 90°C. Again, SiC-hier showed the highest activity (Entry 5) than SiC-micro (90%) and SiC-meso (64%, see entries 4, 6 in Table 1). At this temperature no further hydrogenation of phenol to cyclohexanol was observed provi-

-ding phenol in 99% selectivity. Hierarchically porous SiC-hier, because of its higher activity than the other two catalysts (SiC-micro and SiC-meso) was chosen for the selective cleavage of  $\beta$ -O-4 linkage to phenol and ethylbenzene (see Fig. S10, SI). No conversion was observed at 120°C in the absence of base and TBAB (Entry 1, Table 2) or in the presence of TBAB alone (Entry 2). A minor conversion (27%) was achieved by the addition of a base (Entry 3) which increased by many folds (93%) upon the addition of both the base and TBAB (Entry 4). Whereas lower conversion and selectivity was obtained using  $K_2CO_3$  as base (Entry 5), other bases (NaOtBu and KOtBu) provided good yields and selectivities (Entries 6-7). In comparison to SiC-hier, the other two materials (SiC-micro and SiC-meso) had lower activities (Entries 8-9). A minor conversion of phenol (hydrogenation product of phenol) was observed in all cases indicating a high chemoselectivity of hydrogenolysis over hydrogenation provided by the catalysts.

The effect of the amount of TBAB and base was also investigated. On increasing the amount of TBAB, conversion increased with up to 0.3 mole equivalents of the ether used and then became almost constant (see Fig. S11a, SI). Keeping the amount of TBAB to 0.3 equivalents, an increase in the concentration of base (NaOtBu) increased the overall conversion up to 1 mole equivalent of base relative to the ether. With more than 1 equivalent of base, the conversion decreased (see Fig. S11b, SI).

These optimized conditions were also applied to selectively cleave the 4-O-5 linkage of DPE, the model compound for 4-O-5 linkage (see Fig. 1). 50% of DPE was converted into phenol and toluene (Entry 10) with very high selectivity (98%). The phenol selectivity was nearly quantitative. By doubling the amount of the catalyst, base and phase transfer catalyst, almost quantitative conversion of DPE was achieved (Entry 11). The selectivity towards phenol and benzene was again as high as 97%. These results showed the hierarchical Ni@SiC materials to be highly selective towards hydrogenolysis of  $C_{Ar}$ -O bond without hydrogenation of aromatic ring(s). In comparison to previous works, we have achieved the selective cleavage of  $C_{Ar}$ -O in water (avoiding the use of organic solvents) and with a lower nickel content (4.3wt %).

The recycling of the catalyst (SiC-hier) was tested at almost 50% conversion of PEB at 120°C under 6 bar of hydrogen. No prominent loss in the activity was observed up to five consecutive catalysts runs (see Fig. S12, SI).

In summary, we have developed a robust porous SiC materials with integrated Ni NPs. A tunable porosity could be accomplished *via* the self assembly of organic-inorganic block copolymers. Depending upon the molecular weight of the organic block (inexpensive polyethylene), the fabrication of micro-, meso- and hierarchically porous Ni@SiC catalysts is possible. All catalysts were found to be active in ether hydrogenolysis. Hierarchical Ni@SiC materials were found to be the most active catalyst. It is a reusable catalyst and is efficient in the selective hydrogenolysis of diaryl ethers, a challenging lignin model compound.

## 7.1 Experimental

The starting materials 4-methyl-2-((trimethylsilyl)amino)pyridine,<sup>[27]</sup> the Ni complex<sup>[28]</sup> and phenethoxybenzene<sup>[13a]</sup> were synthesized following reported methods.

Micro (SiC-micro) and hierarchical (SiC-hier) Ni@SiC materials were fabricated by the reaction of PE-326 and PE-550 with polycarbosilane in THF respectively. In a vial placed in a Schlenk tube, PE (1 g) was dissolved in THF (8 mL) followed by the addition of polycarbosilane (1 g) and Ni complex (0.400 g,  $4.79 \times 10^{-4}$  mole, Ni/Si = 1/20). The solution was annealed at 80 °C for 24 hours during which the solvent comes out of the vial into the Schlenk. Finally the solid was slowly cooled to room temperature.

For the synthesis of mesoporous (SiC-meso) materials, polycarbosilane SMP-10 (1 g) and PE-1739 (1 g) were dissolved in 10 mL of cumene at 150 °C. Afterwards, Ni complex (0.400 g,  $4.91 \times 10^{-4}$  mole) solution in 7 mL of cumene was added. The mixture was cooled to 140 °C and annealed at this temperature for 24 hours. Lastly, obtained solid was slowly cooled to room temperature and traces of the solvent were removed under vacuum.

The catalytic selective hydrogenolysis of lignin model compounds was done in Parr autoclave under a hydrogen pressure. A glass tube was charged with magnetic bar and milled catalyst (particle size: <100 μm) and placed in the reactor which was then filled with hydrogen at room temperature. The reactor was heated to respective temperature within 20 minutes and stirring was continued at this temperature for 20 hours. Afterwards, dodecane was added and mixture was extracted with ethylacetate (3x2 mL). The conversion and selectivity were determined by GC.

For the reusability studies, catalyst was washed with ethanol and water and dried at 80 °C under vacuum.

## Acknowledgements

This work was financially supported by Deutsche Forschungsgemeinschaft, SFB 840. Authors are thankful to Bernard Putz for PXRD analysis. Dr. C. D. Keenan, Dr. Y. S. Avadhut and Prof. Dr. J. Senker are acknowledged for the solid state NMR measurements and discussions. M. Zaheer expresses his gratitude for HEC Pakistan and DAAD for the fellowship.

## 7.2 References

- [1] C. O. Tuck, E. Perez, I. T. Horvath, R. A. Shelden, M. Poliakoff, *Science* **2012**, 337, 695-699.
- [2] a) C. –H. Zhou, X. Xia, C. –X. Lin, D. –S. Tong, J. Beltramini, *Chem. Soc. Rev.* **2011**, 40, 5588-5617; b) P. Gallezot, *Chem. Soc. Rev.* **2012**, 41, 1538-1558; c) M. Alonso, S. G. Wettstein, J. A. Dumesic, *Chem. Soc. Rev.* **2012**, DOI: 10.1039/c2cs35188a; d) R. Rinaldi, F. Schueth, *Energy Environ. Sci.* **2009**, 2, 610-626; e) Y. –C. Lin, G. W. Huber, *Energy Environ. Sci.* **2009**, 2, 68-80; f) J. Q. Bond, D. M. Alonso, D. Wang, R. M. West, J. A. Dumesic, *Science* **2010**, 327, 1110-1114; g) Y. –R. Leshkov, C. J. Barret, Z. Y. Liu, J. A. Dumesic, *Nature* **2007**, 447, 982-986; h) P. Anbarasan, Z. C. Baer, S. Sreekumar, E. Gross, J. B. Binder, H. W. Blanch, D. S. Clark, F. D. Toste, *Nature* **2012**, 491, 235-239.
- [3] a) A. Corma, S. Iborra, A. Velty, *Chem. Rev.* **2007**, 107, 2411-2502; b) G. W. Huber, S. Iborra, A. Corma, *Chem. Rev.* **2006**, 106, 4044-4098.
- [4] a) E. Furimsky, *Appl. Catal. A.* **2000**, 199, 147-190; b) J. Z. Pieter, C. A. Bruijninx , A. L. Jongerius, B. M. Weckhuysen, *Chem. Rev.* **2010**, 110, 3552–3599.
- [5] M. Stöcker, *Angew. Chem. Int. Ed.* **2008**, 47, 9200-9211.
- [6] J. R. Regalbuto, *Science* **2009**, 325, 822-824.

- [7] S. Son, F. D. Toste, *Angew. Chem. Int. Ed.* **2010**, *49*, 3791-3794.
- [8] J. M. Nichols, L. M. Bishop, R. G. Bergman, J. A. Ellman, *J. Am. Chem. Soc.* **2010**, *132*, 12554-12555.
- [9] a) A. G. Sergeev, J. F. Hartwig, *Science*, **2011**, *332*, 439-443; b) M. Tobisu, K. Yamakawa, T. Shimasaki, N. Chatani, *Chem. Commun.* **2011**, *47*, 2946-2948; c) B. S. Samant, G. W. Kabalka, *Chem. Commun.* **2012**, *48*, 8658-8660.
- [10] a) X. Wang, R. Rinaldo, *ChemSusChem*. **2012**, *5*, 1455-1466; b) A. G. Sergeev, J. D. Webb, J. F. Hartwig, *J. Am. Chem. Soc.* **2012**, *134*, 20226-20229; c) E. M. Van-Duzee, H. Adkins, *J. Am. Chem. Soc.* **1935**, *57*, 147-151.
- [11] T. H. Parsell, B. C. Owen, I. Klein, T. M. Jarrell, C. L. Marcum, L. J. Hauptert, L. M. Amundson, H. I. Kenttämä, F. Ribeiro, J. T. Miller, M. M. Abu-Omar, *Chem. Sci.* **2013**, *4*, 806-813.
- [12] V. M. Roberts, R. T. Knapp, X. Li, J. A. Lercher, *ChemCatChem*. **2010**, *2*, 1407-1410.
- [13] a) C. Zhao, J. A. Lercher, *Angew. Chem. Int. Ed.* **2012**, *51*, 5935-5941; b) C. Zhao, J. A. Lercher, *ChemCatChem*. **2012**, *4*, 64-68.
- [14] J. He, C. Zhao, J. A. Lercher, *J. Am. Chem. Soc.* **2012**, *134*, 20768-20775.
- [15] a) G. Glatz, T. Schmalz, T. Kraus, F. Haarmann, G. Motz, R. Kempe, *Chem. Eur. J.* **2010**, *16*, 4231-4238; b) M. Zaheer, G. Motz, R. Kempe, *J. Mater. Chem.* **2011**, *21*, 18825-18831; c) T. Schmalz, T. Kraus, M. Guenther, C. Liebscher, U. Glatzel, R. Kempe, G. Motz, *Carbon* **2011**, *49*, 3065-3072; d) M. Zaheer, T. Schmalz, G. Motz, R. Kempe, *Chem. Soc. Rev.* **2012**, *41*, 5102-5116.
- [16] M. Kamperman, A. Burns, R. Weissgraeber, N. van Vegten, S. C. Warren, S. M. Gruner, A. Baiker, U. Wiesner, *Nano Lett.* **2009**, *9*, 2756-2762.
- [17] M. Zaheer, C. D. Keenan, J. Hermannsdörfer, E. Roessler, G. Motz, J. Senker, R. Kempe, *Chem. Mater.* **2012**, *24*, 3952-3963.
- [18] Y. Shi, Y. Wan, D. Zhao, *Chem. Soc. Rev.* **2011**, *40*, 3854-3878.

- [19] Y. Mai, A. Eisenberg, *Chem. Soc. Rev.* **2012**, *41*, 5969-5985.
- [20] a) Q. D. Nghiem, D. -P. Kim, *Chem. Mater.* **2008**, *20*, 3735-3739; b) Q. D. Nghiem, D. -P. Kim, S. O. Kim, *J. Nanosci. Nanotechnol.* **2008**, *8*, 5527-5531.
- [21] a) D. A. Rider, K. Liu, J. -C. Eloi, L. Vanderark, L. Yang, J. -Y. Wang, D. Grozea, Z. -H. Lu, T. R. Russel, I. Manners, *ACS Nano* **2008**, *2*, 263-270; b) K. Temple, K. Kulbaba, K. N. Power-Billard, I. Manners, K. A. Leach, T. Xu, T. M. Russel, C. J. Hawker, *Adv. Mater.* **2003**, *15*, 297-300.
- [22] M. Seo, M. A. Hillmyer, *Science* **2012**, *336*, 1422-1425.
- [23] a) B. -H. Kim, M. -S. Cho, M. -A. Kim, H. -G. Woo, *J. Organomet. Chem.* **2003**, *685*, 93-98; b) B. -H. Kim, M. -S. Cho, H. -G. Woo, *Syn. Lett.* **2004**, 761-772; c) E. Lukevics, M. Dzintara, *J. Organomet. Chem.* **1985**, *295*, 265-315.
- [24] S. T. K. Pillai, W. P. Kretschmer, M. Trebbin, S. Förster, R. Kempe, *Chem. Eur. J.* **2012**, *18*, 13974-13978.
- [25] S. K. T. Pillai, W. P. Kretschmer, C. Denner, G. Motz, M. Hund, A. Fery, M. Trebbin, S. Förster, R. Kempe, *Small* **2013**, *9*, 984-989.
- [26] a) T. Taki, M. Inui, K. Okamura, M. Sato, *J. Mater. Sci. Lett.* **1989**, *8*, 918-920; b) C. Hoffmann, T. Biemelt, A. Seifert, K. Pinkert, T. Gemming, S. Spange, S. Kaskel, *J. Mater. Chem.* **2012**, *22*, 24841-24847; c) Q. Liu, H. -J. Wu, R. Lewis, G. E. Maciel, L. V. Interrante, *Chem. Mater.* **1999**, *11*, 2038-2048.
- [27] R. Kempe and P. Arndt, *Inorg. Chem.* **1996**, *35*, 2644-2649.
- [28] S. Deekan, S. Proch, E. Casini, H. F. Braun, C. Mechtler, C. Marschner, G. Motz, R. Kempe, *Inorg. Chem.* **2006**, *45*, 1871-1879.

## 7.3 Supporting data

### 7.3.1 General remarks

All reactions were carried out under dry argon using standard Schlenk and glove box techniques. Solvents were dried and distilled from sodium benzophenone before use. Deuterated solvents obtained from Cambridge Isotope Laboratories were degassed, dried using molecular sieves and distilled prior to use. 2-amino-4-picoline, chlorotrimethylsilane, (Sigma-Aldrich), *n*-butyllithium, dodecane, benzylphenyl ether (ACROS Chemicals) and diphenylether (Alfa Aesar) were used as received without any further purification. Polycarbosilane (SMP-10) was purchased from Starfire Systems, New York, USA. PE-326 (NACOL-22-98, 326 g/mole), and PE-550 (Unilin-550, 550 g/mole) were received from Sasol Germany GmbH and Baker Hughes, respectively.

### 7.3.2 Characterization

**BET.** The specific surface area measurements were carried out on Quantachrome (NOVA 2000 e) surface area and pore size analyzer. The pore width and average pore volume was calculated using nonlocal density functional theory (NLDFIT, adsorption branch) and silica kernel (cylindrical pore geometry) was applied.

**PXRD.** All X-ray powder diffractograms were recorded by using a STOE STADI-P-diffractometer (CuK $\alpha$  radiation, 1.54178 Å) in  $\theta$ -2 $\theta$  -geometry and with a position sensitive detector. All powder samples were introduced into glass capillaries ( $\varnothing = 0.7$  mm, Mark-tubes Hilgenberg No. 10) in a glove box and sealed prior to the measurements.

**Solid state NMR.** Pyrolyzed samples were characterized by ramped  $^{29}\text{Si}\{^1\text{H}\}$  cross-polarization (CP) MAS NMR techniques, recorded on a commercial Avance II 300 Bruker spectrometer equipped with a standard triple resonance 7-mm MAS probe.

**Thermal analysis.** (TGA/DTA) was performed over Thermowaage L81 (Linseis Germany).

**TEM.** Transmission electron microscopy (TEM) was carried out by using a Varian LEO 9220 (200 kV) instrument. The sample was suspended in chloroform and

sonicated for 5 min. Subsequently a drop of the suspended sample was placed on a grid (Plano S 166–3) and allowed to dry.

**GC.** Gas chromatography (GC) analyses were performed by using an Agilent 6890N gas chromatograph equipped with a flame ionization detector (FID) and an Agilent 19091 J-413 FS capillary column using dodecane as internal standard.

**Catalysis.** The catalytic selective hydrogenolysis of lignin model compounds was done in Parr autoclave under a hydrogen pressure (6 bar). A glass tube containing milled catalyst (particle size: <100  $\mu\text{m}$ ) was charged with magnetic bar and placed in the reactor which was then filled with hydrogen at room temperature. The reactor was heated to respective temperature within 20 minutes and stirring was continued at this temperature for 20 hours. Afterwards, dodecane was added and mixture was extracted with ethylacetate (3 $\times$ 2 mL). The conversions and selectivities were determined by GC (Agilent 1100 series) using FID detector.

For the reusability studies, catalyst was washed with ethanol and water and dried at 80°C under vacuum.

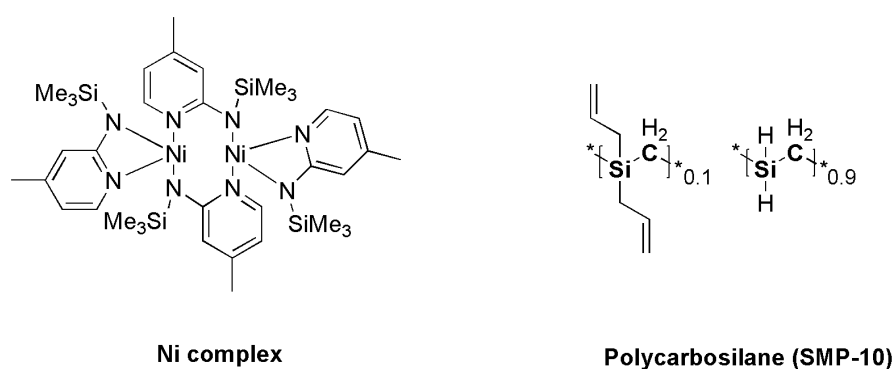


**Figure S1.** Molecular structures of nickel complex and polycarbosilane (SMP-10).

**Table S2.** Tabular presentation of samples codes, PE to PCS ratio, molecular weights of different PEs, yield of ceramics and corresponding metal loading.

Entry	Sample	PE:PCS <sup>[a]</sup>	PE mol wt (g/mole)	Yield <sup>[b]</sup> (%)	Ni loading (wt %)
1	SiC-meso	1:1	1739	54	4.3
2	SiC-micro	1:1	326	57	4.3
3	SiC-hier	1:1	550	50	4.3

[a]PE:PCS stands for polyethylene to polycarbosilane weight ratio. [b] Yield of final materials based on total weight of PE and PCS blend.

**Table S3.** Nitrogen physisorption analysis of composite materials showing surface area (micro and external), pore volume (micro and total) and average pore diameter.

Entry	Sample	$S_{\text{BET}}$ <sup>[a]</sup> (m <sup>2</sup> /g)	$S_{\text{micro}}$ <sup>[b]</sup> (m <sup>2</sup> /g)	$S_{\text{ext}}$ <sup>[b]</sup> (m <sup>2</sup> /g)	$V_{\text{micro}}$ <sup>[b]</sup> (cc/g)	$V_{\text{total}}$ <sup>[c]</sup> (cc/g)
1	SiC-meso <sup>[d]</sup>	450	38	413	0.016	0.332
2	SiC-micro <sup>[e]</sup>	552	482	69	0.198	0.249
3	SiC-hier <sup>[f]</sup>	527	326	202	0.147	0.333

$S_{\text{BET}}$ : Surface area,  $S_{\text{micro}}$ : Microporous surface area,  $S_{\text{ext}}$ : External surface area (meso and macropores),  $V_{\text{micro}}$ : Microporous volume,  $V_{\text{total}}$ : Total pore volume,  $D$ : Pore diameter.[a] BET method,[b] t-plot method, [c] DFT method (NLDFE adsorption branch on silica kernel with cylindrical pore geometry). Hydroxy terminated polyethylene (PE) was added in 1:1 weight ratio to polycarbosilane (SMP-10), the molecular weights of PE used are [d] 1739, [e] 326 and [f] 550 g/mole.

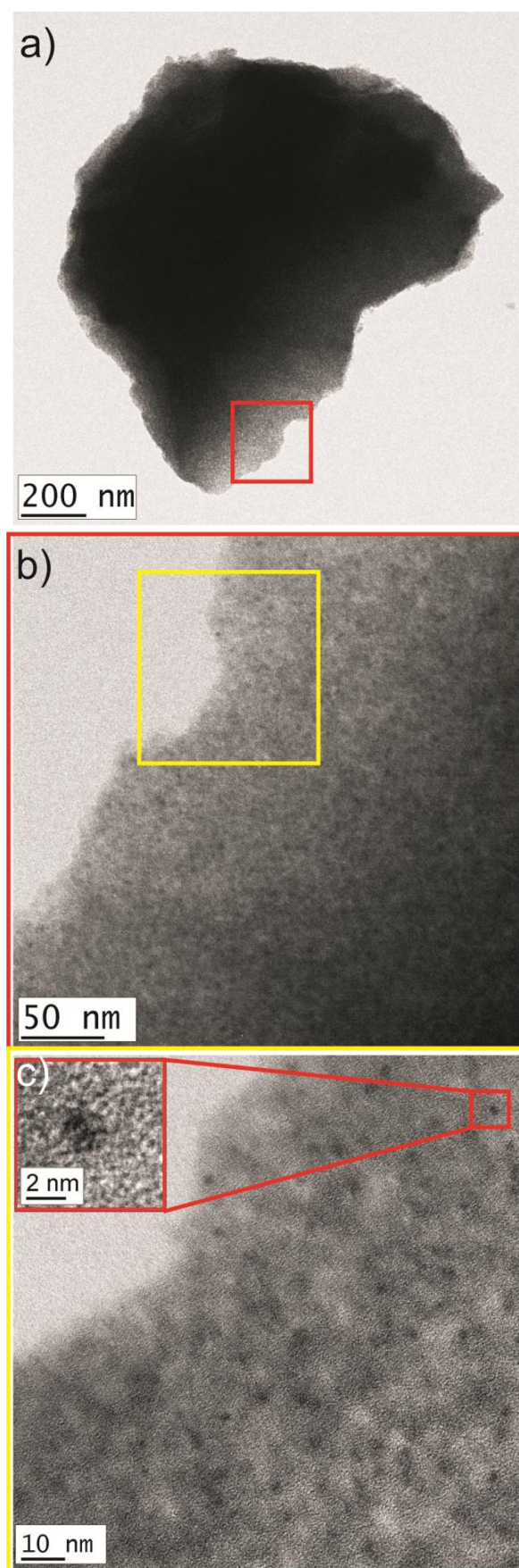


**Figure S4.** TEM micrographs of mesoporous Ni@SiC (SiC-meso) with high resolution insets.

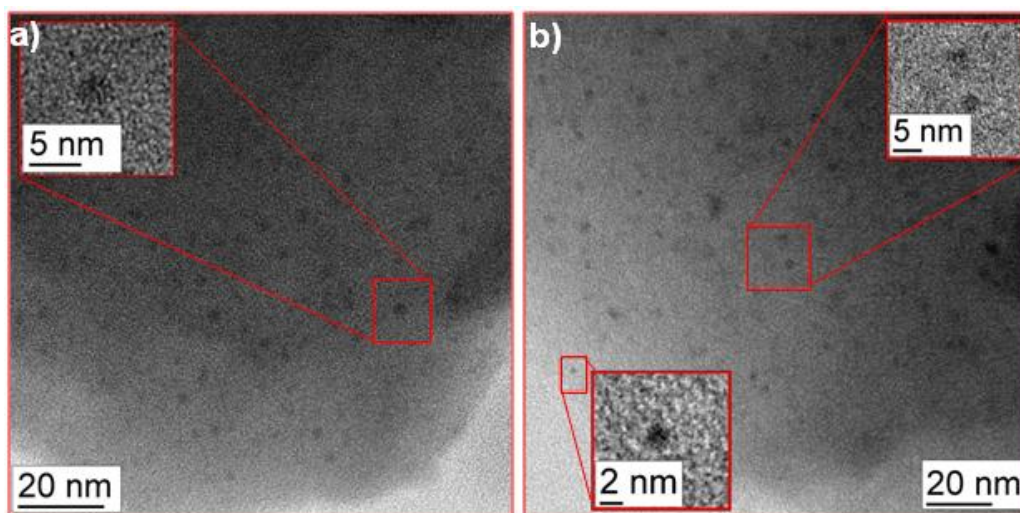


**Figure S5.** a) TEM micrographs of microprorous Ni@SiC (SiC-micro), b) hierarchical Ni@SiC (SiC-hier). The inset show the higher magnification of selected regions with particles.

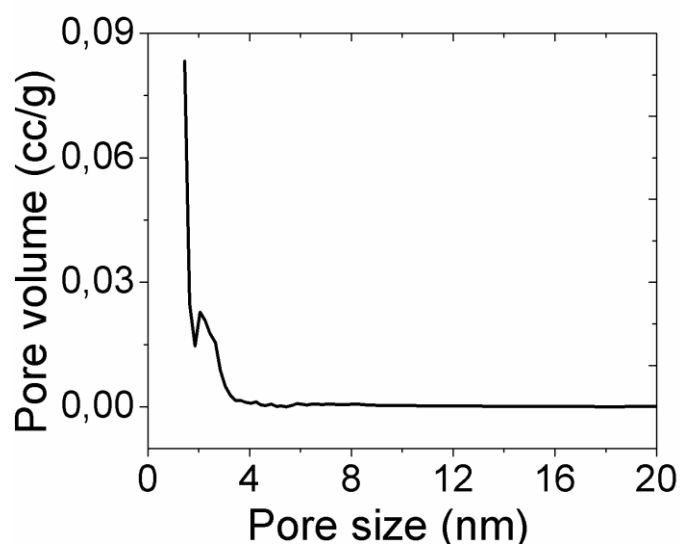


**Figure S6.** Pore size distribution of microporous Ni@SiC (SiC-micro) as calculated from NLDFT model applied to  $N_2$ -adsorption isotherm.

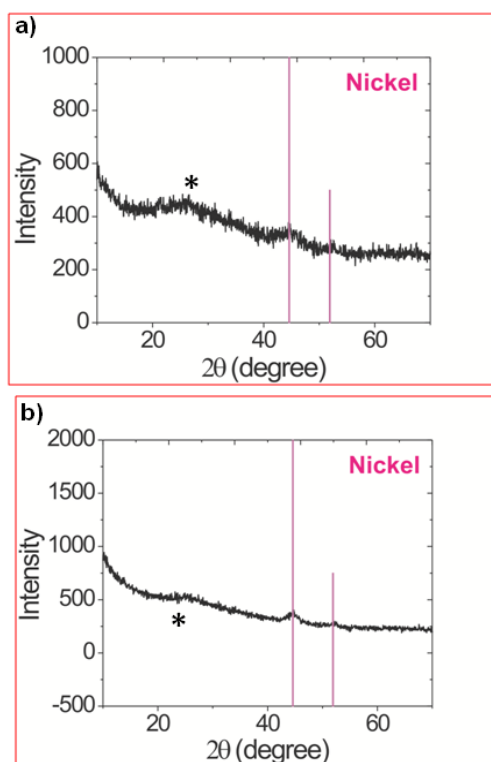


**Figure S7.** a) XRD pattern of SiC-micro and b) SiC-hier. The asterisk denotes the graphitic carbon phase.

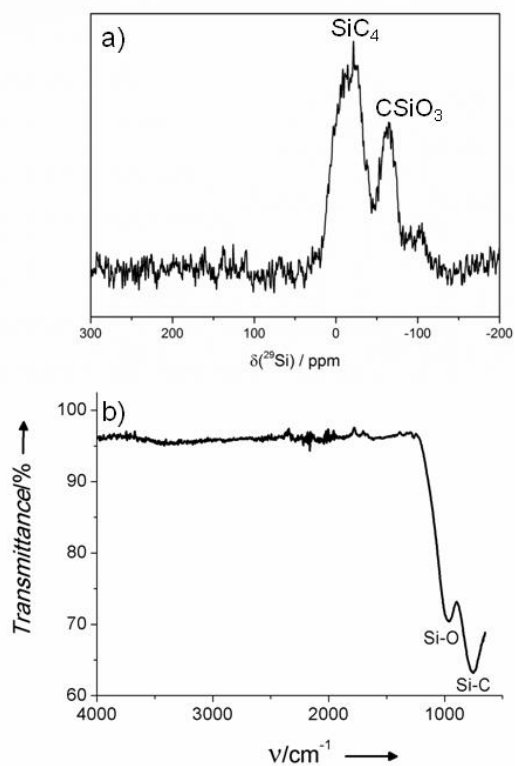


**Figure S8.** a) Solid state  $^{29}\text{Si}$  MAS NMR of SiC-hier shows characteristic peaks for  $\text{SiC}_4$  ( $\sim -16$  ppm) and  $\text{CSiO}_3$  ( $-65$  ppm) silicon environments. b) FT-IR spectrum of SiC-hier showing peaks typical of stretching vibrations of Si-O ( $960 \text{ cm}^{-1}$ ) and Si-C ( $760 \text{ cm}^{-1}$ ) bonds.

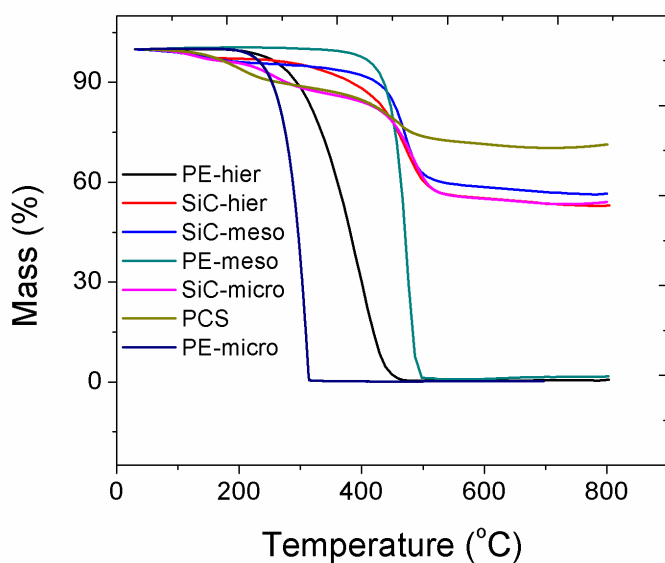


**Figure S9.** TGA (5 K/min, Ar) of polyethylene (PE) and polycarbosilane in comparison to that of micro, meso and hierarchical Ni@SiC materials. PE-micro: polyethylene (326 g/mole); PE-hier: polyethylene (550 g/mole); PE-meso: polyethylene (1739 g/mole); PCS: polycarbosilane.

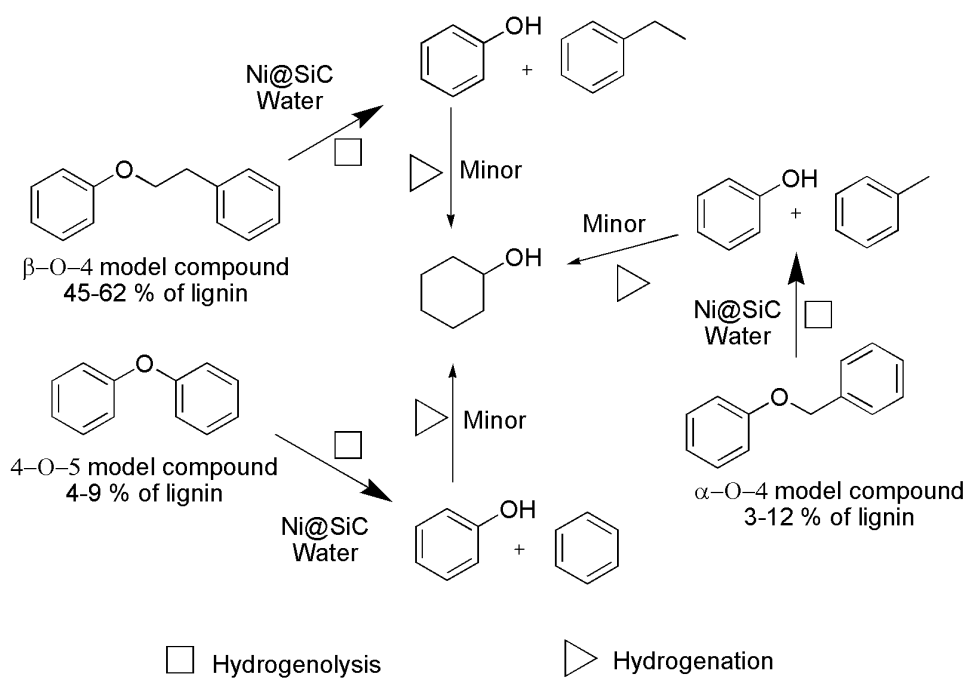


**Figure S10.** Schematic presentation of hydrogenolysis of the lignin model compounds with Ni@SiC materials in water. Catalysts show chemoselectivity for hydrogenolysis over hydrogenation.

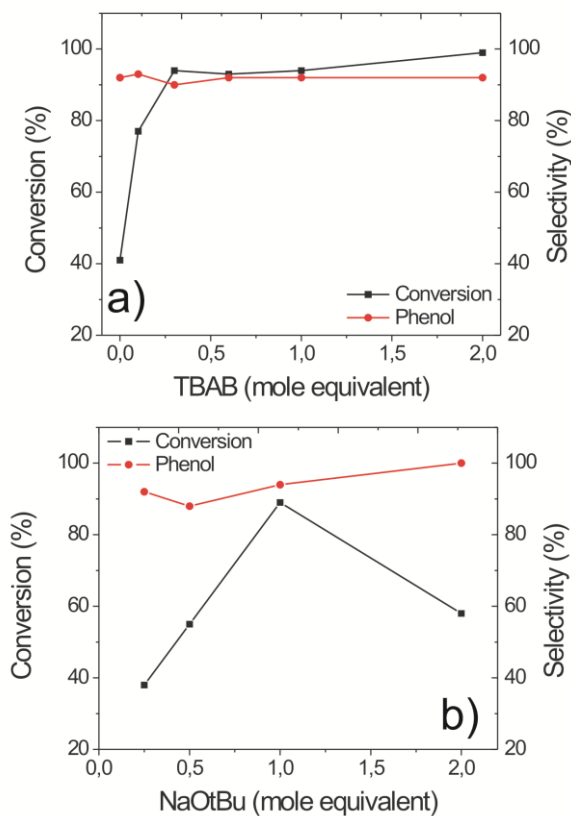


**Figure S11.** a) Effect of the amount of TBAB and b) base on the conversion of phenethoxybenzene (PEB). Conditions: 0.5 mmol of ether was mixed with 15 mg of catalyst (SiC-13,  $1.17 \times 10^{-5}$  mole Ni) in 2 mL water at a hydrogen pressure of 6 bar and then stirred (1000 rpm) at 120°C for 20 hours.

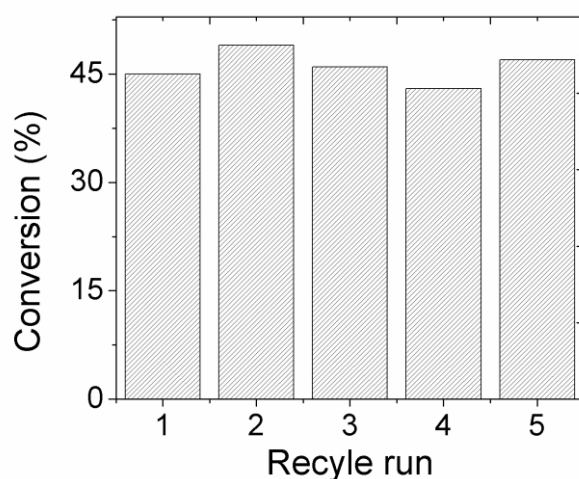


**Figure S12.** Recycling of SiC-hier (15 mg;  $1.17 \times 10^{-5}$  mole Ni) in successive hydrogenolysis of PEB (0.5 mmol) in water (2 mL) at 120°C under 6 bar of hydrogen for 8 hours. Stirring velocity: 1000 rpm

## 8. Robust Nanoporous Palladium Catalysts for Oxidant Free Dehydrogenation of Alcohols under Mild Conditions

---

Muhammad Zaheer,<sup>[a]</sup> Guenter Motz,<sup>[b]</sup> Rhett Kempe<sup>[a]\*</sup>

[a] Inorganic Chemistry II, University of Bayreuth, 95440 Bayreuth, Germany. E-mail: kempe@uni-bayreuth.de [b] Ceramic Materials Engineering, University of Bayreuth, 95447 Bayreuth, Germany

### To be submitted:

Palladium nanoparticles (PdNPs) supported on various solid supports find intensive applications as recyclable catalysts in organic synthesis and in the production of fine chemicals.<sup>[1]</sup> Among others (PdNPs supported on metal oxides,<sup>[2]</sup> zeolites,<sup>[3]</sup> clay,<sup>[4]</sup> MOFs<sup>[5]</sup> and polymers<sup>[6]</sup>) palladium supported on activated carbon/charcoal (Pd/C) is perhaps the most widely used heterogeneous catalyst. It is used, for instance, in hydrogenation,<sup>[7]</sup> oxidation,<sup>[8]</sup> coupling (C-C,<sup>[9]</sup> C-S,<sup>[10]</sup> C-P<sup>[11]</sup>), hydrodechlorination (HDC)<sup>[12]</sup> alkylation,<sup>[13]</sup> cyanation,<sup>[14]</sup> dehydrogenation,<sup>[15]</sup> electrocatalysis,<sup>[16]</sup> organic synthesis<sup>[17]</sup> and more recently in deriving fuels from biomass.<sup>[18]</sup> The activity of the supported catalysts is broadly affected by the factors like the size, shape and the dispersion of metal NPs<sup>[19]</sup> polarity, porosity and size of the pores contained by the support, acid-base and redox properties of support and metal-support interactions.<sup>[20]</sup> High surface area allows effective mass transport,<sup>[21]</sup> while with the decrease in the size of metal NPs, altered electron structure plays a part in the enhancement of their catalytic activity.<sup>[22]</sup> Pd/C is very often used as catalyst because of its high surface area (> 800 m<sup>2</sup>/g) exclusively contributed by micropores (< 2 nm in diameter),<sup>[23]</sup> the stability at higher temperatures and under harsh chemical environment,<sup>[24]</sup> as well as the rather low cost of the support. Nevertheless, leaching of PdNPs from supported carbon catalysts cannot be avoided because of the lack of metal-support interaction necessary to anchor NPs.<sup>[25]</sup> Another challenge is the stabilization of very small NPs on carbon support, in particular when the metal loading is high due to the tendency of

NPs towards agglomeration.<sup>[26]</sup> Furthermore, carbon support is simply burnt off in the presence of oxygen at higher temperatures which makes them unfit for the high temperature oxidation catalysis<sup>[27]</sup> and restricts catalyst recycling. Recently we have successfully used metal organic frameworks (MOFs) for the stabilization of very small palladium particles<sup>[28]</sup> but MOFs are limited only to low temperature catalytic transformations. On the other hand, polymer derived M@SiCN catalysts possess high thermal stability, oxidation resistance and can withstand harsh chemical environment.<sup>[29]</sup> Unfortunately, these catalysts are highly dense nano-composite materials possessing very low surface area. Moreover, during polymer to ceramic transformations at 1100°C, the alloying of noble metals (for instance Pd) with silicon leads to the formation of metal silicides.<sup>[30]</sup> By performing the controlled pyrolysis of metal modified silazane polymer in the presence of Ni, others and we recently managed to get microporous materials at lower temperatures.<sup>[31]</sup> Unfortunately, this material is rather sensitive to hydrolysis and was found to be more like a highly cross-linked silazane polymer than a robust SiCN material.

By fine tuning of the pyrolysis we managed (here) to synthesize nanoporous SiCN materials with small and highly dispersed palladium NPs. The size of the NPs remained small (~2.5 nm) even with a palladium loading as high as 14 wt%. In comparison to the commercial Pd/C (10 wt%), the SiCN-support can resist oxidation. Moreover, the materials can be nicely dispersed in water and therefore can be used as potential catalysts for green oxidation of substances.

The oxidation of alcohols to carbonyl compounds is a fundamental transformation in synthetic organic chemistry and allows the synthesis of a wide variety of compounds. Tremendous efforts have been devoted to the design of catalysts that can oxidize aliphatic, cyclic and aromatic alcohols to their corresponding carbonyl counterparts under mild and environmentally benign conditions.<sup>[32]</sup> The dehydrogenative oxidation of alcohols is interesting in particular in the sense that it avoids the use of hazardous oxidizing agents and the liberated hydrogen can be used as a green source of energy. Homogeneous catalysts in this regard provide high activity and selectivity under mild reaction conditions but are active mostly in basic conditions.<sup>[33]</sup> Heterogeneous catalysts (Ag<sup>[34a-b]</sup>, Au<sup>[34c]</sup>, Cu<sup>[34d-e]</sup>, Co<sup>[34f]</sup>, Ni<sup>[34g]</sup>, Pt<sup>[34h]</sup>) on the other hand offer an ease of separation and reusability but are rather less active and require

organic solvents and high reaction temperatures ( $>100^{\circ}\text{C}$ ). Here we report on a nanoporous Pd catalyst which can efficiently dehydrogenate alcohols at near ambient conditions without the use of a base in a green solvent (water). To the best of our knowledge there are no reports on the base free acceptorless dehydrogenation of alcohols at near ambient conditions using heterogeneous catalysts. The base free dehydrogenation of alcohols is advantageous in the sense that it avoids the formation of unwanted side products *via* condensation reactions.

Nanoporous Pd@SiCN materials were synthesized by the pyrolysis of palladium modified polysilazane (HTT 1800) under argon atmosphere at  $700^{\circ}\text{C}$  (Fig. 1). An amido palladium complex, upon its reaction with HTT 1800, initiates the cross-linking of the polymer along with the transfer of palladium to its nitrogen functions providing a metallopolymer. The loading of palladium was adjusted in terms of palladium to silicon ratio and ranged from 1/10, 1/40 and 1/100 (Table S1, supporting data (SI)). The emission of gases (ammonia and hydrocarbons) during pyrolysis generates micropores within the materials which can be retained even up to  $700^{\circ}\text{C}$  *via* con-

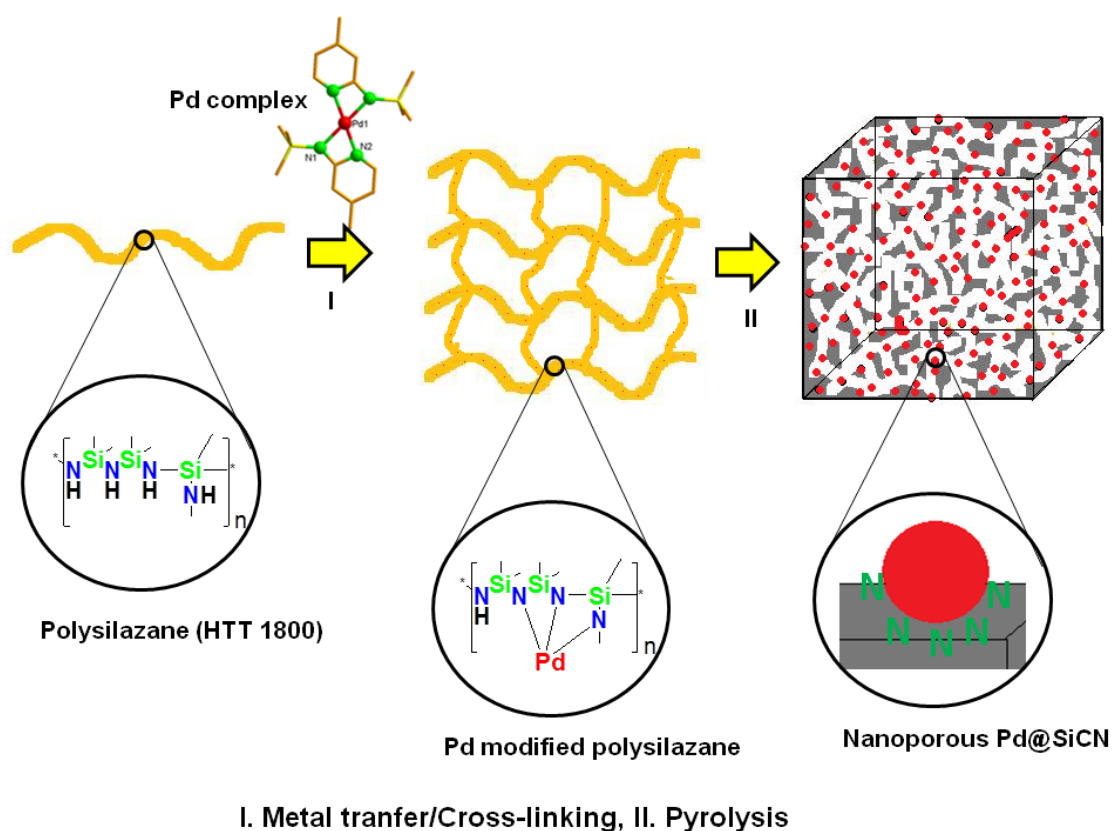


**Figure 1.** Synthesis of nanoporous SiCN materials containing Pd NPs *via* the pyrolysis of palladium modified polysilazane.

-trolled pyrolysis of the metallopolymer. Slow heating rates (1K/min) and long dwelling times (4 hours each at 200, 300, 400, 500 and 600°C) were used to avoid pore collapse due to the rapid escape of gases. FT-IR analysis of the final materials showed broad bands in  $1200-700\text{ cm}^{-1}$  range corresponding to Si-C and Si-N bonds of SiCN network (Fig. S2, SI). The microstructure of the Pd-10 (14 wt% Pd) as investigated by TEM, shows homogeneous distribution of palladium particles all over the surface (Fig. 2a-b) with an average size of  $\sim 2.5\text{ nm}$  (Fig. 2c). Despite of high metal loading and longer holding time during pyrolysis, synthesis of small sized Pd

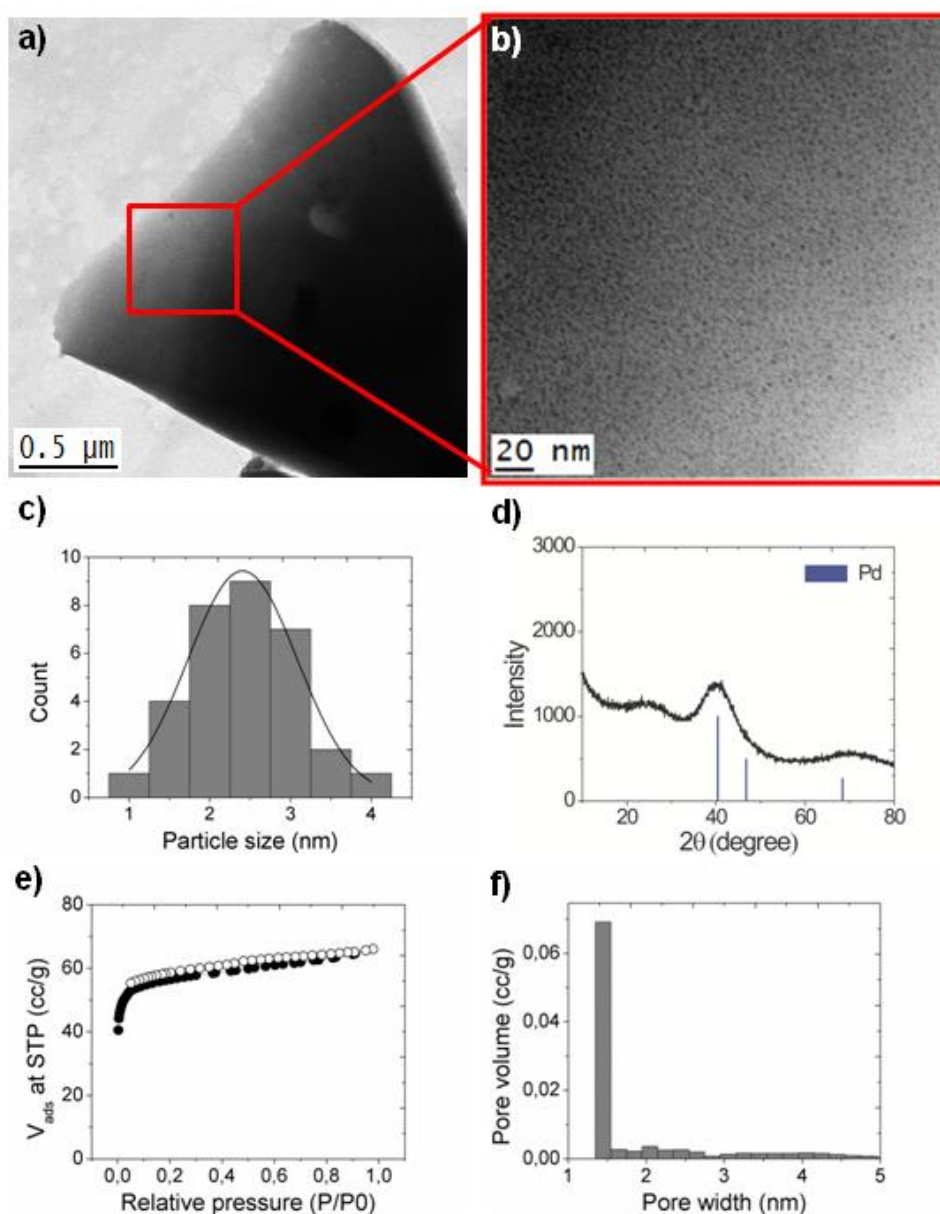


**Figure 2.** a-b) Pd-10 material as investigated by TEM, (b) Particle size distribution, d) PXRD and e) N<sub>2</sub>-adsorption isotherm and f) pore size distribution calculated by NLDFT method.

NPs was achieved. The formation of very small PdNPs can be explained in terms of coordinative saturation of the isolated metal ions during the cross-linking and pyrolysis steps. Nitrogen functions of the polysilazane covalently bond with the palladium ions which upon their reduction to elemental PdNPs, are capped by the nitrogen functions of the SiCN network which would have avoided their possible agglomeration during heating. The presence of palladium was confirmed by PXRD which shows a broad reflection at 40.4° corresponding to (111) plane of cubic palladium (ICDD PDF Card No. 00-001-1201) (Fig. 2d). N<sub>2</sub>-adsorption studies showed that materials possess porosity with an apparent surface area of 290 m<sup>2</sup>/g. Typical type-I adsorption isotherm is indicative of the existence of micropores with an average size of 1.4 nm as calculated by NLDFT method (see Fig. 2e-f).

When the loading of palladium was decreased, the size of the particles increased (see Fig.S3, supporting data) from 2.0 nm (Pd-10) to 2.5 nm (Pd-40) and 3.5 nm (Pd-100). Whereas the pore width decreases with increasing palladium content (see Fig. S3, SI and table 1), apparent surface area however increases (Table 1) which shows the role the palladium content in the retention of the porosity. The palladium content would increase the formation of sp<sup>2</sup> carbon which would provide mechanical strength to material so that they resist the pore rupture during rapid gaseous emissions.

**Table 1.** Nitrogen adsorption analysis of Pd@SiCN materials.

Entry	Material	S <sub>BET</sub> <sup>[a]</sup> (m <sup>2</sup> /g)	Pore volume <sup>[b]</sup> (cc/g)	Pore width <sup>[b]</sup> (nm)
1	Pd-10	290	0.244	1.4
2	Pd-40	158	0.088	2.0
3	Pd-100	70	0.056	2.1

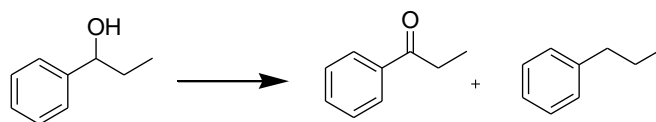
[a] Apparent surface area calculated by BET method [b] pore volume and pore size distribution was calculated by NLDFT (adsorption branch) on silica kernel with cylindrical pore geometry.

Metal dispersion (active metal sites on surface) was determined by pulse titration analysis using hydrogen as titration gas. As compared to the fresh sample, metal dispersion increased from 0.25% to 22% when catalyst was activated at 90°C for 24 hours in a basic methanol-water mixture. In comparison to commercial Pd/C (10 wt% Pd), Pd-10 material (14 wt% Pd) showed higher metal surface area (14 m<sup>2</sup>/g), higher

accessibility of surface palladium (22%) and smaller crystallite size (~2.5 nm) as calculated by hydrogen pulse titration (see Table S4, SI).

The catalytic activity of Pd-10 material was tested in dehydrogenation of 1-phenyl-1-propanol (PP). The conversion increased with temperature from 14% at room temperature to 99% at 90°C (Entries 1-4, Table 2). Amount of water seemed to play a vital role in the dehydrogenative oxidation of alcohols as very low conversions were observed in the absence of it (Entry 5). The optimum conversion was obtained by the use of 1 mL of water (Entry 7) and it decreased with further dilution of substrate with water (Entries 8-9).

**Table 2.** Optimization of reaction conditions in the oxidant free dehydrogenation of 1-phenyl-1-propanol in water.



Entry	Temperature (°C)	Water (mL)	Conversion (%)	Yield (%)
1	RT	5	14	99
2	50	5	62	91
3	70	5	99	96
4	90	5	99	92
5	50	-	9	99
6	50	0.5	74	98
7	50	1	85	98
8	50	3	68	97
9	50	5	62	91

Conditions: 1-phenyl-1-propanol (1mmol), Pd-10 (20 mg, 26  $\mu$ mol Pd), stirring speed (1100 rpm), reaction time (20 hours), argon atmosphere. Conversion and yield of the ketonic product were calculated by GC using dodecane as standard.

The conditions optimized for the dehydrogenation of PP were extended to other alcohols (see Table 3). It was found that under the experimental conditions a variety

of alcohols including aromatic (Entries 1-3) and cyclic (Entries 4-5) ones can be dehydrogenated to their corresponding carbonyl compounds with high selectivity.

**Table 3.** Acceptor free dehydrogenation of alcohols in water catalyzed by Pd@SiCN at 50 °C.

$$\text{R}_1\text{-CH(OH)-R}_2 \longrightarrow \text{R}_1\text{-C(=O)-R}_2 + \text{H}_2$$

Entry	Substrate	Conversion (%)	Yield (%)
1		99	97
2		95	90
3		99	98
4		56	97
		98*	97
5		66	96
		97*	96

Conditions: Substrate (0.5 mmol), Pd-10 (20 mg, 26  $\mu\text{mol}$  Pd), stirring speed (1100 rpm), water (1 mL), reaction time (20 hours), argon atmosphere. Conversion and yield of the ketonic product were calculated by GC using dodecane as standard.\*90°C.

In summary we have successfully developed highly robust nanoporous SiCN materials with integrated PdNPs by the pyrolysis of a Pd modified polysilazane. Controlled pyrolysis plays a vital role both in the generation of porosity as well in the stabilization of small Pd NPs. Despite of the high metal loading (14 wt% Pd) the agglomeration of NPs was avoided due to the stabilization effect of the nitrogen functions of SiCN network. The materials were found efficient catalysts in acceptorless and oxidant free dehydrogenation of alcohols to the carbonyl compounds in a green solvent with high selectivity at near ambient conditions.

## 8.1 References

- [1] a) M. L. Toebes, J. A. Van Dillen, K. P. De Jong, *J. Mol. Catal. A: Chem.* **2001**, *173*, 75-98; b) A. Molnar, *Chem. Rev.* **2011**, *111*, 2251-2320.
- [2] a) V. Polshettiwar, C. Len, A. Fihri, *Coord. Chem. Rev.* **2009**, *253*, 2599-2626; b) Y. Usami, K. Kagawa, M. Kawazoe, Y. Matsumura, H. Sakurai, M. Haruta, *Appl. Catal. A: Gen.* **1998**, *171*, 123-130; c) K. Köhler, M. Wagner, L. Djakovitch, *Catal. Today* **2001**, *66*, 105-114.
- [3] M. Dams, L. Drijik oningen, B. Pauwels, G. Van Tendeloo, D. E. De Vos, P. A. Jacobs, *J. Catal.* **2002**, *209*, 225-236.
- [4] T. Mitsudome, K. Nose, K. Mori, T. Mizugaki, K. Ebitani, K. Jitsukawa, K. Kaneda, *Angew. Chem. Int. Ed.* **2007**, *46*, 3288-3290.
- [5] a) J. Hermannsdörfer, R. Kempe, *Chem. Eur. J.* **2011**, *17*, 8071-8077; b) A. Dhakshinamoorthy, H. Garcia, *Chem. Soc. Rev.* **2012**, *41*, 5262-5284.
- [6] S. Ogasawara, S. Kato, *J. Am. Chem. Soc.* **2010**, *132*, 4608-4613.
- [7] a) J. C. Chaston, E. J. Sercombe, *Platinum Metals Rev.* **1961**, *5*, 122-125; b) A. Mori, Y. Miyakawa, E. Ohashi, T. Haga, T. Maegawa, H. Sajiki, *Org. Lett.* **2006**, *8*, 3279-3281; c) P. K. Mandal, J. S. McMurray, *J. Org. Chem.* **2007**, *72*, 6599-6601; d) E. Guillen, R. Rico, J. M. Lopez-Romero, J. Bedia, J. M. Rosas, J. Rodriguez-Mirasol, T. Cordero, *Appl. Catal. A: Gen.* **2009**, *368*, 113-120.
- [8] a) S. Carrettin, P. McMorn, P. Johnston, K. Griffin, C. J. Kiely, G. J. Hutchings, *Phys. Chem. Chem. Phys.* **2003**, *5*, 1329-1336; b) M. Lim, S. Oh, H. Rhee, *Bull. Korean Chem. Soc.* **2011**, *32*, 3179-3182; c) T. V. Trebushat, N. I. Kuznetsova, S. V. Koschcheev, L. I. Kuznetsova, *Kinet. Catal.* **2013**, *54*, 233-242.
- [9] a) L. Yin, J. Liebscher, *Chem. Rev.* **2007**, *107*, 133-173; b) Y. Kitamura, S. Sako, T. Udzu, A. Tsutsui, T. Maegawa, Y. Monguchi, H. Sajiki, *Chem. Commun.* **2007**, 5069-5071; c) C. R. LeBlond, A. T. Andrews, Y. Sun, J. R. Sowa, Jr. *Org. Lett.* **2001**, *3*, 1555-1557; d) M. Seki, *Synthesis* **2006**, *18*, 2975-2992.

- [10] Z. Jiang, J. She, X. Lin, *Adv. Synth. Catal.* **2009**, *351*, 2558-2562.
- [11] S. M. Rummelt, M. Ranocchiari, J. A. Van Bokhoven, *Org. Lett.* **2012**, *14*, 2188-2190.
- [12] a) C. Amorim, G. Yuan, P. M. Patterson, M. A. Keane, *J. Catal.* **2005**, *234*, 268-281; b) H. Sajiki, A. Kume, K. Hattori, K. Hirota, *Tetrahedron Lett.* **2002**, *43*, 7247-7250.
- [13] C. S. Cho, *J. Mol. Catal. A: Chem.* **2005**, *240*, 55-60.
- [14] a) M. Hatsuda, M. Seki, *Tetrahedron*, **2005**, *61*, 9908-9917; b) Y. -Z. Zhu, C. Cai, *Eur. J. Org. Chem.* **2007**, 2401-2404.
- [15] a) Z. -L. Wang, J. -M. Yan, H. -L. Wang, Y. Ping, Q. Jiang, *Sci. Rep.* **2012**, doi:10.1038/srep00598; b) J. Xu, X. Yu, J. Ni, Z. Zou, Z. Li, H. Yang, *Dalton Trans.* **2009**, 8386-8391.
- [16] a) C. Xu, P. K. Shen, Y. Liu, *J. Power Sources* **2007**, *164*, 527-531; b) Z. -B. Wang, G. -H. Yuan, K. Zhou, Y. -Y. Chu, M. Chen, *Fuel Cells* **2011**, *11*, 309-315; c) Y. Huang, J. Liao, C. Liu, T. Lu, W. Xing, *Nanotechnol.* **2009**, *20*, 105604.
- [17] a) D. Rambabu, G. P. Kumar, B. D. Kumar, R. Kapavarapu, M. V. Basaveswara, M. Pal, *Tetrahedron Lett.* **2013**, *54*, 2989-2995; b) Y. Monguchi, S. Mori, S. Aoyagi, A. Tsutsui, T. Maegawa, H. Sajiki, *Org. Biomol. Chem.* **2010**, *8*, 3338-3342.
- [18] P. Anbarasan, Z. C. Baer, S. Sreetkumar, E. Gross, J. B. Binder, H. W. Blanch, D. S. Clark, F. D. Toste, *Nature* **2012**, *491*, 235-239.
- [19] a) C. Burda, X. Chen, R. Narayanan, M. A. El-Sayed, *Chem. Rev.* **2005**, *105*, 1025-1102; b) P. Ehrburger, O. P. Mahajan, P. L. Walker. Jr. *J. Catal.* **1976**, *43*, 61-67.
- [20] a) R. J. White, R. Luque, V. L. Budarin, J. H. Clark, D. J. MacQuarrie, *Chem. Soc. Rev.* **2009**, *38*, 481-494; b) A. T. Bell, *Science* **2003**, *299*, 1688-1691.

- [21] a) N. Gunasekaran, S. Saddawi, J. J. Carberry, *J. Catal.* **1996**, *159*, 107-111; b) J. Laine, F. Serverino, M. Labady, *J. Catal.* **1994**, *147*, 355-357.
- [22] a) M. Turner, V. B. Golovko, O. P. H. Vaughan, P. Abdulkin, A. Berenguer-Murcia, M. S. Tikhov, B. F. G. Johnson, R. M. Lambert, *Nature* **2008**, *454*, 981-983; b) M. Arenz, K. J. J. Mayrhofer, V. Stamenkovic, B. B. Blizanac, T. Tomoyuki, P. N. Ross, N. M. Markovic, *J. Am. Chem. Soc.* **2005**, *127*, 6819-6829; c) G. C. Bond, *Surf. Sci.* **1985**, *156*, 966-981.
- [23] a) P. A. Simonov, S. Y. Troitskii, V. A. Likholobov, *Kinet. Catal.* **2000**, *41*, 281-297; b) L. B. Okhlopkova, A. S. Lisitsyn, V. A. Likholobov, M. Gurrath, H. P. Boehm, *Appl. Catal. A: Gen.* **2000**, *204*, 229-240.
- [24] F. Rodriguez-Reinoso, *Carbon* **1998**, *36*, 159-175.
- [25] X. Xu, Y. Li, Y. Gong, P. Zhang, H. Li, Y. Wang, *J. Am. Chem. Soc.* **2012**, *134*, 16987-16990.
- [26] F. Mailard, S. Schreier, M. Hanzlik, E. R. Savinova, S. Weinkauff, U. Stimming, *Phys. Chem. Chem. Phys.* **2005**, *7*, 385-393.
- [27] E. Auer, A. Freund, J. Pietsch, T. Tacke, *Appl. Catal. A: Gen.* **1998**, *173*, 259-271.
- [28] J. Hermannsdörfer, M. Friedrich, N. Miyajima, R. Q. Albuquerque, S. Kümmel, R. Kempe, *Angew. Chem. Int. Ed.*, **2012**, *51*, 11473-11477
- [29] M. Zaheer, T. Schmalz, G. Motz, R. Kempe, *Chem. Soc. Rev.* **2012**, *41*, 5102-5116.
- [30] M. Zaheer, G. Motz, R. Kempe, *J. Mater. Chem.* **2011**, *21*, 18825-18831.
- [31] M. Zaheer, C. D. Keenan, J. Hermannsdörfer, E. Roessler, G. Motz, J. Senker, R. Kempe, *Chem. Mater.* **2012**, *24*, 3952-3963.
- [32] a) C. Parmeggiani, F. Cardona, *Green Chem.* **2012**, *14*, 547-564; b) B. -Z. Zhan, A. Thompson, *Tetrahedron* **2004**, *60*, 2917-2935; c) T. Mallat, A. Baiker, *Chem. Rev.* **2004**, *104*, 3037-3058; d) S. E. Devis, M. S. Ide, R. J. Davis, *Green Chem.* **2013**, *15*, 17-45; e) T. Matsumoto, M. Ueno, N. Wang, S.

- Kobayashi, *Chem. Asian J.* **2008**, *3*, 196-214; f) H. –B. Ji, K. Ebitani, T. Mizugaki, K. Kaneda, *Catal. Commun.* **2002**, *3*, 511-517; g) S. Proch, J. Hermannsdörfer, R. Kempe, C. Kern, A. Jess, L. Seyfarth, J. Senker, *Chem. Eur. J.* **2008**, *14*, 8204-8212; h) M. Schrunner, S. Proch, Y. Mei, R. Kempe, N. Miyajima, M. Ballauf, *Adv. Mater.* **2008**, *20*, 1928-1933.
- [33] a) T. C. Johnson, D. J. Morris, M. Willis, *Chem. Soc. Rev.* **2010**, *39*, 81-88; b) M. Nielsen, A. Kammer, D. Cozzula, H. Junge, S. Gladioli, M. Beller, *Angew. Chem. Int. Ed.* **2011**, *50*, 9593-9597; c) R. Kawahara, K. Fujita, R. Yamaguchi, *Angew. Chem.* **2012**, *124*, 12962-12966.
- [34] a) T. Mitsudome, Y. Mikami, H. Funai, T. Mizugaki, K. Jitsukawa, K. Kaneda, *Angew. Chem.* **2008**, *120*, 144-147; b) K. Shimizu, K. Sugino, K. Sawabe, A. Satsuma, *Chem. Eur. J.* **2009**, *15*, 2341-2351; c) W. Fang, J. Chen, Q. Zhang, W. Deng, Y. Wang, *Chem. Eur. J.* **2011**, *17*, 1247-1256; d) V. Z. Fridman, A. A. Davidov, *J. Catal.* **2000**, *195*, 20-30; e) T. Mitsudome, Y. Mikami, K. Ebata, T. Mizugaki, K. Jitsukawa, K. Kaneda, *Chem. Commun.* **2008**, 4804-4806; f) K. Schimizu, K. Kon, M. Seto, K. Shimura, H. Yamazaki, J. N. Kondo, *Green Chem.* **2013**, *15*, 418-424; g) K. Shimizu, K. Kon, K. Shimura, S. S. M. A. Hakim, *J. Catal.* **2013**, *300*, 242-250; h) K. Kon, K. Shimura, S. M. A. Hakim Siddiki, K. Schimizu, *J. Catal.* **2013**, *304*, 63-71.

## 8.2 Supporting data

### 8.2.1 General remarks

All reactions were carried out under dry argon using standard Schlenk and glove box techniques. Solvents were dried and distilled from sodium benzophenone before use. 2-amino-4-picoline, chlorotrimethylsilane, (Sigma-aldrich), *n*-butyllithium, and dodecane were used as received without any further purification. Polysilazane (HTT 1800) was provided by Clariant GmbH, Germany. Dichloro(1,5-cyclooctadiene) palladium (II) was synthesized from palladium (II) chloride (Alfa Aesar) by a reported method.<sup>[1]</sup> The starting material 4-methyl-2-((trimethylsilyl)amino)pyridine<sup>[2]</sup> and palladium complex (I)<sup>[3]</sup> were prepared as reported.

### 8.2.2 Characterization

**BET.** The specific surface area measurements were performed on Quantachrome (NOVA 2000 e) surface area and pore size analyzer. The pore width and average pore volume was calculated using non localized density functional theory (NLDFT, adsorption branch) and silica kernel (cylindrical pore geometry) was applied.

**Pulse titration analysis.** Pulse titration of the material with hydrogen was performed over ChemBET Pulsar TPR/TPD (Quantachrome). 100 mg of the materials was first heated at 300°C for 4 under helium stream. A known volume of hydrogen (74  $\mu$ l) was injected *via* a precalibrated injection loop and amount of hydrogen chemisorbed by the material was calculated by TCD. Metal surface area, average crystallite size and metal dispersion were calculated by the software provided with the instrument.

**PXRD.** All X-ray powder diffractograms were recorded by using a STOE STADI-P-diffractometer (CuK $\alpha$  radiation, 1.54178 Å) in  $\theta$ -2 $\theta$  -geometry and with a position sensitive detector. All powder samples were introduced into glass capillaries ( $\varnothing$  = 0.7 mm, Mark-tubes Hilgenberg No. 10) in a glove box and sealed prior to the measurements.

**Elemental analysis.** The samples were digested with HF followed by their analysis with inductively coupled plasma optical emission spectrometry (ICP-OES) using a Varian, Vista-Pro radial.

**TEM.** Transmission electron microscopy (TEM) was carried out by using a Varian LEO 9220 (200 kV) instrument. The sample was suspended in chloroform and sonicated for 5 min. Subsequently a drop of the suspended sample was placed on a grid (Plano S 166–3) and allowed to dry.

**GC.** Gas chromatography (GC) analyses were performed by using an Agilent 6890N gas chromatograph equipped with a flame ionization detector (FID) and an Agilent 19091 J-413 FS capillary column using dodecane as internal standard.

**Catalysis.** Dehydrogenation of alcohols was performed under argon in a Schlenk tube. The catalyst was weighed in a prebacked Schlenk tube followed by the removal of air by argon-vacuum cycle. Finally, water and alcohol were added *via* a septum and tube was agitated in a preheated oil bath. Afterwards, the mixture was extracted with diethylether (6 mL) and products were quantified by GC (Agilent 1100 series) using dodecane as standard.

**Table S1.** Table shows the sample IDs, amount of palladium complex reacted with polysilazane, yield of materials at 700°C and amount of palladium contained by the materials.

Entry	Material	HTT 1800 (g)	Pd complex (g)	Pd/Si	Yield (%)	Pd loading (wt %)	
						theoretical	Actual
1	Pd-10	3.218	2.325	1/10	62	14.1	14.0
2	Pd-40	3.218	0.581	1/40	73	4.7	4.0
3	Pd-100	3.218	0.232	1/100	79	1.9	1.8

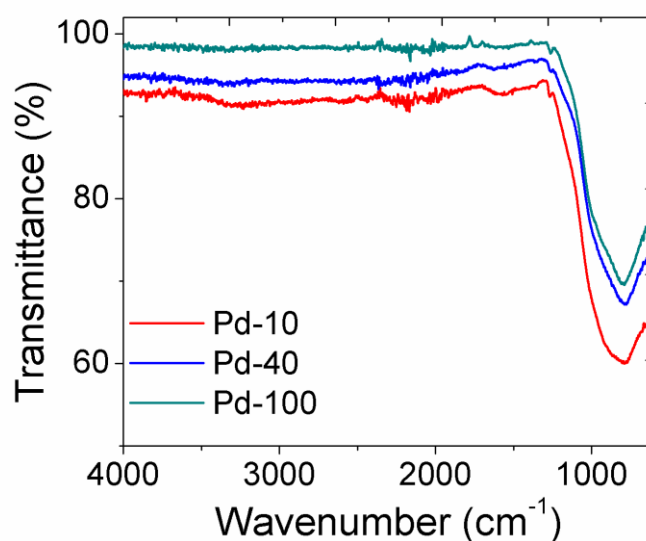


**Figure S2.** FT-IR spectra of Pd@SiCN materials showing broad bands assigned to Si-C and Si-N bonds. A very weak peak at 1250  $\text{cm}^{-1}$  shows the existence of Si-CH<sub>3</sub> groups.

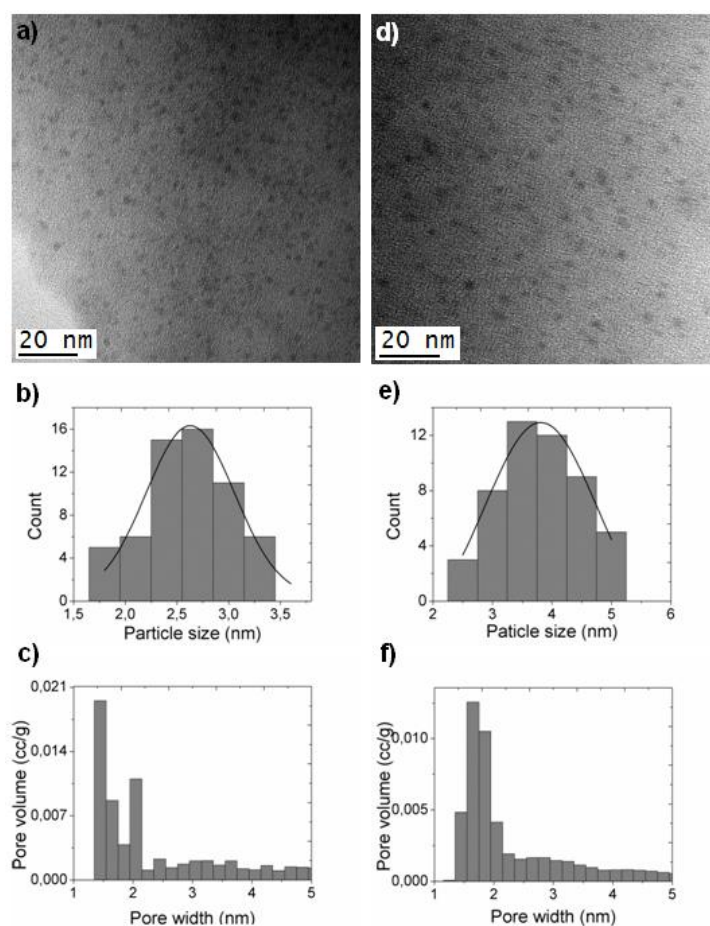


**Figure S3.** a-c) TEM micrographs, particle size and pore size distribution of Pd-40 and d-f) Pd-100.

**Table S4.** Metal surface area, average crystallite size and dispersion of palladium at surface calculated by hydrogen pulse titration.

Entry	Material	$S_{\text{metal}}^{\text{[a]}}$ ( $\text{m}^2/\text{g}$ )	Crystallite size (nm)	Metal dispersion (%)
1	Pd-10	14	1.6	22
2	Pd/C	9	3.3	20

[a] Metal surface area

### 8.2.3 References

- [1] J. Wiedermann, K. Mereiter, K. Kirchner, *J. Mol. Catal. A: Chem.* **2006**, *257*, 67-72.
- [2] R. Kempe, P. Arndt, *Inorg. Chem.* **1996**, *35*, 2644-2649.
- [3] A. Spannenberg, P. Arndt, R. Kempe, *Angew. Chem. Int. Ed.* **1998**, *37*, 832-835.

## 9. List of Publications

---

Following research articles have been published during the course of this thesis.

- 1) M. Zaheer, G. Motz, R. Kempe, *J. Mater. Chem.* **2011**, *21*, 18825-18831.  
'The Generation of Palladium Silicide Nanoalloy Particles in a SiCN Matrix and Their Catalytic Applications'
- 2) M. Zaheer, T. Schmalz, G. Motz, R. Kempe, *Chem. Soc. Rev.* **2012**, *41*, 5102-5116.  
'Polymer Derived Non-oxide Ceramics Modified with Late Transition Metals'
- 3) M. Zaheer, C. D. Keenan, J. Hermannsdörfer, E. Roessler, G. Motz, J. Senker, R. Kempe' *Chem. Mater.* **2012**, *24*, 3952-3963.  
'Robust Microporous Monoliths with Integrated Catalytically Active Metal Sites Investigated by Hyperpolarized  $^{129}\text{Xe}$  NMR'
- 4) M. Zaheer, J. Hermannsdörfer, W. P. Kretschmer, G. Motz, R. Kempe, *ChemCatChem* **2013**, DOI: 10.1002/cctc.201300763.  
'Robust and Reusable Nickel Catalysts with Hierarchical Porosity for Hydrogenolysis of Aryl Ethers'

The research article listed below is to be submitted for its publication in a scientific journal.

- 5) M. Zaheer, G. Motz, R. Kempe, to be submitted:  
'Robust Nanoporous Palladium Catalysts for Oxidant Free Dehydrogenation of Alcohols under Mild Conditions'

## 10. Acknowledgments/Danksagung

---

### Acknowledgments

I would like to express my gratitude for my supervisor Prof. Dr. Rhett Kempe, firstly, for providing me an opportunity to work under his kind supervision and secondly, for the growth of scientific thinking and creativity in me. He has been a source of inspiration for me throughout my Ph.D with his motivation, commitment and enthusiasm for the research. Undoubtly, it was him who taught me how to tackle with everyday scientific problems patiently, think logically and come up with new ideas. The research environment provided by him was friendly, supportive and comfortable. I also learned a lot from him how to prepare and present your work to the scientific community in an appealing way. Other than research activities, I would remember some of the co-curricular activities like the skiing in Austria with him where he taught me how to ski confidently on the mountains.

Dr. Günter Motz is acknowledged for his contributions in scientific discussions.

I am obliged to Higher Education Commission of Pakistan (HEC) for sponsoring my studies here in Germany and to Deutscher Akademischer Austausch Dienst (DAAD) for hosting. My academic advisors at DAAD have been wonderful with their philanthropic attitude in taking care of all my problems regarding my admission, accommodation and money issues. I am grateful to Tobias Ebel, Irina Turner, Kerstin Richter, Hellen Sahlmann and Angele Becher in this regard for their help, support and guidance.

I would like to mention my colleagues who in one way or the other have helped me during my research work. Many thanks go to Dr. Germund Glatz with whom I learned the basic things of my work. I am thankful to Dr. Beniot Blank, Dr. Christian Döring, Dr. Kathrin Kutlescha, Dr. Muhammad Hafeez, Dr. Awal Noor, Dr. Winfried Kretschmer, Dr. Torsten Irrgang and Dr. Sadaf Qayyum for their help and support.

For a wonderful working atmosphere, I would like to thank my laboratory colleagues Dr. Christine Denner, Julia Ewert, Franziska Klemm, Saravana Pillai, Theresa Winkler, Daniel Forberg, Sonja Lippert and Sabrina Sachau. A lot of thanks go to Justus Hermannsdorfer, Tobias Bauer, Adam Sobaczynski, Stephan Michilik,

Isabelle Hass and Emmanuel Sobgwi for the wonderful company. Also, Dr. Benjamin Oelkers, Johannes Obenauf, Georg Lochner, Sina Rösler, Susane Ruch, Janina Lauer, Martin Friedrich and Toni Hille are acknowledged as a part of our research group.

For administrative work Marlies Schilling has been wonderful and I express my gratitude for her help. For the management of safety and chemicals, I would like to thank Walter Kremnitz for his efforts. Thanks to Anna-Maria Dietel, Heide Maisel and Simone Ott for providing dry solvents.

I am indebted to the support and encouragement provided by my family during the course of my work. Especial thanks to my father, mother, sister and my elder brothers for their efforts in the completion of this work.

## **Danksagung**

Ich möchte meine tiefe Dankbarkeit meinem Doktorvater, Prof. Dr. Rhett Kempe, Ausdruck verleihen, erstens dafür, dass er mir die Gelegenheit gegeben hat, unter seiner freundlichen Betreuung zu arbeiten und zweitens für die Förderung des wissenschaftlichen Denkens und der Kreativität in mir. Er ist eine Quelle der Inspiration für mich gewesen, während meiner gesamten Doktorandenzeit, mit seiner Motivation, seiner Hingabe und seinem Enthusiasmus für die Forschung.

Zweifelsohne war er es, der mich lehrte, wie man mit den täglichen wissenschaftlichen Problemen geduldig umgeht, logisch denkt und neue Ideen entwickelt.

Das Forschungsumfeld, das er mir stellte, war freundlich, unterstützend und sehr angenehm. Ich lernte auch sehr viel darüber, wie ich meine Arbeiten, der wissenschaftlichen Gemeinschaft auf eine attraktive Art und Weise vorbereiten und zeigen kann. Außer an die Forschungsaktivitäten erinnere ich mich gerne an manche außer lehrplanmäßigen Aktivitäten wie das Skifahren in Österreich, wo er mir beibrachte, wie man sicher und selbstbewusst auf Skiern den Berg runterfahren kann.

Meine Anerkennung gebührt auch Dr. Günter Motz für seine Beiträge in wissenschaftlichen Diskussionen.

Ich bin der höheren Bildungskommission von Pakistan (HEC) dankbar dafür, dass sie mein Studium hier in Deutschland gefördert haben und auch dem Deutschen Akademischen Austausch Dienst (DAAD) für mein Stipendium.

Meine akademischen Berater bei DAAD haben sich mit ihrer sehr menschenfreundlichen Haltung um all meine Schwierigkeiten, wie Zulassung, Wohnung und Geldangelegenheiten gekümmert, sie sind wunderbar gewesen. In diesem Zusammenhang bin ich Tobias Ebel, Irina Dreher, Kerstin Richter, Hellen Sahlmann und Angele Becher für ihre Hilfe, Unterstützung und Beratung sehr dankbar.

Auch möchte ich hier meine Kollegen erwähnen, die mir auf die ein oder andere Weise während meiner Forschungsarbeit geholfen haben. Mein Dank geht an Dr. Germund Glatz, mit dem ich die Grundlagen meiner Arbeit lernte. Für ihre Hilfe und Unterstützung bin ich Dr. Beniot Blank, Dr. Christian Döring, Dr. Kathrin Kutlescha,

Dr. Muhammad Hafeez, Dr. Awal Noor, Dr. Winfried Kretschmer, Dr. Torsten Irrgang und Dr. Sadaf Qayyum zu großem Dank verpflichtet.

Für die wunderbare Arbeitsatmosphäre möchte ich meinem Laborkollegen Dr. Christine Denner, Julia Ewert, Franziska Klemm, Saravana Pillai, Theresa Winkler, Daniel Forberg, Sonja Lippert und Sabrina Sachau danken.

Ein großer Dank geht auch an Justus Hermannsdörfer, Tobias Bauer, Adam Sobaczynski, Stephan Michilik, Isabelle Hass und Emmanuel Sobgwi für die wunderbare Begleitung.

Auch sollten Dr. Benjamin Oelkers, Johannes Obenauf, Georg Lochner, Sina Rösler, Susane Ruch, Janina Lauer, Martin Friedrich und Toni Hille als Mitarbeiter unserer Forschungsgruppe dankend erwähnt werden.

Für die administrative Arbeit möchte ich Marlies Schilling meinen herzlichsten Dank für Ihre Hilfe aussprechen. Sie ist wunderbar gewesen.

Für die Verwaltung von Sicherheit und Chemikalien möchte ich Walter Kremnitz für seine Bemühungen danken. Dank auch an Anna-Maria Dietel, Heide Maisel und Simone Ott für das bereitstellen getrockneter Lösungsmittel.

Ich bin meiner Familie zu tiefsten Dank verpflichtet, für Ihre Unterstützung und Ermutigung während meiner Arbeitsphase. Besonderer Dank geht an meinen Vater, meine Mutter, meine Schwester und meine älteren Brüder für ihr Bestreben und ihre Unterstützung, die ich brauchte in der Zeit der Fertigstellung dieser Arbeit.

## 11. Declaration/Erklärung

---

I hereby declare that I have written this work by myself and that no other sources than those mentioned in this work have been used.

This work has so far neither been submitted to the Faculty of Biology, Chemistry and Earth Sciences at the University of Bayreuth nor to any other scientific institution for the purpose of a doctoral thesis.

Hiermit versichere ich dass ich die vorliegende Arbeit selbständig und nur unter Verwendung der angegebenen Hilfsmittel und Quellen angefertigt habe.

Diese Arbeit wurde bisher weder an der Fakultät für Biologie, Chemie und Geowissenschaften der Universität Bayreuth noch einer anderen wissenschaftlichen Einrichtung zum Zwecke der Promotion eingereicht.

**Muhammad Zaheer**